Satellite observations of lake surface state to improve weather forecasting in a lake-rich region

by

Homa Kheyrollah Pour

A thesis
presented to the University of Waterloo
in fulfillment of the
thesis requirement for the degree of
Doctor of Philosophy
in
Geography

Waterloo, Ontario, Canada, 2015

AUTHOR'S DECLARATION

I hereby declare that I am the sole author of this thesis. This is a true copy of the thesis, including any required final revisions, as accepted by my examiners.

I understand that my thesis may be made electronically available to the public.

Abstract

The thermal and dynamic properties of water bodies are important factors affecting the structure of the atmospheric boundary layer which stores and transports energy and mass. The storage and heat transfer of lakes play an essential role in energy and water exchanges with the atmosphere. At high latitudes, the effects of lake ice on climate mostly occur at the local/regional scale, with the degree of influence dependent on the magnitude, timing, location, duration of ice cover and the size of the water body. Ground-based lake temperature and ice observations have been used to investigate the role of lakes in the weather and climate, and the response of lakes to climate. However, in the last two to three decades, it has been observed that the number of ground-based observations, lake ice in particular, has been decreasing dramatically in several countries across the northern hemisphere. In this context, remotely sensed earth observations represent a practical tool in support of the scientific and operational modeling communities, permitting to monitor Lake Surface Water Temperature (LSWT) and ice cover.

Data assimilation methods have been used widely to solve the initial value problem in numerical weather prediction (NWP) models. There is a variety of users and applications of space-borne observations in NWP systems; however, not much attention has been paid on the assimilation of remotely-sensed LSWT data in pre-operational NWP environments for improvement of the weather forecast using the optimal interpolation method. This thesis aimed to demonstrate how retrieved remotely-sensed LSWT observations can improve the representation of lake-atmosphere interactions in NWP models. More specifically, LSWT observations were used to improve the representation of lake surface state in the High Resolution Limited Area Model (HIRLAM), a three-dimensional numerical weather prediction (NWP) model.

To attain this goal, satellite-derived LSWT observations from the Moderate Resolution Imaging Spectroradiometer (MODIS) and the Along-Track Scanning Radiometer (AATSR) sensors onboard the Terra/Aqua and ENVISAT satellites, respectively, were first evaluated against in-situ measurements collected by the Finnish Environment Institute (SYKE) for a selection of large to medium-size lakes during the open-water season. Results show a good agreement between MODIS and in-situ measurements from 22 Finnish lakes, with a mean bias of -1.13 ˚C determined over five open water seasons (2007-2011). Evaluation of MODIS during an overlapping period (2007-2009) with the AATSR-L2 product currently distributed by the European Space Agency (ESA) shows a

mean bias error of -0.93 ˚C for MODIS and a warm mean bias of 1.08 ˚C for AATSR-L2. Two additional LSWT retrieval algorithms were applied to produce more accurate AATSR products. The algorithms use ESA's AATSR-L1B brightness temperature product to generate new L2 products: one based on Key et al. (1997) and the other on Prata (2002) with a finer resolution water mask than used in the creation of the AATSR-L2 product distributed by ESA. The accuracies of LSWT retrievals are improved with the Key and Prata algorithms with biases of 0.78 ˚C and -0.11 ˚C, respectively, compared to the original AATSR-L2 product (3.18 ˚C).

The impact of remotely-sensed LSWT observations in the analysis of lake surface state of HIRLAM forecasting system was then investigated. Data assimilation experiments were performed with the HIRLAM model. Selected thermal remote-sensing LSWT observations provided by MODIS and AATSR sensors were included into the assimilation. The domain of the experiments, which focused on two winters (2010-2011 and 2011-2012), covered northern Europe. Validation of the resulting objective analyses against independent observations demonstrated that the description of the lake surface state can be improved by the introduction of space-borne LSWT observations, compared to the result of pure prognostic parameterizations or assimilation of the available limited number of in-situ lake temperature observations. Further development of the data assimilation methods and solving of several practical issues were found to be necessary in order to fully benefit from the space-borne observations of lake surface state for the improvement of the operational weather forecast.

Lastly, the lake-specific autocorrelation function based on LSWT remotely sensed observations was approximated in HIRLAM. A new autocorrelation function of lake pairs was approximated and compared against the original function utilized in current version of HIRLAM to investigate potential improvements demonstrated through HIRLAM sensitivity experiments. The autocorrelation function is calculated based on distance and lake depth differences for each lake pairs. Results show that large lakes are more sensitive to the impact of the autocorrelation. These results also suggest that the high concentrated observations can improve the enhanced result; however, ground-based observations of LSWT are barely available for NWP applications.

Overall, results from this thesis clearly demonstrate the benefits of assimilating space-borne LSWT observations into a weather forecasting system such as HIRLAM, and that comprehensive assimilation of LSWT observations can improve NWP results.

Acknowledgements

This thesis has been kept on track and been seen through to completion with the support and encouragement of numerous people.

First and foremost I want to thank my advisor *Prof. Claude Duguay*. It has been an honor to be his PhD student. I appreciate all his contributions of time, ideas, and funding to make my PhD experience productive and stimulating. Claude has been supportive and has given me the freedom to pursue various projects without objection. The joy and enthusiasm he has for his research, was contagious and motivational for me and his advices on research as well as on my career have been invaluable.

The outcomes in this thesis would not have been obtained without a close collaboration with *Dr. Laura Rontu*, *Mr. Kalle Eerola* and *Dr. Ekaterina Kourzeneva* at Finnish Meteorological Institute (FMI) in Helsinki, Finland. This work would not have been possible without their guidance, support and encouragement.

I also have to thank the members of my PhD committee, *Dr. Chris Fletcher*, *Dr. Ram Yerubandi*, and *Dr. Andrea Scott* for serving as my committee members and their helpful advices and suggestions. I also want to thank *Dr. Stéphane Bélair*, who agreed to be the external examiner for my PhD defense.

I thank my colleagues in *"Duguay Research Group"* and in the Department of Geography and Environmental Managements (too many to list here but you know who you are!) for providing support and friendship.

A journey is easier when you travel together. Interdependence is certainly more valuable than independence. Words fail me to express my appreciation to my beloved husband *Dr. Fereidoun Rezanezhad* and my wonderful son *Hooman* for their support, generous care, great patience and tolerance. Without *you*, none of these could happen.

I also would like to pay high regards to my parents for their sincere encouragement and inspiration from far away. I owe everything to them!

This research was supported by European Space Agency (Support to Science Element, North Hydrology Project) and a Discovery Grant from the Natural Sciences and Engineering Research Council of Canada (NSERC) to C. Duguay, as well as a NSERC Canadian Graduate Scholarship to H. Kheyrollah Pour.

List of Abbreviations

AATSR	Along-Track Scanning Radiometer
AMSR-E	Advanced Microwave Scanning Radiometer for EOS (Earth Observation System)
ASTER	Advanced Spaceborne Thermal Emission and Reflection Radiometer
AVHRR	Advanced Very High Resolution Radiometer
COSMO	Consortium for Small-scale Modeling
CLIMo	Canadian Lake Ice Model
CRCM	Canadian Regional Climate Model
DA	Data Assimilation
EASE-GRID	Equal-Area Scalable Earth Grid
ECMWF	European Centre for Medium-Range Weather Forecasting
EOS	Earth Observation System
ESA	European Space Agency
FLake	Freshwater Lake model
FMI	Finnish Meteorological Institute
GABLS	Atmospheric Boundary Layer Studies
GCM	Global Circulation Models
GCOM	Global Change Observation Mission
GEOS	GEOStationary Satellite server
GEWEX	Global Energy and Water Exchange
GLCC	Global Land Cover Characteristics
GLWD	Global Lakes and Wetlands Database
HIRLAM	High Resolution Limited Area Model
IASI	Infrared Atmospheric Sounding Interferometer
JAXA	Japanese Aerospace Exploration Agency
LIC	Lake Ice Concentration
LIST	Lake Ice-snow Surface Temperature
LST	Land Surface Temperature
LSWT	Lake Surface Water Temperature
LWD	Long-Wave Radiation
MBE	Mean Bias Error
MERIS	MEdium Resolution Imaging Spectrometer
MODIS	Moderate Resolution Imaging Spectrometer
NEMO	Nucleus for European Modeling of the Ocean
NOAA	National Oceanic and Atmospheric Administration
NPP	National Polar-Orbiting Partnership
NSIDC	National Snow and Ice Data Center
NWP	Numerical weather prediction model
OI	Optimal Interpolation
OSTIA	Operational Sea Surface Temperature and Ice Analysis
POM	Princeton Ocean Model
QC	Quality Control
RCA	Rossby Centre Regional Atmospheric Model
RMSE	Root Mean Squared Error
SAMS	Scottish Association for Marine Science
SD	Standard Deviation
SGLI	Second-generation GLobal Imager
SIC	Sea Ice Concentration
SIMB	Sea Ice Mass Balance buoy
SSM/I	Special Sensor Microwave Imager
SST	Sea Surface Temperature
SYKE	Finnish Environment Institute (Suomen Ympäristökeskus)
UW	University of Waterloo
VIIRS	Visible Infrared Imaging Radiometer Suite

Table of Contents

List of Figures

List of Tables

Preface

In addition to a general introduction, a background chapter and a general conclusion, the thesis contains three journal articles that examine how retrieved remote sensing Lake Surface Water Temperature (LSWT) observations can improve the representation of lake-atmosphere interactions in a numerical weather prediction (NWP) model. The first and second papers are published in the peer-reviewed international journal *Tellus Series A: Dynamic Meteorology and Oceanography*. The first paper presents the development of new algorithms and assessment of the accuracy of LSWT datasets derived from thermal remote sensing sensors to be applied in NWP models. The second paper presents the improvement of the High Resolution Limited Area Model (HIRLAM) NWP model analysis through assimilation of the developed satellite-derived LSWT observations. The third paper, submitted to the international journal *Boreal Environment Research,* investigates the potential improvement of the lake-specific autocorrelation function implemented in HIRLAM using the remotely-sensed LSWT observations studied in the previous papers.

The work presented in this thesis is the result of a direct collaboration between the University of Waterloo (Professor Claude R. Duguay) and the Finnish Meteorological Institute (FMI), in Helsinki, Finland (Dr. Laura Rontu, Dr. Ekaterina Kourzeneva, and Mr. Kalle Eerola). Professor Duguay aided a great deal with the initial proposal and facilitated collaboration with FMI through North Hydrology project he led, funded by the Support to Science Element of the European Space Agency (ESA). This collaboration provided a great opportunity to work with weather forecasting specialists at FMI, which complemented the University of Waterloo's expertise in remote sensing. This project provided an opportunity to develop the basis of a long-term collaboration with FMI.

Chapter 1
General Introduction

1.1 Motivation

Climate change, especially in the context of contemporary temperature rise, has become a topic of intensive scientific research since the mid-1980s. High northern latitude regions have been identified as the most vulnerable ones to recent global climate warming, where lakes occupy a significant fraction of the landscape. Lakes are a fundamental component of climate on the local and regional scales, functioning much as oceans do on the global scale (Schertzer, 1997). Therefore, monitoring and study of lakes hydrodynamic changes in high latitude regions are important as they contribute to a better understanding of lake-atmosphere interactions (role and response of lakes) in a warming climate.

The thermal and dynamic properties of water bodies are important factors affecting the structure of the atmospheric boundary layer which stores and transports energy and mass. The heat transfer and storage of lakes play an essential role in energy and water exchange with the atmosphere. The exchanges occurring at the air/water interface are complicated as water is a fluid and thus, the heat transfer is not only by conduction and radiation, but also by convection and advection (Oke, 1978). The surface heat flux over lakes significantly depends on Lake Surface Water Temperature (LSWT). LSWT influences regional heat, moisture content and circulation of the atmosphere. The study of LSWT is important because the energy exchange between the surface and subsurface of a lake influences the static stability of the water column, which is essential in determining the lake hydrodynamics (Lofgren and Zhu, 2000).

Another important factor in the study of lakes is ice cover since it strongly affects the thermal and hydrologic behavior of lakes. At northern latitudes, seasonal lake ice forms in the fall, thickens during the course of winter and melts in the spring. The effects of lake ice on weather and climate mostly occur at the local/regional scale, with the degree of influence dependent on the magnitude, timing, location, duration of ice cover and the size of the water body. Lake ice formation, growth, decay, break-up and freeze up are also influenced by climatic variables that control surface heat fluxes. Ground-based lake temperature and ice observations have been used to investigate the role of lakes in the weather and climate, and the response of lakes to climate. However, in the last two to three decades, it has been observed that the number of ground-based observations, lake ice in particular, has been decreasing dramatically in several countries across the northern hemisphere. The decline in the ground-based observational network limits the use of such lake data into numerical weather

prediction (NWP), climate and hydrologic models. As the spatial resolution of these models is increasing, a better description of energy exchange between the atmosphere and the earth's surface is required. The development of computational methods has the ability to support the sharp reduction in observational practices using one-dimensional (1-D) to three-dimensional (3-D) lake models; however, they could have significant errors (Mironov et al., 2010; Rontu et al., 2012). In this context, remotely sensed earth observations represent a practical tool to support the scientific and operational communities to monitor LSWT and ice thermodynamic/dynamic processes. The advantage of remotely sensed data is that unlike much of the in-situ measurements, it can be obtained over very large geographic areas rather than just at a single point or a few points.

Generally speaking, one of the main reasons that forecasting for tomorrow is not accurate enough, especially in lake-rich regions, is that there are not sufficient and accurate observations over lakes giving the information of the state of lakes for today. Mathematically speaking, NWP models have an initial-value problem in which the necessary initial values are known only incompletely and inaccurately. Therefore, new observing systems such as satellite-based observations, which provide continuous observations, make it obviously necessary to find new and more sophisticated methods of assimilating observations in NWP models.

1.2 Objectives

The overall goal of this research is to demonstrate how retrieved remote sensing LSWT observations can improve the representation of lake-atmosphere interactions in NWP models. The specific objectives of this thesis are to: 1) develop satellite-based observations of lakes surface state and evaluate with ground-based measurements, 2) apply the combination of satellite-based LSWT observations and a numerical lake model to define the initial state of lake surface in the High Resolution Limited Area Model (HIRLAM) forecasting system using optimal interpolation assimilation methods, and 3) investigate possible improvement of the lake-specific autocorrelation function in HIRLAM using the developed satellite-based LSWT observations.

1.3 Thesis Structure

This manuscript-based thesis consists of six chapters aimed at investigating the benefits of using remotely sensed lake surface state observations to improve weather forecasting. The current chapter presents the rationale and objectives of the thesis, outlining the need for monitoring and assimilating lake surface state observations in numerical weather forecasting systems.

Chapter 2 provides a review of evolution of NWPs, the general methods of data assimilation, specifically optimal interpolation. The chapter also reviews the representation of lakes in NWPs, more specific in HIRLAM system, and the available satellite based observations for lake studies.

Chapter 3 addresses the first objective of the thesis by evaluating the Moderate Resolution Imaging Spectroradiometer (MODIS) and the Along-Track Scanning Radiometer (AATSR) LSWT observations with in-situ measurements collected by the Finnish Environment Institute (SYKE) for a selection of large- to medium-size lakes over Europe. This paper is published in a thematic cluster of *Tellus Series A: Dynamic Meteorology and Oceanography*:

> **Kheyrollah Pour, H.**, Duguay, C.R., Solberg, R., and Rudjord, Ø. (2014a). Impact of satellite-based lake surface observations on the initial state of HIRLAM. Part I: Evaluation of remotely-sensed lake surface water temperature observations. *Tellus Series A: Dynamic Meteorology and Oceanography.* 66, 21534, DOI: 10.3402/tellusa.v66.21534.

Chapter 4 addresses the second objective by applying the evaluated LSWT products in the HIRLAM forecasting system. It investigates the issue of improving the analysis of the HIRLAM model using LSWT observations from space. This paper is published in a thematic cluster of *Tellus Series A: Dynamic Meteorology and Oceanography*:

> **Kheyrollah Pour, H.**, Rontu, L., Duguay, C. R., Eerola, K. and Kourzeneva, E. (2014b). Impact of satellite-based lake surface observations on the initial state of HIRLAM. Part II: Analysis of lake surface temperature and ice cover. *Tellus Series A: Dynamic Meteorology and Oceanography.* 66, 21395, DOI: 10.3402/tellusa.v66.21395.

Chapter 5 investigates the potential improvement of the lake-specific autocorrelation function used in current version of the HIRLAM model using MODIS LSWT observations. This paper has been submitted to the international journal *Boreal Environment Research*:

> **Kheyrollah Pour, H.**, Kourzeneva, E., Eerola, K., Rontu, L., Duguay, C. R., and Pan, F. Preliminary assessment of lake surface water temperature statistical properties for objective analysis in a NWP model using satellite observations.

Chapter 6 presents a summary of the key findings of this research, and also includes suggestions for further research directions.

Finally, research results from Chapters 3 and 4 led to further developments and the preparation of two additional co-authored journal publications. These were published in a thematic cluster of *Tellus*

Series A: Dynamic Meteorology and Oceanography. They are included in Appendix A and B of the thesis:

> Cheng, B., Vima, T., Rontu, L., Kontu, A., **Kheyrollah Pour, H.**, Duguay, C. R., and Jouni Pulliainen. (2014). Evolution of snow and ice temperature, thickness and energy balance in Lake Orajärvi, northern Finland. *Tellus A: Dynamic Meteorology and Oceanography*. 66, 21564.

In this publication, snow and ice observations collected on a northern lake in Finland were used to investigate the seasonal evolution of snow and ice. The observed snow and ice temperature from ice mass balance buoys (SIMB) and the MODIS observations are compared to a snow/ice model (HIGHTSI) and the uncertainty in snow/ice model simulations originating from precipitation was investigated. This project also showed the large inter-annual variability of precipitation, long-wave radiative flux and air temperature during the winter season.

> Eerola, K., Rontu, L., Kourzeneva, E., **Kheyrollah Pour, H.**, and Duguay, C.R. (2014). Impact of partly ice-free Lake Ladoga on temperature and cloudiness in an anticyclonic witer situation- a case study using HIRLAM model. *Tellus A: Dynamic Meteorology and Oceanography*. 66, 23929.

This publication followed the results from Chapter 4, which improved analysis of HIRLAM using Lake Ladoga as a case study. The study showed improvement of forecast (2-m air temperature and cloud cover) using satellite observations of lake surface state and the 1-D Flake model.

Chapter 2
Background

2.1 Numerical weather prediction

2.1.1 Evolution of numerical weather prediction

Numerical weather prediction (NWP) focuses on taking current meteorological observations and processing them by integrating primitive-equation models to forecast the future state of weather. The observations are used as input to NWP through a process called data assimilation. The state of the weather is described as the series of grid-boxes by a set of state variables such as temperature, humidity, and pressure.

At the beginning of the 20th century, weather forecasting was very imprecise and unreliable as observations were scarce and irregular and the theoretical physics played a relatively minor role in practical forecasting. Forecasting was more like an art than a science. The first explicit analysis of the weather prediction problem from a scientific viewpoint was undertaken when the Norwegian scientist Vilhelm Bjerknes set down a two-step plan for rational forecasting (Bjerknes, 1904). He used diagnostic and prognostic terms for these two steps. The diagnostic step required adequate observational data at the particular time and prognostic step was to be taken by assembling a set of equations for each variable describing the atmosphere such as temperature, humidity, and pressure. So that the idea of solving the equations to calculate future weather was promoted by Bjerknes, but he did not construct a detailed plan for implementing his program or attempt to carry it through a practical realization. The first attempt to put his idea into practice was by Lewis Fry Richardson. He constructed a systematic mathematical method for predicting weather and the methodology proposed by him is essentially that used in practical weather forecasting today (Charney, 1950).

Numerical methods used in NWP for solving the equations have naturally evolved in the last few decades, partly due to research advances and partly because of changes in the available computing resources. The model equations in NWPs are solved at points defined by a three-dimensional spatial grid that covers the region of interest. NWP models of the 1950s had grid-points spaced every few hundreds kilometers in the horizontal direction, whereas today, models use grid-points every 1-100 km. The resolution of models depends on the area coverage so that general circulation models (GCMs) have generally coarse resolution and are necessary for long-range forecasts; however,

regional models often called limited area models, have finer resolution and are used for short-range forecasts (Collins et al., 2013).

Over time, the complexity and sophistication of NWP models increased and most of the improvements have been in better model resolution, numerical techniques and model physics. As the resolution of a model increases, more and more fine scale effects in the atmosphere from the underlying surface become apparent and should be taken into account. Meteorological observations made all over the world are used to provide the best estimate of the NWPs initial conditions. Some of the observations, such as the ones from weather stations, weather balloons or radio sounders, are taken at specific times at fixed locations (Figure 2.1). Other data, such as aircraft, ships, or satellites, are not fixed in space. Observations cannot be used directly to start model integration as initial conditions, but must be modified in a dynamically consistent way, which is referred to as data assimilation.

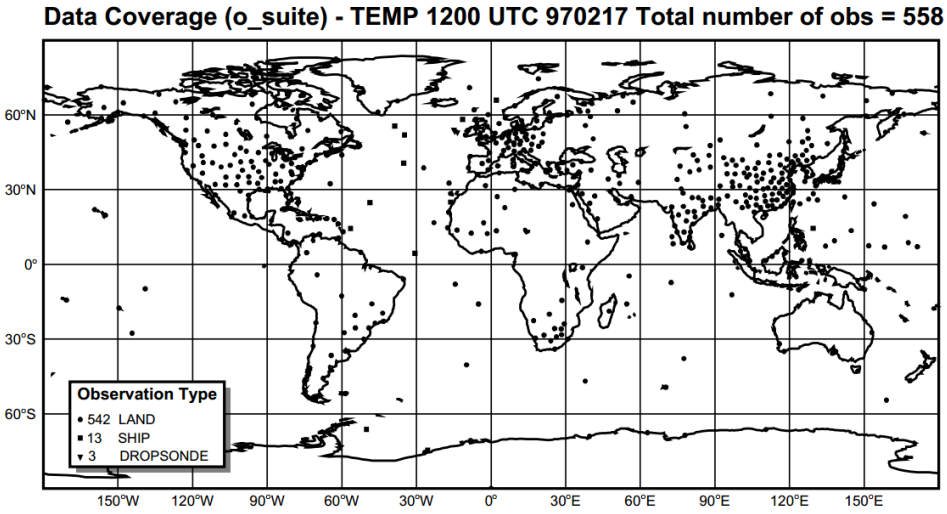

Figure 2.1 Map of radiosonde locations (ECMWF report).

2.1.2 General methods of data assimilation

NWP models are "initial value problem" for which initial data are not available in sufficient quantify and with sufficient accuracy (Daley, 1991). Moreover, computed weather forecasts are of operational use only if they are available well ahead of verifying time. Therefore, it was essential to automate the process of preparing the initial fields, called objective analysis. Objective analysis method is the process of interpolating the available observations onto a regular grid in NWP in order to define the initial conditions. To do this, first guess field or background field (provided for example by the earlier forecast) should be blended with the observations. As the background field is consistent

with the physical relationship implemented by the model equations, it helps to introduce the dynamical consistency between the analysis and the model. In the case that there is no direct connection between observations and background values or there are no observations available for a grid-box, data assimilation method is needed to connect the observed information into a model state (Lynch**,** 2006). Therefore, observations from regions with good data will be blended to the regions with no or sparse data. An example of the intermittent analysis /forecast cycle is shown in Figure 2.2.

The better objective analysis will improve the forecasting model result and therefore will improve the background. To achieve this, the following steps should be applied: a) the weight factor should be taken into account so that data should be weighted to their distance from the grid-point; b) the error in each type of observations should be estimated; c) the error of the background field should be estimated; and d) the effect of clustering data should be considered to avoid an exaggerated effect on the analysis value (if there are many observations in one area).

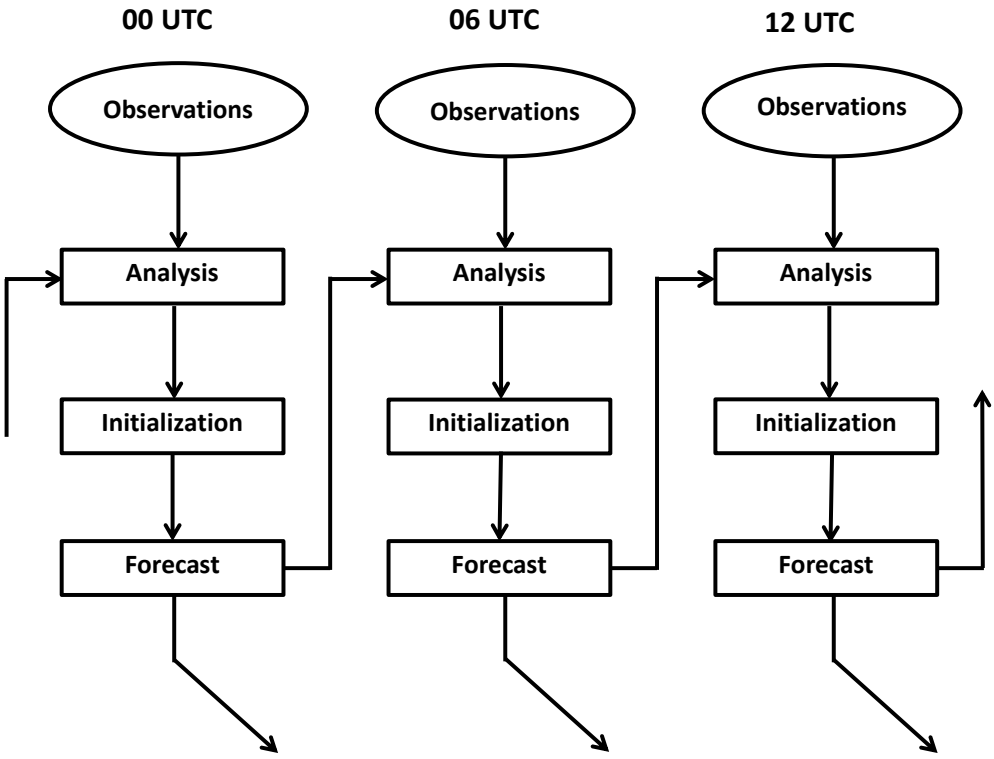

Figure 2.2 Intermittent analysis/forecast cycle. Observations in a window surrounding each analysis time are used at the nominal analysis time. After initialization, the forecast is performed. A short-range forecast (6 hours) is illustrated here (Lynch, 2006).

2.1.3 Optimal interpolation

Optimal Interpolation (OI) is an objective analysis procedure that incorporates all four steps listed above when performing an analysis. OI is based on a statistical estimation approach, which minimizes the analysis error. The method of optimizing the use of information in the background field and in the observations was first proposed by Arnt Eliassen and was developed in more detail by Gandin (1965) and in Chapter 5.

In the OI method, the state of the atmosphere at a particular time will be given in terms of vector **X** of the variables at all model grid-points. The aim is to deduce the best estimate $\mathbf{X}_A$ (vector of analyzed value) of **X** from the available data. The vector of analyzed value can be expressed as (Daley, 1991):

$$\boldsymbol{X_A = X_B + K[Y - H(X_B)]} \qquad \mathbf{2.1}$$

Where $\mathbf{X}_B$ is background model state, **K** is gain, or weight matrix, **Y** is vector of observations, and **H** is observation operator. Observation operator converts the background field into first guess values of the observations. The operator includes spatial interpolation to observation points and transformation to observed variables based on physical laws. Based on Eq. 2-1, the analysis is obtained by adding to the background field a weighted sum of the difference between observed and background values by the gain matrix **K**, where the **K** is given by:

$$\boldsymbol{K = BH^T(R + HBH^T)^{-1}} \qquad \mathbf{2.2}$$

Where **B** is the covariance matrix of background field error and **R** is the observational error covariance matrix. In OI, the background and observational matrices are assumed to be constant in time. The analysis error covariance (**A**) is then given by:

$$\boldsymbol{A = (I - KH)B} \qquad \mathbf{2.3}$$

2.2 Representation of lake observations in NWP

The thermal and dynamic properties of water bodies make them important climatological substances. As the first law of thermodynamics states, energy can be neither created nor destroyed; therefore, the transmission of energy in the lake-atmosphere system is converted from one form to another in three different modes such as conduction, convection, and radiation. In the lake-atmosphere system, the amount of energy as an input is equal to the energy output over a long period of time (*e.g.*, a year) and during shorter periods (*e.g.*, hourly to monthly); the energy balance differs significantly based on the amount of stored energy.

Water stores energy well due to its high heat capacity (Oke, 1978). Due to their high heat capacity, lakes take much more energy input to rise their temperature in comparison to land surfaces, and take longer to cool down or warm up.

In NWP models, at a minimum, the lower boundary of the model atmosphere over water bodies must have specified the water surface temperature. In today's NWP models, the effect of lakes are either ignored or accounted for very crudely, affecting the quality of simulation of atmospheric boundary-layer structure. Figure 2.3 illustrates some of the processes that can be represented, explicitly or through parameterization, in NWP models to couple the atmosphere-water system.

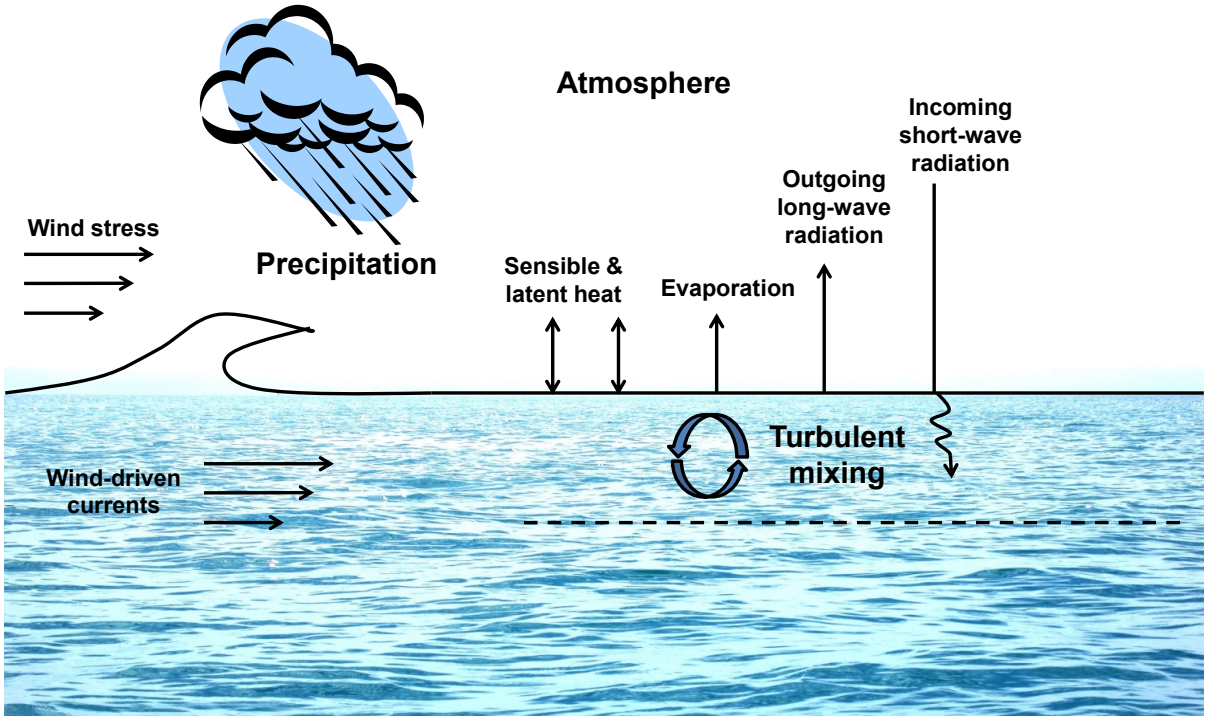

Figure 2.3 Physical and heat-exchange processes associated with the movement of heat and mass between lake and the atmosphere and within the lake (modified from Warner, 2011).

Wind at the lake surface causes waves, where the wind strength is a function of wind speed and fetch. Wind causes the water to mix (the mixed layer) and the density of water produces different temperature layers within the water column (stratification). The more stable the surface water causes

a weaker and shallower mixing. The near surface stability depends on the vertical distribution of energy exchange from atmospheric incoming fluxes and the lake surface (Warner, 2011).

The importance of a correct description of lake physical processes in weather predictions is well known (Niziol, 1987; Niziol et al., 1995; Zhao et al., 2012). During freezing and melting of lakes, the surface radiative and conductive properties as well as latent and sensible heat released from lakes to the atmosphere change dramatically leading to a completely different surface energy balance. Earlier break-up takes advantage of strong solar insolation in the high sun season and gives an earlier start to the heating of the lake due to the small surface albedo. Low albedo and high absorption of solar radiation result in a strongly positive radiation balance with small sensible and latent heat exchanges. The overlaying atmospheric condition becomes stable and it persists until the LSWT exceeds atmospheric temperature to create unstable atmosphere (transition time varies by different lake characteristics and latitude). With earlier break-up and heating storage, a lake reaches its maximum temperature and heat storage earlier (Schertzer et al., 2002) and stable to unstable atmospheric regime change occurs sooner. Subsequently, the period of maximum sensible and latent heat exchanges increases. Rouse et al. (2003) showed that the total sensible and latent heat fluxes are 9 times larger during unstable atmospheric condition than stable atmospheric condition in a study conducted on Great Slave Lake, NWT, Canada (late August-November). Peaks in sensible and latent heat fluxes are due to strong winds that promote larger vertical temperature and vapor pressure gradients (Blanken et al., 2000; Blanken et al., 2003).

Understanding lake ice processes and the corresponding interactions with the atmosphere allow for better weather forecasting (Eerola et al., 2010). In most NWP models, this is often ignored or parameterized very roughly (Brown and Duguay, 2010) as obtaining spatially detailed in-situ observations such as lake surface temperature, ice thickness, or albedo are challenging, especially for large lakes. The influence of inland water in regional climate has been confirmed in previous studies using simple lake simulations. The land surface parameterizations in climate models have been developed to represent sub-grid scale inland surface water in terms of prescribed fractional surface water area (Pitman, 1991; Henderson-Sellers and Pitman, 1992; Hostetler and Giorgi, 1992; Bates et al., 1993; Bonan, 1995; Ljungemyr et al., 1996; Lofgren, 1997). Coe (1998) developed a terrain-based hydrologic model to simulate rivers, lakes, wetlands on the continental scale. Ljungemyr et al. (1996) developed a model for parameterization of lake temperature and lake ice thickness in atmospheric models and they applied the model within HIRLAM for short-range weather forecasting. They also showed that replacing lake climatology within HIRLAM with modeled LSWT changed modeled low

level 2-m air temperature in Sweden by 3K. Since the cumulative effect of lakes on climate is important, 1-D models have also been implemented in climate models in previous studies (*e.g.* Samuelsson et al., 2010). A list of lake models most commonly used as the lake parameterization schemes in NWP and RCMs, and their strengths and weaknesses are summarized in Table 2.1. Some models assume complete mixing down to the lake bottom and characterize the entire water column by a single value of temperature. This assumption can reduce the computational costs; however, it neglects the lake thermocline, which results in large errors in the surface temperature. Other models, such as turbulence closure models (Tsuang et al., 2001), are based on the transport equation for turbulent kinetic energy and describe the lake thermocline better, but they are expensive computationally. Samuelsson et al. (2010) investigated the impact of lakes on the European climate by coupling the Freshwater Lake (FLake) model to the Rossby Centre Regional Climate Model (RCA3.1), and compared the simulations with those in which all lakes in the model domain were replaced by land. Their results showed that lakes have a warming effect on the European climate, especially in fall and winter.

Although the 1-D models are able to simulate surface temperature and the thermal structure of a lake, they cannot simulate lateral flow in the lake and do not take into account the numerous mixing mechanisms present in deep and large lakes, such as mechanical mixing caused by 3-D water circulation, horizontal transfer of water by currents, etc. For these reasons, various attempts have been made over the past few years to couple 3-D lake models with atmospheric models. Recent studies show that atmospheric models coupled with 3-D lake models could provide more realistic local temperature and evaporation in comparison to simulations without lake effects (Song et al., 2004; Long et al., 2007; Huang et al., 2010; Dupont et al., 2011). Sophisticated 3-D lake/ocean models, such as the Princeton Ocean Model (POM) and the Nucleus for European Modeling of the Ocean (NEMO) have been shown in the past to be able to simulate water circulation in lakes and interactive coupling of climate models (Song et al., 2004; Dupont et al., 2011).

The majority of previous studies have discussed the prognostic parameterization of lakes in NWP models (Kourzeneva et al., 2012a, b; Mironov et al., 2012), but assimilation of lake observations in NWP has received much less attention. Eerola et al. (2010) investigated the performance of HIRLAM using the FLake model as a parameterization scheme. They suggested that assimilation of lake surface temperature observations would likely improve the results. Rontu et al. (2012) studied the applicability of the prognostic and observation-based approaches of LSWT in NWP and showed that the lake model provides a better background for data assimilation than lake surface temperature

climatology. They suggested that improvement could be achieved using in-situ and space-borne observations of LSWT and ice cover for real-time operational NWP.

In particular, methods to retrieve LSWT data from satellite sensors offer the opportunity to apply remote sensing technology for obtaining a consistent coverage of a key parameter for climate and hydrological research. This study demonstrates how satellite remote sensing of lakes can help improve weather forecasting. It also identifies existing satellite data products specific to lakes, discusses the limitations of the currently available remote sensing products, and describes expected future improvements (see Section 2.4).

Table 2-1 Lake models most commonly used as lake parameterization schemes in NWP and RCMs.

Study	Lake Model	Short description	Strengths and weakness
Hostetler (1993) Bates et al. (1993)	Hostetler model	A 1-D energy balance model that simulates the vertical transfer of heat as well as ice cover using ice model. It coupled interactively with the RCMs to simulate the precipitation and air temperature in the vicinity of water bodies	The model is simple and flexible and insensitive to the lake depth for a broad range of depth value, which is important when coupling with RCMs, where numerous lakes have to be simulated. But the formulations of physical processes, which determine the water temperature, need to be improved.
Ljungemyr et al., (1996)	Mixed model	A simple thermodynamic lake model used for parameterization of lake effects in in HIRLAM system. It's a well-mixed model to simulate lake water temperature, ice thickness, and break –up dates.	The model uses a simple approach but it assume a complete mixing down to the lake bottom and characterize the entire water column by a single value of temperature.
Goyette et al. (2000)	Goyette model	The model is based on GCM mixed-layer ocean model. It simulates LSWT using a mixed-layer model and a thermodynamic ice model to simulate evolution of ice cover, which coupled with CRCM.	The model use a simple mixed-layer model to estimate mixed-layer but the seasonal variation of mixed-layer depth is not considered.
Mironov (2008) Kourzeneva et al. (2008) Mironov et al. (2010) Samuelsson et al. (2010) Eerola et al. (2010) Balsamo et al. (2012) Kheyrollah Pour et al. (2014b)	FLake model	A 1-D model, which is based on a two-layer water temperature profile. The structure of the stratified thermocline layer is described using the concept of self-similarity (assumed shape) of the temperature depth curve.	The model is simple and not expensive but very sensitive to the lake depth. For deep lakes, a virtual bottom depth of 40-60 m is typically used in simulations. FLake considers the snow cover over on ice but the snow module needs to be improved.
Blumberg and Mellor (1987) Schwab and Bedford (1994) Song et al. (2004) Long et al. (2007) Huang et al. (2010)	The Princeton Ocean Model (POM)	A 3-D model, which solves the conservation equations of heat, mass, and momentum on staggered grids using the finite difference method. POM is able to simulate temporal and vertical variation of currents.	The model uses the bottom bathymetry and surface elevation of lakes and is widely used for major lakes with realistic estimation. However, it has a high computational cost and requires detailed input data.
Dupont et al. (2011)	Nucleus for European Modeling of the Ocean (NEMO) model	A 3-D atmospheric-lake modeling system that being developed by Environment Canada to represent the complex atmosphere-lake interaction over the Great Lakes region. It uses two layer of ice and one layer of snow to simulate ice condition on Great Lakes.	The advantage of NEMO model is its wide spread use and continue tuning by the scientific community, however, it is computationally expensive.

2.3 HIRLAM forecasting system

The numerical short-range weather forecasting system HIRLAM (Undén et al., 2002) has been used for operational weather prediction at the Finnish Meteorological Institute (FMI) since 1990. Currently, version 7.4 is implemented over the European-Atlantic domain with a 7.5-km horizontal grid spacing and 65 levels in vertical (Figure 2.4). HIRLAM considers five surface types within each grid square such as sea/lake water, ice, bare land, forest and agricultural terrain/low vegetation. Diagnostic fields, such as 2-m air temperature, relative humidity, and 10-m height wind are available for each grid-box fraction separately. In HIRLAM, the LSWTs are treated by the prognostic model and also data assimilation using OI method (Gandin, 1965 and Mahfouf, 1991). With increasing computing power, higher resolutions in limited area models become more feasible and the horizontal/vertical resolutions of HIRLAM improved from 55km/16 levels to 7.5km/65 levels. This resolution improvement allows resolving lakes with sufficient accuracy in a local weather forecast.

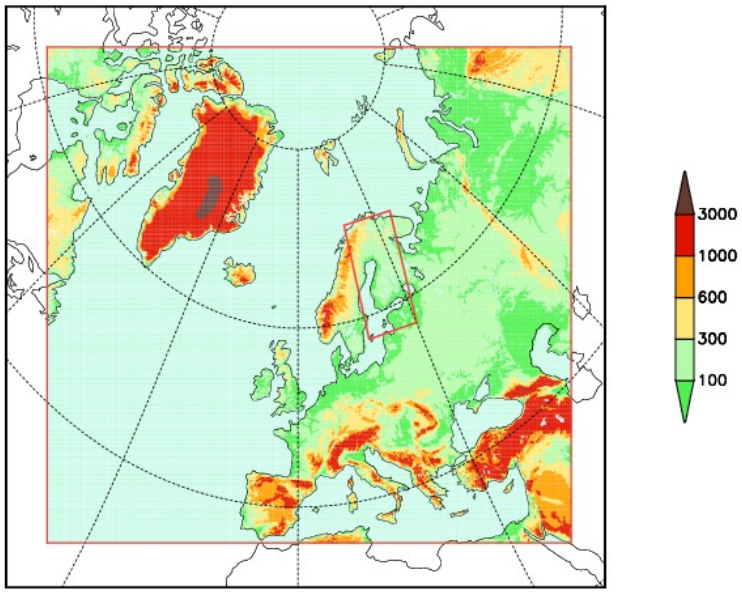

Figure 2.4 HIRLAM v7.4 operational domain (elevation in red box).

2.3.1 Treatment of LSWT in the operational HIRLAM

The treatment of lakes became relevant when the resolution of models became high enough to resolve them, even smaller ones. In the HIRLAM system, sea and lakes are treated together, but there is an extra variable such as fraction of lake, in every grid-point. In the first implementation of HIRLAM, monthly climatological water surface temperature was used both over sea and lakes. However, for

lakes the climatology values were achieved by extrapolating the values over sea to lakes. The reason was that no suitable lake climatology was available at that time and, consequently, the values were not representative for lakes. Especially, in Scandinavia, this meant that lakes that were close enough to the Atlantic or Arctic oceans never froze in winter. An example of this is given in Eerola (1996) using Lake Inari in northern Finland (Figure 2.5). In the HIRLAM climatology, extrapolated from the Arctic Ocean, the lake remained free of ice all year round, but the lake water temperature never rose over 10°C in summer. In the real climate, the lake is ice-covered from early November to late May and in summer the temperature rises to 16°C.

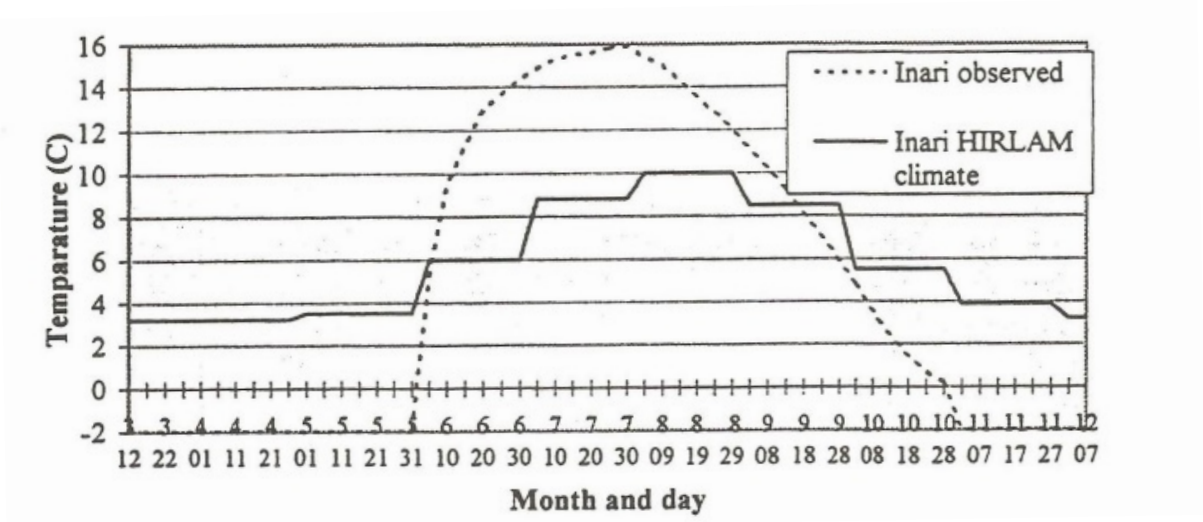

Figure 2.5 Surface temperature of Lake Inari (68.878°N, 28.101°E) in northern Finland from the HIRLAM climate system, and corresponding observed long-term averages as a function of the calendar date (Eerola, 1996).

To obtain a better climatological LSWT over the Finnish lakes, a procedure called Finlake was created (no observed values were available in real-time). In every HIRLAM run, climatological LSWT pseudo observations were created for 20 lakes in Finland by linear interpolation in time from the climatological values of every 10 days. These pseudo observations were then used in the LSWT analysis. Note that in the HIRLAM surface analysis, sea observations do not affect the lakes and vice versa. Another problem in Finland was is Lake Ladoga (61°N, 31°E), a huge lake at the boundary of Finland and Russia, since no climatological values were available and it behaved totally differently than the smaller Finnish lakes. However, it was close enough to affect the weather; at least in eastern

Finland (Eerola et al., 2014). To solve this, an assumption was made that Lake Ladoga behaves in a way similar to the eastern part of the Gulf of Finland, when the spatial resolution of the European Centre for Medium-Range Weather Forecasting (ECMWF) Sea Surface Temperature (SST) analysis was high enough to resolve the Gulf of Finland. A few pseudo observations on the eastern part of the Gulf of Finland were copied to Lake Ladoga and used as lake observations there. The assumption was still crude; however, it was better than assuming that Lake Ladoga behaves like the Finnish lakes.

At the same time, in other meteorological services, it was also recognized that sea climatology is not representative of lakes. In Germany, Deutsher Wetterdienst, a prognostic lake parameterization scheme started to be developed (Mironov 2008, 2010, 2012) where the FLake model was applied instead of the observation-based approach. In the ECMWF, time-lagged monthly mean screen-level temperatures from the forecast model were introduced to the LSWT analysis over the large lakes. Kourzeneva (2008) coupled the FLake model as a parameterization scheme in HIRLAM, and showed that the simulated LSWT is quite sensitive to the lake parameterization. Eerola et al. (2010) discussed the specific features of the implementation of FLake into HIRLAM as a parameterization scheme, and then Rontu et al. (2012) continued this work by integrating the data assimilation system with FLake. Results showed that the lake model provides a better background for data assimilation than LSWT climatology.

The next step was to use real LSWT observations of the Finnish Lakes. This took place in fall 2010 when real-time in-situ observations from 27 lakes, made by SYKE (Finnish Environment Institute) became available. In March 2012, the FLake model was implemented into the operational HIRLAM at FMI. From that time, the lake state was totally handled by FLake and the analysis of LSWT only offered another independent analysis of LSWT that had to be solved, as discussed in Kourzeneva et al. (2014) and Kheyrollah Pour et al. (2014). Therefore, the methods to retrieve LSWT data from satellite thermal remote sensing, and then assimilate these observations into analysis or 1-D lake models, are very promising in order to reduce errors of the lake models used in NWP systems and to improve HIRLAM analysis in particular.

2.4 Satellite remote sensing of lakes

The decrease of cryospheric in-situ observations and limitation of lake models can be compensated by the use of satellite imagery. The network of in-situ observations dataset has plummeted at a time when there was an increase demand of lake ice observations by the modellers' community. Over the past years, innovations in satellite technology and processing algorithms have generated data to improve earth observation. The advantage of using satellite data is that they provide: continuous measurements, sufficiently high spatial resolutions, accessibility to remote areas and provide global retrieval of observations. Several prior studies have looked into the ability of data assimilation of remotely sensed observations in order to improve estimation of model simulations of the land surface state (e.g. Houser et al., 1998; Reichle et al., 2002a,b; Slater et al., 2005) or sea ice (e.g. Lisaeter et al., 2003; Lindsay and Zhang 2006; Stark et al. 2008; Scott et al., 2012), with the overall objective of increasing the skill of weather and climate forecast. Based on previous investigations, assimilation of lake variables in current NWP using satellite observations has received less attention. The operational analysis of LSWT was developed at Met Office, UK, for NWP purposes on the Operational Sea Surface Temperature and Ice Analysis (OSTIA) system (Donlon et al., 2012; Fiedler at al., 2014). The LSWT observations used in this system are part of SST products from AATSR and MetOp-AVHRR (Infrared Atmospheric Sounding Interferometer (IASI)). These data are based on SST retrievals as none of them include lake-specific processing; therefore, they introduce inaccuracies to the LSWT data over lakes.

Remote sensing is widely used as a tool in lake studies such as for the determination of surface water temperature (e.g. Wan et al., 2002; Bussières et al., 2002; Bussières and Schertzer, 2005; Oesch et al., 2005; Crosman and Horel, 2009; Coll et al., 2009; Schneider et al., 2009; Arp et al., 2010; Reinart and Reinhold, 2008; Hulley et al., 2011; Kheyrollah Pour et al., 2012; Liu et al., 2014), albedo (e.g. Savacina et al., 2014a, b), ice phenology (Hall et al., 1981, 2002; Duguay and Lafleur, 2003; Jeffries et al., 2005; Latifovic and Pouliot, 2007; Leshkevich and Nghiem, 2007; Howell et al., 2009; Kang et al., 2010, 2012; Brown and Duguay, 2010, 2011), water transparency (e.g. Sydor, 2006; Heim et al., 2008) and lake depth (e.g. Duguay and Lafleur, 2003). The existing remotely sensed data products specific to lakes in visible and infrared spectrum are summarized in Table 2.2.

Table 2-2 Most available satellite data products in visible and infrared spectrum (the grey color represents the existing data).

	Platforms	Sensors	Products (Pixel size- km)	Revisit time					
				Daily	3 Days	Weekly	8 Days	16 Days	Monthly
Visible and Infrared Spectrum	**Terra**	MODIS	LST (1)	■		■	■		
			LST (5.6)	■			■		■
			LST (6)	■		■			
			Albedo (0.5)	■			■		
			Snow cover (0.5)	■			■		
			Surface reflectance (0.25 & 0.5)	■			■		
			Surface reflectance (1 & 5.6)	■					
		ASTER	Surface reflectance (0.013 & 0.03)					■	
	Aqua	MODIS	LST (1)	■		■	■		
			LST (5.6)	■			■		■
			LST (6)	■		■			
			Albedo (0.5)	■			■		
			Snow cover (0.5)	■			■		
			Surface reflectance (0.25 & 0.5)	■			■		
			Surface reflectance (1 & 5.6)	■					
	Aqua/Aqua combined	MODIS	LST (1 & 6)	■		■	■		■
			Albedo (0.5 & 1 & 5.6)					■	
	Envisat	AATSR	LST (1)	■		■	■		■
			LST (6)	■		■	■		■
			Ice cover (1)	■					■
		MERIS	Ice cover (0.3)	■					
			Water optical properties (0.3)	■					
	NOAA	AVHRR	LST (1)	■					
			Albedo (1)	■					
		AVHRR-APP	LST (5)	■					
			Albedo (5)	■					
	ERS-1/2	ATSR	LST (1)	■					
	Suomi-NPP	VIIRS	LST (0.38 & 0.75)	■					
	NOAA-GEOS		LST (4)	15-30 minutes					

In principle, for successful parameterization of lakes, it is necessary to describe the distribution of water, ice and snow over water bodies in the model domain. This description can be derived from observational points to the model grid. There are currently no operational NWP models, which include, for instance, a full prognostic treatment of lake thermodynamics (Rontu et al., 2012). Thus, these values usually remain unchanged during the forecast. Advanced lake models can help in this matter to make progress but is challenging. Mironov et al. (2010) implemented FLake into the NWP model COSMO (the Consortium for Small-scale Modeling) and they noted the challenge of the quantitative evaluation of snow and ice in the model. No method has yet been developed to estimate on-ice snow depth on lakes. However, Duguay et al. (2005) discussed that Advanced Microwave Scanning Radiometer for EOS (AMSR-E) and the Special Sensor Microwave Imager (SSM/I) sensors at 37 GHz frequency becomes sensitive to snow depth when the ice is thick enough so that the measured brightness temperature is not influenced by the radiometrically cold water under the ice. The higher frequency could probably be considered in the earlier winter season when ice is thinner relative to the depth of emission of the microwave signal.

2.4.1 Development of MODIS UW-L3 LSWT product

A previous study by Rontu et al. (2012) reported the large differences between the analyzed and predicted LSWT fields in spring involving the FLake model into the HIRLAM system. Therefore, applying frequent acquisitions of LSWT satellite observations is of interest to the weather forecasting community. A new data set, known as MODIS UW-L3 LSWT, was developed at University of Waterloo (Duguay Research Group) by combining MODIS-Terra and Aqua data to produce regional and global scale products. This data set provides daytime and nighttime LSWT at hourly, daily, weekly, monthly, and yearly time scales. The new algorithm was developed because there are no combined Terra and Aqua LSWT products currently available. The main advantage of combining data from these two satellites is to increase the number of observations due to the limitation of optical sensors during cloudy conditions (Kheyrollah Pour et al., 2012).

In this algorithm, first, the section of the file intersecting the region of interest is read, and then the latitude/longitude coordinates and time values are calculated for each pixel. The domain is split into approximately square tiles, which are re-projected to the Equal-Area Scalable Earth Grid (EASE-GRID) projection. The EASE-GRID projection consists of a set of three equal-area projections and developed at the National Snow and Ice Data Center (NSIDC) for the distribution of snow and ice

products. It is intended to be a flexible tool for users of global scale gridded data. The re-projection is carried out by first calculating the projection coordinates of each observation and then using linear interpolation to calculate a value for the center of each EASE-GRID cell. Tiles of the selected regions of interest are then projected onto the target grid with the desired output resolution (1 km in this thesis) by averaging all pixels that fall into the target grid cell. The algorithm distinguishes daytime/nighttime average data to be able to use each of them individually if needed. As there are two satellites (Terra and Aqua) operating a MODIS sensor, when combined it offers the possibility of four observations per day (two days and two nights). To produce daily LSWT products (day/night equal weight average), at least one daytime and one nighttime observation is considered to keep the balance. For the entire domain of interest, two sets of data are produced, one containing the average of all observations during the day and the other containing the observation during the night. Then, the intermediate sum of all MODIS Terra/Aqua day/night observations for each pixel is calculated. These values are averaged together to produce the final lake surface temperature average with equal weighting between day and night values. These data, along with the day and night averages and the number of observations that went into producing each average, and output to a GEOTIFF file. Figure 2.6 shows an example of monthly LSWT maps (1 km resolution) for June and July 2011 over the main study area of this thesis. The differences of LSWT of lakes for June and July in this region can be determine from Figure 2.6. For example, the LSWT for Lake Ladoga is between 5-10 ˚C, where the LSWT for the same lake is between 14-21 ˚C.

2.4.2 Limitation of optical sensors

Optical sensors provide data with relatively high spatial and temporal resolutions, which allows the Earth's surface to be covered in a high frequency of acquisition. Despite these advantages, there are some limitations using optical sensors over lakes, especially in the fall and early winter when lakes are often covered with cloud. Data from optical sensors may not be updated for several days or, on occasion, clouds may not be detected by the algorithm, resulting in anomalous errors and lowering the temporal resolution of sensors. Therefore, upgrading the cloud cover algorithm is necessary to improve the optical sensors abilities to observe the Earth's surface. Optical sensors are also limited by fluctuations in atmospheric conditions, calibration differences of sensors or by prolonged darkness or low sun elevation at northern latitudes, which can cause over- or under-estimation of ice formation and melt onset dates. Microwave sensors are effective instruments for monitoring lake ice, being

unaffected by cloud cover or low sun elevation, which cover some limitations of optical sensors; but the most current passive microwave satellite sensors are of very coarse resolutions. Synthetic aperture radar (SAR) sensors are a viable alternative or complement, but more efforts are necessary on the development of automated algorithms for ice cover mapping/monitoring before operational usage (e.g. Duguay et al., 2015).

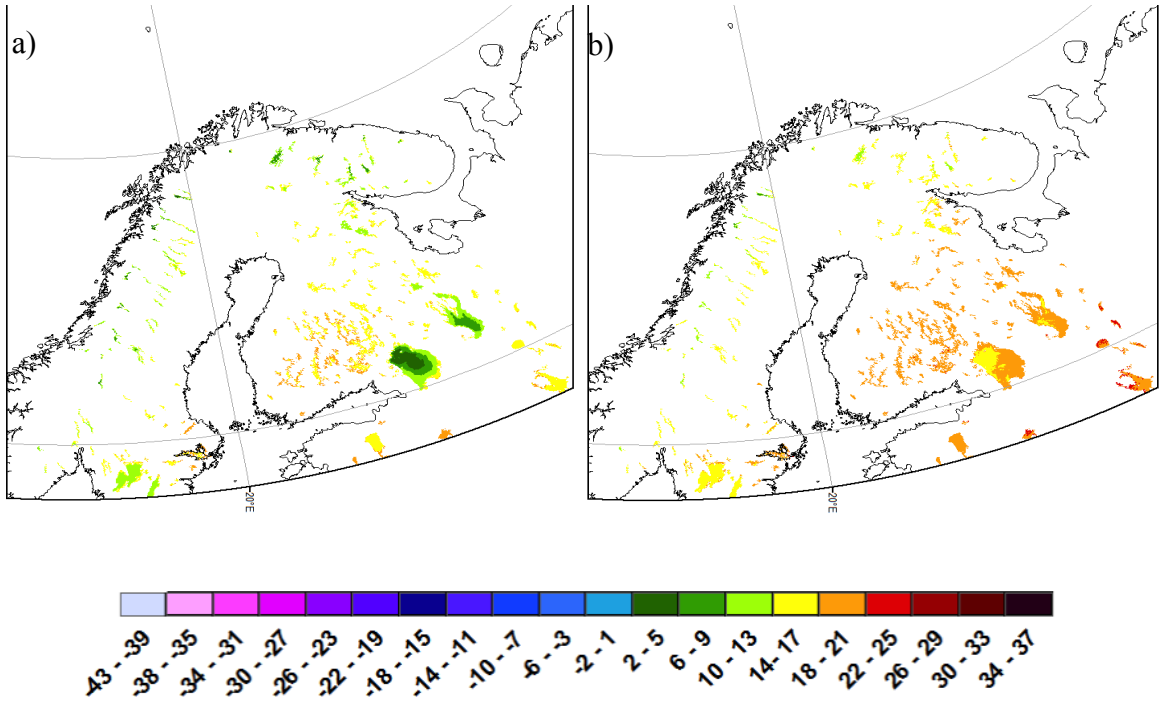

Figure 2.6 Monthly LSWT maps derived from MODIS-Aqua/Terra (1-km resolution- UW-L3) for (a) June and (b) July 2011 over northern Europe.

The complexity of the Earth system, in which spatial and temporal variability exists on a range of scales, makes it necessary to consider the development of future mission portfolios. The Global Change Observation Mission (GCOM) is an observation program of the Japanese Aerospace Exploration Agency (JAXA). The spacecraft GCOM-C, which is planned for launch in 2016, will carry the Second-generation Global Imager (SGLI) sensor with visible/infrared (VNIR, SWIR, TIR) channels. The TIR1 and TIR2 channels will have a spatial resolution of 500 m. ESA's Sentinel-3, which will provide atmospheric and land applications, provide data continuity for the ERS, Envisat and SPOT satellites. Sentinel-3 will make use of multiple sensing instruments to accomplish its

objectives; SLSTR (Sea and Land Surface Temperature Radiometer), OLCI (Ocean and Land Colour Instrument), SRAL (SAR Altimeter), DORIS, and MWR (Microwave Radiometer). The thermal sensors on Senrinal-3A and 3B with 1 km resolution allow for continuity of monitoring LSWT observation in a daily revisit time. Sentinel-3A is scheduled to be launched in 2015 and Sentinel- 3B and 3C are planned to be launched ~18 months after the first one.

Chapter 3

Impact of satellite-based lake surface observations on the initial state of HIRLAM- Evaluation of remotely-sensed lake surface water temperature observations

3.1 Introduction

Lake surface temperature observations collected by space-borne thermal sensors are increasingly being used in climate and weather-related investigations (e.g. Duguay et al., 2011, 2012a, 2013; Kheyrollah Pour et al., 2012; Schneider et al., 2009). Knowledge of Lake Surface Water/Ice-Snow Temperature (LSWT/LIST) is important for coupling the lake surface with the atmosphere in order to better represent exchanges of heat and moisture. Satellite remote sensing platforms can provide the LSWT/LIST observations required for this purpose. As thermal sensors are limited in terms of consistency due to the presence of cloud cover, which hinders surface observations, a scientific priority is to seek the best combination of tools such as space-borne observations, in-situ measurements, and numerical models to optimize the information content of LSWT/LIST data using Data Assimilation (DA) methods.

The Moderate Resolution Imaging Spectroradiometer (MODIS) aboard NASA's Aqua and Terra Earth Observation System (EOS) satellites (2000-present) and the Along-Track Scanning Radiometer (AATSR) onboard the European Space Agency (ESA) environmental satellite ENVISAT (2002-2012) have been two of the main sensors providing land and lake surface temperature observations since 2000. The MODIS sensor, launched on Terra (EOS AM, 18 December 1999) and Aqua (EOS PM, 4 May 2002), scans the Earth surface at ±55° viewing angle from nadir in 36 bands with 16 thermal infrared (TIR) bands located in the 3 to 15 µm range. MODIS-derived Level 2 surface temperature products (MOD/MYD 11-L2, Collection 5, each pixel is 1km by 1km in size) have been validated in various studies over lakes against in-situ measurements acquired during the open water season. The reported accuracies vary depending on the validation method employed (i.e. direct LSWT measurements with thermometers at some depth near the surface or non-contact, skin, LSWT measurements with thermal infrared radiometers) and the observational periods (i.e. hourly, daytime, nighttime or average daily). Biases of -0.22 ˚C for daytime and -0.39 ˚C for nighttime observations have been reported for MODIS-Terra over Lake Tahoe (California/Nevada, USA) during 2002-2005

(Hook et al., 2007) and a bias of 0.1 ˚C for nighttime observations in 2000-2008 (Schneider et al., 2009). A validation study conducted over the same lake by Hulley et al. (2011) showed a bias of -0.21 ˚C and 0.064 ˚C for daytime and nighttime observations (2002-2010 period), respectively, for both MODIS-Aqua/Terra L2 products. Crosman and Horel (2009) reported a bias of -1.5 ˚C between MODIS L2 (combined daytime and nighttime observations) and in-situ water temperature measurements from Great Salt Lake (Utah, USA) obtained at a depth of 0.5 m. The larger bias from the study of Crosman and Horel (2009) is expected since their in-situ measurements correspond to a bulk water temperature (0.5 m depth) rather than a surface (skin) temperature which is the quantity retrieved from MODIS and measured with thermal infrared radiometers deployed in the field (e.g. Hook et al., 2007; Schneider et al., 2009; Hulley et al., 2011).

The AATSR, which operated on the ENVISAT satellite until April 2012, crossed the equator at 10:00 A.M. local time for the descending orbit. AATSR acquired data in seven bands from visible to infrared with TIR bands centered at 10.85 and 12 μm. The sensor scanned the Earth with a dual view (i.e. forward view at an angle of around 55˚ and the nadir view at an angle of around 21.7˚). The nominal spatial resolution of the AATSR is 1 km for the nadir view and 1.5 km by 2 km for the forward view. Coll et al. (2009) evaluated the accuracy of LSWT retrieved with the algorithm of Prata (2002) (described in section 2.1.2), based on AATSR Level-1B (L1B) brightness temperature observations over Lake Tahoe between July-December 2002 and July 2003. The authors reported an average bias of -0.17 ˚C and Standard Deviation (SD) of 0.37 ˚C for both daytime and nighttime observations.

The purpose of this study is to assess the accuracy of a relatively new Level 3 (L3) LSWT product (referred to here onward as UW-L3 LSWT), generated from the combination of Terra and Aqua (MOD/MYD11_L2) observations, as well as ESA's current AATSR-L2 data product and two new AATSR-L2 products derived from algorithms proposed by Key et al. (1997) and Prata (2002), which make use of an improved lake mask over Finland. The acronym UW-L3 (University of Waterloo-Level 3) is used to describe the MODIS LSWT product utilized in this paper as it differs from the L3 product distributed by NASA. The UW-L3 LSWT/LIST product has previously been compared with surface water/ice temperature outputs from 1-D lake models (Kheyrollah Pour et al. 2012, Cheng et al. 2014). Kheyrollah Pour et al. (2012) showed a good agreement between daily averaged MODIS-derived and simulated (using Canadian Lake Ice Model (CLIMo)) LSWT/LIST for different depths in Great Bear Lake and Great Slave Lake, Northwest Territories, Canada, (mean bias error of less than 1

˚C) when compared over a full annual cycle or broken down into open-water and ice-cover seasons. Cheng et al. (2014) evaluated MODIS temperature observations with in-situ (snow and ice temperatures measured by an ice mass balance buoy (SIMB)) and simulated snow/ice model (HIGHTSI) LIST in three ice-cover seasons (2009-2012). They showed that MODIS observations agree with SIMB (R = 0.9, MBE = -3.1 ˚C) and HIGHTSI (R = 0.9, MBE = 3.2 ˚C) results. This study differs from previous investigations since it is the first time that the UW-L3 LSWT product is evaluated against in-situ LSWT/LIST measurements.

The study area for this investigation covers a large domain, which encompasses many lakes in Finland (Figure 3.1 and Table 3.1), and therefore addresses the need of continuous lake temperature measurements to improve the forecast of weather phenomena in this region. This paper is the first of a series of two articles that describe our recent efforts aimed at improving the treatment of lake surface state in the HIgh Resolution Limited Area Model (HIRLAM) Numerical Weather Prediction (NWP) system. In the study described herein, in-situ measurements of lake water temperature collected by the Finnish Environment Institute (Suomen Ympäristökeskus (SYKE)) are compared to MODIS- and AATSR-derived LSWT products to investigate the bias of satellite observations for a selection of large to medium-size lakes in Finland. SYKE and satellite-derived LSWT observations are then applied in the analysis of the HIRLAM NWP system (Undén et al., 2002; Eerola, 2013) in Chapter 4 using the optimal interpolation (OI) method. Chapter 4 develops the OI method and discusses analysis results of time-series of observed, analyzed and predicted LSWT, and ice cover obtained by applying MODIS/AATSR/SYKE observations and a lake parameterization scheme, the FLake model (Mironov et al., 2008, 2010).

3.2 Data and methods

3.2.1 Satellite observations

The reliability of MODIS and AATSR LSWT products was assessed using in-situ water temperature measurements from Finnish lakes. The MODIS UW-L3 daily averaged product was evaluated against SYKE observations from 22 lakes over five open water seasons (2007-2011), as well as during an overlapping period (2007-2009) along with AATSR-L2 products. Being onboard of two satellite

platforms (Aqua and Terra), MODIS provides a greater temporal coverage than AATSR (Soliman et al., 2012).

3.2.1.1 MODIS LSWT

MODIS Aqua and Terra Land Surface Temperature and Emissivity (MYD/MOD 11-L2, Collection 5, 1 km) products were acquired from the NASA Land Processes Distributed Active Archive Center (LP DAAC) for the period of 2007-2011. The products are generated with the generalized split window approach (Wan and Dozier, 1996) using the MODIS sensor radiance data (MYD/MOD021KM), the geolocation (MYD/MOD03), the atmospheric temperature and water profile (MYD/MOD07_L2), the cloud mask (MYD/MOD35_L2), the quarterly land cover (MYD/MOD12Q1), and the snow cover (MYD/MOD10_L2) products. The Land/Lake surface temperature retrieval in a MODIS swath is made by using L1B radiance data in thermal bands 31 and 32 on land or inland water under clear-sky conditions with a confidence of ≥ 66 % over lakes (Wan, 2005).

MODIS UW-L3 Land Surface Temperature (LST) (Duguay et al., 2012b; Soliman et al., 2012) and LSWT/LIST products (Kheyrollah Pour et al., 2012) are generated from Aqua and Terra MYD/MOD 11-L2 data. A new algorithm was developed to create products at various temporal resolutions (daily, weekly, and monthly) from the combination of MODIS data from the Aqua and Terra satellites, which were not available otherwise. The Aqua and Terra satellite platforms follow the same orbit within 3 hours of each other. However, at higher latitudes, it is possible to monitor the same location from both sensors within an hour, considering different viewing angles. In such case, it is feasible to combine observations from both sensors in each pixel during an hour. For the daily-averaged UW-L3 product, observations are separated into either a daytime bin (from 6 A.M. to 6 P.M.) or a nighttime bin (from 6 P.M. to 6 A.M. of the next day), not by solar angle such as the number of hours of daylight and darkness. To ascertain a balance between daytime and nighttime observations in the creation of the daily averaged product, pixels must contain at least one daytime observation and one nighttime observation for a daily value to be calculated. For the geographical region of interest, two sets of data are produced, one containing the average of all daytime observations and the other containing those of all nighttime observations. Then, the intermediate sum of all MODIS Aqua/Terra daytime/nighttime observations for each pixel is calculated. These values are averaged together to produce the final surface temperature average with equal weighting between daytime and nighttime values. Daytime average, nighttime average, daily average and the number of

clear-sky observations (counts) are recorded in separate images for each pixel during the period of interest as GEOTIFF files (GEOTIFF refers TIFF data format, which contains geographic information embedded within the TIFF file).

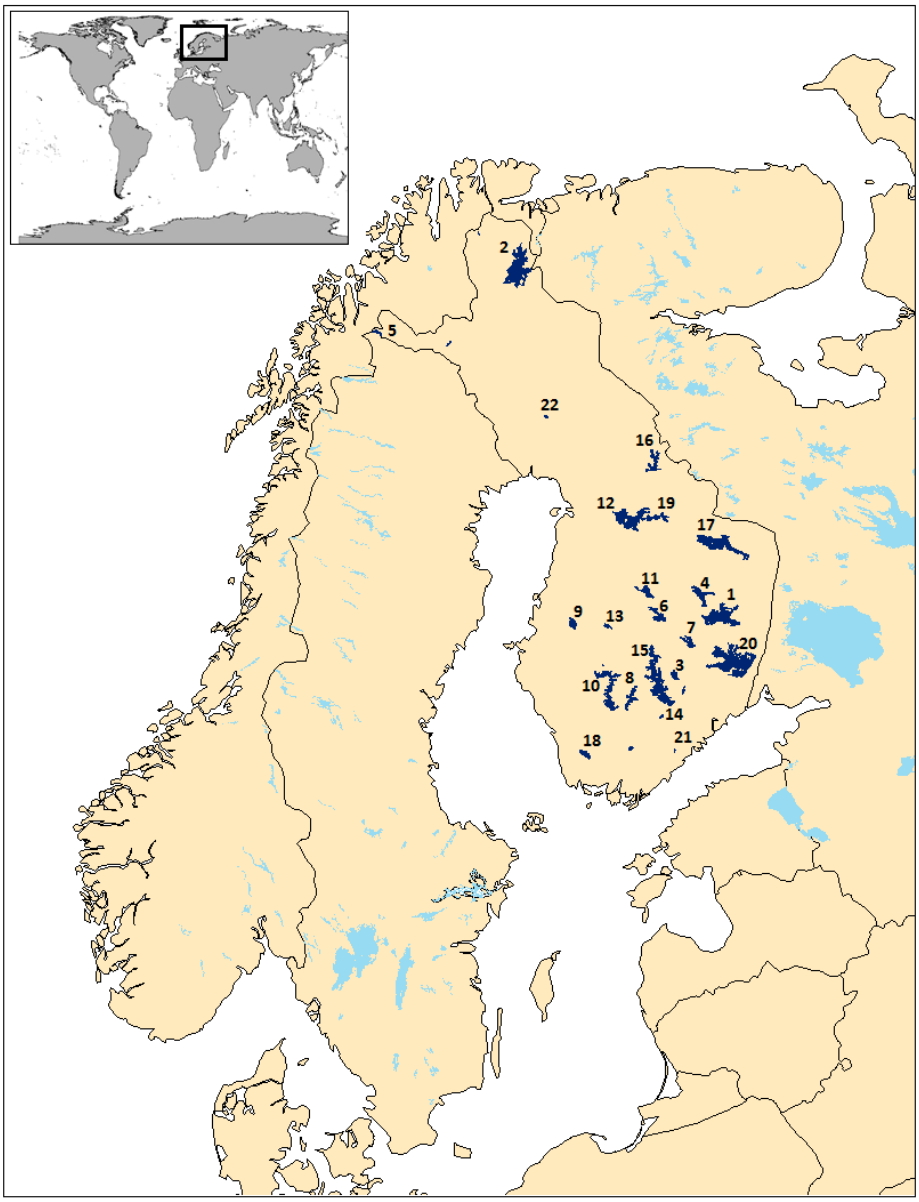

Figure 3.1 Location of lakes within the HIRLAM domain over Northern Europe (light blue) and selected lakes (dark blue) from SYKE's in-situ measurement sites in Finland.

The Equal-Area Scalable Earth Grid (EASE-Grid), Lambert's Equal Area Azimuthal projection is the projection selected for the UW-L3 product, based on a sphere datum with a radius of 6,371.228 km. Each domain is split into approximately square tiles, which are re-projected to the EASE-Grid projection. The EASE-Grid projection consists of a set of three equal-area projections and developed at the National Snow and Ice Data Center (NSIDC) for the distribution of snow and ice products. It is intended to be a flexible tool for users of global scale gridded data. The re-projection is carried out by first calculating the projection coordinates of each observation, and then using linear interpolation to calculate a value for the center of each EASE-Grid cell. Tiles of the selected regions of interest are then projected onto the target grid with the desired output resolution (1 km for this study) by averaging all pixels that fall into the target grid cell. Local time is calculated for each EASE-Grid cell using UTC acquisition time and longitude of MODIS L2 products with an accuracy of ±15 minutes.

Table 3-1 List of 22 selected Finnish lakes with coordinates, mean depth and statistics of the evaluation results for MODIS.

	Lake Name (Finnish name)	Longitude (Decimal Degree, WGS84)	Latitude (Decimal Degree, WGS84)	Mean depth (m)	MBE (°C)	RMSE (°C)	*n*
1	Hauki (Haukivesi)	14.752	56.637	10	−1.15	2.08	519
2	Inari	27.924	69.082	14	−1.87	2.31	244
3	Jaasj (Jääsjärvi)	26.135	61.631	10	−1.64	2.12	412
4	Kalla (Kallavesi)	27.782	62.761	10	−0.47	2.14	407
5	Kilpi (Kilpisjärvi)	20.815	69.006	22	−0.67	2.13	297
6	Konne (Konnevesi)	26.604	62.632	10	−1.24	1.98	382
7	Kyyve (Kyyvesi)	27.079	61.998	10	−1.14	2.16	492
8	Lange (Längelmävesi)	24.370	61.535	10	−1.42	2.27	349
9	Lappa (Lappajärvi)	23.670	63.147	10	−1.24	2.20	463
10	Nasij (Näsijärvi)	23.750	61.631	10	−1.31	2.13	428
11	Nilak (Nilakka)	26.526	63.114	10	−0.96	2.06	286
12	Ouluj (Oulujärvi)	26.965	64.450	10	−1.33	2.02	361
13	Paaj1 (Pääjärvi1)	24.789	62.863	3	−1.27	2.25	401
14	Paaj2 (Pääjärvi2)	25.047	61.052	15	−1.02	2.07	502
15	Paija (Päijänne)	25.482	61.613	10	−1.84	2.35	322
16	Pesio (Pesiöjärvi)	28.650	64.945	7	−1.10	2.20	322
17	Pieli (Pielinen)	29.606	63.270	10	−0.95	2.39	367
18	Pyhaj (Pyhäjärvi)	22.291	61.001	5	−0.79	2.04	420
19	Rehja (Rehja-Nuasjärvi)	28.016	64.184	10	−1.58	2.24	324
20	Saima (Saimaa)	28.115	61.337	10	−0.78	2.12	468
21	Tuusu (Tuusulanjärvi)	25.054	60.441	3	−0.25	2.19	385
22	Unari	25.711	67.172	10	−0.92	2.28	184
Average					−1.13	2.17	8135

MBE: mean bias error, RMSE: root mean square error, *n*: number of observations.

3.2.1.2 AATSR LSWT

The current AATSR-L2 (land and lake) product distributed by ESA is generated from AATSR-L1B data based on the algorithm of Prata (2002). The basic algorithm for the retrieval of surface temperature is:

$$T_s = a_0 + b_0 T_{11} + c_0 T_{12} \qquad 3.1$$

where a_0, b_0, and c_0 are coefficients that depend on the surface type (including lakes), viewing angle, and atmospheric water vapor. T_{11} and T_{12} represent the brightness temperature values in channels 11 and 12, respectively. The L2 algorithm expresses the surface temperature as a nearly linear combination of the brightness temperatures in each channel using only the nadir view ($\theta < 21.7^{o}$); therefore the equation is modified as:

$$T_s = a_0 + b_0 (T_{11} - T_{12})^n + (b_0 + c_0) T_{12} \qquad 3.2$$

where the index n depends on the incident angle θ as follows:

$$n = 1 / cos(\theta - m) \qquad 3.3$$

where m is an empirical constant. Coefficients for (Eq. 3.2) were determined for 13 different land cover classes including lakes, in which two separate sets of coefficients are specified for each class. For the lake class, different coefficients are given for day and night. However, in this study, only day coefficients are used due to the AATSR morning overpass for Finnish lakes (a_0= -0.0005, b_0= 2.4225, c_0= -1.4344). The algorithm operates using a low-resolution ($0.5^{o} \times 0.5^{o}$) map of land cover classes. Due to this coarse-resolution land cover type map, the algorithm misses many small to medium-size lakes. These lakes are often confounded with land. As a result, evaluation of this product was only possible for 11 of the 22 lakes monitored by SYKE.

To improve the currently available AATSR-L2 product, two additional algorithms were implemented from ESA's AATSR-L1B brightness temperature data using a finer resolution lake mask in order to minimize the possibility of land contamination (mixed land-water pixels) within the 1 km spatial resolution pixels of the AATSR satellite sensor (i.e. identify pure lake water pixels located as close as possible to the in-situ water temperature measurement sites). For this purpose, the Global Lakes and Wetlands Database (GLWD) data (~1 km^2 resolution) was applied over satellite images as the lake mask (Lehner and Doell, 2004) when selecting the pixels on each lake for evaluation.

More specifically, algorithms presented in Key et al. (1997) and Prata (2002) were applied on the AATSR-L1B product to derive new AATSR-L2 products (AATSR-L2-PR; PR stands for Prata Revised and AATSR-L2-NCC; NCC referring to the Norwegian Computing Center), and then evaluated against SYKE observations for the month of August 2009. The Prata algorithm described above (Eq. 3.2) was used to derive LSWT for each pixel from top-of-the-atmosphere cloud-free, calibrated and navigated day and night AATSR-L1B brightness temperatures. Regression coefficients for LSWT have been developed by analysis of a set of in-situ radiometric measurements made in a previous study on Lake Tahoe in 1999. The anticipated accuracy of the algorithm is ±0.3 ˚C (Prata, 2002).

In addition to the AATSR-L2-PR, AATSR-L2-NCC was generated following the algorithm proposed by the Key et al. (1997) for the ATSR sensor (the predecessor of AATSR). For surface temperature retrieval, Key's algorithm uses both nadir and forward viewing angles, and is expressed as follows:

$$\boldsymbol{T_s = a_0 + b_0 T_{11\,nadir} + c_0 T_{11\,forward} + d_0 T_{11\,nadir} + e_0 T_{12\,forward}} \qquad \textbf{3.4}$$

where a_0, b_0, c_0, d_0 and e_0 are coefficients derived for different temperature ranges (T_{11}< 240 K, 240 K < T_{11} < 260 K, T_{11} > 260 K) rather than the defined seasons to provide greater flexibility of the algorithm (a_0= -0.56158, b_0= 2.23152, c_0= -0.91817, d_0= -0.40756, and e_0= 0.09610).

The Key algorithm has previously been implemented by Amlien and Solberg (2003) and Solberg et al. (2011) as part of a snow processing chain for snow surface temperature retrieval as well as temperature of melting snow in mountainous areas of southern Norway using ESA's AATSR-L1B data. As snow, water and ice have similar emissive properties, the same approach was used for the retrieval of LSWT. The AATSR-L1B data are geo-corrected and corrected for radiometric drift. Similar to the generation of the AATSR-L2-PR product, a lake mask was also applied, defining the regions of surface temperature retrieval. The mask was produced from vector data provided by SYKE containing all large Finnish lakes. The lake mask was then eroded using a 3 × 3 kernel so that the lakes in the mask were somewhat smaller than the actual lakes. This was done in order to avoid evaluating mixed pixels, containing fractions of water and land along shorelines.

3.2.2 In-situ lake water temperature measurements

There are 187,888 lakes in Finland with a surface area larger than 500 m^2. The lakes cover 9 % of the land surface. SYKE regularly measures lake water temperature at 32 sites on a selection of these lakes. The water temperature measurements are recorded every morning at 8.00 A.M. local time, close to shore and at a depth of 0.2 m below the water surface. In this study, 22 observation sites were utilized. The selection of sites was based on the location of in-situ measurements to be compared with the satellite-derived LSWT pixel values. The measurements from SYKE are either made automatically (13 stations) or manually and are performed only during the open water season (ice-free conditions) (Rontu et al., 2012). The in-situ lake water temperature observations from SYKE were also assimilated into HIRLAM experimental model runs in Chapter 4.

3.2.3 Evaluation of satellite-derived LSWT products

The lakes were selected on the basis of their size and the ability to select a pure pixel (1 km by 1 km) from the satellite images. Pixels were chosen manually over each lake considering only lake water and to avoid land contamination. Since most of the in-situ measurements are made close to the shore, it was not possible to select pixels at exactly the same location as the SYKE measurements. Therefore, it is expected that a systematic error will result from the comparison between the satellite-derived LSWT observations (middle of the lake) and the in-situ water temperatures (closer to shore, which is warmer than middle of the lake in early spring and colder in autumn).

The Mean Bias Error (MBE), Root Mean Squared Error (RMSE), and Standard Deviation (SD) were calculated from the comparison of the satellite-derived LSWT from MODIS and AATSR and in-situ water temperature measurements from SYKE for the various time periods and sites described in the previous section. Before discussing the evaluation results, a few general remarks are needed with regards to the accuracy of the in-situ and the satellite observations.

1. The LSWT values within each satellite pixel represent an average value over a 1-km^2 area while the in-situ water temperature measurements are limited spatially (i.e. point observations).
2. The in-situ measurements were usually taken close to shore or sometimes on a river channel connected to the lake (see the location of in-situ and satellite pixels in Figure 3.2). The MODIS and AATSR pixels were chosen as close as possible to the location

of SYKE observations, but far enough to prevent land contamination. Therefore, the satellite pixels and in-situ measurements are not from the exact same location.

3. The in-situ measurements represent the lake water temperature taken at 0.2 m below the water surface. The satellite observations, however, provide a "skin" temperature of the lake water surface. Since the outgoing and incoming long-wave radiation as well as sensible and latent heat fluxes add or remove heat directly from the top few microns of the lake surface, the water temperature across the sub-layer (~2 mm) tends to be colder than the bulk temperature.
4. SYKE lake water temperature measurements are made every morning at 8.00 A.M. local time, which is not the exact time as the satellite overpasses over the studied lakes.

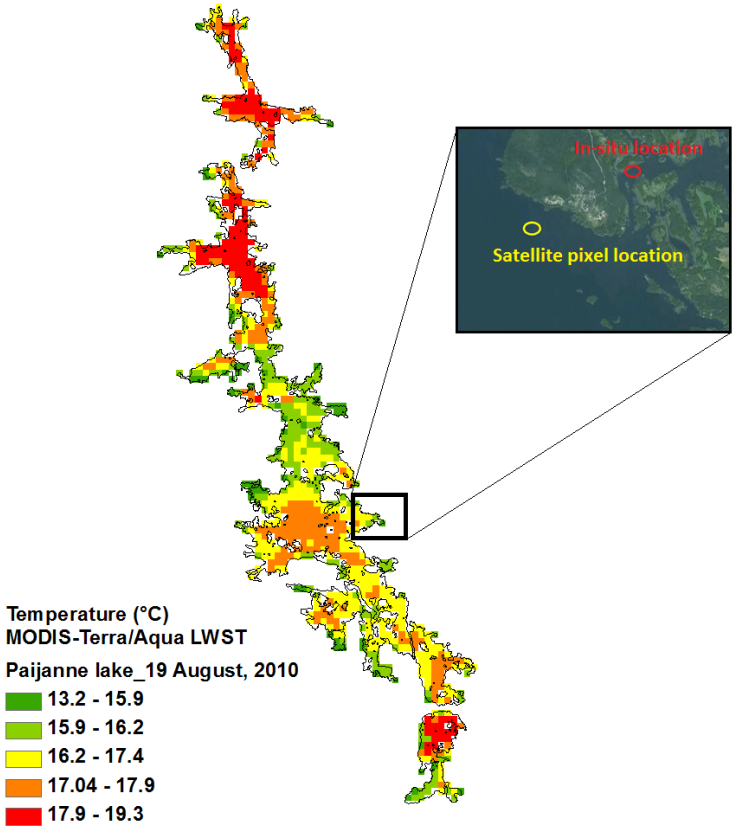

Figure 3.2 Map showing combined MODIS-Aqua/Terra LSWT of Lake Päijänne (August 19, 2010) and the location of MODIS and SYKE observations used for comparison.

3.3 Results

3.3.1 Comparison between MODIS UW-L3 product and in-situ measurements

The quality of the daily averaged UW-L3 MODIS LSWT product was evaluated against SYKE temperature recordings for 22 lakes over the open water season from 2007 to 2011. The MBE, RMSE and the number of observations (n) for each site are summarized in Table 3.1. The MBE values for all 22 lakes show a minimum of -0.25 ˚C for Lake Tussu and maximum of -1.87 ˚C for Lake Inari, and the RMSE cover the range of 1.98 to 2.39 ˚C for Lake Konnevesi and Lake Pielinen, respectively. A temperature map produced from the combination of MODIS-Aqua/Terra data on August 19, 2010 and the time series of LSWT from MODIS and SYKE data for Lake Päijänne (2007-2010) are shown in Figures 3.2 and 3.3, respectively, as an example of one site. Lake Päijänne was chosen to show a case when the location of the in-situ measurement and the satellite pixel selected are not close to each other (Figure 3.2). On August 19, 2010, Lake Päijänne had a mean LSWT of 16.2 ˚C ($LSWT_{min}$ = 13.2 ˚C and $LSWT_{max}$ = 19.3 ˚C) as retrieved from MODIS-Aqua/Terra, over the entire lake. The selected pixel (61.613 N, 25.282 E) from MODIS on the same day had a temperature value of 16.8 ˚C, which was recorded to be 20.1 ˚C by SYKE. Due to the same limitation, Lake Päijänne and Lake Inari, both have the largest MBE of -1.84 ˚C and -1.87 ˚C (SD = 1.46 ˚C and 1.36 ˚C), respectively (Table 3.1).

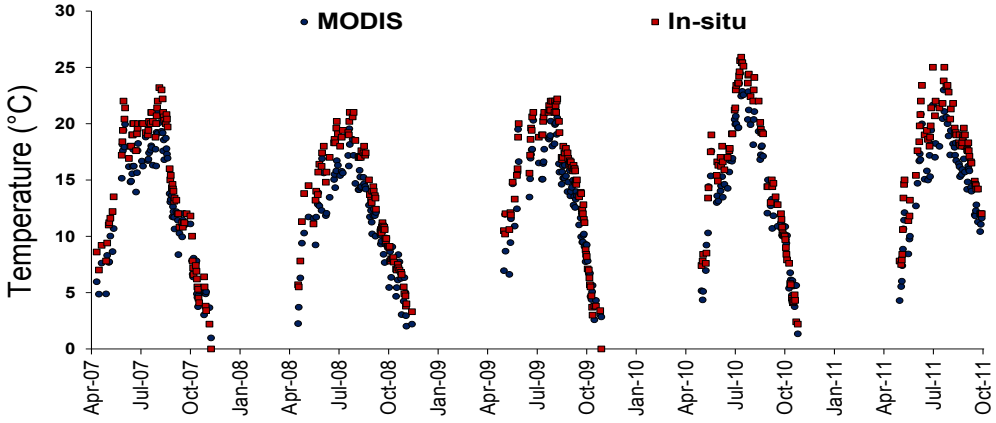

Figure 3.3 Time-series of MODIS-Aqua/Terra LSWT (blue) versus SYKE (red) at Lake Päijänne during open water season (2007-2011).

Figure 3.4 shows a scatterplot of the MODIS-derived LSWT and in-situ measurements along a 1:1 relation line for all 22 sites during open water season. The MBE is -1.13 and RMSE 2.17 ˚C for 8,135

observations available for comparison (Figure 3.4). Results from the analysis of all lake sites reveal that MODIS LSWT observations are on average colder than the in-situ measurements with a negative bias (MODIS minus in-situ).

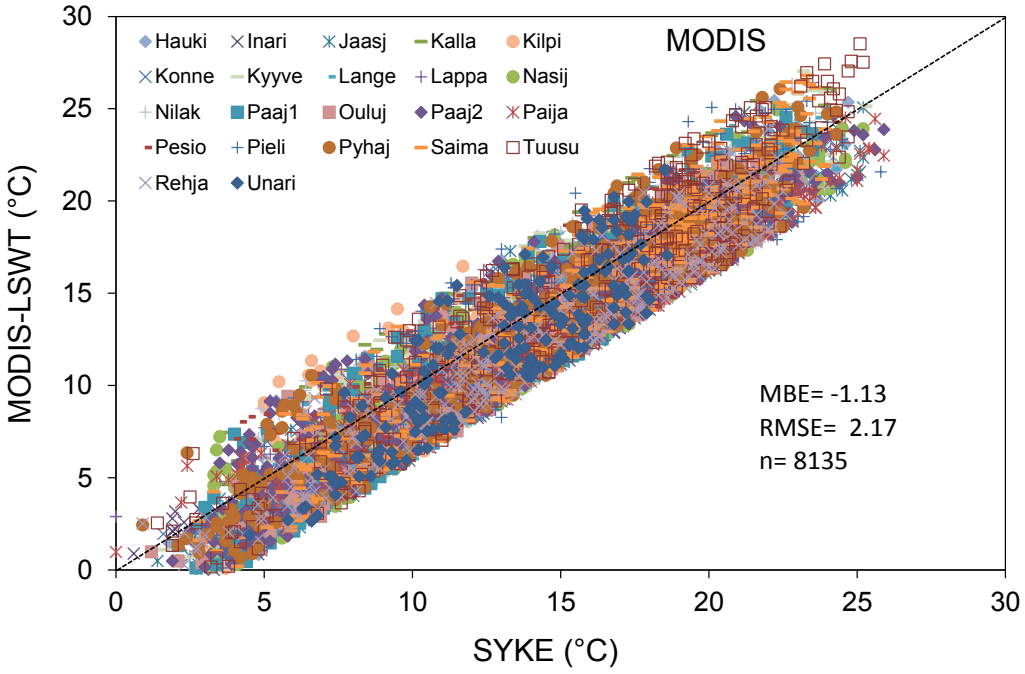

Figure 3.4 Scatter plot of MODIS-Aqua/Terra LSWT in comparison with SYKE water temperature data for all 22 Finish lakes during (2007-2011).

3.3.2 Comparison between MODIS UW-L3 and ESA AATSR-L2 products relative to in-situ measurements

Daily averaged MODIS UW-L3 and AATSR-L2 LSWT products were both evaluated against in-situ measurements and contrasted between each other during the open water season for three years. MODIS LSWT observations were selected for 11 lakes for which AATSR-L2 data were also available during an overlapping period (2007-2009) (see Figure 3.5). MODIS provided 2,733 LSWT observations in total in contrast to only 569 for the AATSR-L2 product. MODIS provides more observations than AATSR-L2 since it is onboard of both the Aqua and Terra satellites, and the sensor covers a larger swath on the Earth's surface.

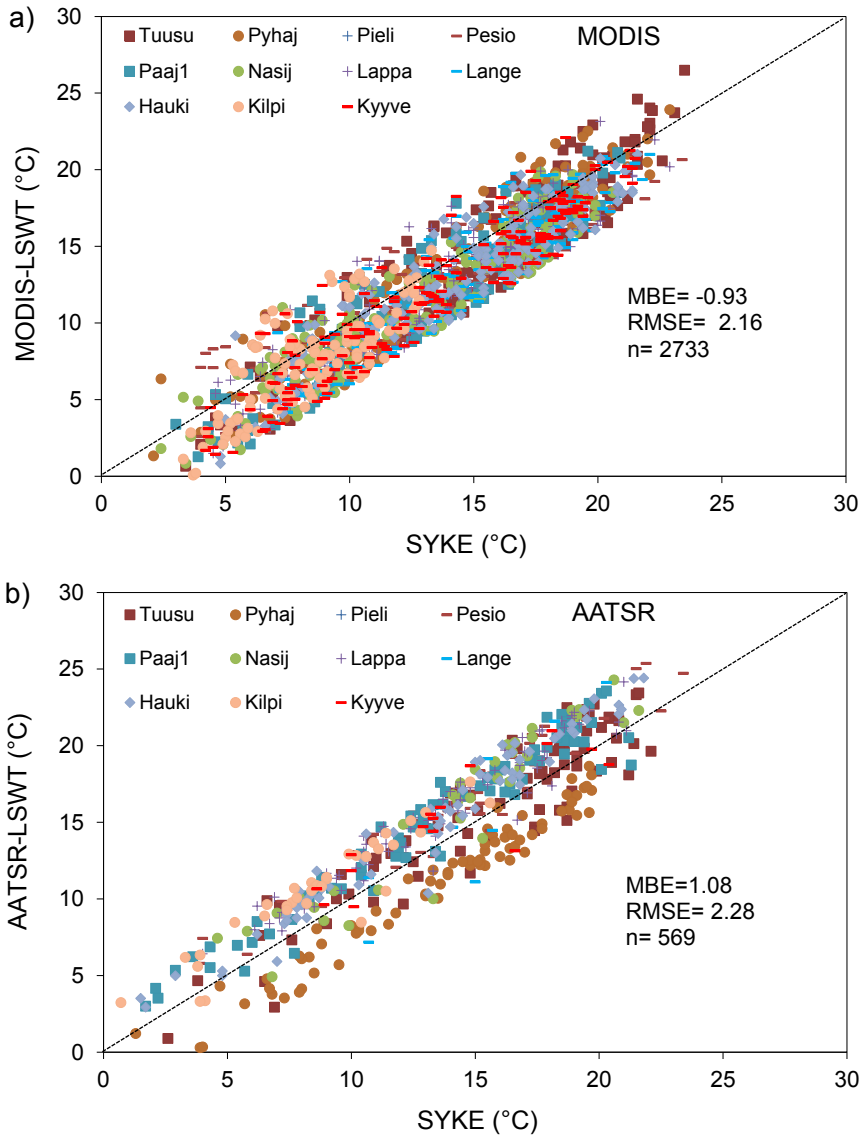

Figure 3.5 Scatter plot of (a) MODIS-Aqua/Terra and (b) AATSR-L2 LSWT in comparison with SYKE water temperature data for 11 Finish lakes during open water period (2007-2009).

Overall, the MODIS LSWT observations are colder (MBE = -0.93 and RMSE = 2.16 ˚C) and AATSR-L2 warmer (MBE = 1.08 and RMSE = 2.28 ˚C) when evaluated against in-situ measurements. In Figure 3.5a, most of the paired observations (dots) are located below the 1:1 relation line showing the cold bias of MODIS observations and, in Figure 3.5b, most of the paired

observations (dots) are located above the line indicating the warm bias of the ESA AATSR-L2 product.

3.3.3 Comparison between AATSR-L2-NCC, AATSR-L2-PR, and ESA AATSR-L2 products relative to in-situ measurements

ESA's AATSR-L2 product as well as the new products based on the Key (AATSR-L2-NCC) and Prata (AATSR-L2-PR) algorithms with the finer resolution lake mask were evaluated against SYKE water temperature measurements during the month of August 2009 for a selection of nine lakes, when overlapping data were available for all three sets of satellite products (Figure 3.6). LSWT products generated from both the Key and Prata algorithms provide comparable results when evaluated against SYKE water temperature measurements with MBE (RMSE) of 0.78 (3.69) ˚C and -0.11 (2.91) ˚C, respectively (Figure 3.6). A MBE of 3.18 (RMSE= 5.25) ˚C was calculated for the AATSR-L2 product over the same time period and number of lake sites. The evaluation results show small biases for both the Prata and Key algorithms when compared to in-situ observations, in contrast to the larger positive bias of the original AATSR-L2 product (Figure 3.6).

3.4 Discussion

Results reveal a good agreement between daily-averaged UW-L3 MODIS-Aqua/Terra data and in-situ observations for the 22 lakes examined with an overall average bias of ~ -1 ˚C. The UW-L3 MODIS-Aqua/Terra and ESA's AATSR-L2 products were also compared for a selection of 11 lakes for an overlapping time period (2007-2009). AATSR-L2 showed a positive MBE of 1.08 ˚C (SD = 2 ˚C) over these lakes most likely due to the utilization of a coarse spatial resolution land cover type map ($0.5^o \times 0.5^o$). Because of this, entire lakes or lake sections may not be classified into the proper land cover type in ESA's AATSR-L2 product (Noyes et al., 2006; 2007). Open-water lake temperatures are colder than that of land usually from the beginning of April until August at high latitudes. Water has a higher heat capacity than land and therefore requires more energy to heat up

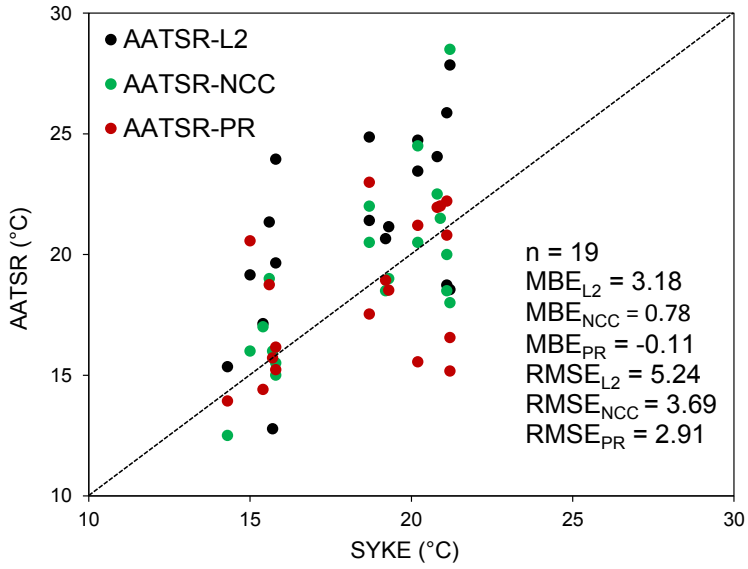

Figure 3.6 Comparison between AATSR-derived LSWT (AATSR-L2, AATSR-L2-NCC and AATSR-L2-PR products; see text for details) and SYKE in-situ water temperature measurements for nine lakes during open water season of August 2009.

and cool down. Therefore, mix of land and lake in each pixel can result in warmer temperatures within each 1 km × 1 km pixel of the AATSR-L2 product. In addition, MODIS LSWT values were derived using daytime and nighttime acquisitions from Aqua and Terra, while AATSR LSWT observations were available mostly at daytime. This also provides a further explanation for the different biases calculated for the two LSWT products.

In order to produce a more accurate AATSR dataset, in which land contamination effects would be minimized, the two new algorithms (Key and Prata algorithms described earlier) were applied along with the GLWD lake mask with the objective of improving the accuracy of LSWT product from AATSR. The newly developed AATSR products as well as ESA's original L2 product were evaluated against in-situ measurements during August 2009, when overlapping data were available. The new AATSR products provide comparable results with MBE of 0.78 ˚C (SD = 3.61 ˚C) and MBE of -0.11 (SD = 2.91 ˚C), with implementation of the Key and Prata algorithms, respectively.

In a previous study, Kheyrollah Pour et al. (2012) compared the UW-L3 MODIS-Aqua/Terra product against LSWT (open water season) and LIST (ice season) simulated with two 1-D lake models for two large Canadian lakes, Great Bear and Great Slave lakes. The authors found a mean bias of magnitude (~ -1 ˚C) as the one from this study. Crosman and Horel (2009) also reported a bias

of -1.5˚C when comparing MODIS-Terra L2 (combined daytime and nighttime observations) against in-situ water temperature measurements (at a depth of 0.5 m) from Great Salt Lake (Utah, USA). Smaller biases are expected when comparison is only during daytime or nighttime and when in-situ observations are of surface water (skin) temperature measured with thermal infrared radiometers (e.g. Hook et al., 2007; Schneider et al., 2009; Hulley et al., 2011).

Similar to the present study, the limitation of ESA's AATSR-L2 product over lake regions has also been recognized by Coll et al. (2009) and Hulley et al. (2011). The authors applied the Prata algorithm to AATSR-L1B data acquired over Lake Tahoe (California/Nevada, USA). Coll et al. (2009) calculated a bias of -0.178 K during July-December 2002 and July 2003 for day and night observations, while Hulley at al. (2011) reported a mean bias of -0.326 K for the period 2000-2010. The biases reported in these two studies are close to the bias of -0.11 ˚C calculated herein, which also used the Prata algorithm to generate a new AATSR-L2 product (i.e. AATSR-L2-PR).

The lakes selected for evaluation of the satellite-based LSWT products in this study ranged in depth between 3 and 22 m. No particular relationship was found between the mean depth and the magnitude of the biases calculated for the different lakes (R = -0.116 and p-value = 0.607). The could be due to the location of in-situ measurement sites, which are always located in the shallow section of the lakes, compared to the 1 km^2 satellite pixels that needed to be selected further from the shore to avoid possible land contamination. However, in some instances, the large distance between the location of in-situ observations and satellite pixels can affect the statistics. Lake Päijänne and Inari are two examples that showed larger biases (MBE = -1.84 and SD = 1.46 ˚C and MBE = -1.87 and SD = 1.36 ˚C, respectively) due to the large differences between in-situ and pixel locations. Evaluation of the satellite products using in-situ surface water temperature measurements collected by buoys at the same location as the satellite pixels, further from shore, would provide a closer correspondence (smaller bias) between the two sets of observations.

In addition to lake depth, the shape of the lakes of this study may also have had an impact on the accuracy of the retrieved LSWT when selecting the satellite pixels. Most of the lakes in Finland tend to be irregular in shape. They have arisen during post-glacial times and were formed mostly during glacier movement and scraped of rocks and soils (e.g. Tikkanen 2002; Hakala, 2004). Lake Päijänne is an example of a very irregular lake (MBE = -1.84 and RMSE = 2.35 ˚C for MODIS versus in-situ). Lake Pyhäjärvi, on the other hand, is an example of a more regular shaped lake and its bias was less than 1 ˚C (MBE of -0.79, RMSE: 2.04 ˚C and SD = 1.88 ˚C for MODIS versus in-situ). The shape

and lakeshore topography are important factors that influence the mixing of lakes (Imboden and Wüest, 1995). Some irregular shaped lakes may not undergo complete mixing in the spring or fall if there is not enough wind action as the irregular shape/lakeshore topography may block the wind and affect the mixing, resulting in a complex circulation pattern. Moreover, it is more challenging to select a pure pixel in an irregular shaped lake with many small islands, which could be missed in the 1 km^2 lake shape files applied over thermal images.

3.5 Conclusion

The accuracy of MODIS UW-L3 and AATSR-L2 products was assessed as a step prior to performing data assimilation experiments in the HIRLAM NWP model using LSWT as a surface state variable (Kheyrollah Pour et al., 2014; Kalle Eerola, personal communication, 2014). To create a AATSR LSWT product that can be used with greater confidence in HIRLAM analysis, algorithms presented by Key et al. (1997) and Prata (2002) were applied to AATSR-L1B brightness temperature data, which had the effect of reducing the LSWT biases to 0.79 ˚C and -0.11 ˚C, respectively. Based on the results presented in this study, the MODIS UW-L3 and the improved AATSR-L2 (Key algorithm) products were selected for integration into HIRLAM analysis using the OI data assimilation method in Chapter 4. During the data assimilation process, the statistical properties of the observational error are taken into account in the interpolation as well as in the preceding quality control of observations. During these experiments, all lake observations were assumed to have similar statistical properties. The assumed observational error standard deviation was set to 1.5 ˚C for both in-situ and remotely sensed LSWT observations. Observations were used to correct the background provided by FLake model or by previous analysis in HIRLAM. The quality control of the observations is performed prior to the actual analysis in two consequent phases: first observations are tested against the background, and then each observation is compared to the surrounding observations (see Chapter 4).

The satellite products evaluated in this research are a promising source of LSWT data for the description of lake surface state in HIRLAM and are expected to improve the NWP results as they can provide frequent surface temperature measurements of many lakes over large geographical areas. The ESA's Sentinel-3 with two satellites (first Sentinel-3A is expected to be launched in 2015, followed by the second one, Sentinel-3B, ~18 months after), in addition to the two MODIS sensors already in orbit, should generate increased interest in the assimilation of satellite-derived LSWT

products in operational NWP models. However, cloud cover is known to significantly impact its full utilization in NWP models. In this study, we took advantage of the short time interval between MODIS-Aqua and Terra acquisitions by combining them together and therefore increasing the number of observations. Further studies are still needed to assess the quality of the cloud cover masks used in the satellite retrieval algorithms (e.g. errors due to undetected thin clouds). In the present study, the outliers of LSWT due to the presence of undetected cloud cover were removed from the database by monitoring the error and quality control values calculated in each pixel. However, more robust algorithms are needed in order to improve the quality of cloud cover masks from MODIS, AATSR and future satellite missions.

Chapter 4

Impact of satellite-based lake surface observations on the initial state of HIRLAM- Analysis of lake surface temperature and ice cover

4.1 Introduction

The importance of a correct description of the lake surface state in climate (Duguay et al., 2006; Brown and Duguay, 2010; Samuelsson et al., 2010; Krinner and Boike, 2010; Ngai et al., 2013) and weather prediction (Niziol, 1987; Niziol et al., 1995, Zhao et al., 2012) is well known. Particularly during freezing and melting of lakes, the surface radiative and conductive properties as well as latent and sensible heat released from lakes to the atmosphere change dramatically leading to a completely different surface energy balance. Recent studies (Eerola et al., 2010; Rontu et al., 2012) have demonstrated the possibility of improving the description of the lake surface state in a numerical weather prediction (NWP) model by replacing climatological information with the objective analysis of observations. A good background for the analysis provided by the prognostic parameterization of lake temperatures using the Freshwater Lake model (FLake) (Mironov, 2008; Mironov et al., 2010) was also shown to be important. In fact, lake parameterizations alone seem to lead to (locally) improved NWP results even without the introduction of Lake Surface Water Temperature (LSWT) observations (Eerola et al., 2010; Rontu et al., 2012).

However, application of thermodynamic lake parameterizations in NWP has its limitations. A prognostic lake parameterization encounters difficulties over lakes with poorly defined properties due to the complex geometry or complex topography around the lake. These are often poorly resolved by the NWP model; even if the parameterizations are able to treat the lake physical processes correctly (Semmler et al., 2012; Manrique-Suñén et al., 2013; Yang et al., 2013). The thermodynamic lake parameterizations work independently under each grid-box (column), thus not taking into account horizontal exchange on or in the lakes. Thus they are not able to handle, for example, the small-scale inhomogeneity or drifting ice on the large lakes. Objective analysis of remote-sensing observations could help the NWP model to treat the horizontal variability over lakes.

A possibly improved description of the initial state of the lakes is expected to lead to an improved weather forecast, if there is a real connection between the analyzed (based on observations) and predicted (seen by the atmospheric model) state of lakes. However, in present NWP models, a prognostic lake temperature parameterization is applied independently from the analysis (Rontu et al., 2012). To our knowledge, results of the first studies aimed at bridging the gap between the analyzed and predicted state of lakes in NWP models by using the methods of Extended Kalman Filter (Kurzeneva, 2014) and nudging (Mironov, 2012, personal communication), have been only recently reported (e.g. in the third workshop on "Parameterization of Lakes in Numerical Weather Prediction and Climate Modelling", http://netfam.fmi.fi/Lake12). Application of these methods requires, in addition to a good thermodynamic lake parameterization, that the observations on lake surface state are first interpolated to the NWP model grid. Hence the objective analysis of LSWT is their starting point.

The aim of this paper is to determine if the inclusion of remote-sensing observations on LSWT can improve the analysis of lake surface state in a NWP model, compared to the description based on the thermodynamic lake parameterization alone. By the analyzed lake surface state (analysis, objective analysis), we mean here the description of LSWT and fractional ice cover over lakes at the time when each forecast cycle by the NWP model starts. This analysis results from application of a specialisation method such as Optimal Interpolation (OI, based on Gandin (1965)) to the observed variables over lakes. We report results from data assimilation experiments performed with the three-dimensional NWP model HIRLAM (High Resolution Limited Area Model), (Undén et al., 2002; Eerola et al., 2013) run over a northern European domain for two winters (2010-2011 and 2011-2012). Our main attention is placed on the objective analysis of the lake surface state in winter-time conditions, over freezing and melting lakes.

Our experiments focus on the use of remote-sensing observations on lakes (>6 km^2) and the ways they can be introduced in the analysis. The influence of larger lakes on weather is expected to be larger than that of a multitude of smaller lakes. On the smaller lakes, there are less space-borne observations available because the number of pixels representative of pure open water or ice is limited by the surrounding land (i.e. by the within-pixel land surface contamination). We included in the HIRLAM analysis archived Moderate Resolution Imaging Spectroradiometer (MODIS) and Advanced Along-Track Scanning Radiometer (AATSR) LSWT observations, provided by the

Terra/Aqua and ENVISAT satellites, and also used MERIS ice cover observations from ENVISAT for evaluation. We compared the result of pure prognostic parameterizations to the analysis based on in-situ and space-borne LSWT observations. For validation, we used additional independent satellite observations of LSWT and lake ice cover, as well as in-situ visual observations of freeze-up and break-up dates of selected lakes. We discuss in detail the maps and time-series of observed, analyzed and predicted LSWT and fractional ice cover, obtained in the different experiments, in order to understand the differences and sensitivities. In the conclusions and outlook section, we discuss the perspectives and practical aspects of further usage of space-borne lake observations in operational NWP.

This chapter focused on improving the objective analysis of lake surface state in HIRLAM. The previous chapter (Chapter 3) documents the processing and evaluation of remote-sensing observations applied herein for the LSWT analysis. Our study is an extension of the work reported by (Eerola et al., 2010) and (Rontu et al., 2012). The main differences compared to these earlier studies lie in the extended usage of remote-sensing observations and exclusion of climatological data in the analysis.

4.2 Observations

In this study, in-situ and remote-sensing observations on lake surface state are introduced into the surface data assimilation system and used for comparison and validation. Table 4.1 summarizes the different observation types and their usage, discussed in this section.

4.2.1 Satellite LSWT observations

Satellite thermal infrared sensors offer a global coverage and high temporal resolution of lake temperature observations (shown in Chapter 3). This represents a significant advantage over in-situ observing systems that provide point measurements, often only close to the shoreline. In the present study, 70 pre-defined pixels were selected over 41 northern lakes (Figure 4.1, large image, black dots). The selection of a limited number of pixels, instead of using all available 1 km × 1 km resolution data, is a limitation which was dictated by practical reasons, and will be discussed in the concluding section. The satellite observations were used at the nearest analysis time within ± 3 h when available, i.e. under cloud-free conditions over each pixel location. A detailed description of the

satellite observations and of the algorithms applied for extraction and screening can be found in Chapter 3, only a short summary is given here.

Table 4-1 Summary of observations used in this study.

Variable	Source of observation	Spatial coverage	Temporal coverage	Usage
LSWT	MODIS (1 km^2)	70 pixels (41 lakes)	2010.11.01–2012.05.31	Objective analysis
LSWT	AATSR (1 km^2)	15 pixels (Lake Ladoga)	April 2011	Objective analysis
LSWT	FMI Marine Services[a]	Swedish lakes[a,b]	Oct.–May, 2010–2012	Objective analysis
Lake water temperature	SYKE measured	27 Finnish lakes	2010.11.01–2012.05.31	Objective analysis
Freeze-up/break-up dates	SYKE visual observation	27 Finnish lakes	2010.11.01–2012.05.31	Evaluation
Ice fraction	MERIS (300 m^2)	Lake Ladoga	April 2011	Evaluation

[a]FMI Marine Services = partly manual interpolation of remote-sensing and ship observations on SST and properties of ice cover.
[b]Swedish lakes = Vänern, Vättern and Mälaren.

LSWT data were derived from the MODIS sensor, which operates on NASA's Terra and Aqua Earth Observation System (EOS) satellites (http://modis.gsfc.nasa.gov). The LSWT level 3 data, referred to as UW-L3 here onwards, were generated at the University of Waterloo. These data were evaluated using ground measurements over lakes in the same study area during the open-water season (Chapter 3) and over two large Canadian lakes (Kheyrollah Pour et al., 2011). For MODIS observations, both daytime and night-time Terra and Aqua LSWT observations were selected in order to maximize the amount of available input data to the analysis. Data from the AATSR, onboard the European Space Agency (ESA) ENVISAT satellite, were extracted over Lake Ladoga for the same 15 pixels as for MODIS (Figure 4.1, Lake Ladoga image, red squares). Aqua and Terra satellites passed over our study area daily around 08-10 UTC and 20-01 UTC. AATSR observations were available 06-08 UTC every third day in April 2011.

4.2.2 In-situ lake water temperature observations

Regular in-situ lake water temperature measurements are provided by the Finnish Environment Institute (Suomen Ympäristökeskus, SYKE). SYKE operates 32 regular lake and river water temperature measurement sites in Finland. The temperature of the lake water is measured every morning at 8.00 AM local time, close to shore, at 20 cm below the water surface. The measurements are either recorded automatically (13 stations) or manually and are performed only during the ice-free season (Rontu et al., 2012). Measurements from 27 lakes (Figure 4.1, upper left map), which are also used by the FMI operational HIRLAM, were included in all experiments reported in this study.

The operational Baltic Sea ice chart (Grönvall and Seinä, 2002) produced by FMI's Marine Service also provides manually processed, satellite-based observations of water temperature and ice properties over Swedish lakes Vänern, Vättern and Mälaren. From these, pseudo-observations of LSWT have been derived since 10 January 2011 for the FMI operational HIRLAM at a few selected pixels in winter season approximately between 15 October and 15 May each year. In this derivation, ice fractions are converted to LSWT and ice flag temperatures by applying the inverse of the method described in section 4.3.3. These data were included in the present experiments when available, but their influence is not discussed herein.

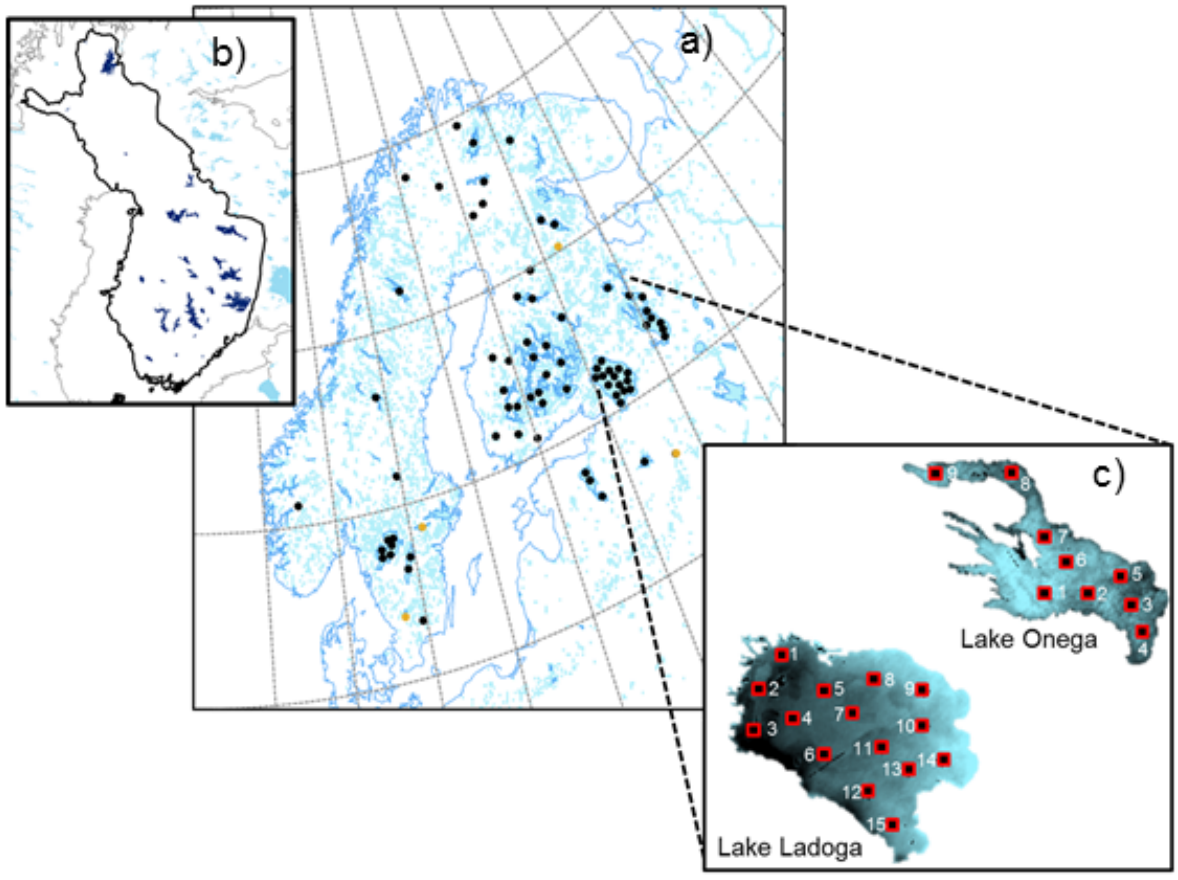

Figure 4.1 (a) Location of the MODIS pixels over the northern lakes. Independent lakes are marked with orange dots. (b) Location of 27 lakes (dark blue polygons) with SYKE measurement sites in Finland. (c) Detailed view of the selected MODIS and AATSR pixels over the lakes Ladoga (left) and Onega (right).

4.2.3 Data for comparison and validation

Historical freeze-up and break-up dates from SYKE for most of the 27 Finnish lakes (Figure 4.1) were used for comparison with MODIS observations and HIRLAM analysis results. These freeze-up and break-up dates are based on visual observations from shore and represent the complete freezing and melting in small lakes. For the large lakes, separate freeze-up and break-up dates for the central open waters and coastal areas may be given by SYKE. Among the lakes discussed in this study, this is the case only for Lake Inari, where we used central open water dates. The visual observations are made independently of the water temperature measurements. These observations are made over a larger number of lakes in Finland than was used here, thus available for further studies.

MODIS UW-L3 LSWT observations were prepared but withheld from the HIRLAM analysis, in order to be used as independent data for comparison over Lakes Bolmen and Hjälmaren in Sweden and Lakes Valday and Kuito in Russia (orange dots in Figure 4.1, coordinates shown in Table 4.3). MERIS-derived ice fraction observations for Lake Ladoga were utilized in this study for the month of April 2011. The ice fraction data were produced by the Norwegian Computer Center as part of the European Space Agency's (ESA) North Hydrology project (http://env-ic3-vw2k8.uwaterloo.ca:8080). MERIS was a core instrument of ESA's ENVISAT satellite platform that operated between March 2002 and April 2012.

4.3 Analysis of lake surface state

Over water bodies in HIRLAM surface water temperature observations are treated with OI (Gandin, 1965). The methods of OI analysis of LSWT are based on those applied for sea surface temperature (SST). We summarize the method briefly here, and present in the conclusions our findings concerning the needs of its further development.

4.3.1 OI of LSWT

OI analysis, integrated into the framework of HIRLAM, is applied for SST (Undén et al., 2002). More recently, the same method has been extended for the analysis of LSWT (Eerola et al., 2010, Rontu et al., 2012). In the near-surface analysis of HIRLAM, OI is applied to spread the information from irregularly located observations to regularly located grid-points for the initialization of the next

forecast cycle. This is done by correcting the background field with observations. For lakes, the background can be provided either by the previous analysis or by a short forecast. In the latter case, the background LSWT is derived from the surface temperature forecast by the lake model (FLake), which is incorporated in HIRLAM as a parameterization scheme. Here, the evolving three-dimensional state of the atmosphere also influences the predicted state of lakes and hence the background for the LSWT analysis. A good background is especially important over lakes where observations are sparse or not available at all.

The analysis at a grid-point k is determined by a linear combination of the observed departures from the background

$$\boldsymbol{a_k = b_k + \sum_{i=1}^{N} w_{ki}\,(y_i - b_i)} \qquad \textbf{4.1}$$

where a_k is the analysis, b_k the background and w_{ki} are the weights given to observations $i = 1, \ldots, N$, y_i the observations and b_i the background values interpolated to the observation points.

Derivation of the weights relies on the assumption that observation and background errors are uncorrelated. In OI, the weights w_{ki} in Eq. 4.1 are determined by inverting a matrix which represents the background and observation error covariances (Daley, 1991). For the SST and LSWT analysis applied in HIRLAM, the background error covariance, which to a large extent determines the resulting analysis, is treated by modelling the autocorrelation and standard deviation of the background error separately. A Gaussian autocorrelation function is applied, which depends on distance

$$\boldsymbol{g(\rho) = e^{-0.5\rho^2/L_H^2}} \qquad \textbf{4.2}$$

where $g(\rho)$ is the autocorrelation function, ρ is the distance and $L_H$is a horizontal length scale (L_H = 80 km). So $g(\rho)$ depends only on distance between the points. The observation and background error variances, which enter the diagonal of the matrix, are assigned prescribed constant values (we assumed a standard deviation error 1.5 °C for observations and 1.0°C for the background).

The OI analysis integrated into the NWP model differs from the stand-alone analysis approach, as applied for SST and LSWT (e.g. by the Operational Sea surface Temperature and sea and lake Ice Analysis (OSTIA) (Donlon et al., 2012; Fiedler et al., 2014) in two essential aspects. In OSTIA, the background is always provided by the previous analysis done (e.g. on the previous day), and relaxed towards the LSWT climatology, which is taken from ARC-lake database (Hook at al., 2012;

MacCallum and Merchant, 2012). If the observations are missing for a long time or not available at all over some lakes, climatology gets a large weight. In the case of OSTIA, realistic lake climatology is available over lakes of the ARC-lake database (ca. 250 lakes worldwide, around 15 over our present study area). More importantly, no climatology is able to represent the current and near past atmospheric conditions, which basically determine the current lake temperatures. In our case, it is also possible to use previous analysis as the background and relax to climatology at each HIRLAM grid-box, where a fraction of lake is detected. However, in our case, this is even more problematic, because our LSWT climatology was extrapolated to any lake from SST climatology instead of using lake climatology, which is unrealistic. This is why we prefer the background provided by the prognostic lake parameterization, calculated within HIRLAM for each time step at each grid-box which contains a lake fraction.

Another point is that our OI method works also across the lakes, sometimes interpolating LSWT observations from nearby lakes if these are close enough to influence. Thus, an analyzed LSWT value is always available in every lake grid-point of HIRLAM. In this respect, we are again not limited by the choice of pre-selected large lakes, between which OSTIA can also interpolate. In HIRLAM, special care is taken not to mix sea and lake observations in the analysis near the sea coast. However, to fully benefit from the across-lake interpolation possibility, it will be necessary to derive autocorrelation (structure) functions, depending not only on the horizontal distance but also at least on the depth and possibly on the elevation differences within and between the lakes.

4.3.2 Quality control

In HIRLAM, quality control (QC) of the observations is performed prior to the actual analysis. QC is done in two consequent phases: first the observations are tested against the background, then each observation is compared to the surrounding observations. For the background check, a normalized difference Δ_i between the observed value and the background value interpolated to the observation point is calculated as

$$\Delta_i = (\boldsymbol{y_i} - \boldsymbol{b_i})^2/(\boldsymbol{\sigma_b^2} + \boldsymbol{\sigma_0^2}) \qquad \textbf{4.3}$$

where σ_b and σ_0 denote the background and observation error standard deviations. If Δ_i is larger than a prescribed threshold value, the observation is rejected by the background check. The check against surrounding observations first excludes the observation to be checked, and then performs OI analysis

to this point by using the nearby observations. The difference between the analyzed and the observed value, again normalized by the observation and background error standard deviations, is tested against a prescribed threshold value. It is difficult to choose optimal criteria for this threshold. In order to retain a maximum number of observations, a quite liberal approach was adopted here: the threshold was set so that only those LSWT observations which deviated from the background by more than 10 °C were rejected (Eq. 4.3).

4.3.3 Treatment of ice fraction

In HIRLAM, a diagnostic ice fraction is derived from the analyzed LSWT. Thus, neither space-borne nor in-situ ice concentration, ice thickness, and ice temperature observations are directly analyzed. The diagnostic ice fraction is estimated in a simple way: we assume that a lake grid-square is fully ice-covered when LSWT falls below -0.5 °C and fully ice-free when LSWT is above 0 °C. Between these temperature thresholds, the fraction of ice changes linearly. A range from -0.5 to 0 °C has been chosen to account for the variability and uncertainty of the analyzed LSWT within the model resolution. A corresponding ice flag value of -0.6 °C was assigned to LSWT while creating the background to LSWT analysis in such grid-squares, where the ice thickness predicted by FLake exceeded a threshold value of 1 mm. An observation ice flag value of -1.2 °C was assigned to all MODIS surface temperature values below -0.5 °C over lakes. These were assumed to represent full ice cover in their surroundings. In the case of SYKE observations the ice flag value was given to all measurements showing 0 °C water temperature. If we had instead assigned LSWT observations a missing value under the observed ice, we would have excluded from the analysis all observations representing ice conditions, thus letting the background (FLake or previous analysis) alone to determine. In the melting and freezing conditions, removal of all information about ice would give more weight to the water observations and most probably lead to incorrect spread of open water information into the near-by ice-covered part of the lake.

This kind of procedure, which was inherited from the SST analysis and sea ice diagnostics, represents a simplified but non-physical way of handling ice concentration. Here a single variable, namely LSWT, is taken to represent in the analysis both itself, i.e. the water temperature, and another variable, ice cover. This is why the LSWT flag values enter the OI analysis and QC together with the real observations. However, the choice of the ice concentration versus LSWT range and the flag values is rather arbitrary. The sensitivity of the resulting LSWT and ice cover to these choices should

be systematically studied. The eventual solution of the problem could be found in assimilation of the observed and predicted physical properties of ice, such as ice thickness (see Section 4.6 for discussion).

4.4 Description of the analysis-forecast system and setup of experiments

All our experiments were run in the framework of HIRLAM version 7.4 (www.hirlam.org). This HIRLAM version incorporates fully integrated FLake model, applied as a parameterization scheme for prediction of lake water, ice and snow temperatures and ice thickness and snow depth over lakes (Rontu et al., 2012). We used a model setup with a horizontal resolution of 6.8 km over a northern Europe experimental domain (Figure 4.1) with 65 levels in vertical between the surface and the 10 hPa level in the atmosphere. Four data assimilation-forecast cycles were run every day, starting at 00, 06, 12 and 18 UTC. For the upper-air data assimilation, three-dimensional variational method was used. The lateral boundary conditions for the atmospheric model were provided by the fields of the European Centre for Medium-Range Weather Forecasts (ECMWF) analysis.

Three initial sets of experiments were designed to study the impact of assimilated remote-sensing LSWT observations over the major northern European lakes (Table 4.2). In the baseline experiment TRULAK (SYKE water temperature observations, FLake parameterizations), the prognostic lake parameterizations inside the forecast model provided the background for the LSWT analysis. This follows the setup of the reference HIRLAM used for the FMI operational NWP. No satellite observations were used in the baseline experiment, just SYKE in-situ water temperature measurements over Finland. In the second experiment, called NHFLAK (SYKE water temperature and MODIS LSWT observations, Flake parameterizations), remote-sensing LSWT observations were also included. In the last experiment, referred to as NHALAK (SYKE water temperature and MODIS LSWT observations), LSWT observations were used to correct the background provided by the previous analysis, which was relaxed towards “ocean-derived” LSWT climatology of the reference HIRLAM (Rontu et al., 2012). AATSR observations over Lake Ladoga only were included in two additional short experiments, called NHALAA (AATSR LSWT observations) and NHFLAA

(AATSR LSWT observations , Flake parameterizations), run for April 2011. SYKE in-situ water temperature observations from the Finnish lakes were included in all experiments.

For the lake analysis and parameterizations, information about the lake depth and fraction of lake in each grid-box is needed. Lake depths were obtained from the lake data base for NWP and climate models (Kourzeneva et al., 2012a). Fraction of lakes was taken from the HIRLAM physiography description (Undén et al., 2002). The lake fraction was originally derived for HIRLAM using the 1 km resolution Global Land Cover Characteristics (GLCC) data base (Loveland et al., 2000). For the

Table 4-2 Definition of the HIRLAM experiments.

Experiment	Period	Observations	Background
TRULAK	2010.11.01–2012.05.31	SYKE[a]	FLake+6 h[c]
NHFLAK	2010.11.01–2012.05.31	SYKE[a] + MODIS[b]	FLake+6 h[c]
NHALAK	2012.01.01–2012.05.31	SYKE[a] + MODIS[b]	previous analysis
NHFLAA	2011.04.01–2011.04.30	SYKE[a] + AATSR[d]	FLake+6 h[c]
NHALAA	2011.04.01–2011.04.30	SYKE[a] + AATSR[d]	Previous analysis

[a]SYKE = Measured LSWT over 27 lakes in Finland.
[b]MODIS = MODIS observations in 70 pixels.
[c]FLake+6 h = Freshwater Lake model parameterisations within HIRLAM, 6 h forecast.
[d]AATSR = AATSR observations over Lake Ladoga only.

very first cycle, prognostic inside-lake variables were initialized with gridded lake climatology (Kourzeneva et al., 2012b). The very first LSWT analysis was replaced by the reference HIRLAM LSWT climatology when starting each of the experiment series. Note that these two climatologies are different - the first is the climatology of Flake prognostic variables, the second has been extrapolated from SST for LSWT analysis only.

4.5 Results and discussion

4.5.1 Freeze-up and break-up dates

Freeze-up and break-up dates interpreted from SYKE, MODIS, and MERIS observations were compared with the dates given by HIRLAM experiments for selected representative lakes (Table 4.3). Lake Lappajärvi is a regular-form, medium-size, and relatively shallow lake located in western Finland. SYKE water temperature measurements are available for this lake. Lakes Bolmen, Hjälmaren, Valday and Kuito whose MODIS observations were excluded from HIRLAM analysis,

resemble Lake Lappajärvi. Lake Inari in the Finnish Lapland is large, with islands, a complex coastline and bathymetry, and is also represented in HIRLAM analysis by SYKE water temperature observations. Over the large, deep and open Lakes Ladoga and Vänern the break-up and freeze-up processes progress differently than over smaller lakes: ice forms, cracks and drifts depending on the wind speed and direction. However, for simplicity, only one point is chosen to illustrate the surface state of these lakes here. Coordinates of the chosen locations and the mean depth of lakes are shown Table 4.3. A few preliminary remarks related to the accuracy of the dates are necessary before discussion:

- *SYKE freeze-up and break-up dates:* These dates are based on visual ground-based observations, which are independent of the SYKE water temperature measurements used by the HIRLAM analysis.
- *MODIS dates:* Especially during the freezing period, which is often cloudy and dark, the MODIS observations over a chosen location may be missing for several days, even weeks. During the freezing and melting periods, MODIS LSWT may oscillate from one measurement to another by several degrees, sometimes jumping to both sides of zero. Some subjective reasoning was applied when determining the dates from this information.
- *HIRLAM dates:* In Table 4.3, the dates are shown based on the OI analysis of HIRLAM, which used either the prognostic temperatures from FLake (experiments NHFLAK and TRULAK) or the previous analysis (experiment NHALAK) as background. For various reasons, the analyzed temperature also has a tendency to oscillate between analysis cycles, which during the freezing and melting periods may lead to oscillation of the ice fraction. Thus, here again some subjective reasoning was needed to determine the freezing and melting dates. In some cases, a transition period up to three weeks is shown to indicate the uncertainty related to this oscillation.
- *MERIS ice fraction:* Data were prepared for comparison in 2011 for Lake Ladoga. MERIS-derived ice fraction information was obtained from pixels, each representing an area of 300 m x 300 m.

SYKE and MODIS freeze-up and break-up dates were first compared over two Finnish lakes, Lake Lappajärvi and Lake Inari. During lake melt, SYKE and MODIS dates differed from each other

by less than ten days. During freezing, the difference could be several weeks. It is possible that the MODIS LSWT observations on selected 1 km × 1 km pixels may indicate melting or freezing before the SYKE observer determines that the whole lake is unfrozen or frozen. To avoid this error, MODIS visible images (bands 7, 2, and 1) were used to make sure that the chosen pixel values represented correctly the whole lake area. The difference between SYKE and MODIS freeze-up and break-up dates, shown in Table 4.3 for Lake Inari and Lake Lappajärvi, was similar over the other Finnish lakes (not shown). The uncertainty of a lake melting date, derived from MODIS by a couple of weeks compared to the in-situ data could be due to the visual in-situ observation as the observer cannot monitor the whole area of the lake from the lake shoreline. The uncertainty of the freezing dates could be up to one month.

Over Lake Ladoga, no SYKE freeze-up and break-up dates observations were available to be compared with MODIS. Melting dates interpreted from MERIS measurements in spring 2011 over Lake Ladoga (shown for pixel 9 in Table 4.3, see Figure 4.1 for the map), seem to agree with the dates interpreted from MODIS LSWT measurements. Thermal satellite observations from AATSR-L1B are used to develop MERIS lake ice products to detect cloud cover, therefore both MERIS ice cover and MODIS temperature observations represent the surface only under clear-sky conditions. This limits the accuracy of the dates derived from these measurements in a similar way.

The freezing dates given by the analysis of the experiment NHFLAK (FLake + MODIS LSWT + SYKE water temperature) came in general closer to the observed dates compared to the dates from experiment TRULAK (in the area of the analysis domain outside Finland, where no SYKE temperature observations are available, FLake alone was used). In spring, the analyzed melting dates by both TRULAK and NHFLAK were always earlier than those indicated by MODIS observations at the selected pixels. The largest differences between melting dates interpreted from HIRLAM analysis and directly from MODIS observations were more than one month when the analysis was determined by the Flake background alone. This was the case for TRULAK over all lakes and NHFLAK over the independent lakes Bolmen, Hjälmaren, Kuito and Valday. Over the Finnish lakes, SYKE temperature observations were available only well after melt. Thus, during the melting period, the warm FLake background dominated over the (sparse) MODIS observations also in NHFLAK.

In cases when the inclusion of MODIS observations to NHFLAK did not change the analyzed state of lakes significantly, the reasons may have been due to the fact that: 1) MODIS data were

seldom or not at all available for analysis, 2) the prognostic parameterizations were good and agreed with MODIS, or 3) the difference between MODIS and Flake was so large that the observations were rejected by the quality control while comparing the background and observations. Rejections were, however, uncommon in autumn and when the lakes were frozen (between the dates shown in Table 4.3), but became more frequent at the end of May with rising lake water temperatures after the ice melt. It is possible that the FLake background dominates in the analysis over the large lakes because the information brought by the selected MODIS pixels is simply insufficient there (see also Section 4.5.2).

The NHALAK experiment combined SYKE water temperature and MODIS LSWT observations with the background given by the previous analysis, which had been relaxed towards the LWST climatology. This experiment, which was run only for January-May 2012, followed the observations more closely than the prognostic experiments TRULAK and NHFLAK, but only when observations were available on the lake or close to it (i.e. when the effect of background field was small). Elsewhere, the analysis tended towards the (wrong ocean-derived) climatology, possibly resulting in a completely useless description of lake surface state [not shown in Table 4.3, see an example in Rontu et al. (2012)]. Over Lakes Lappajärvi and Inari, NHALAK improved the analysis so that the melting dates became closer to the SYKE temperature observation. Over Lakes Ladoga and Vänern, the dates became closer to the MODIS observations. In spring, interpretation of the point values over the large lakes may be affected by the uneven melting and drifting ice. The NHALAK melting dates over the selected lakes seem to agree with MODIS observations within about one week. The agreement is better than in the case of NHFLAK, whose analysis was dominated by the FLake parameterizations. Freezing dates from NHALAK were available only over a few lakes because this experiment was started in the middle of winter.

4.5.2 April 2011 comparison

For visual comparison of the full-resolution satellite observations with the NWP analysis during melt, MODIS (daytime and nighttime) and AATSR (morning) LSWT, as well as MERIS ice fraction on 12 April 2011 were mapped (Figure 4.2) and compared with the HIRLAM analysis and background by experiments NHFLAK and NHFLAA (Figure 4.3). In April, the ice cover on Lake Ladoga started to break, which makes comparison of observations and simulations both interesting and challenging due to the moving ice on the lake.

Table 4-3 Freezing and melting dates of selected lakes given by observations (SYKE and MODIS) and analyses by experiments (TRULAK, NHALAK, NHFLAK as defined in Table 4.2)

	Melting 2010	Freezing 2010/11	Melting 2011	Freezing 2011/12	Melting 2012
Lappajärvi, Finland	23.67E 63.14N	Mean depth 7 m			
SYKE	20100504	20101122	20110503	20111231	20120502
MODIS	20100505	20101105	20110501	20111203	20120429
TRULAK	–	20101108	20110418	20111217	20120424
NHFLAK	–	20101117	20110421	20111213	20120424
NHALAK	–	–	–	–	20120429
Inari, Finland	28.10E 68.87N	Mean depth 14 m			
SYKE	20100603	20101126	20110603	20111230	20120531
MODIS	20100512	20101106	20110515	20111201	20120527
TRULAK	–	Before 20101101	20110506	20111121	20120509
NHFLAK	–	20101107	20110507	20111125	20120507
NHALAK	–	–	–	–	20120526
Ladoga,[a] Russia	32.50E 60.82N	Mean depth 33 m			
MODIS	20100513	20110115	20110508	20120125	20120501
MERIS	–	–	20110509	–	–
TRULAK	–	20101206–20110111	20110404–16	20120123	20120401–13
NHFLAK	–	20101213–20110101	20110430	20120127	20120428
NHALAK	–	–	–	20120128	20120511
Vänern,[b] Sweden	13.75E 59.15N	Mean depth 50 m			
MODIS	20100410	20110206	20110409–0429	Partial ice	Partial ice
TRULAK	–	20101108	20110410–0430	Almost no ice	Almost no ice
NHFLAK	–	20101223	20110412	Almost no ice	Almost no ice
NHALAK	–	–	–	Almost no ice	Almost no ice
Bolmen, Sweden	13.69E 56.87N	Mean depth 5 m			
MODIS	20100409	20101130	20110328	20120115	20120223
TRULAK	–	20101127	20110320	20120123	20120312
NHFLAK	–	20101127	20110321	20120123	20120312
NHALAK	–	–	–	20120206	20120226
Hjälmaren, Sweden	15.85E 59.24N	Mean depth 10 m			
MODIS	20100418	20101121	20110414	20110108	20120326
TRULAK	–	20101108–1202	20110408	20120108–0130	20120316
NHFLAK	–	20101128	20110404	20120119	20120325
NHALAK	–	–	–	20120203	20120329
Kuito, Russia	31.42E 65.14N	Mean depth 19 m			
MODIS	20100514	20101115	20110519	20111121	20120513
TRULAK	–	20101105	20110425	20111129	20120417
NHFLAK	–	20101108	20110427	20111122–29	20120417
NHALAK	–	–	–	–	20120516
Valday, Russia	33.31E 57.99N	Mean depth 14 m			
MODIS	20100507	20101122	20100508	20111122	20120412
TRULAK	–	20101127	20110403	20111225	20120327
NHFLAK	–	20101202	20110404	20111225	20120329
NHALAK	–	–	–	–	20120420

[a]Ladoga, pixel 9, see Fig. 1 for map.
[b]Vänern, pixel 4.

MERIS estimation of ice fraction (Figure 4.2b) agrees well with the MODIS visible image (Figure 4.2a), indicating an area consisting of a mixture of ice and water (MERIS: values between 0 and 54%

ice fraction) in the northeastern part and, to a lesser extent, in the southwestern part of the lake. On the northeastern part of Ladoga, MODIS daytime observations (between 08 and 10 UTC) show temperatures just above 0 °C and around 2-3 °C lower at night-time (between 20 and 01 UTC) (Figures 4.2d and e). The daytime MODIS observations show warmer temperatures compared to AATSR (Figure 4.2c). The AATSR observations were available earlier in the morning (06-08 UTC) than MODIS. Thus the stronger heating of the surface by solar radiation at noon may explain the difference.

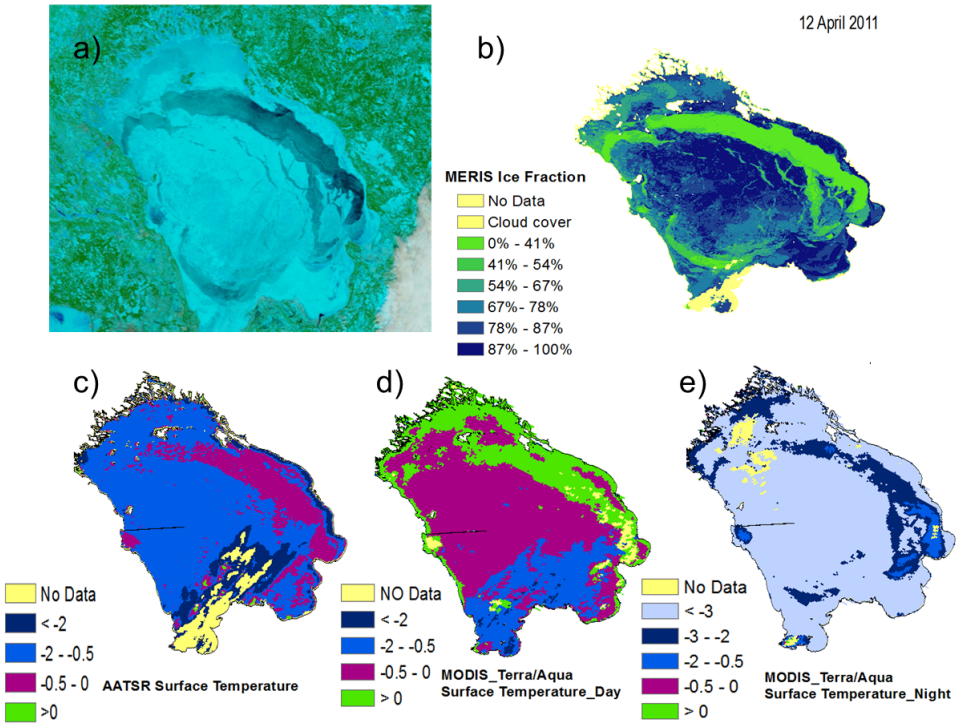

Figure 4.2 Surface temperature on 12 April 2011: (a) MODIS visible image, light blue represents snow/ice and dark blue indicate open water area (b) MERIS ice fraction, (c) AATSR surface temperature (between 8 and 10 AM local time), (d) MODIS daytime surface temperature (between 10 AM and 12 PM local time) and (e) MODIS nighttime (between 10 PM and 3 AM local time).

The ice fraction from HIRLAM (Figure 4.3, left column) was derived from the analysis of LSWT (for the method, see Section 4.3.3), which was based on the combination of MODIS (experiment NHFLAK) or AATSR (experiment NHFLAA) observations (Figure 4.4) and the background field by FLake. For comparison, the ice fraction diagnosed from the +6h ice thickness forecast by FLake parametrization is shown (Figure 4.3, middle column). In this diagnosis, the lake within each grid

square is assumed to be either completely ice-covered or completely ice-free, i.e. no fractional ice is assumed. Both the analyzed and predicted ice patterns differ from those of the mid-day and night-time satellite observations (Figure 4.2). According to the background forecast, Lake Ladoga should have been almost ice-free during the day, while at night and in the morning the northern part seems frozen. Similarly, the analysis indicates a frozen lake at night (based on MODIS) and early morning (based on AATSR) but partially melted during the day.

Three technical comments are needed for understanding the possible reasons of the difference between the analysis and the satellite observation. First, the horizontal resolutions of the model and satellites are different: 7 km for HIRLAM (the boxes visible on the maps in Figure 4.3 represent grid squares), 1 km for MODIS and AATSR, and 300 m for MERIS. Thus we would not expect HIRLAM to represent all details of the ice cover detected by the satellites. Second, the diagnostic ice fraction of the HIRLAM analysis is derived from the analyzed LSWT in a very simple ad-hoc way (Section 4.3.3). Consequently, all HIRLAM ice fractions are derived from temperatures between the freezing temperature and an artificially set lower limit of - 0.5 °C. This is not the same variable as the MERIS ice fraction, which can represent physically realistic ice properties within its 300 m × 300 m pixels. In addition, the method involves unphysical ice flag temperatures (see section 4.3.3), which may enter the analysis together with the real observations, thus adding uncertainty to the resulting analysis. Third, the LSWT analysis of the HIRLAM experiment NHFLAK over Ladoga is based on a selection of observed LSWT from a maximum of 15 MODIS or AATSR pixels (see Figures 4.1 and 4.4), combined with the FLake +6h forecast which is used as the background. This means that over Lake Ladoga, the largest part of the information from the ca. 30000 theoretically possible MODIS pixels remains unused in the analysis at the ca. 600 HIRLAM grid-squares, and the result is compared to ~300000 MERIS pixels.

Of the 15 possible MODIS pixels, 14 were available and accepted for the analysis at 00 UTC on 12 April (MODIS observation at 23 UTC, 11 April 2011, Figure 4.4a). They all show the flag value of ice, assumed for MODIS when the observed LSWT is below -0.5 °C. Twelve hours later, at 12 UTC on 12 April (MODIS observations at 9 and 11 UTC, Figure 4.4b) the analysis input also included 14 observed values, the most northeastern one (pixel 8) indicating unfrozen conditions and the other temperatures slightly under the freezing point. AATSR observations assimilated at 06 UTC

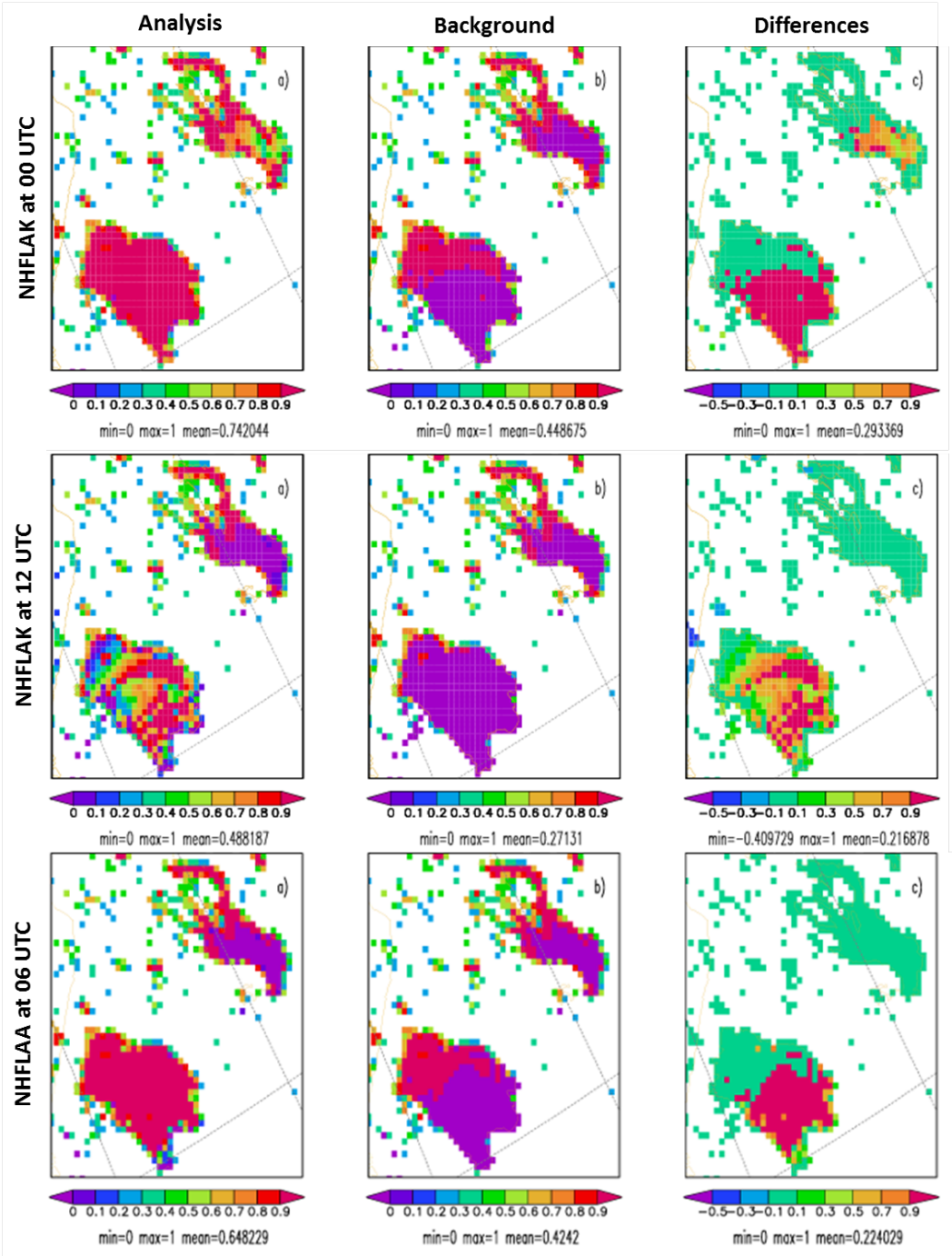

Figure 4.3 HIRLAM ice fraction (0-1) on 12 April 2011, diagnosed from LSWT: (a) analysis, (b) background and (c) their differences. NHFLAK (SYKE, FLake, MODIS) at 00 UTC (upper panel) and at 12 UTC (middle panel), and NHFLAA (SYKE, MODIS) at 06 UTC (lower panel).

indicated that the northeastern (pixel 1) and western (pixel 6) areas may have been unfrozen, while the remaining 15 pixels were frozen (Figure 4.4c).

AATSR observations were extracted for the chosen 15 pixels and applied for HIRLAM analysis on the 5-6 days in April 2011 when they were available. AATSR observations always represent morning conditions. An example of their influence in the experiments NHFLAA (with FLake background) and NHALAA (with previous analysis background), as compared to the influence of

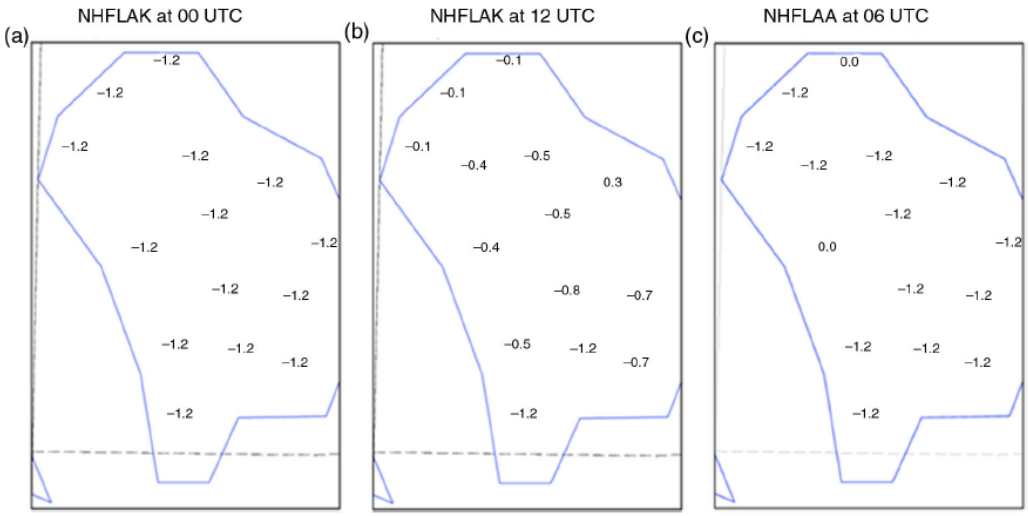

Figure 4.4 LSWT observations used for HIRLAM analysis over Lake Ladoga on 12 April 2011: (a) MODIS for NHFLAK (SYKE, FLake, MODIS) at 00 UTC, (b) MODIS for NHFLAK at 12 UTC and (c) AATSR for NHFLAA (SYKE, FLake, AATSR) at 06 UTC.

MODIS observations in the experiments NHFLAK (with FLake background) and NHALAK (with previous analysis background), is shown in Figure 4.5 for the centre of Lake Ladoga at pixel 7 during April 2011. The background given by FLake (experiment NHFLAA) and by the previous analysis (NHALAA), which was relaxed towards climatology, was very different. FLake would indicate melting during the first week of the month, while the MODIS and AATSR observations pointed to melting during the last week. Both MODIS and AATSR provided enough observations to modify the analysis accordingly, so that the analyses indicated melting closer to the end of April. Without observations and FLake (i.e. relying on climatology only), melting would have occurred after the end of April.

Only those days when observations were available are shown in Figure 4.5. When observations are sparse, the Flake background dominates the analysis outcome. The behaviour of FLake may vary between individual grid-columns because of their different lake depths. For large lakes such as Ladoga, an approximate bathymetry is available in HIRLAM (Kourzeneva et al., 2012). However, to a large extent, the conditions over the lake remain homogeneous, also from the point of view of the atmospheric forcing. This means that the background for LSWT analysis, given by FLake, also contains little horizontal variability. In addition, the analysis at each grid-point is influenced by all nearby observations, whose values and availability may vary in time. Over Lake Ladoga, these nearby observations consisted of the selected 15 pixels, each of which would have an influence to some extent over the whole lake, according to Eq. 4.2.

The different behaviour of MODIS observations during day and night contributed to an unrealistic jumping of the HIRLAM NHFLAK analysis from frozen to unfrozen conditions: during the day unfrozen conditions prevailed, during the night the lake seemed frozen. This was typical during the melting period over Lake Ladoga, also over the other lakes (not shown). Jumping of the MODIS observations between sequential observations is confirmed by Figure 4.5. AATSR may suffer less from this feature, perhaps because observations at the selected pixels were quite sparse in time but representing always the similar morning conditions. Also the lake parameterization may contribute to the unrealistic oscillation across the freezing temperature (e.g., by absorbing solar radiation too effectively during daytime.)

The reason for the difference between the cold nighttime and warm daytime MODIS lake surface temperatures remains to be understood. At night, water on ice may refreeze due to long-wave radiative cooling of the surface. In this case, the MODIS temperature would not represent that of the lake, but the temperature of the refrozen melt water on ice. One could also speculate on the possibility of formation of fog during the night over the melting ice. This type of fog, perhaps quite impossible to distinguish from the underlying surface in the satellite image, would show colder temperature than the surface, due to the long-wave cooling of the upper boundary of the fog layer.

4.5.3 Melting of Lake Lappajärvi

Features of the OI analysis over a medium size lake are illustrated by an example of the melting of Lake Lappajärvi in HIRLAM experiments NHFLAK (with FLake background) and NHALAK (with previous analysis background) in spring 2012. Over Lake Lappajärvi, SYKE temperature

observations were included in a slightly different location (closer to the shore) than MODIS. Figure 4.6 shows more details of the OI analysis during the melt period at the MODIS and SYKE points of Lake Lappajärvi.

FLake parameterization in the NHFLAK experiment suggests open water already around 10 April, while MODIS indicates a complete break-up (water clear of ice) around the first day of May (Figures 4.6b and 4.6d). Analysis of the experiment NHFLAK indicates water clear of ice a few days earlier (24 April) than that of the experiment NHALAK (28 April) (Figures 4.6b and 4.6a). The visible MODIS-Aqua images (Figure 4.7) indicate that Lake Lappajärvi is clear of ice on 1 May but still ice-covered on 25 April. The SYKE observer recorded 2 May as the water clear of ice date for Lake Lappajärvi (see Table 4.3). SYKE temperature measurements started only on 10 May when the water temperature had already reached 3 °C (Figures 4.6c and 4.6d).

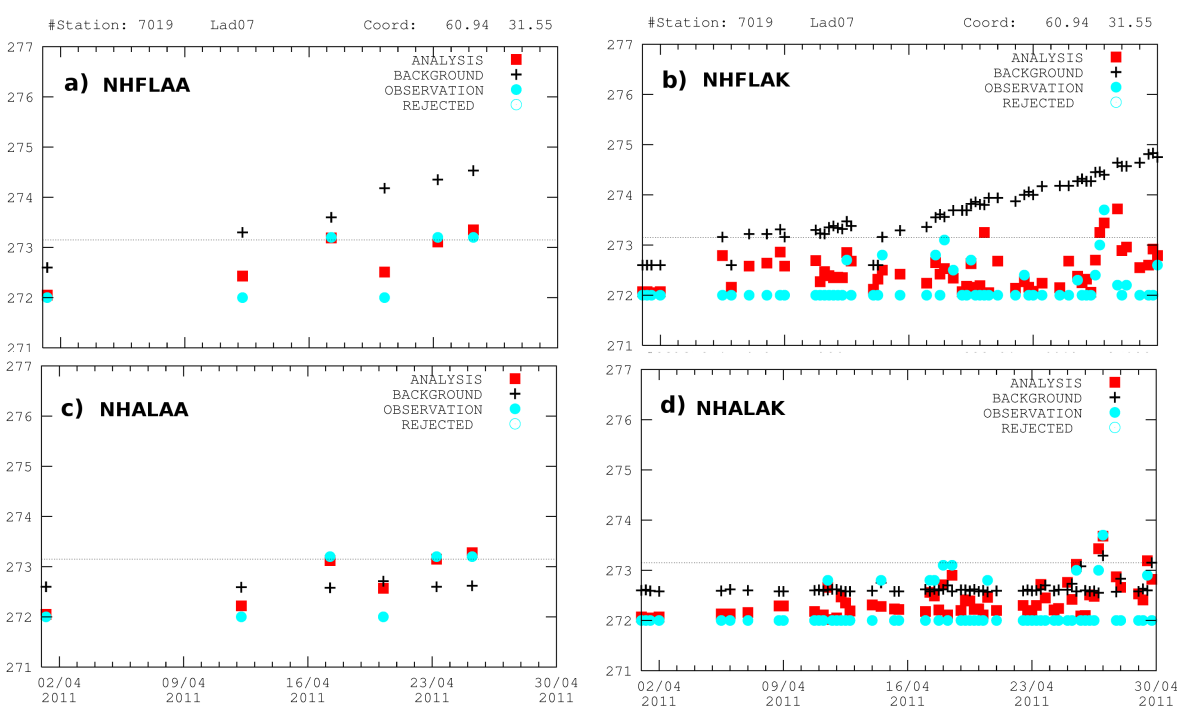

Figure 4.5 Analysis (red), background (black) and observation (blue) of LSWT in the grid point nearest to pixel 7 over central Ladoga during April 2011 in the experiments (a) NHFLAA (SYKE, FLake, AATSR), (b) NHFLAK (SYKE, FLake, MODIS), (c) NHALAA (SYKE, AATSR) and (d) NHALAK (SYKE, MODIS). Only times when MODIS observations were available are shown. No data are rejected here.

The analysis of NHALAK followed MODIS observations more closely than that of NHFLAK, which was influenced by the warmer background suggested by FLake. SYKE temperature measurements were not available before 10 May, entering the NHALAK analysis only well after the observed ice break-up. When there were no MODIS observations over Lake Lappajärvi, the previous analyses that were applied as background in NHALAK would have converged to the climatological values, which still represented ice-covered conditions. If break-up was interpreted from NHALAK analyses based on the observations at the SYKE point alone, it would have occurred two weeks later than when MODIS observations were included. In general, melting of Lake Lappajärvi could be described realistically due to the MODIS observations both with and without FLake parameterizations. FLake alone would have led to too early and OI, based only on the (missing) SYKE water temperature measurements and climatology, to too late melting of this lake in the HIRLAM analysis. This is because a lake grid-point is assumed to retain its state given by the background field when there are no observations available to correct it.

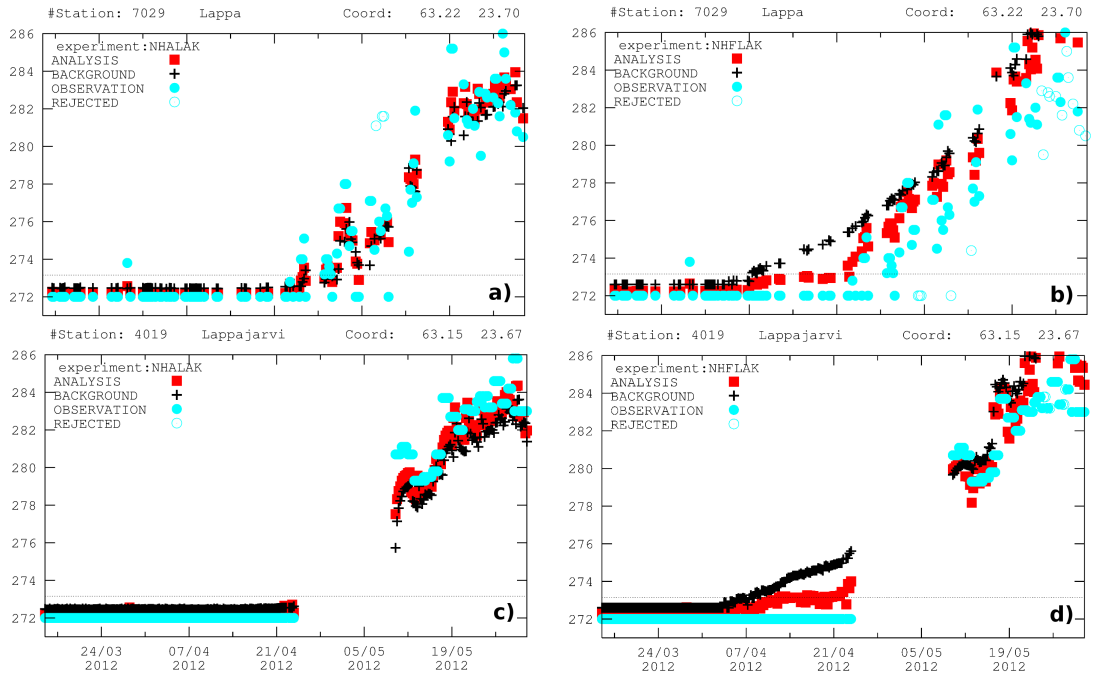

Figure 4.6 Same as in Fig. 5 but over Lake Lappajärvi (15 March _ 31 May 2012) in the experiments (a) NHALAK (SYKE, MODIS) and (b) NHFLAK (SYKE, FLake, MODIS) for the selected MODIS pixel (23.70 E, 63.22 N), (c) NHALAK (SYKE, MODIS) and (d) NHFLAK (SYKE, FLake, MODIS) for the SYKE measurement point (23.67 E, 63.15 N).

The reason of the too-early warming of lakes by FLake (noted also in Section 4.5.2 and in Table 4.3) requires further study. One possible reason may be related to the missing of snow on lake ice. In these experiments snow parameterization was included in FLake, as in the reference HIRLAM v.7.4, but in fact snow never accumulated on lake ice in the model. This was due to a technical error that has lately been corrected.

The rather large variation of MODIS LSWT observations from day to day (Figure 4.6), which may result from unsuccessful removal of the signals due to high-level clouds during preprocessing of the data, poses a problem to the quality control within the HIRLAM analysis system. On the other hand, FLake reached unrealistically high LSWT after the melt of ice on Lake Lappajärvi. Around 25 May, many MODIS and some SYKE observations were rejected in the background check by the quality control, which was not correct in this case. Relations between the adjacent observations of different types (SYKE and MODIS) on the lake and its neighbourhood would require further study. In the present experiments, all lake observations were assumed to have similar statistical properties. For example, the assumed observational error standard deviation was set to 1.5 °C for both in-situ and remote-sensing LSWT observations. This value is supported by the evaluation study in Chapter 3, where a standard deviation of around 1.8 °C was estimated for the satellite measurements for selected 22 Finnish lakes during open water season when SYKE temperature observations were available.

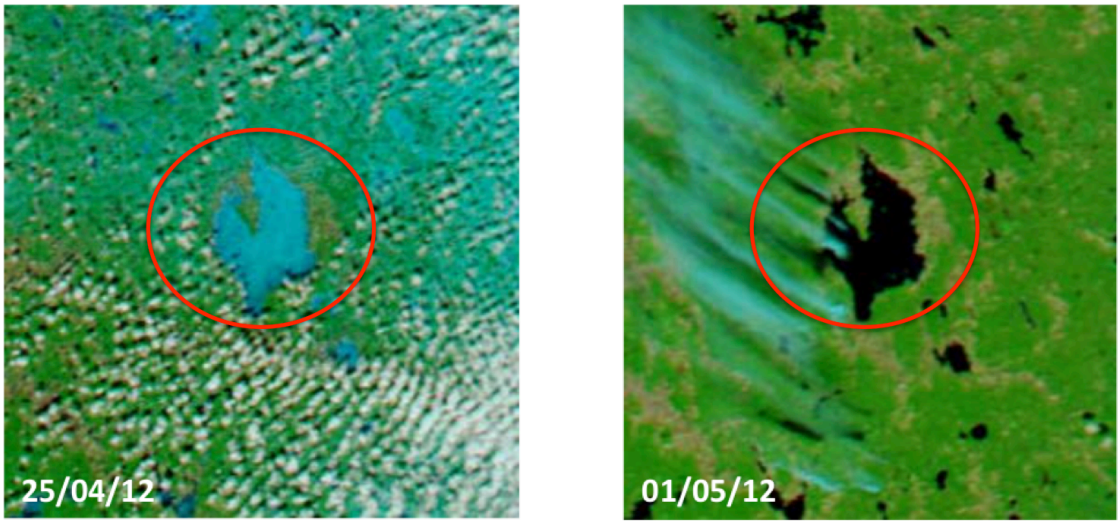

Figure 4.7 MODIS-Aqua visible images over Lake Lappajärvi on 25 April (left, 8:30-12:10 UTC, light blue color represent snow/ice) and 1 May (right, 9:50-11:30 UTC, black color represents open water), 2012.

4.5.4 Validation of analysis over independent lakes

MODIS UW-L3 LSWT observations were derived but withheld from the HIRLAM analysis over four lakes in Sweden and Russia (see Section 4.2.3). The Russian Lake Kuito and Lake Valday are chosen for comparison between analyses and observed MODIS LSWT (Figure 4.8). These two lakes were chosen for illustration because they are located far enough from the nearest lakes included in the analysis, so that analyses on them are not significantly influenced by the nearby observations. The results for the Swedish Lake Hjälmaren and Lake Bolmen (not shown) confirm the results presented here. The analyses of the three main experiments TRULAK, NHFLAK and NHALAK (Table 4.2) were compared to MODIS observations during January to May 2012 when results from all experiments were available. MODIS observations with the ice flag -1.2 °C (indicating measured temperatures below -0.5 °C) were excluded from the set of validation observations. Over these lakes, the analysis by TRULAK and NHFLAK is interpreted directly from the FLake forecast, thus this validation measures the quality of FLake, not that of the analysis method. Similarly, as observations were not applied, validation of NHALAK compares the available climatology to MODIS observations.

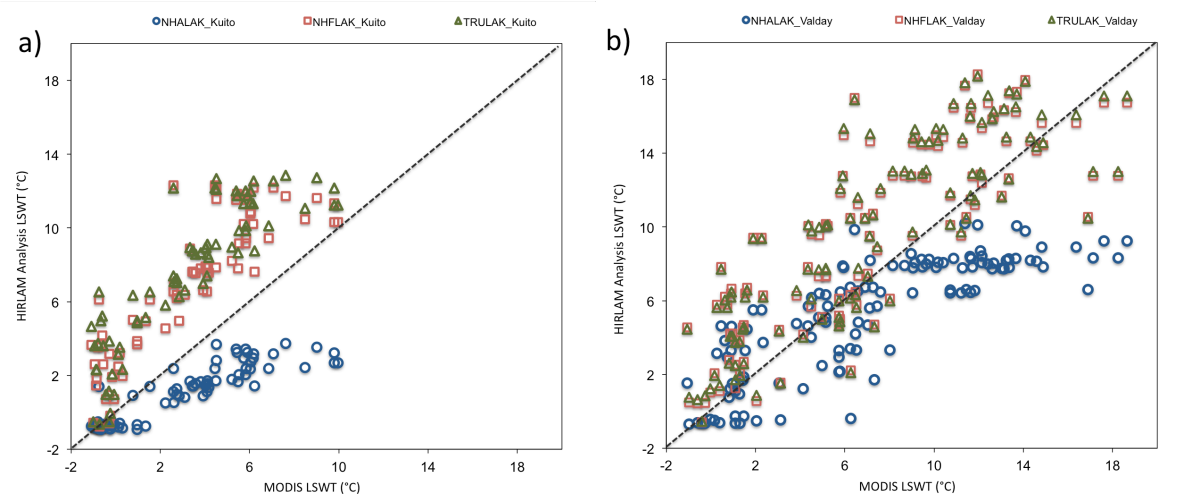

Figure 4.8 Comparison of LSWT derived by MODIS with LSWT analysed by experiments NHFLAK (SYKE, FLake, MODIS; red), NHALAK (SYKE, MODIS; blue) and TRULAK (SYKE, FLake; green) for (a) Lake Valday and (b) Lake Kuito.

We can see in Figure 4.8 that the analyses based on different backgrounds - NHALAK on the previous analysis relaxed towards climatology, TRULAK and NHFLAK on the 6-hour forecast by FLake - started to diverge as soon as the observed LSWT clearly rose above the freezing point.

Typically, NHALAK analyses remained significantly colder than MODIS observations, while TRULAK and NHFLAK tended to be significantly warmer. According to the applied climatology, these lakes normally stay ice-covered longer than was observed in spring 2012. Relaxation of the NHALAK towards such a climatology forced the analyses towards freezing temperatures when no observations were available to correct the situation. The warm bias of FLake led the analyses TRULAK and NHFLAK to too high analysed LSWT. This bias has been detected earlier in this study as well as by Eerola et al. (2010) and Rontu et al. (2012).

4.6 Conclusions and outlook

We have reported the first steps in utilizing satellite-based observations to define the initial state of lake surfaces in a NWP model. We have applied the HIRLAM surface analysis by introducing new lake observations. While not focusing on optimization of the analysis methods for LSWT and lake ice, we did however detect their limitations and provided suggestions for improvements. Many questions will require further investigation on the road towards a completely integrated lake data assimilation system for NWP.

In our experiments, we included MODIS and AATSR temperature observations over lakes in HIRLAM. When temperatures below freezing were detected, LSWT was given an ice-flag value, otherwise the observation was assumed to represent the measured LSWT. A limited number of 70 MODIS pixels over 41 large- and medium-size Scandinavian, Karelian and Baltic lakes and a sample of AATSR data over Lake Ladoga were selected for the analysis input. Pre-processing of these data for the analysis is described in Chapter 3. To understand the sensitivity of the resulting LSWT analysis to the new data, the analyzed LSWT and diagnosed lake ice concentration were compared with those by the experiments where space-borne observations were not included. The initial states of every forecast-analysis cycle of each experiment were validated, mostly qualitatively, against locally recorded freezing and melting dates of the lakes as well as against independent satellite LSWT and ice cover observations. Introduction of space-borne observations led to an improvement of the description of lake surface state, especially during the melt period when in-situ LSWT observations were not yet available and the prognostic lake parameterizations suffered of a significant warm bias. During the freezing period, when the sun was low and weather typically cloudy, only few thermal

satellite data were available. In the conditions of well-mixed lake water, typical of the freezing period, the Flake prognostic parameterizations also worked reasonably well, making the additional observations less necessary in autumn.

The background LSWT for the optimal interpolation analysis was provided either by the prognostic lake parameterizations of the Freshwater Lake model integrated in HIRLAM, or by the previous analysis backed up by climatology. FLake provides background for the LSWT analysis at every HIRLAM grid-point containing a lake fraction. In the case of sparse and missing observations, this ensures on average a better result than an analysis that uses the previous analysis as background, especially when the lake is frozen and the background relaxes to climatology. However, in cases where a sufficient quantity of good (satellite-based) observations was regularly available, the analysis using the previously analyzed LSWT as the background followed observations closer than when the background LSWT was diagnosed from the predicted FLake lake temperature.

In a case study, MERIS ice fraction over Lake Ladoga was found to qualitatively agree with the ice fraction derived from the HIRLAM lake temperature analysis. Due to the finer spatial resolution of MERIS observations, they provided a more detailed picture than the HIRLAM analysis. However, MERIS is an optical sensor whose data coverage is limited by the presence of clouds. Ice cover observations derived from passive microwave sensors do not suffer from this problem. However, they are presently of a coarse spatial resolution (ca 10 km) and would thus only represent large lakes. The Interactive Multisensor Snow and Ice Mapping System (IMS) product (4 km resolution) could be the other alternative, which utilizes a variety of multi-sourced datasets such as passive microwave, visible imagery, operational ice charts and other ancillary data (Helfrich et al., 2007; Ramsay, 1998). IMS data has been shown to be an effective product for lake ice (Brown and Duguay, 2012; Duguay et al., 2011, 2012, 2013; Kang et al., 2012) and sea ice (Brown et al., 2014) phenology studies.

In the long term, for a direct assimilation of ice concentration from optical sensors, some spatialisation methods such as OI should be used. However, solutions for several theoretical and technical problems need to be found. The error distribution of the ice concentration is probably non-Gaussian and needs application of specific methods (Lisaeter et al., 2003; Qin et al., 2009; Simon and Bertino, 2009). For the background, the FLake ice fraction can at the moment only be 0 or 1. This means that it is only known if the lakes in the grid-box are ice-covered or not. Such information is in principle qualitative, when defined within the relatively coarse resolution of the NWP model.

Methods to assimilate qualitative information are poorly developed in NWP. For example, an algorithm for assimilation of remotely sensed snow extent (Drusch et al., 2004) uses a quite simple and ad-hoc approach. When utilizing LSWT and ice cover observations together, it will be necessary to ensure their consistency in the resulting analysis. Experience from simplified methods, where the observed ice fraction is converted to temperature, which is then treated by the OI algorithm together with SST (Canadian Meteorological Centre), may also be helpful. In addition to the horizontal spacialisation, methods to assimilate ice information with respect to the prognostic variables of FLake (such as ice thickness) should be developed.

Extended application of remote-sensing LSWT measurements is a novel feature in this paper, compared to the previous studies (Eerola et al., 2010; Rontu et al., 2012). However, significantly more data, potentially available from satellites, still remain unused with the approach of predefined pixels over the lakes (70 pixels used in this study versus several tens of thousands pixels covered by the satellite measurements). By using the fine-resolution land-cover information available in the NWP model, it is possible to classify if a satellite pixel (with known coordinates) is located over a lake resolved by the model. Thus, it would be possible to utilize high-resolution near-real time satellite LSWT/ice cover observations without pre-selection of pixels. Methods to reduce the amount of input data over large lakes (thinning, screening, creation of super-observations) should be developed and applied in order to avoid giving too much weight to the large amount of mutually correlated satellite data compared to possible in-situ measurements, and also in order to keep the amount of input data reasonable compared to the resolution of the NWP model. Certain preprocessing of these data, including cloud clearance, identification of missing data, and estimation of the measurement error in each pixel would be preferable before entering the OI quality control within the model.

Improvement of the operational analysis of remote-sensing LSWT measurements in NWP models requires development of the optimal interpolation methods. Derivation of the autocorrelation functions (structure functions), which take into account lake depth and elevation, as well as calculation of observation error statistics of different measurement types is believed to be important. Practical questions should be resolved in the future, such as: how to obtain near-real-time daily observational data of reasonable volume in a universal format; how to introduce more than selected pixel observations into the analysis; how to improve the quality control before and within the NWP application. For the operational NWP models, the analysis of the transient surface properties is

crucial, but handling of the observational data and computations should be highly optimized in order to allow timely production of the full three-dimensional weather forecast. Input information should be processed without manual intervention, but well enough to allow only reliable observations to influence the analysis.

It is worth mentioning that presently, the analyzed state of the lake surface creates no feedback to the FLake parameterization, which is coupled to the atmospheric model during the forecast run. Thus, the improved LSWT analysis remains as a possibly useful independent by-product of the NWP model. In order to really utilize the space-borne and in-situ observations on lake surface state for the improvement of the weather forecast and prediction of lake temperatures, methods to connect the analyzed LSWT and ice cover to the prognostic in-lake variables are needed. Such methods for NWP models are currently under development (Kurzeneva, 2014).

To conclude, it has been learned that space-borne LSWT observations are beneficial for the description of lake surface state in HIRLAM. Satellite observations provide frequent observations over large areas. The large spatial coverage of satellite-based data at a high resolution is a major advantage but also an application challenge when compared to in-situ measurements.

Chapter 5

Preliminary assessment of lake surface water temperature statistical properties for objective analysis in a NWP model using satellite observations

5.1 Introduction

The importance of energy exchange processes between the Earth's surface and the atmosphere is increasingly being recognized in weather forecasting. The surface heat, moisture and momentum fluxes, which provide the coupling between the atmosphere and the Earth's surface, depend not only on atmospheric conditions but also on surface characteristics, in which inland water bodies are known to play an important role on lake-rich areas. The importance of a correct description of inland water (lake) surface state in climate (Duguay et al. 2006, Brown and Duguay 2010, Krinner and Boike 2010, Samuelsson et al. 2010, Ngai et al. 2013) and weather prediction (Niziol 1987, Niziol et al. 1995, Zhao et al. 2012) models is well known. Particularly during freezing and melting of lakes, the surface radiative and conductive properties as well as the latent and sensible heat released from lakes to the atmosphere change dramatically, leading to a completely different surface energy balance. By affecting the surface fluxes, lakes modify the structure of atmospheric boundary layer.

Lake Surface Water Temperature (LSWT) is a critical variable to measure, assimilate and predict in numerical weather prediction (NWP) models, because it is directly related to the heat fluxes. The quality of observation-based lake surface state description (result of the numerical analysis) depends to a large extent on the availability and selection of the observations influencing each grid-point of a NWP model. Obtaining reliable observations on lakes in real-time, especially at high latitudes, is challenging. Satellite-based observations are the only realistic way of getting frequent observations over large areas. However, various types of satellite observations collected over lakes represent different scales and have different accuracies, depending on the observing system, and they are irregularly distributed in space and time. Considering the various sources of information, a number of necessary processes have to be considered prior to and during assimilation of the observations into the

NWP model grid. Quality control, filtering systematic errors and interpolation of the observations in time and space require knowledge of the statistical properties and error characteristics of the observations and model background.

A correct description of the lake surface state started to be relevant in NWP models when the horizontal resolution of models became high enough to resolve lakes, even the smaller ones. For example, in the first implementation - with a horizontal resolution of ca. 50 km - of the High Resolution Limited Area Model (HIRLAM; Undén et al. 2002), applied since 1990 for the numerical short-range weather forecast over northern Europe, monthly climatological water surface temperature was used both over sea (Sea Surface Temperature or SST) and lakes. The LSWT climatology was achieved by extrapolating the SST values to lakes as no suitable climatological data for lakes were available. The analysis of SST observations by the method of successive corrections (Cressmann 1959) followed in early 1990s by utilizing pseudo observations created from ECMWF SST analysis (Chelton 2005). The first improvement to the treatment of LSWT over the Finnish lakes was to use real lake climatology (Eerola et al. 2010). Daily climatological LSWT pseudo observations were created for 20 lakes in Finland based on long-term statistics of measurements. The pseudo observations were applied for the LSWT analysis instead of real observations but using similar methods as for SST over the sea. To avoid drifting far from realistic values, the background (first guess) SST and LSWT values, given by the analysis of the previous forecast cycle, were still relaxed towards the (extrapolated) SST climatology and the statistical properties derived for SST were used everywhere. In addition, the fractional ice cover over the sea and lakes was diagnosed from SST and LSWT in the same way.

It was obvious that the SST climatology cannot be used to represent LSWT (Eerola 1996, Eerola et al. 2010). Instead of the observation-based approach, a prognostic lake parametrization for NWP and climate models, the Freshwater Lake Model (FLake), was developed (Mironov 2008, Mironov et al. 2010). FLake was implemented to the HIRLAM forecast model (Kourzeneva et al. 2008, Eerola et al. 2010) utilizing external data sets on lake depth (Kourzeneva et al. 2012a) and climatology of the predicted variable (Kourzeneva et al. 2012b). At the same time, in-situ lake water temperature observations from 27 Finnish lakes were implemented into the operational HIRLAM LSWT analysis (Eerola et al. 2010, Rontu et al. 2012), based on real-time in-situ measurements by SYKE (Finnish Environment Institute) and application of the method of optimal interpolation (OI, Gandin 1965).

FLake now provides the background LSWT for the analysis, but the analysis does not influence the prognostic FLake. The approach and its limitations have been studied and discussed by Kheyrollah Pour et al. (2014b) and Kourzeneva (2014).

Work to develop the analysis of LSWT continued also elsewhere. An operational stand-alone analysis of LSWT was developed at U.K. Met Office for NWP purposes in the Operational Sea Surface Temperature and Ice Analysis (OSTIA) system (Donlon et al. 2012, Fiedler at al. 2014). The LSWT observations used in OSTIA are part of Sea Surface Temperature (SST) products from AATSR and MetOp-AVHRR (Infrared Atmospheric Sounding Interferometer (IASI)). These data are based on SST retrievals as none of them include lake-specific processing. On the other hand, the background LSWT for the large lakes (ca. 248 globally) in OSTIA is backed up by lake climatology (Fiedler et al. 2014).

Numerical methods, which are essential to solve the problem of initial analysis, were developed by several groups of meteorologists for atmospheric models (Panofsky 1949, Gilchrist and Cressman 1954, Bergthorsson and Döös 1955, Cressman 1959). The OI (also called as statistical interpolation), introduced by Eliassen (1954) and Gandin (1965), was applied for the upper air analysis in operational numerical weather prediction systems (e.g. Lorenc 1981, Hollingsworth and Lönnberg 1986, Lönnberg and Hollingsworth 1986, Daley 1991) until the early 2000s. OI is based on the idea of minimizing the mean analysis error in the statistical sense. It is still applied for the analysis of the near-surface variables such as SST, LSWT, soil and screen-level temperature (Thiebaux 1975, Julian and Thiebaux 1975, Sattler and Huang 2002, Donlon et al. 2012). In NWP models, it is applied both for the definition of the analyzed value in the grid-point and for the quality control of the observations. The OI method relies on the knowledge of the statistical properties and error estimates of the observations and the background (e.g. the short forecast) variables. Structure (autocorrelation) functions, depending on distance (and possibly on other characteristics) between the observations and between observations and grid-points, are derived for determination of the weight of individual observations in the analysis.

In the current version of HIRLAM, the model used in this study, the autocorrelation function used for LSWT is represented in the form of an exponential function depending on the distance and is the same as that of SST. The length scale (influence radius) has been set to work properly for SST. However, this has never been studied for lakes using LSWT observations. The depth of the lake is a

major factor determining the thermal regime of lakes (Walsh et al. 1998), in addition to size, shape, and elevation. Therefore, it is of interest to derive and evaluate the impact of function, depending not only on the horizontal distance but also at least on depth differences, and possibly elevation differences between lakes.

In this paper, we seek answers to several questions concerning the improvement of the autocorrelation function used in the analysis of LSWT. Can the current autocorrelation function be improved using LSWT observations instead of the current assumption based on SST? Can lake depth differences influence the function beside lake distances? Are LSWT data obtained from thermal satellite remote sensing sensors appropriate for calculation of the autocorrelation function? How sensitive is the resulting objective analysis of LSWT in HIRLAM to the choice of autocorrelation function? To answer these questions, the spatial coherence of LSWT observations derived from the Moderate Resolution Imaging Spectroradiometer (MODIS) for lakes located in Scandinavia and Karelia was first investigated (Section 3.1). Empirical autocorrelation function were fitted to the observational data and a new influence radius for The HIRLAM model was approximated (Section 3.2). Simultaneously, the sensitivity of HIRLAM LSWT analysis to the formulation of autocorrelation function was tested in numerical simulation experiments (Section 4). To our knowledge, this is the first study of its kind, which could lead to future improvement of LSWT autocorrelation function not only in HIRLAM system, but also in any other analysis system of LSWT.

5.2 Data and methods

5.2.1 Autocorrelation function for objective analysis of LSWT by optimal interpolation

Data assimilation is the process of using all variable information to define as accurately as possible the initial state of the atmospheric variables. The information contains both observations and model state. To do this, first guess field or background field provided by the earlier forecast is blended with the observations. As the background field is produced by the forecast model and therefore is physically consistent, this helps maintain the dynamical consistency between the analyzed model variables. In the case when there is no direct connection between observations and background values or there are no observations available for a grid-box, data assimilation methods give the possibility to

use information from other meteorological variables. The purpose of data assimilation is to provide the best possible analysis (initial value) of model variables in grid-points. In the case when there are no observations available that influence the value in the grid-point, the analysis is the same as the first guess value. A improved objective analysis result a better forecast, and eventually an improved background field.

Optimal Interpolation (OI) is one objective analysis procedure that uses weighting factors and observational errors. The weight of an observation depends on the distance between the observations and the grid-point and the distance between observations to each other, and the error of each type of observation is taken into account. The method was introduced into the field of meteorology by Gandin (1965). In this paper, we are concerned with properties of the statistical information incorporated into the OI objective analysis in the form of autocorrelation function of the LSWT variables. This method gives the state of LSWT at a particular time at all model grid-points. The aim is to deduce the best estimate (analyzed value) from the available data. The analyzed value ($f_A\,(r_i)$) can be expressed as:

$$\boldsymbol{f_A(r_i) = f_B(r_i) + \sum_{k=1}^{K} W_k\,[f_O(r_k) - f_B(r_k)],} \qquad \boldsymbol{i = 1, \dots, I} \qquad \textbf{5.1}$$

where f is the value of the surface variable (LSWT) at the analyzed grid-point defined by its radius-vector r_i (the arrow sign is omitted for simplicity), I is the number of grid-points, $f_B\,(r_i)$ is the background value of f at r_i, and $f_O\,(r_k)$ and $f_B\,(r_k)$ are the observed and background values, respectively, at the observation point r_k. K is the number of influencing observations and W_k are the weights given to each observation increment $[f_O(r_k) - f_B(r_k)]$ in the analysis at the grid-point r_i. Weights are defined as a solution of the following system of linear equation:

$$\boldsymbol{\sum_{j=1}^{K} W_j\,\mu(r_j, r_k) + W_k\eta = \mu(r_i, r_k),} \quad \boldsymbol{k = 1, \dots, K} \qquad \textbf{5.2}$$

where $\mu(r_i, r_k)$is the normalized autocorrelation function of the analyzed value between points r_i and r_j and η is the normalized observational error:

$$\boldsymbol{\eta = \frac{\sigma_f^2}{\bar{f}^2}} \qquad \textbf{5.3}$$

where $\sigma_f$is an observational error and $\bar{f}$ is a variance of the analyzed value (LSWT). Therefore, the autocorrelation function (or the structure function in some notations) is used in OI to calculate the interpolation weight of different observations.

Here, a mathematical definition of the structure function and the autocorrelation function is given according to Gandin (1965). If r_1 and r_2 are two observation points on the surface, then the mean square difference of $\acute{f}$ at r_1 and $r_2$is defined as the structure function $\mathrm{b}_f(r_1, r_2)$:

$$\mathbf{b}_f(\boldsymbol{r_1}, \boldsymbol{r_2}) = \overline{[\acute{\boldsymbol{f}}(\boldsymbol{r_1}) - \acute{\boldsymbol{f}}(\boldsymbol{r_2})]^2} \quad \textbf{5.4}$$

where the bar denotes averaging and the function is considered for deviations of f from its mean value $\bar{f}$ which being defined as

$$\acute{\boldsymbol{f}}(\boldsymbol{r}) = \boldsymbol{f}(\boldsymbol{r}) - \bar{\boldsymbol{f}}(\boldsymbol{r}) \qquad \textbf{5.5}$$

Another important characteristic of the statistical structure of this field is the correlation function, which is defined as the mean product of the values of two LSWT values at two observation points. If these two elements are identical, it is called autocorrelation function:

$$\boldsymbol{m_f}(\boldsymbol{r_1}, \boldsymbol{r_2}) = \overline{\acute{\boldsymbol{f}}(\boldsymbol{r_1})\, \acute{\boldsymbol{f}}(\boldsymbol{r_2})} \qquad \textbf{5.6}$$

There is a simple relationship between the structure function and the autocorrelation function for the same elements so that:

$$\boldsymbol{b_f}(\boldsymbol{r_1}, \boldsymbol{r_2}) = \boldsymbol{m_f}(\boldsymbol{r_1}, \boldsymbol{r_1}) + \boldsymbol{m_f}(\boldsymbol{r_2}, \boldsymbol{r_2}) - \boldsymbol{2m_f}(\boldsymbol{r_1}, \boldsymbol{r_2}) \qquad \textbf{5.7}$$

If the field is homogeneous and isotropic, the structure function and autocorrelation functions do not depend on the location of each observational point $r_1$and r_2 but only on distance between them (ρ), so we use ρ onward instead of the pair of $r_1$and r_2.

The normalized autocorrelation function $\mu_f(\rho)$ is defined as

$$\boldsymbol{\mu_f}(\boldsymbol{\rho}) = \frac{\boldsymbol{m_f}(\boldsymbol{\rho})}{\boldsymbol{m_f}(\boldsymbol{0})} \qquad \textbf{5.8}$$

From Eq. 5.7 we can derive the expression:

$$\boldsymbol{b_f}(\infty) = \boldsymbol{2m_f}(\boldsymbol{0}) \qquad \textbf{5.9}$$

and also:

$$\boldsymbol{b_f}(\boldsymbol{\rho}) = \boldsymbol{b_f}(\infty) - \boldsymbol{2m_f}(\boldsymbol{\rho}) \qquad \textbf{5.10}$$

Consequently, $\mu_f(\rho)$ can be calculated as:

$$\boldsymbol{\mu_f}(\boldsymbol{\rho}) = \frac{\boldsymbol{2\, m_f}(\boldsymbol{\rho})}{\boldsymbol{b_f}(\boldsymbol{\rho}) + \boldsymbol{2\, m_f}(\boldsymbol{\rho})} \qquad \textbf{5.4}$$

5.2.2 Determination of autocorrelation function

The structure function and the autocorrelation function may be calculated from observations. In our case, the determination of the functions needs a reliable and homogeneous observational network to determine a distance-dependent function for horizontal distance or differences between depth of lakes in all available observation points (vertical distance) or both. In this study, the LSWT observations derived from MODIS sensors are used to calculate the autocorrelation function, not only distance-dependent but also lake-depth dependent. To calculate the function, LSWT values at 74 observational points (pixels) are selected over 44 lakes. The calculations are performed for the period covering summer (June-July-August) 2010-2011 when lakes were free of ice and snow. Data are used at each observation period successively and the structure function and the autocorrelation function are determined according to Eq. 5.4 and 5.6**.**

First, the coordinates of each of the selected pixels are defined and the horizontal distance between these points (ρ) is calculated. The value of ρ is then compared with the limit of the gradations of ρ, in order to determine to which gradation the calculated value of ρ refers. The gradations of ρ are design as categories (14 categories) of lakes observational point (lake pairs) within each 100km distances from 100-1300km and 1300km above due to the low number of lake pairs in the last category. After, the calculated $b_f\ (\rho)$ and $m_f\ (\rho)$ are recorded for the first and second observation points in this gradation in each distance categories, the second observation point is replaced by the third observation point and then the fourth, etc.

As the next step, the normalized autocorrelation function ($\tilde{\mu}_f(\rho)$) is calculated. It is essential to consider the normalized observational error (η) when calculating the autocorrelation function (Eq. 5.3). The normalized autocorrelation function with consideration of normalized observations error is calculated as follow:

$$\tilde{\mu}_f(\rho) = \frac{\mu_f(\rho)}{1+\eta_f} \qquad \textbf{5.5}$$

5.2.3 Approximation of LSWT autocorrelation function in HIRLAM

5.2.3.1 Dependence on distance

The HIRLAM system uses a homogeneous anisotropic analytical approximation of the autocorrelation function (Rodriguez et al. 2002) for SST. Currently, the same function is also used for

lakes in the HIRLAM forecasting system. It is defined as a Gaussian function representing dependence on the horizontal distance:

$$\boldsymbol{\mu(\rho) = e^{-0.5\rho^2/L_H^2}} \qquad \textbf{5.6}$$

where L_H is a horizontal length scale (influence radius). So, $\mu(\rho)$ only depends on the distance between lake pairs. The value for L_H is defined as 80 km, which is a tuning value selected to give more weights on the near-by observations; however, this follows a pragmatic approach. The same value for L_H is also applied in HIRLAM for lakes and, to our knowledge, no statistical methods are used to adjust this value to be relevant for lakes.

In this study, $b_f\,(\rho)$ and $m_f\,(\rho)$ are calculated for each lake pair and for each distance categories from the approach described in section 2.1 using MODIS-derived LSWT observations. Then $\tilde{\mu}_f(\rho)$ is calculated from Eq. 5.11 and 5.12 and an exponential function is derived from the regression of $\tilde{\mu}_f(\rho)$ values against distance.

5.2.3.2 Dependence on lake depth

The autocorrelation function was examined to understand the influence of lake depth beside distance. Lake depths are categorized in 10-m intervals (5 categories) from the minimum depth differences (0 m when lake pairs had a similar depth) to the maximum of 50 m. The normalized autocorrelation function is calculated for each depth category (including distance categories) separately in order to understand the influence of lake depth in the static intervals. The calculations are performed during two summers 2010-2011 (JJA). The hypothesis is that the influence decreases from category one (lake depth differences between 0-10m) to category five (lake depth differences between 40-50m).

5.2.4 Satellite-derived observations

The LSWT observations (UW-L3 dataset described below) are derived from the thermal remote sensing sensor MODIS aboard the Aqua and Terra satellites. MODIS pixels were extracted from 44 Scandinavian lakes (> 6 km^2) of various depths (Figure 5-1). Lakes of dissimilar sizes and shapes over northern Europe were chosen. The LSWT observations derived from MODIS are at a grid resolution of 1 km × 1 km. For most of the lakes, one pixel was selected to represent the observation points; however, for large lakes, more pixels were chosen (e.g. nine pixels for Lake Onega and fifteen pixels for Lake Ladoga, in Russia).

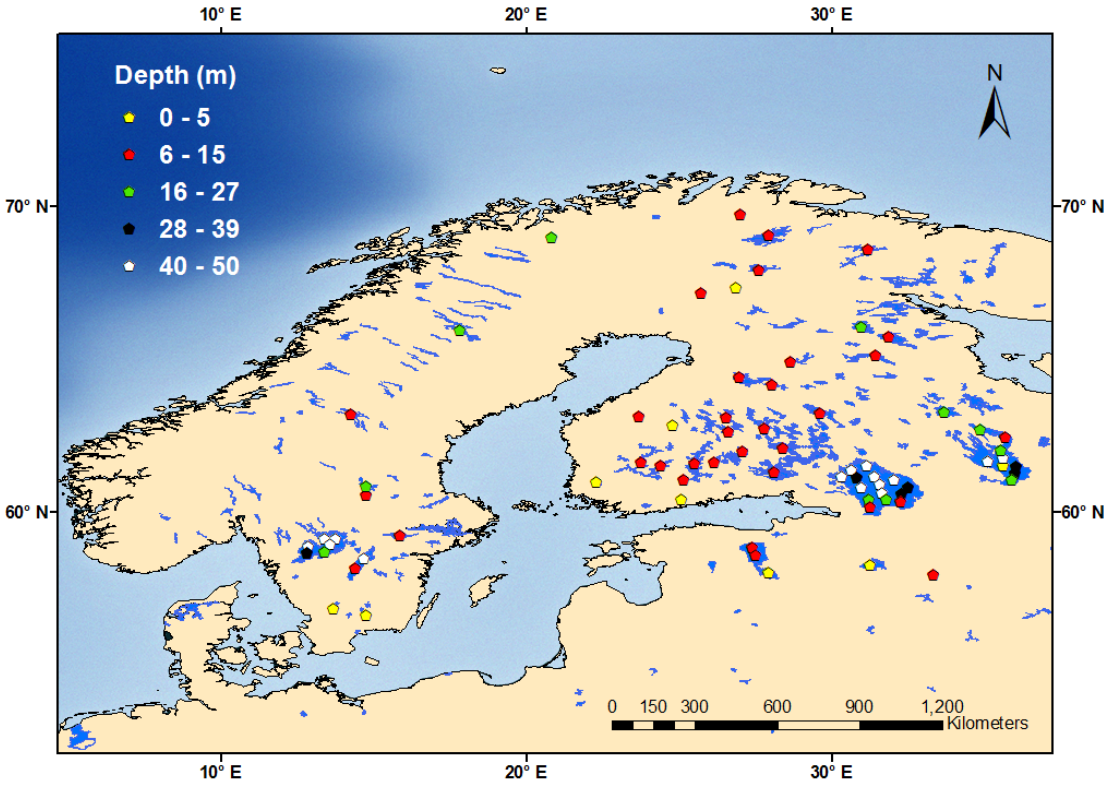

Figure 5.1 Location of lakes within the HLRAM domain over northern Europe. The colors correspond to different lake depth classes (in meters).

MODIS Aqua and Terra Land Surface Temperature and Emissivity (MOD11-L2, collection 5, 1 km) data were acquired from the NASA Land Processes Distributed Active Archive Center (LP DAAC). These data were produced using the generalized split window approach (Wan and Dozier 1996) and the MODIS sensor radiance data product (MOD021KM), the geolocation product (MOD03), the atmospheric temperature and water profile (MOD07-L2), the cloud mask (MOD35-L2), the quarterly land cover (MOD12Q1), and snow product (MOD10-L2) (Wan, 2005).

The MODIS science team generates Land Surface Temperature (LST) and Emissivity data. MODIS Terra was launched on 18 December 1999 (EOS AM) and MODIS Aqua (EOS PM) on 4 May 2002. They scan the Earth with ±55° from Nadir in 36 bands within the thermal infrared (TIR) in the range of 3 to 15 µm. MODIS-derived LST products (MOD/MYD 11-L2, Collection 5, 1-km) has been validated using a radiance-based approach in the mid and south US states. The bias of L2

MODIS LST observations from LST estimates obtained with a radiative transfer model ranged from −0.8 to 0.1 K, with a general tendency of underestimation of LST values from MODIS (Wan 2008). MODIS LSWT have been used and evaluated in various studies over lakes using in-situ observations and the reported accuracy varies between validation methods and the observation periods (Wan et al. 2002, Oesch et al. 2005, Hook et al. 2007, Reinart and Reinhold 2008, Crosman and Horel 2009, Schneider et al. 2009, Hulley et al. 2011, Liu et al. 2014).

The UW-L3 MODIS dataset has been developed for LSWT (Kheyrollah pour et al. 2012, 2014a) from both Terra and Aqua satellites (the algorithm's details can be found in Kheyrollah Pour et al. 2014a). Both day-time and night-time observations are used to maximize the number of observations. However, there are some limitations using thermal sensors over lakes, especially in late summer and fall when the lakes are covered by cloud cover and thin clouds may not be detected by the cloud mask algorithm. Therefore, additional filtering (the negative temperature values are removed as only open water season was used in this study) is applied to avoid the odd values due to the undetected thin clouds for this study.

5.3 Result

5.3.1 Statistics of satellite-derived LSWT observations

The histogram of LSWT observations in JJA 2010-2011 is shown in Figure 5-2, upper panel. A statistical one-sample t-test was applied to determine if data are normally distributed as it is requeied to estimate a autocorrelation function. It is important to test the normality to prove the homogeneity of data and ensure that data are not influenced by the annual cycle. The details statistics are summarized in Table 5-1. Results show that data are normally distributed in summer (statistically significant at the 0.04 significance level) with a small skewness (= 0.058). In addition, the Q-Q plot (Figure 5-2, lower panel) shows the validity of the distribution assumption for the data based on mean and standard deviation of data. As plot shows, points are falling approximately on a straight line, which supports the normal distribution of the data. As the graph shows, the theoretical distribution fit and data distribution agree and the points fall near the fit line.

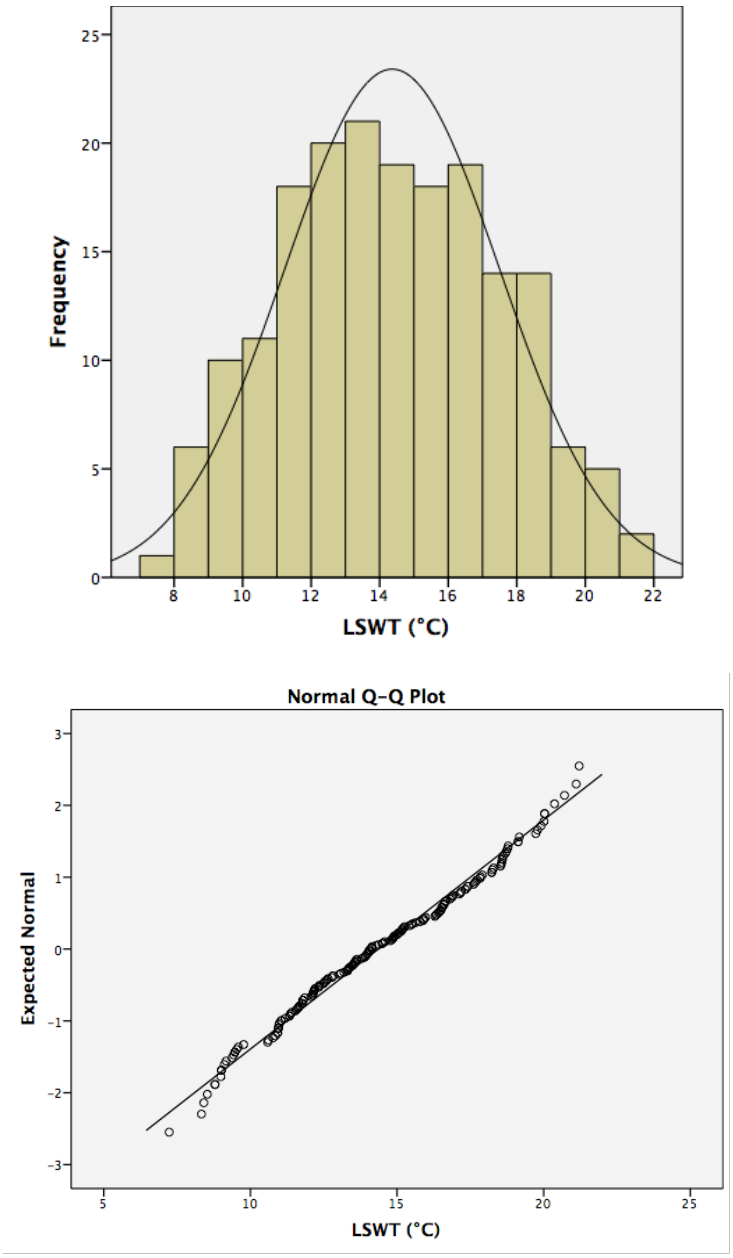

Figure 5.2 Histogram and normal Q-Q plot of MODIS LSWT observations (^{o}C) for JJA 2010-2011.

Table 5-1 Statistics of MODIS LSWT data (^{o}C) in June 2010.

LSTW (°C)-JJA 2010-2011		Statistic	Std. Error
Mean		14.3646	0.23122
95% Confidence Interval for Mean	Lower Bound	13.9084	
	Upper Bound	14.8208	
Sig.		0.04	
Median		14.1000	
Variance		9.837	
Std. Deviation		3.13644	
Minimum		7.23	
Maximum		21.21	
Range		13.98	
Skewness		0.058	0.179

5.3.2 Estimation of the autocorrelation based on LSWT observations

5.3.2.1 Dependency on distance

The LSWT autocorrelation depending on distance between the measurement points was calculated first during three months (JJA) of summer 2010 and 2011. The observations were those derived from MODIS pixels (74 pixels) from 44 lakes. The $b_f(\rho)$ and $m_f(\rho)$ were computed from approach described in section 2.1 (Eq. 5.4 and 5.6) for all observation pairs in 14 different mentioned categories (2701 lake pairs for n=74).

The distribution of points in each distance category is shown in Figure 5-3 for both $b_f(\rho)$ and $m_f(\rho)$. After calculating $b_f(\rho)$ and $m_f(\rho)$ for each lake pair (in each specified distance category) using MODIS-derived LSWT observations, the normalized autocorrelation function is calculated from Eq. 5.11 and 5.12 for each lake pair and an exponential function is derived from the regression of $\tilde{\mu}_f(\rho)$ values against distance.

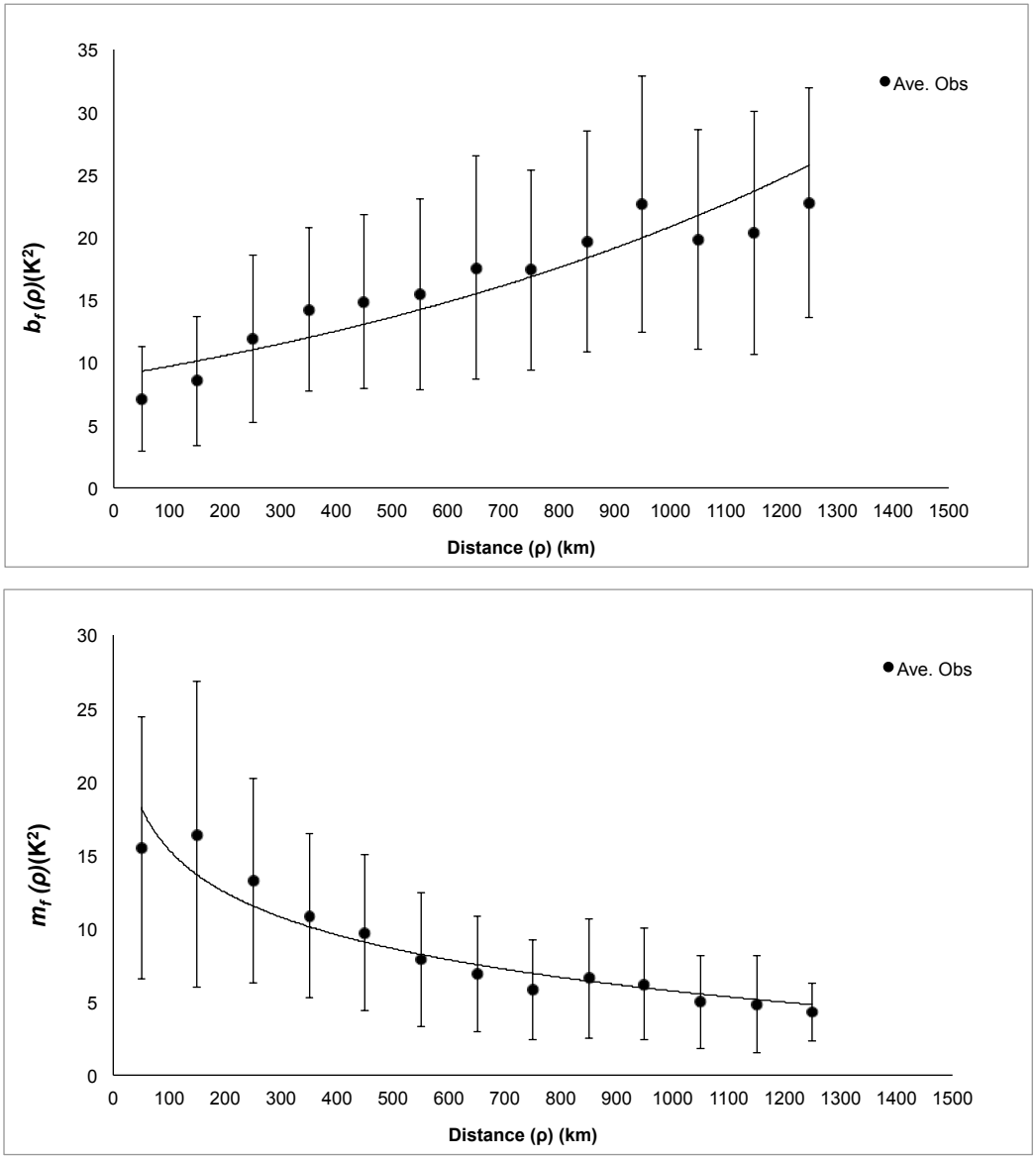

Figure 5.3 The distribution of points in each distance category for (a) the structure function ($b_f(\rho)$) and (b) autocorrelation function ($m_f(\rho)$) and the standard deviations from MODIS LSWT observations pairs for summer (JJA) 2010-2011.

The normalized autocorrelation function is calculated considering observations error for all lake pairs for each category shown in Figure 5-4. The function is approximated as:

$$\tilde{\mu}_f(\rho) = e^{-c\rho} \quad \textbf{5.7}$$

where c_1 is 0.001 km^{-1}.

In the case of the Gaussian function (Eq. 5.13), the correlation for the zero distance is assumed to be one (a perfect correlation). Therefore, based on the estimated function (Eq. 5.14), the best correlation value is calculated for lake pairs with the zero distance (fitting equation in Figure 5-4*)*. Correlations decrease more rapidly for distances of less than 300 km and are smoother for distances above 800 km. It verifies that the correlation magnitude of radius influence is high for distances of less than 300 km and decreases.

To estimate which L_H value in Eq. 5.13 fits best for calculation of autocorrelation relevant for lakes, L_H is plotted with different values (80, 300, 400 and 500 km) in Figure 5-4, together with the autocorrelation calculated from LSWT observations and the calculated values from fitting equation. Based on the results, the candidate radius for the best fit with LSWT observations correlation is selected between 300-500 km. This range of L_H is estimated from LSWT observations during summer. To understand the seasonal behavior of the correlation, $\tilde{\mu}_f(\rho)$ is also calculated during fall (September-October). The results show that the correlation of LSWT of lake pairs is weaker in comparison with summer (not shown) suggesting that data were not normally distributed during fall. As freeze onset on most of the lakes in this region occurs around mid-October, a filter was applied to remove LSWT below zero degrees, which consequently reduced the number of observations. To study the sensitivity of L_H in HIRLAM autocorrelation function, two sets of HIRLAM sensitivity experiments were designed and tested in the next chapter.

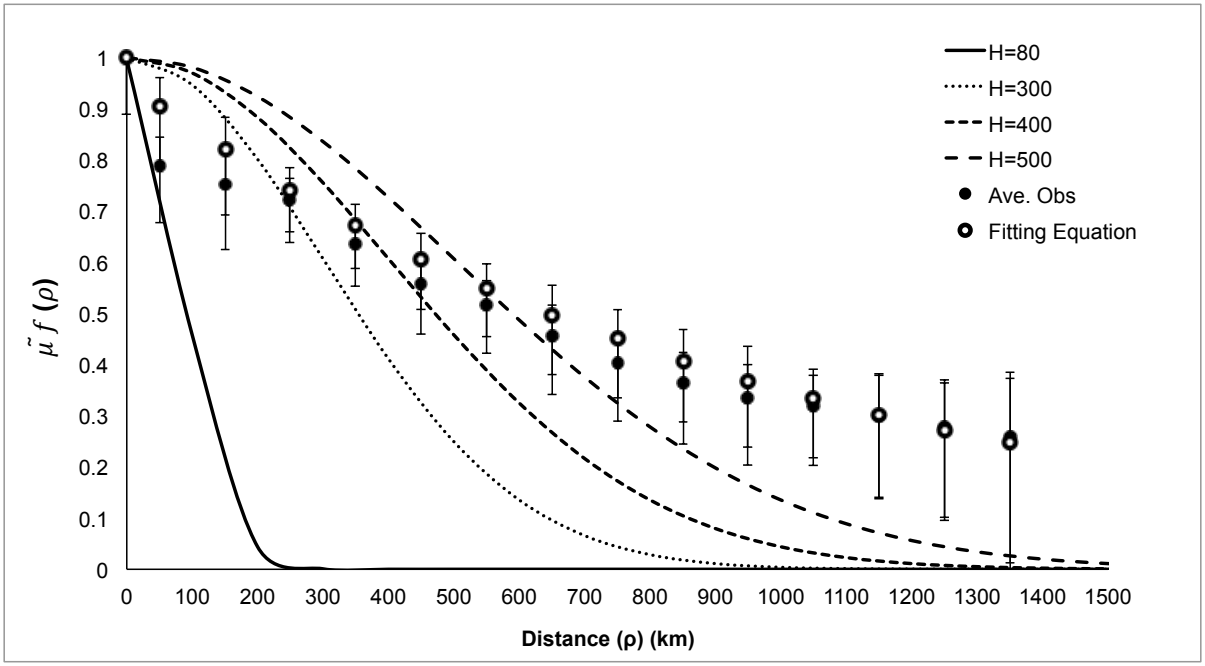

Figure 5.4 The autocorrelations for MODIS LSWT observations pairs for summer (JJA) 2010-2011 in comparison with the default Gaussian autocorrelation (Eq. 5.13) function with different assumed length scale.

5.3.2.2 Dependency on lake depth

The lake depth effect is examined in this section with the hypothesis that the correlation of LSWT of lake pairs decrease when lake depth differences increase. However, the magnitude of the influence of lake depth on correlations should not be as big as distance. The lake depth differences were categorized in 10 m intervals from 0 m (when lake pairs have similar depth) to 50 m shown in different colors in Figure 5-1. Figure 5-5 shows the normalized autocorrelation in all 5 lake depth categories. The magnitude of the influence of lake depth is significantly less than that of distance; however, still conspicuous as shown in Figure 5-6.

Lakes with larger depth differences (30-50 m depth differences) correlate less in comparison to lakes with less depth differences. Figure 5-6 shows that lakes with moderate depth differences (10-30 m depth differences) have a close correlation as lakes with almost the same depth (0-10 m depth differences); however, their correlation is a bit higher in shorter distances. Result from Figure 5-6 confirmed that the larger is the depth differences, the smaller is the autocorrelation. Conversely the

magnitude of differences is not absolutely significant especially for lakes with smaller depth differences (0-30 m), which can be explained by frequency and error of observations.

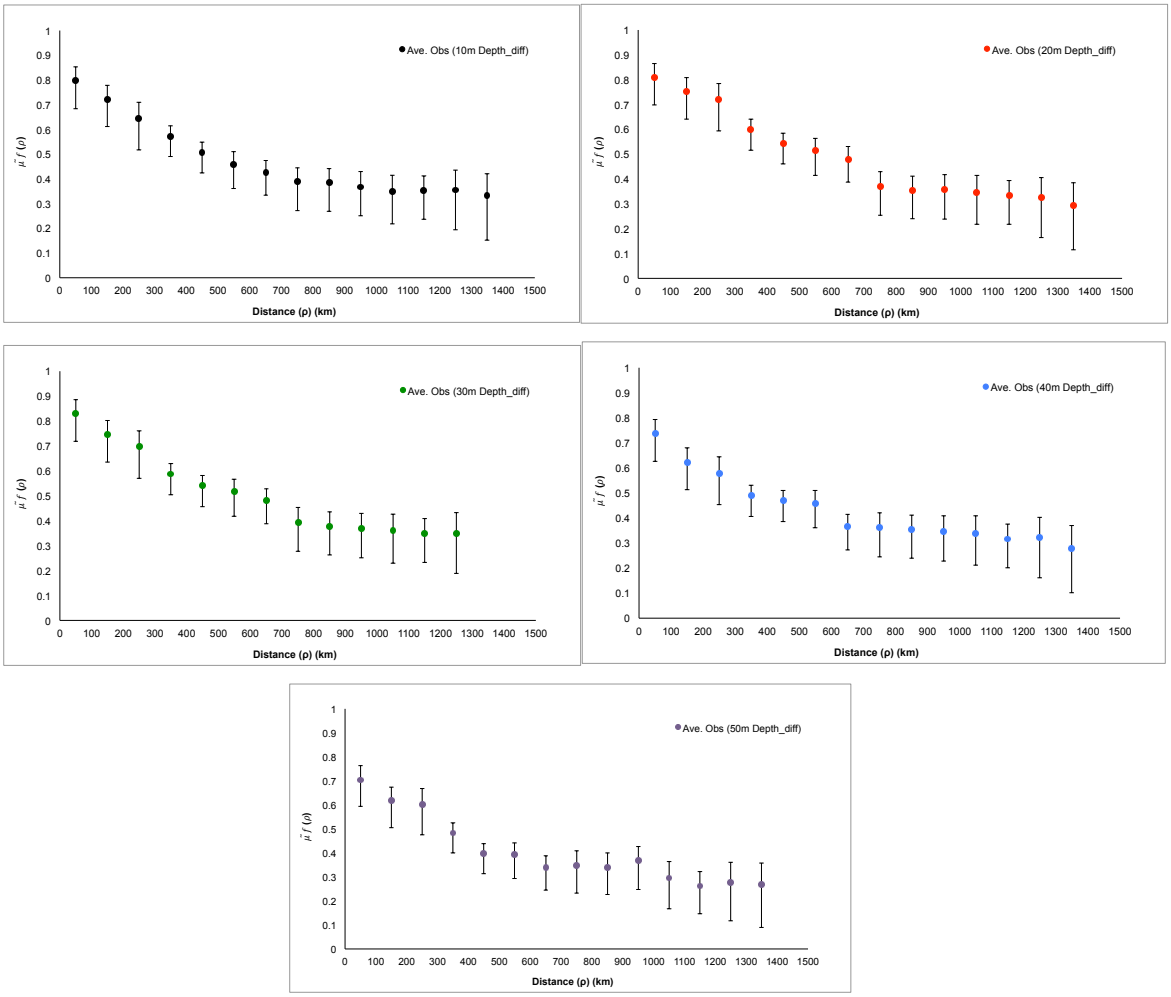

Figure 5.5 The calculated normalized autocorrelation function from MODIS LSWT observations pairs in 5 different lake categories for summer (JJA) 2010 and 2011.

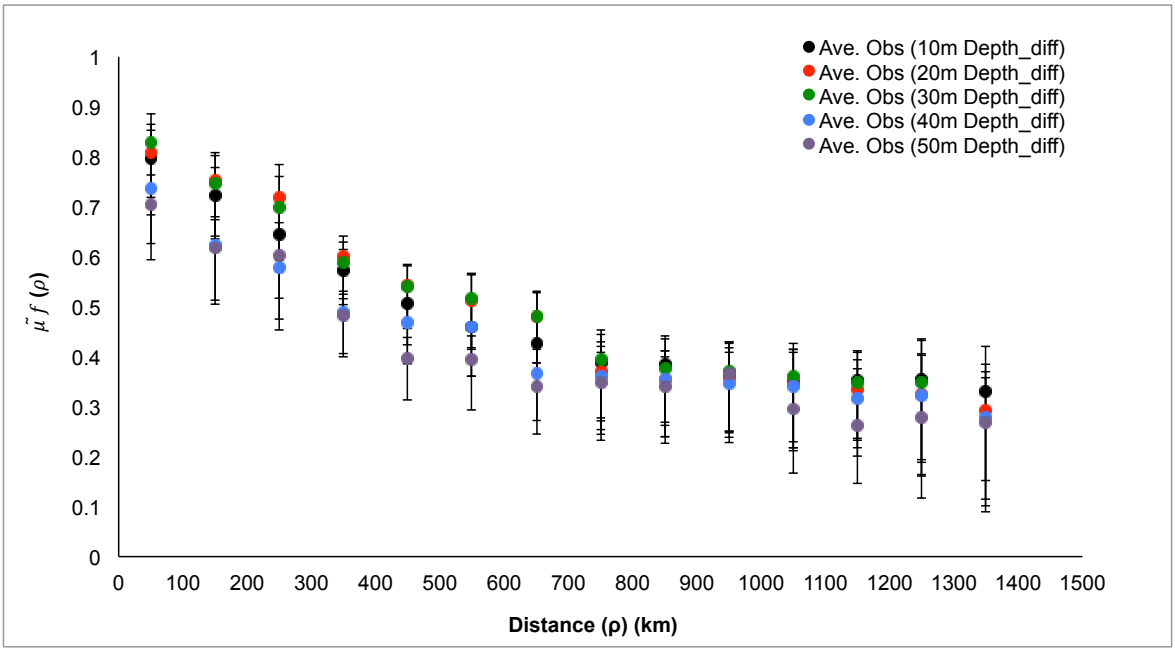

Figure 5.6 The normalized autocorrelation function derived from MODIS LSWT observations in summer (JJA) 2010-2011.

5.4 Sensitivity experiments with HIRLAM

Two sets of HIRLAM sensitivity experiments were designed to test the sensitivity of the LSWT analysis to the selection of observations and application of different autocorrelation functions (Table 5-2). In this experiment, the lake depth differences were not considered. Results were compared to those of experiment NHFLAK (Kheyrollah Pour et al. 2014b). The study period is chosen from the 1st of May to the 31st of August 2011. In the LAKEREF and LAKE300 experiments, only MODIS observations were included into the analysis and SYKE observations (in-situ water temperature observations on 20cm below water) were handed as passive, while NHFLAK contained both SYKE and MODIS observations. The length scale L_H in the autocorrelation function (Eq. 5.13) was given the default value of 80 km in the experiments LAKEREF and NHFLAK, and 300 km in LAKE300. The selection of the L_H of 300 km was based on the preliminary result that LSWT may have larger length scale than the reference value of 80 km.

Comparison between LAKEREF and NHFLAK allows estimating the uncertainty related to the choice of observations while keeping the autocorrelation function fixed. This comparison illustrates

also the properties of the remote sensing and local lake water temperature measurements during summer. It shows how the HIRLAM quality control treats the different observations during the OI analysis. Comparison between LAKE300 and LAKEREF allows understanding the impact of autocorrelation function formulation alone and the passive SYKE observations can be used as independent data for validation.

Table 5-2 Definition of the HIRLAM experiments.

Experiment	Observations	Background	Length scale (km)
LAKEREF	MODIS[2]	FLake+6h[3]	80
LAKE300	MODIS[2]	FLake+6h[3]	300
NHFLAK	SYKE[1] & MODIS[2]	FLake+6h[3]	80

[1]SYKE = Measured LSWT over 27 lakes in Finland; [2]MODIS = MODIS observations in 70 pixels; [3]FLake+6h = Freshwater Lake Model parameterizations within HIRLAM, 6h-forecast

The setup of the sensitivity experiments was similar to that described by Kheyrollah Pour et al. (2014b). All experiments were run in the framework of HIRLAM version 7.4 (wwww.hirlam.org). This HIRLAM version incorporates fully integrated FLake model (Rontu et al. 2012), which provided the background for LSWT analysis in all three experiments. The lateral boundary conditions for the atmospheric model were provided by the fields of the European Centre for Medium-Range Weather Forecasts (ECMWF) analysis. Only the surface data assimilation was applied in the sensitivity experiments LAKEREF and LAKE300, where the upper air analysis was replaced by the interpolation of the ECMWF analysis in the sensitivity experiments. In the baseline experiment NHFLAK, three-dimensional variational data assimilation was applied for upper air analysis.

Figure 5-7 shows an example of time-series of the analyzed LSWT for July 2011 by the three experiments for four different lake locations: a) medium size lake where both MODIS and SYKE observations are available for assimilation (Lappajärvi, SYKE 23.67°E, 63.15°N; MODIS 23.6983°E 63.2204, b) a large lake with only MODIS observations available (Ladoga, MODIS pixel 30.939°E, 60.818°N in the central western part of the lake), c) a small lake with only SYKE observations available (Kuivajärvi, 23.86°E, 60.79°N), d) a small lake in the Eastern Finland with no own observations (Kolkonjärvi, 28.144°E, 62.004°N).

In all cases, the comparison shows that the differences between the experiments LAKEREF and LAKE300 is minor in comparison with the difference between them and NHFLAK. This is due to the

different selection of observations entering the experiments: only MODIS for the sensitivity experiments, both MODIS and SYKE for NHFLAK. The impact of the different formulation of the autocorrelation function is largest at Lake Ladoga, where it may reach ca. 0.5 ^{o}C. At Lake Ladoga, the typical difference between NHFLAK and the sensitivity experiments is less than one degree. At the other lakes shown this difference is up to two degrees. This is because only MODIS observations were available over Lake Ladoga in all three experiments while over the other lakes also SYKE observations influenced the result of NHFLAK.

Another feature shown by this example is the quite large difference between the observed and analyzed values. Figure 5-8 shows another view to the Lake Lappajärvi analysis and observation usage for the experiments LAKE300 (MODIS only) and NHFLAK (MODIS + SYKE). In LAKE300 (also in NHFLAK for the MODIS observation location, not shown) the MODIS observations are less frequently available and show much more variability than the SYKE observations. Consequently, a significant part of the MODIS observations are rejected by the HIRLAM quality control before the actual LSWT analysis (Figure 5-8, top panel). In this case, all rejections were done by the test against background, not by the OI quality control against nearby observations. There are no rejections in the case of SYKE observations (Figure 5-8, bottom panel). In both cases, the resulting analysis seems to be dominated by the background, i.e. by the FLake short forecast but the more abundant and consistent SYKE observations are able to influence the result more than the MODIS observations. Note that SYKE and MODIS observations are not representing exactly the same temperature. MODIS measures skin temperature of lakes' surface while SYKE measurements represent water temperature at a depth of 20 cm below the water surface.

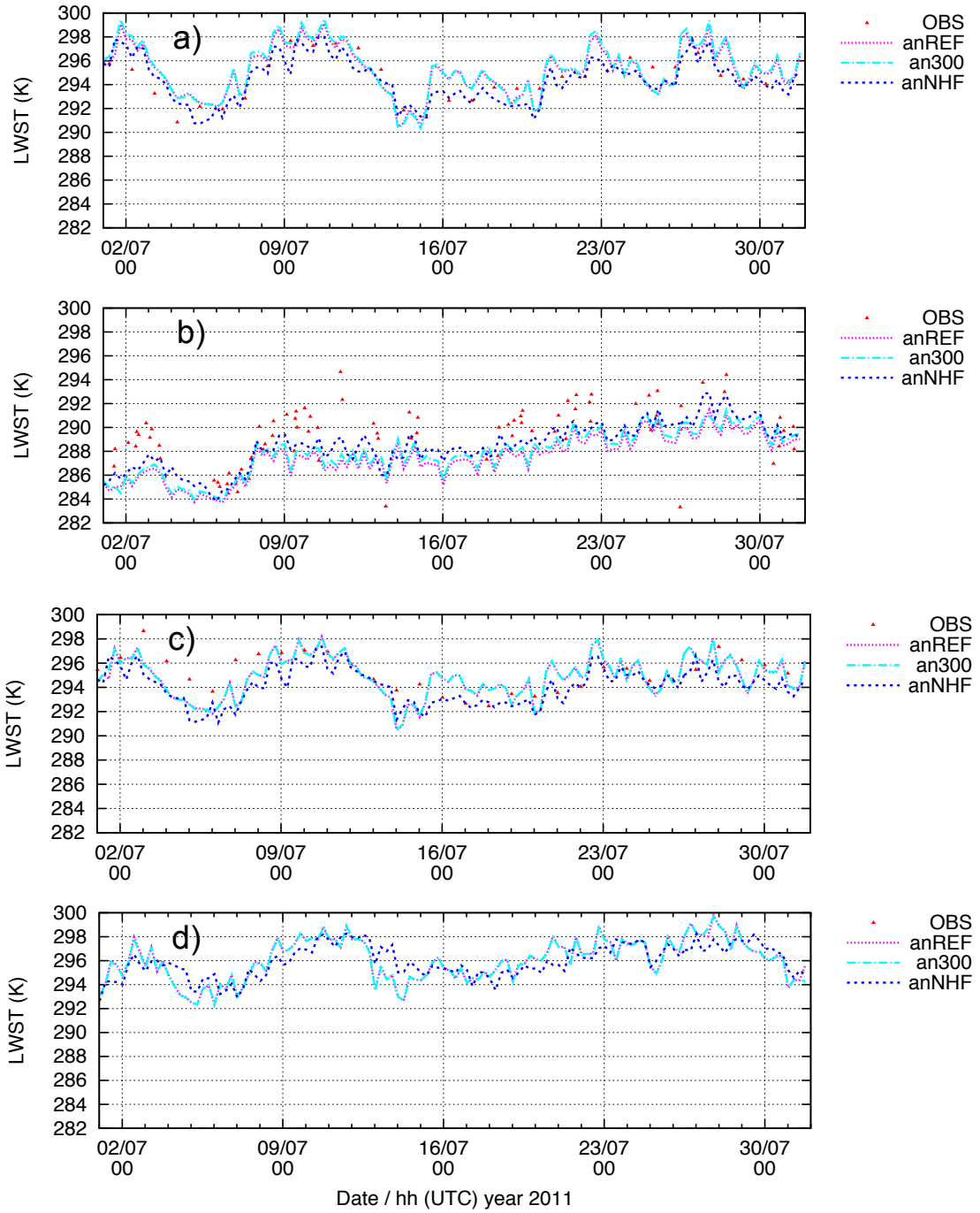

Figure 5.7 Analyzed by the experiments LAKEREF (anREF), LAKE300 (an300) and NHFLAK (anNHF) LSWT (K) over four lakes: (a) Lappajärvi, (b) Ladoga western pixel, (c) Kuivajärvi, and (d) Kolkonjärvi. The red dots show observations by SYKE in (a) and (c), by MODIS in (b). There are no observations in (d). In (b), original MODIS observations before HIRLAM quality control are shown.

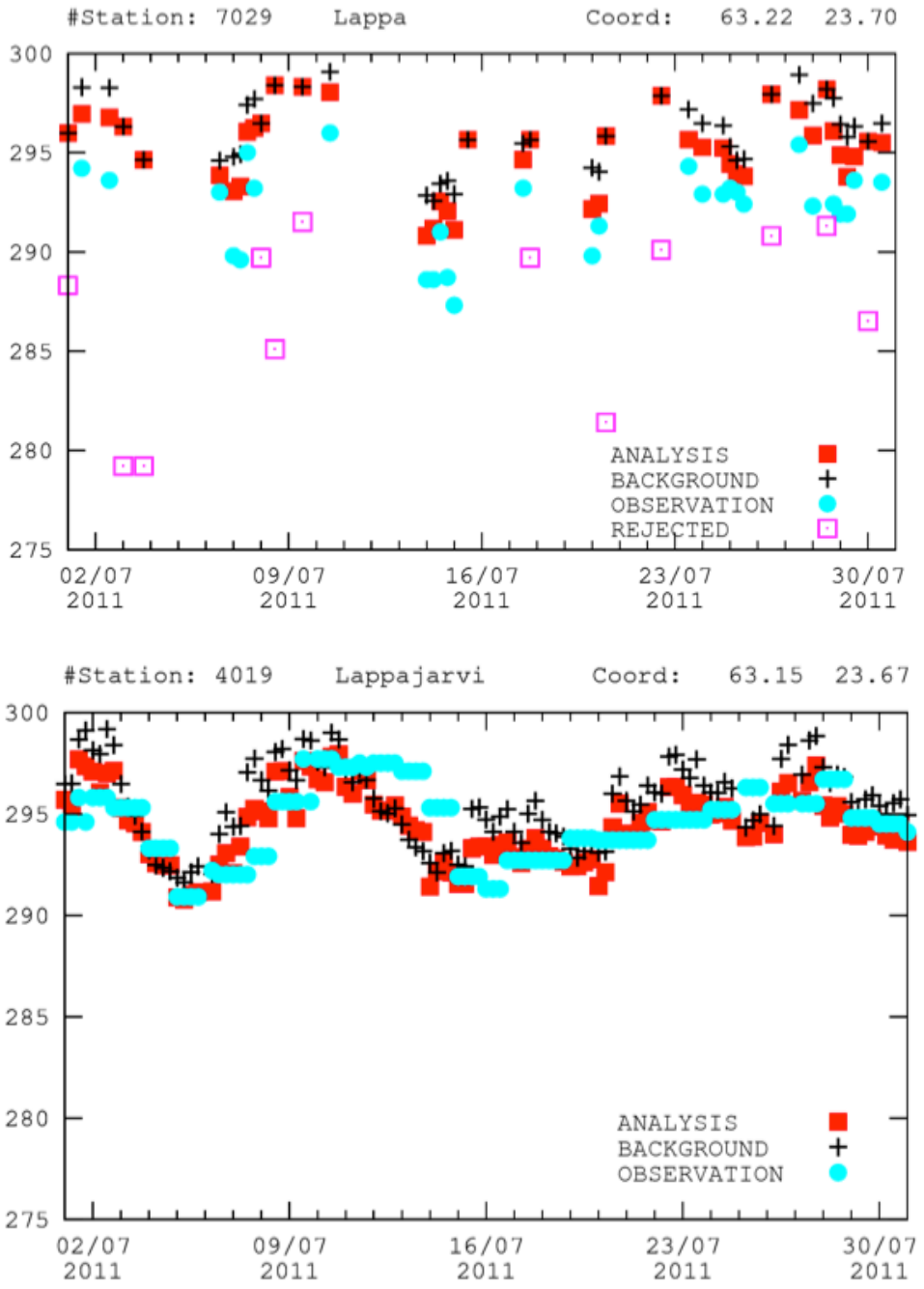

Figure 5.8 Analysis, background, used and rejected LSWT observations for the locations of MODIS (top panel) and SYKE measurement (bottom panel) at lake Lappajärvi, June 2011. Legend is included in the figures.

In the experiments LAKEREF and LAKE300, SYKE observations were imported to HIRLAM as passive observations, i.e. excluded from the analysis but included in the quality control and available for validation. Figures 5-9a and b compare the maps of available and rejected MODIS observations versus the potentially available SYKE observations on one of the days when MODIS observations were rejected at Lake Lappajärvi. The comparison shows that MODIS observations were rejected by the background test over a large area over western Finland while the more homogeneous SYKE observations would have covered the whole country. The analysis based on MODIS and FLake was up to five degrees warmer than indicated by the SYKE observations, while in the NHFLAK the corresponding difference was about half of this (not shown).

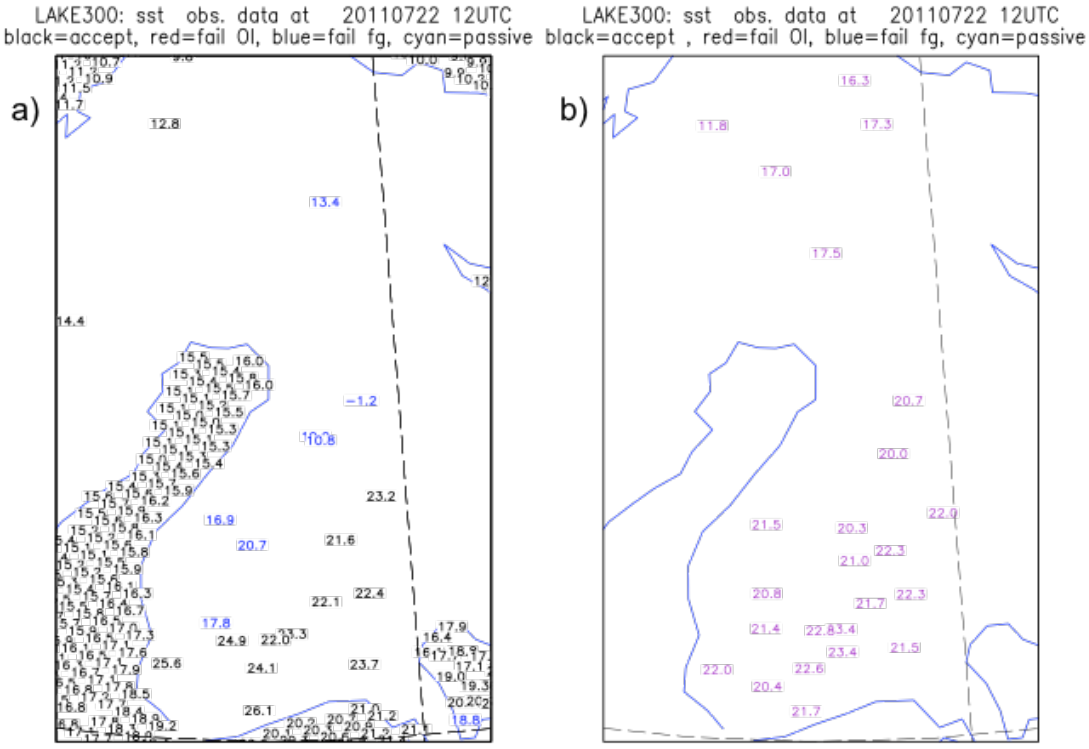

Figure 5.9 Map of a) used (black) and rejected by the background check (blue) of MODIS observations in the experiment, and b) potentially available SYKE observations (cyan) in the experiment LAKE300 at 12UTC 22th July 2011. The color code is also given in the title of the figures.

5.5 Summary and outlook

This study investigated for the first time an approach for calculating the autocorrelation function derived from satellite-based LSWT observations. MODIS LSWT observations were derived for 44 Scandinavian lakes (74 pixels) within the HIRLAM domain in two summers (JJA) 2010 and 2011. The current autocorrelation function used in HIRLAM is not based on observations and is generated for SST and consequently the length scale ($L_H = 80$ km) is set to work properly for SST. Moreover, the function has been developed depending only on distance between lakes. Here, we estimated the autocorrelation function based on observations not only dependent on horizontal distance but also accounting for lake depth differences for each lake pair. The estimated length scale calculated from observations would be between 300 and 500 km. In addition, LSWT may be correlated between different lakes only due to the similar surface energy balance in similar weather conditions, i.e. only via the atmosphere and air-water interaction. Within the same (large) lake, also horizontal and vertical mixing connects the temperatures in a similar way as in sea. There is no reason why the statistical properties of lake and sea temperatures should be generally similar.

Autocorrelation functions were also estimated for 5 depth categories in summer (JJA) when lakes were free of snow and ice. Results based on LSWT observations show that the autocorrelation function is distance as well as lake depth differences dependence. The same result was obtained for fall when autocorrelation function was estimated for September-October; however, the correlation of LSWT of lake pairs was weaker than in summer. The number of observations used in fall to calculate the autocorrelation function was significantly less than the number of observations used in summer due to the increase of number of days with cloud cover. Moreover, data were filtered when temperatures were below zero in order to remove possible snow/ice cover temperature measurements, knowing that most of the lakes in this area start freezing around mid-October.

Two sets of HIRLAM sensitivity experiments were designed and run for a preliminary assessment of the sensitivity of the LSWT analysis to the selection of observations and application of different autocorrelation functions with default (80 km) and a new length scale (300 km). These preliminary examples suggest that the resulting LSWT analysis in HIRLAM is not highly sensitive to the formulation of the autocorrelation function of OI. This is true at least in the conditions where the background (short forecast) dominates over the highly variable and sparse MODIS observations. The quality control by OI is in practice rarely applied in HIRLAM LSWT analysis due to the preliminary

quality control by first guess, which already removes the unreliable observations from the analysis. Thus the autocorrelation function may not influence the selection of observations.

The impact of the autocorrelation was the largest for large lakes, with a good coverage of satellite LSWT measurements availability, which suggests future examination of the effect of a stand-alone OI system (like OSTIA) that focuses on large lakes and derives the background from the previous analysis cycle instead of the short forecast by the model. These results also suggest that the in-situ observations (like SYKE) can improve the result (for example repeating the analysis using 5-years of SYKE observations); however, they may not be available in real-time.

This study was the first step toward improving the autocorrelation function used in analysis of LSWT by using satellite observations. Remote sensing provides data with a spatial coverage better than in-situ measurements. The combination of more years of data and checking the quality of data in a more systematic approach before feeding into the autocorrelation calculation could be an option for future improvement of lake surface state in NWP models. Moreover, combining different satellite observations such as VIIRS (the Visible Infrared Imaging Radometer Suite on the Suomi-NPP satellite) or EUMETSAT's MetOp-AVHRR (the Advanced Very High Resolution Radiometer on board of MetOp-A, B, and C) could be another option for future improvement. ESA's Sentinel-3 will provide atmospheric and land applications with multiple sensing instruments such as SLSTR (Sea and Land Surface Temperature Radiometer) to monitor LSWT. The thermal sensors on Sentinal-3A and 3B with 1 km resolution will allow for continuity of LSWT observations on a daily revisit time. Sentinel-3A is scheduled for launch in 2015 and Sentinel- 3B is planned for launch ~18 months after. The Global Change Observation Mission (GCOM) is an observation program of the Japanese Aerospace Exploration Agency (JAXA), which is planned for launch in 2016 and will carry the Second-generation Global Imager (SGLI) sensor which will provide thermal data at a spatial resolution of 500 m.

The results suggest an adaptation of HIRLAM's autocorrelation function for lakes by increasing the influence radius; on the other hand, it is important to note that this function is calculated only during summer. Seasonal changes should be taken into account when calculating the autocorrelation function in the future. Results further indicate that lake depth has to be considered in the function, however a future investigation is needed to identify more thoroughly the lake depth effect. A

systematic exploration of this method, especially for lake depth and size, is needed in order to improvement the autocorrelation function suitable for lakes in NWP models.

Chapter 6
General Conclusion

6.1 Overall summary

The overall aim of this research was to demonstrate the benefits of assimilating space-borne LSWT observations into a weather forecasting system such as HIRLAM model. There is a variety of users and applications of space-borne observations in NWP systems; however, not much attention has been paid on the assimilation of satellite derived LSWT observations in pre-operational NWP models for improvement of the weather forecast. A correct description of the lake surface state started to be relevant in NWP models when the horizontal resolution of models became high enough to resolve lakes, even the smaller ones. Here, we showed how retrieved remotely-sensed LSWT observations can improve lake surface state in HIRLAM, therefore, improve the forecast results such as 2-m air temperature and cloud cover. This work is not only a contribution to lake satellite observation studies involving optimization of the analysis methods using data assimilation in a NWP model, but also extends to mathematical aspect of the optimal interpolation assimilation using LSWT data. The research context (Chapter 2) provided an overview of the evolution of NWP models from subjective to object analysis using mathematical or statistical models. In that chapter, the term data assimilation and the technique of statistical interpolation were discussed. The chapter also reviewed the representation of lakes in the HIRLAM system, and available satellite-based observations for lake studies.

The accuracy of the satellite observations used in this work was assessed in Chapter 3 prior to performing data assimilation experiments (Chapter 4), showing that incorrect observations can have a negative influence that can spread over a large area in the model, and potentially affect the entire model solution. Results revealed a good agreement between daily-averaged UW-L3 MODIS-Aqua/Terra data and in-situ observations for the 22 lakes examined with an overall average bias of ~ -1 ˚C. The quality control of the observations also was performed prior to the actual analysis in NWP models in two consequent phases: first observations were tested against the background, and then each observation was compared to the surrounding observations, which was discussed in Chapter 4.

A correct description of lakes surface state such as LSWT and ice cover is essential during freezing and melting of lakes as the surface radiative and conductive properties as well as latent and sensible heat released from lakes to the atmosphere change dramatically, leading to a completely different surface energy balance. Introduction of space-borne observations led to an improvement of the description of surface state during the melting period, when in-situ observations were not yet available and the prognostic lake parameterization suffered from a significant warm bias.

Improvement of the operational analysis of remote-sensing LSWT measurements in NWP models requires development of OI methods. Derivation of an autocorrelation function, which takes into account lake depth as well as calculation of observation error statistics of different measurement types, was presented in Chapter 5. The autocorrelation function determines the weights for the individual observations in the analysis and quality control by OI. The length scale of the autocorrelation function determines from how large an area around each point the observations are allowed to influence. In the current version of HIRLAM, the autocorrelation function, represented in the form of an exponential function, depends on the distance and was generated for SST. The influence radius is set to work properly for SST. The autocorrelation function and influence radius specific for lakes was approximated directly from LSWT observations and illustrated a larger radius for lakes in comparison with the default value. The HIRLAM sensitivity experiments with adjusted radius showed quite large differences between the observed and analyzed values for large lakes and they are more sensitive to the impact of the autocorrelation function.

Overall, this thesis has shown the utility of optical sensors for monitoring LSWT and ice cover on lakes and those space-borne LSWT observations are beneficial for the description of lake surface state in HIRLAM. Satellite observations provide frequent observations over large areas. The large spatial coverage of satellite-based data at moderate resolution is a major advantage but when compared to in-situ measurements.

6.2 Limitations

Despite the advantages of using optical sensors for monitoring LSWT and ice cover, there are some limitations, especially in the fall and early winter when lakes are often covered with cloud. Data from optical sensors may not be updated for several days or, on occasion, clouds may not be detected by

the algorithm, resulting in anomalous errors and lowering the temporal coverage of sensors. Therefore, upgrading the cloud cover algorithm is necessary to improve the optical sensors' abilities to observe the Earth's surface. Optical sensors are also limited by fluctuations in atmospheric conditions, calibration differences of sensors or by prolonged darkness or low sun elevation at northern latitudes, which can cause over- or under-estimation of ice formation and melt onset dates.

Regarding assimilation of remote-sensing LSWT observations in HIRLAM, pre-defined pixels were selected over various lakes; however, significantly more data were potentially available from satellites, which still remain unused. By using the relatively fine-resolution land cover information available in the NWP model, it is possible to classify if a satellite pixel (with known coordinates) is located over a lake resolved by the model. Thus, it would be possible to utilize near-real time satellite LSWT/ice cover observations without pre-selection of pixels.

Finally, toward improving the current version of HIRLAM's autocorrelation function it has been found that the number of observations is not satisfactory. The number of observations has a significant influence on the accurate estimation of a autocorrelation function. Remote sensing provides data with a good spatial coverage, however, observations derived from satellite sensors are limited to the overpass time in comparison with in-situ observations. In-situ observations can provide more frequent data but they are rarely available and limited in area. Therefore, combination of various sensors and in-situ observations would be the best solution considering the error of each observing system.

6.3 Future Directions

There is a great potential for future research regarding satellite remote sensing of lake surface temperature. Optical sensors provide data with moderate spatial and temporal resolutions, which allows the Earth's surface to be covered in a high frequency of acquisition.

For operational NWP models, the analysis of the transient surface properties is crucial, but handling of the observational data and computations should be highly optimized in order to allow timely production of the full three-dimensional weather forecast. Input information should be processed without manual intervention, but well enough to allow only reliable observations to influence the analysis.

Presently, the analyzed state of the lake surface creates no feedback to the FLake parameterization in HIRLAM, which is coupled to the atmospheric model during the forecast run. Thus, the improved LSWT analysis remains as a possibly useful independent by-product of the NWP model. In order to really utilize the space-borne and in-situ observations on lake surface state for the improvement of the weather forecast and prediction of lake temperatures, methods to connect the analyzed LSWT and ice cover to the prognostic in-lake variables are needed. Such methods for NWP models are currently under development.

Finally, in order to fully improve the autocorrelation function suitable for lakes in NWP models, more work is needed. An interesting research avenue is the systematic exploration of this method, especially for lake depth, elevation, and size.

Appendix A

Evolution of snow and ice temperature, thickness and energy balance in Lake Orajärvi, northern Finland

Bin Cheng[1], Timo Vihma[1], Laura Rontu[1], Anna Kontu[1], Homa Kheyrollah Pour[2], Claude Duguay[2] and Jouni Pulliainen[1]

[1] Finnish Meteorological Institute
[2] Interdisciplinary Centre on Climate Change and Department of Geography & Environmental Management, University of Waterloo, Waterloo, Canada

Abstract

The seasonal evolution of snow and ice on Lake Orajärvi, northern Finland, was investigated for three consecutive winter seasons. Material consisting of numerical weather prediction model (HIRLAM) output, weather station observations, manual snow and ice observations, high spatial resolution snow and ice temperatures from ice mass balance buoys (SIMB), and Moderate Resolution Imaging Spectroradiometer (MODIS) lake ice surface temperature observations was gathered. A snow/ice model (HIGHTSI) was applied to simulate the evolution of the snow and ice surface energy balance, temperature profiles, and thickness. The weather conditions in early winter were found critical in determining the seasonal evolution of the thickness of lake ice and snow. During the winter season (Nov. – Apr.), precipitation, longwave radiative flux, and air temperature showed large inter-annual variations. The uncertainty in snow/ice model simulations originating from precipitation was investigated. The contribution of snow to ice transformation was vital for the total lake ice thickness. At the seasonal time scale, the ice bottom growth was 50 – 70 % of the total ice growth. The SIMB is suitable for monitoring snow and ice temperatures and thicknesses. The Mean Bias Error (MBE) between the SIMB and borehole measurements was -0.7 cm for snow thicknesses and 1.7 cm for ice thickness. The temporal evolution of MODIS surface temperature (three seasons) agrees well with SIMB and HIGHTSI results (correlation coefficient, R=0.81). The HIGHTSI surface temperatures were, however, higher (2.8 °C ≤ MBE ≤ 3.9 °C) than the MODIS observations. The development of HIRLAM by increasing its horizontal and vertical resolution and including a lake parameterization

scheme improved the atmospheric forcing for HIGHTSI, especially the relative humidity and solar radiation. Challenges remain in accurate simulation of snowfall events and total precipitation.

1 Introduction

Lake ice cover has wide ranging impacts on hydrology (Walsh et al., 2005), lake biology and ecology (Prowse and Brown, 2010), local weather and climate (Rouse et al., 2008; Brown and Duguay, 2010), recreation, and transportation. Lake ice is also a sensitive indicator of climate change (e.g., Brown and Duguay, 2010). During the last decades, climate warming has been more significant at high latitudes than over other regions of the globe, and this has caused remarkable decreases in lake ice thickness (Surdu et al., 2014) and phenology (freeze-up and break-up dates, and ice cover duration). According to Prowse et al., (2011), long-term observational records (from 1840s to 2005) for the Northern Hemisphere show that freeze-up (ice-on) dates have been occurring later by 10.7 d / 100 years and break-up earlier by 8.8 d/100 years. According to climate model scenarios, lake ice will decline at an even faster rate during the next 100 years (e.g. Brown and Duguay, 2011).

The processes controlling lake ice thickening are the energy balance at the snow surface (or bare ice surface, if there is no snow on top of ice), energy balance at the ice bottom, heat conduction through ice and snow, penetration of shortwave radiation into snow and ice, as well as formation of snow ice and superimposed ice. From the point of view of modelling, all these processes include uncertainties. Considering the surface energy balance, downward longwave radiation is a challenge for models particularly at high latitudes due to the common presence of mixed-phase clouds and strong temperature and humidity inversions (Tjernström et al., 2008). Downward solar radiation is also very sensitive to cloud cover and cloud properties, and a good parameterization of surface albedo is a major challenge (Pirazzini, 2009). Furthermore, the modelled near-surface temperature, humidity, wind speed, and the turbulent fluxes of sensible and latent heat often have large errors over snow and ice surfaces, where stable stratification prevails (Atlaskin and Vihma, 2012). The energy balance at the ice bottom controls the bottom growth and melt of ice: if the upward conductive heat flux in the ice exceeds the heat flux from the lake water to ice bottom, the ice grows. Due to very limited number of observations on the heat fluxes at the ice bottom, the model parameterizations are not on a solid basis. The ice growth is, however, not only due to bottom growth. In addition, superimposed ice may form, typically at the snow-ice interface, due to refreezing of surface melt water or rain, and snow ice

may form due to refreezing of flooding slush on the ice surface (Semmler et al., 2012). According to Archimedes Law, snow ice formation takes place when the snow mass is large enough to depress the ice below its hydrostatic water level. To better understand the physical processes involved in snow and ice mass balance in lakes, we need to carry out more research on the modelling of lake ice thermodynamics.

Precipitation is an essential process for lake ice thickening, as it strongly affects the surface albedo, snow thickness, and formation of superimposed ice and snow ice. Snowfall usually increases surface albedo, but rain strongly reduces it. Accumulation of snow insulates the lake ice from the atmosphere, and controls the formation of the snow ice and ice growth rate (Morris et al., 2005). Several studies have, however, revealed that climate and numerical weather prediction (NWP) models as well as atmospheric reanalyses have large uncertainties in both the amount and phase of precipitation at high latitudes (Bosilovich et al., 2008; Jakobson and Vihma, 2010). The accuracy of modelled precipitation is usually not known, as precipitation measurements at high-latitudes are sparse. Furthermore, the spatial distribution of snow thickness is often strongly affected by re-distribution of snow by wind (Duguay et al., 2003; Leonard and Maksym, 2011). The climate modelling community has started to take this process into account for ice sheets (Lenaerts and van den Broeke, 2012) but, to our knowledge, not in a lake environment.

Besides the importance of atmospheric forcing on lake ice, the lake ice cover information is, in turn, important for weather and climate locally. Lakes affect the air temperature: in autumn, winter, and spring, the effect strongly depends on the presence of lake ice (e.g. Brown and Duguay, 2010). In addition, lake-induced snowfall is common in winter over and downwind of large open lakes, for example the North American Great Lakes (Niziol, 1987) and Lake Ladoga. The occurrence and amount of snowfall is very sensitive to the existence of lake ice (Wright et al., 2013). Recently, the parameterization of lake ice thickness, temperature and snow cover on ice in NWP models has also received increased attention, along with development of assimilation methods for lake water surface temperature and ice cover observations (e.g. Eerola et al., 2010; Rontu et al., 2012).

The evaluation and further improvement of lake ice models is dependent on the availability of accurate observations. Although the freeze-up and break-up of ice in large lakes can be monitored reasonably well via satellite remote sensing (Duguay et al., 2012, 2013), similar success has yet to be achieved in the estimation of snow thickness on lake ice. Limited success has been obtained,

however, in the estimation of lake ice thickness for very large lakes on the basis of satellite passive microwave observations (Kang et al., 2010) as well as in the estimation of the temperature of lake ice and the overlying snow cover from thermal remote sensing (Kheyrollah Pour et al., 2012). Furthermore, over the past two decades the number of in-situ ice observations has significantly decreased (e.g. Duguay et al., 2006; Prowse et al., 2011). This calls for the development of novel approaches for measuring or estimating the thickness of lake ice and snow on-ice as well as their temperature regime.

In this paper, we simulated the seasonal evolution of lake ice and its snowpack on Lake Orajärvi, in Sodankylä, Finnish Lapland. We applied a high-resolution thermodynamic snow/ice model, forced in various experiments with in-situ observations and the NWP model HIRLAM (High-Resolution Limited-Area Model). The snow/ice model results were compared against buoy observations on snow and ice mass balance and temperature profiles, as well as satellite observations of Lake Ice/Snow Surface Temperature (LIST). Our objectives are to: (1) investigate the performance of a new prototype snow/ice mass-balance buoy in over-winter measurements on a boreal lake; (2) understand how snow and ice mass balance responds to atmospheric forcing during three different winters (among others, what is the relative importance of inter-annual variability in precipitation and the energy fluxes melting snow and ice, and how the temporal evolution of these variables affects the observed and modelled snow and ice mass balance); and (3) identify the main sources of uncertainty in modelling the seasonal evolution of lake ice.

2 Study area and observations

2.1 Research site

Lake Orajärvi (67.36N, 26.83E) is located in Sodankylä about 8 km east from the Finnish Meteorological Institute (FMI) Arctic Research Centre, some 120 km north of the Arctic Circle (Fig. A.1). The surface area of the lake is 11 km^2. The average water depth is 4.4 m and maximum depth is 11 m. The ice season lasts 6 -7 months (from November/December to May/June), and the maximum ice thickness usually reaches more than 50 cm in late April, just before the onset of ice melt. Snow is present on the ice surface every winter season but its spatial distribution is variable across the lake.

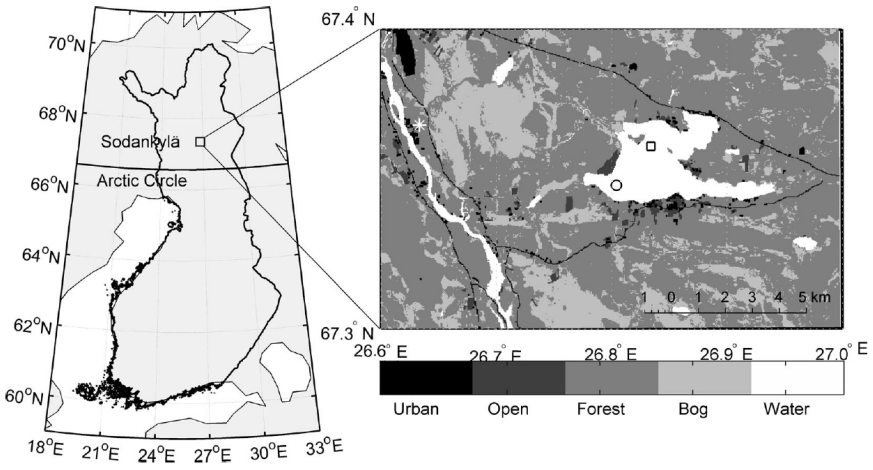

Figure A.1 Geography map of lake Orajärvi in Sodankylä. The symbols in right panel: ○: regular snow and ice thicknesses measurement site; □: SIMB site and, *: Sodankylä weather station.

2.2 Manual measurements

Snow and ice thicknesses have been measured on Lake Orajärvi since the winter season 2009/2010. The measurements are made every second week when the ice is thick enough (for safety reasons), usually through November to April, at approximately the same three sites on the lake. The measurement sites are located at a distance of 400 m from the closest shore and 200 m from a snow mobile route crossing the middle of the lake (Fig. A.1. The measured variables are snow and ice thickness (total ice and granular ice), freeboard (the height difference between the ice surface and the water level) and ice layering. The measurements follow the standard procedures of the Finnish Environmental Institute. In addition, a snow pit with profiles of snow grain size, temperature, density, and layer structure is recorded at one of the three sites each time.

When ice is formed but still thin, heavy snowfall events may result in flooding, formation of a slush layer, and re-freezing to snow-ice. However, if the early winter is very cold and ice gets thick rapidly, the snow load may not be heavy enough to create slush, and the insulation effect of snow will reduce the ice growth from the ice bottom. To fully detect these processes, one would need to install a monitoring system, initially in the open water, to measure the ice formation and growth as well as snow accumulation. Unfortunately, such a system is not yet available.

The snow and ice thickness showed striking inter-annual differences in early winter compared to those in later spring (Fig. A.2). For example, the ice thickness was 24 cm, 39 cm and 14 cm in early December, i.e. Julian day (JD) 341 (7 Dec), JD 343 (9 Dec) and JD 342 (8 Dec) in 2009, 2010 and 2011, respectively, and the corresponding snow thickness was 5 cm, 14 cm and 6 cm, respectively.

In winter 2010/2011, the thicker ice in the early winter season was most probably formed due to the combined effects of lack of snowfall and very low temperatures during the early winter. These three winter seasons demonstrated that once the freeboard is negative (flooding), it is followed by an increase in ice thickness due to snow-ice formation. In mid-winter, the decrease in snow thickness is correlated with an increase in ice thickness. The ice thickness reaches its maximum value toward the end of the season (late April) before melt starts.

Unfortunately, we have in-situ observations neither on ice thickness during the melting seasons nor on the break-up dates in Lake Orajärvi. The break-up dates observed by the Finnish Environmental Institute on Lake Unari, located some 50 km southwest of Lake Orajärvi, are JD 507 (22 May), JD 505 (20 May) and JD 510 (25 May) for these winter seasons, respectively (shown in Fig. A.7 as a reference). The area of Lake Unari is 29 km^2, almost three times that of Orajärvi, but there is a large island in the middle and many small inlets. The maximum water depth is 20 m for Lake Unari and 11 m for Lake Orajärvi, but the average depth of the two lakes is the same within 1 m.

2.3 Buoy observations

In order to make long term sustainable snow and ice measurements, a prototype ice mass balance buoy developed by the Scottish Association for Marine Science (SAMS) was tested in winters 2009/2010 and 2011/2012. The SAMS Ice Mass Balance Buoy (SIMB) consists of a high-resolution ice thermistor chain (2 cm sensor interval with a total of 240 sensors); data logger compartment; a GPS and iridium data transmission board; flush memory data card and high-capacity alkaline batteries. The SIMB measures the vertical temperature profile from water through ice and snow up to the air. In addition, the SIMB is equipped with heating elements to run a 1-2 minute long heating cycle mode once a day.

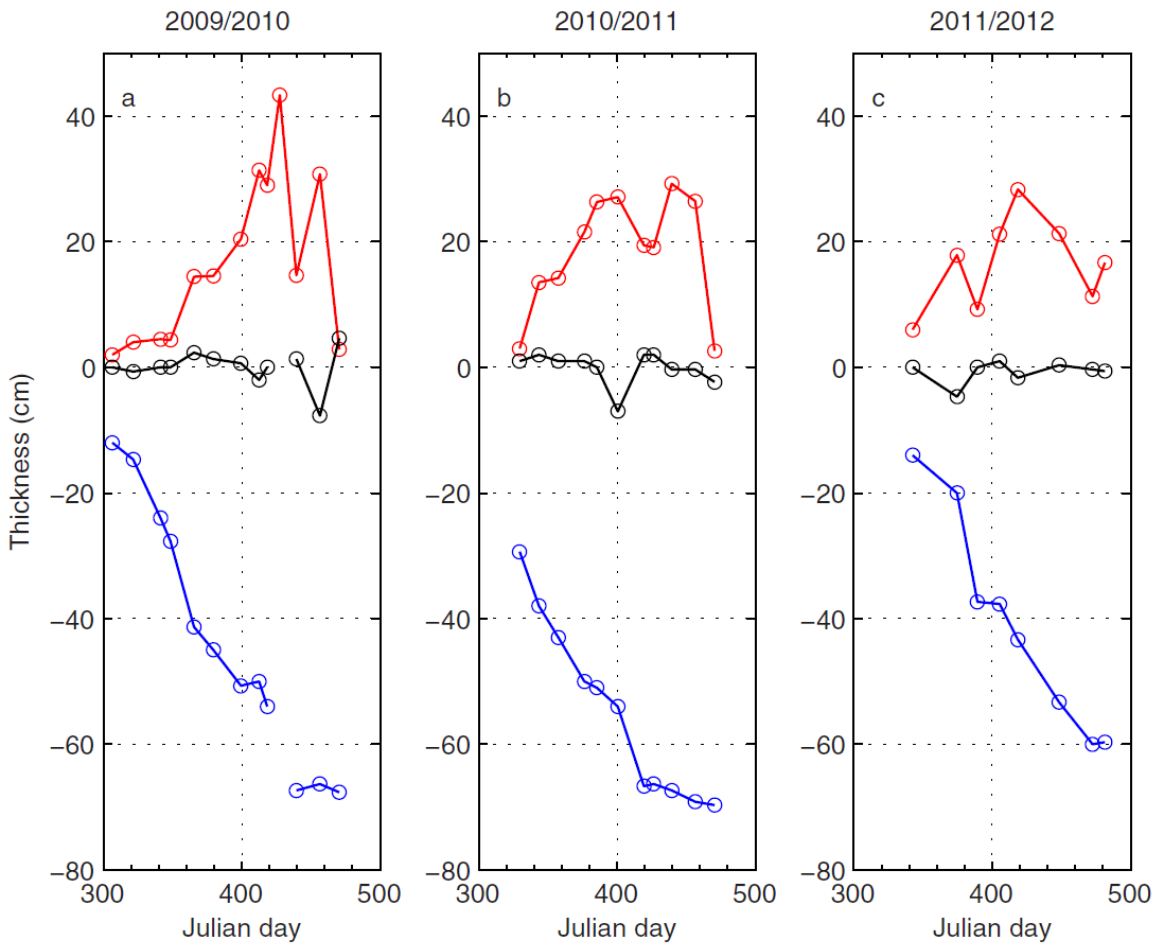

Figure A.2 Measurements of mean snow (red) and ice thickness (blue), and freeboard (black) on Lake Orajärvi for: a) 2009/2010; b) 2010/2011 and c) 2011/2012 winter seasons.

The air/snow interface can be identified based on the fact that a number of sensors located in the air have approximately the same temperature (i.e. vertical temperature gradient is small). Based on the same principle, the sensors located in water yield similar temperatures near the bottom of the ice. The snow/ice interface location can be estimated by investigating the temperature perturbations due to the sensor heating. In air, the heating cycles lead typically to a temperature rise of 2 °C, in ice and water the typical value is about 0.2 °C at least (Jackson et al., 2013). Additionally, since the heat conductivities of snow and ice are different, the temperature gradients in snow and ice are expected to be different. Piecewise linear temperature profiles in snow and ice can, accordingly, be measured

during cold conditions. The evolution of snow and ice thickness can finally be inferred based on all these analyses. The SIMB was designed for Polar ocean deployment. This is the first time that the system was deployed in an Arctic lake in Finland.

The Orajärvi test trial in winter 2009/2010 was not a complete success. The measurements suffered from sensors malfunction from time to time and only partial vertical temperature profiles were obtained. After some major technical innovations and software updates, the SIMB was re-deployed in winter 2011/2012 and successfully operated through the whole winter season. At the time of the initial deployment (19 December 2011), the snow thickness was 16 cm and ice thickness was 14 cm, and lake water flooding occurred. The SIMB operated continuously until 13 April 2012 before it was recovered. In addition to regular snow and ice measurements (Fig. A.2c), measurements were made when the buoy was visited four times for recording the snow thickness and once for ice thickness (Fig. A.3b) before the SIMB was recovered.

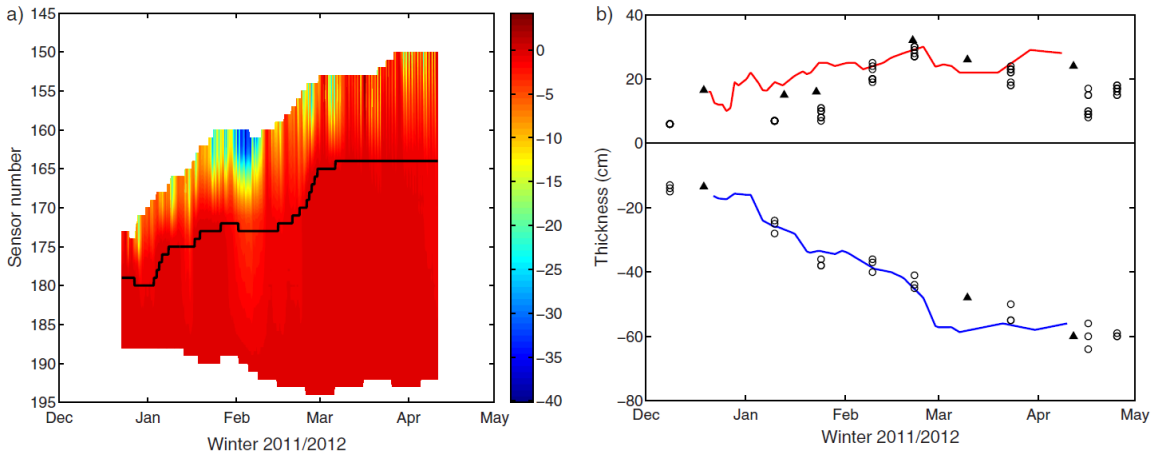

Figure A.3 (a) The SIMB measured snow and ice temperature fields. The number of sensors counts downward from surface to bottom. The snow/ice interface is marked as a black line. (b) SIMB data derived snow and ice thicknesses applying snow/ice interface as zero reference level. The symbols are snow and ice thicknesses measured near the SIMB site (▲) and at regular measurement sites (o).

Figure A.3 shows SIMB measured snow and ice temperatures and thicknesses. For clarity, we plot temperature in snow and ice only, not showing air and water temperatures. The evolving upper and lower boundaries in Figure A.3a represent the evolution of the snow surface and ice bottom along the

thermistor sensor string. The figure also shows the evolution of granular ice thickness: in the beginning of January sensor 180 was in snow, but at the end of the campaign it was 32 cm below the snow/ice interface, indicating the accumulated thickness of snow ice and superimposed ice (the observations do not allow distinguishing between them). The detected maximum bottom ice growth was about 12 cm (distance between sensor 194 and 188) during the SIMB deployment period. In Figure A.3b, the snow/ice interface is set as a reference level to account for the thickness of snow and ice. The independent in-situ snow and ice thickness measurements are plotted in Figure A.3b for comparison. The agreement is reasonably good, especially for the ice thickness evolution (MBE = 1.7 cm). The agreement between the SIMB-based snow thickness evolution and the regular in-situ measurements is not as good (MBE = -6.7 cm) most probably due to the spatial differences of snow distribution (c.f. Fig. A.2). However, for the measurements near the SIMB site, the agreement is better (MBE = -0.7 cm).

We need to emphasise that the absolute air-snow and ice-water interfaces can be estimated reasonable well by looking at the thermistor temperature readings. The large uncertainty comes from the detection of the snow-ice interface. Any inaccuracy from this interface detection will eventually affect the snow and ice thickness estimation because we use it as a reference level. One could consider placing a segment (e.g. 20 cm) of the thermistor string horizontally at the ice surface during the SIMB deployment. A clear mark of the initial snow-ice interface location would minimize the error in snow-ice interface detection later on.

2.4 Satellite observations

Space-borne LIST observations from the Moderate Resolution Imaging Spectroradiometer (MODIS) aboard the Terra and Aqua satellites operated by NASA (http://modis.gsfc.nasa.gov) were derived for comparison of the in-situ observed and HIGHTSI-simulated snow/ice surface temperatures during the ice season. MODIS day-time and night-time observations at 1 km spatial resolution were utilized. For Lake Orajärvi, MODIS overpass times are mostly between 10:00-12:00 and 20:00-22:00 for both ascending and descending modes. In the case of overlapping acquisition times between the Aqua and Terra satellites, the observations were averaged. MODIS data were processed through an algorithm developed in the University of Waterloo (UW-L3 data, see Kheyrollah Pour et al., 2012 for details). For lake Orajärvi, there were about 12 such pixels available that were not contaminated by the surrounding land area. A single (1 km by 1 km) pixel was selected, centred on the location where the

in-situ (buoy) temperature measurements were made during the study period (2009 – 2012) to represent the lake surface skin temperature within the hour of in-situ observations. MODIS observations are available only during clear-sky conditions, due to the limitation of optical sensors during cloudy days. The time series of MODIS LIST observations for the pixel of interest is compared with the SIMB and HIGHTSI model results (see section 5.1 below).

Note that although MODIS observations were included in the optimal interpolation surface analysis in the HIRLAM experiment NHFLAK (Homa Kheyrollah Pour, personal communication, 2014), they did not directly influence the HIRLAM forecasts, which were applied as atmospheric forcing data for HIGHSTI in the present study. This is because, in this HIRLAM experiment, the lake surface state was provided by FLake parameterization during the atmospheric forecast (see Rontu et al., 2012 for further explanation of relations between analyzed and predicted lake variables in HIRLAM). This means that our HIGHTSI results were not influenced by the MODIS observations even indirectly via the atmospheric forcing, hence the MODIS temperatures can be used as independent observations for the evaluation of LIST simulated from HIGHSTI and for comparison with in-situ observations.

3 Thermodynamic snow and ice model

A high-resolution thermodynamic snow and ice model was used to calculate the evolution of snow and ice thicknesses. The HIGHTSI model was initially used to calculate seasonal snow and sea ice thermodynamics (Launiainen and Cheng, 1998; Vihma et al., 2002; Cheng et al., 2003, 2006, 2008). The model has been further developed to investigate snow and ice thermodynamics in lakes (Yang et al., 2012, 2003; Semmler et al., 2012).

The snow and ice temperature regimes are solved by the partial-differential thermal heat conduction equations applied for snow and ice layers, respectively. The surface temperature is defined as the upper boundary condition solved by the Norton iterative method from a detailed surface heat/mass balance equation. The turbulent surface fluxes are parameterized taking the thermal stratification of the atmospheric surface layer into account. Downward short- and longwave radiative fluxes are either parameterized, taking into account cloudiness, or prescribed by observations or NWP model output. The penetration of solar radiation into the snow and ice is parameterized according to

surface albedo, and optical properties of snow and ice. The surface temperature is also used to determine whether surface melting occurs. At the lower boundary, the ice growth/melt is calculated on the basis of the difference between the ice-water heat flux and the conductive heat flux in the ice. At the snow-ice interface, the snow-to-ice transformation processes through re-freezing of flooded lake water or melted snow are considered in the model (Saloranta, 2000, Cheng et al., 2003).

In the HIGHTSI model, we deal with snow (thickness h_s), slush, snow/ice (thickness H_{si}), superimposed ice (thickness H_{su}), columnar ice (thickness H_i), and lake water. The snow thickness is affected by precipitation, snow melting and flooding slush (thickness h_{sL}) formation. The density of snow (ρ_s) is parameterized according to Anderson (1976). The slush is formed by lake water flooding slush (thickness h_{sL}) and snow melting. The density of slush (ρ_{sL}) is calculated as a function of density of snow, ice (ρ_i) and water (ρ_w) (Saloranta, 2000), and its value is very close to that of water density. Snow-ice is formed by refreezing of flooding slush. The flooding slush is a result of isostatic imbalance of overload snow on top of total ice floe. The superimposed ice is formed via refreezing of melt water or rain. For fresh lake water, we assume that the densities of snow-ice (ρ_{si}) and superimposed ice (ρ_{su}) are the same and remain constant. The total ice floe is composed of freezing lake water (columnar ice) and formation of snow-ice and superimposed ice (granular ice). The ice and water densities are constants. The freeboard is defined as the distance between the ice surface and water level. When the freeboard tends to be negative, the flooding slush starts to form, and in freezing conditions it is transformed to snow-ice. Table A.1 shows the calculation of freeboard and new slush formation in terms of different snow/ice compositions. The melting slush is created by surface and sub-surface snow melting and this part of slush is allowed to be re-frozen to create superimposed ice before the onset of ice melt. For the sake of simplicity, snow-ice and superimposed ice are assumed to form at snow-ice interface (Saloranta, 2000; Cheng et al., 2003; Semmler et al., 2012). For lake conditions, the snow-ice and superimposed ice can be regarded as the same kind of meteoric ice since they both are formed by fresh water, but for sea conditions, the snow-ice is different from superimposed ice because it is formed by salty slush. The formation of a slush layer due to heavy snow load needs water paths, which may consist of thermal cracks or drilling holes.

If the conductive heat flux at the ice bottom is larger (smaller) than the heat flux from the lake, the ice grows (melts) from the bottom. In this study, the heat flux from the lake was prescribed to a small

value of 1.5 W/m^2 for the freezing season, increasing to 5 W/m^2 after the onset of ice melt, because penetrating solar radiation heats the lake water below ice.

Table A.1 Calculation of freeboard in terms of various snow/ice compositions present in lake.

$f_b = H_i(\rho_w - \rho_i)/\rho_w$; $B = H_i/(\rho_w - \rho_i)$; $H_{sL} = 0$	ice/water
$f_b = H_i - (h_s\rho_s + H_i\rho_i)/\rho_w$; $B = H_i \times (\rho_w - \rho_i)$ $H_{sLn} = (\rho_w \times ws - B)/(\rho_s + \rho_w)$	snow, ice/water
$f_b = H_i + h_{sL} - (h_s\rho_s + h_{sL}\rho_{sL} + H_i\rho_i +)/\rho_w$; $B = H_i \times (\rho_w - \rho_i) + H_{si} \times (\rho_w - \rho_{sL})$; $H_{sLn} = (\rho_w \times ws - B)/(\rho_s + \rho_w - \rho_{sL})$;	snow, flooding slush and ice/water
$f_b = H_i + H_{si} - (h_s\rho_s + H_{si}\rho_{si} + H_i\rho_i)/\rho_w$; $B = H_i \times (\rho_w - \rho_i) + H_{si} \times (\rho_w - \rho_{si})$; $H_{sLn} = (\rho_w \times ws - B)/(\rho_s + \rho_w - \rho_{sL})$;	snow, snow-ice and ice/water
$f_b = H_i + H_{si} + h_{sL} - (h_s\rho_s + H_{si}\rho_{si} + h_{sL}\rho_{sL} + H_i\rho_i)/\rho_w$; $B = H_i \times (\rho_w - \rho_i) + H_{si} \times (\rho_w - \rho_{si}) + H_{sL} \times (\rho_w - \rho_{sL})$; $H_{sLn} = (\rho_w \times ws - B)/(\rho_s + \rho_w - \rho_{sL})$;	snow, flooding slush, snow-ice and ice/water

B is the buoyancy; ws is the total snow water equivalent in (m).H_{sLn} is the new slush formation.

4 Modelling strategy

4.1 Atmospheric forcing

In this study, local weather station observations and NWP model HIRLAM forecasts were applied as atmospheric forcing for the HIGHTSI experiments.

4.1.1 Weather station data

The weather station nearest to the lake was located at the FMI Arctic Research Centre, about 8 km from Lake Orajärvi. Due to the distance, the conditions over the lake were not necessarily identical to

those observed at the weather station, but the spatial variations are expected to be small as the terrain is almost flat. From this point of view, the weather station data are as representative as the HIRLAM forecasts with a grid spacing of 7.5 – 16 km (Section 4.1.2). In any case, the variability of weather conditions in the region is dominated by synoptic-scale patterns. The variables measured at the weather station consisted of 10-minute averages of 2-m air temperature (T_a, measured with a PT100 sensor), relative humidity (*Rh*, Vaisala HMP45D sensor), and 10-m wind speed (V_a, Vaisala WAA25 sensor). The total cloudiness (*CN*) was measured by a laser ceilometer (Vaisala CT25K), and daily total precipitation (*PrecT*) was measured by a Vaisala all-weather precipitation gauge VRG101. The downward global shortwave (Q_s) and longwave (Q_l) radiative fluxes were measured with Kipp & Zonen CM11 pyranometers and pyrgeometers. All the original measurements were averaged to hourly values and used as external forcing for the ice model. Snow accumulation on land was measured using a Campbell SR50 automatic snow depth sensor every 10 minutes. The data were then averaged to daily means. Snow thickness on land showed large inter-annual variations. The snow season began on JD280 (7 Oct), JD297 (24 Oct) and JD 321 (17 Nov) for winters 2009/2010, 2010/2011 and 2011/2012, respectively. The corresponding snow-season-average snow thicknesses were 45 cm, 39 cm and 53 cm and the snowmelt onset dates were JD 454 (30 Mar) 2010, JD 457 (2 Apr) 2011 and JD 478 (23 Apr) 2012. Table A.2 shows the observed seasonal average weather station data for the three winters. For the ice growth season (November to April), striking inter-annual differences are seen in the air temperature, longwave radiation and precipitation. In May and June, in addition to these variables, the wind and shortwave radiation also differ inter-annually.

4.1.2 HIRLAM forecasts

The HIRLAM NWP model forecasts were utilized in this study as atmospheric forcing. HIRLAM is a short-range NWP model (Undén et al., 2002) developed by an international consortium of 11 European countries (http://hirlam.org). Forcing fields for the first winter (2009/2010) were extracted from the operational HIRLAM archive (3 and 6 h forecasts, see below). The operational model applied version 7.2, with the standard surface data assimilation and four-dimensional atmospheric

Table A.2 The seasonal (Nov. – Apr.) mean values of observed weather data as well as Bias, Root Mean Square Error (RMSE) and correlation coefficient (R) between hourly time series of HIRLAM forecasts and in-situ observed wind, temperature, humidity, downward shortwave and longwave radiation and precipitation for winters 2009/2010; 2010/2011 and 2011/2012.

Winter		V_a (m/s)	T_a (°C)	Rh (%)	Q_s (W/m^2)	Q_l (W/m^2)	Precipitation Total (mm)				Precipitation Snow (mm)			
09/10	Mean	2.3	-9.2	86	42	250	Sum	192			Sum	168		
10/11	(Nov. –	2.3	-10.4	85	46	237	(Nov. –	131			(Nov. –	110		
11/12	Apr.)	2.3	-6.8	87	41	261	Apr.)	271			Apr.)	218		
09/10	Bias	1.1	-0.2	12.8	-9.8	-6.3	(Nov. –	99			(Nov. –	67		
10/11	(Cal. –	0.5	-0.3	7.3	-8.6	-2.2	Apr.)	18			Apr.)	4.8		
11/12	Ob.)	0.8	-0.1	6.4	-8.1	-4.5		32				5.3		
09/10	RMSE	1.7	3.4	18.2	69.3	24.4								
10/11		1.2	3.7	14.2	74.5	22.6								
11/12		1.3	3.5	13.4	67.5	30.2								
09/10	Corr.	0.78	0.94	0.29	0.74	0.89	h	0.64	d	0.83	h	0.66	d	0.85
10/11	Coeff.	0.77	0.93	0.60	0.74	0.88	h	0.45	d	0.68	h	0.51	d	0.74
11/12	R	0.78	0.92	0.48	0.73	0.81	h	0.58	d	0.82	h	0.59	d	0.82

The correlation coefficient (R) between time series of hourly (h) and daily (d) accumulated HIRLAM and in-situ observed total and snow precipitations are given.

data assimilation. A horizontal resolution of 15 km and 60 levels in vertical were used, with the lowest model level centred at 32 m. For winters 2010/2011 and 2011/2012, dedicated HIRLAM model runs were performed for a northern domain (experiment NHFLAK Homa Kheyrollah Pour, personal communication, 2014). These experiments were run with the HIRLAM version 7.4 including renewed surface parameterizations and the Freshwater Lake (FLake) parameterization on lakes. The model resolution was 7 km/65 levels, with the lowest model level centred at the height of ca. 12 m. The lateral boundary conditions for the HIRLAM experiments were obtained from ECMWF analyses, but for the operational HIRLAM of winter 2009/2010 they were derived from ECMWF forecasts. From the three-dimensional HIRLAM output, the lowest model level wind speed (V_a), air temperature (T_a) and relative humidity (Rh) were extracted for the grid point nearest to Lake Orajärvi using 3-hour forecasts. Snow precipitation as well as the downward shortwave (Q_s) and longwave (Q_l) radiative

fluxes were averaged during the first six-hour forecasts, and taken to represent the conditions at the same time as the extracted temperature, humidity and wind. All values were linearly interpolated to one-hour interval for the input of ice model experiments. Note that we did not use the diagnostic 2-m temperature and humidity, neither the diagnostic 10-m wind for forcing. Thus the model-based atmospheric data represents somewhat larger-scale conditions than the local synoptic observations to which they are compared in the next section.

4.1.3 Comparison of weather station data and HIRLAM forecasts

Comparisons between in-situ measurements and HIRLAM forecasts were made. In the different HIRLAM versions, the lowest model level variables represent average conditions between the surface and ca. 64 m in version 7.2 (winter 2009 – 2010) and ca. 25 m in version 7.4 (winters 2010/2011 and 2011/2012). The profiles of wind speed, temperature and water vapour in the surface layer were calculated accordingly based on the Monin-Obukhov similarity theory. It was essential to use the same formulae (Launiainen, 1995) as applied in HIGHTSI when deriving the turbulent surface fluxes from the HIRLAM model level variables. The results were then compared with the observed 2-m air temperature and humidity, and 10-m wind speed. HIRLAM modelled total and snow precipitations (in water equivalent, WE) were compared with observed values. A threshold temperature of 0.5 °C was used to extract snow precipitation (*PrecS*) from the observed total precipitation (Yang et al., 2012). The monthly mean differences between HIRLAM forecasts and weather station observations are shown in Figure A.4. The seasonal statistical error analyses are given in Table A.2.

In general, the agreement between HIRLAM and observations seems better in 2010/2011 and 2011/2012 than in 2009/2010, especially concerning air relative humidity (Fig. A.4h, i, Table A.2). Winter 2011/2012 was relatively warm in Sodankylä compared to the other two winters. Errors in air temperature were variable, the monthly biases ranging from -2 to 1.5 °C, with the largest cold biases in November – January and the largest warm biases in February – April. Shortwave radiation had a negative bias in every season before May. The total precipitation (*PrecT*) was overestimated by HIRLAM in 2009/2010, particularly for May. The exact reason for this large bias (127 mm) still remains unknown. In general, the pointwise validation of simulated and observed precipitation in winter time contains uncertainties due to several reasons related to areal representativeness of the measurements and model results as well as to the known problems of snowfall measurement due to wind effect. In this study, however, the bias of *PrecT* are mostly less than 20 mm WE. In spring, the

bias of *PrecT* is slightly larger (20 – 30 mm WE). The HIRLAM snow precipitation (*PrecS*) agrees better with observed values. The biases are mostly well under 20 mm WE. The bias of accumulated snow precipitation (Nov. – Apr.) is much smaller compared with the corresponding accumulated total precipitation indicating that HIRLAM *PrecS* is pretty reliable for ice modelling. For all seasons, the correlation coefficients between HIRLAM modelled and in-situ observed wind speed, air temperature, shortwave and longwave radiative fluxes as well as the daily accumulated precipitation are quite good (Table A.2).

Despite the dominance of positive biases in air relative humidity and precipitation, the downward shortwave and longwave radiation were underestimated on average. The new HIRLAM version is known to predict less low clouds in spring than the previous one, which may be reflected in the improved scores in the last two springs for the relative humidity, total precipitation, and shortwave radiation (Figure A.4).

4.2 HIGHTSI Experiments

The HIGHTSI experiments are listed in Table A.3. The initial snow and ice conditions were set according to the available in-situ observations. For each of the three winters, two experiments were performed including the snow pack on lake ice: one forced by the weather station data (SL experiments, c.f. Tab.3) and another by HIRLAM forecasts (SH experiments). Model experiments without snow (L and H) were also carried out. In L and H runs, the external precipitation forcing was set to be zero so the ice growth is purely in response to the weather forcing of wind, temperature, moisture, and cloudiness. The purpose of these model runs was to demonstrate the importance of winter precipitation as external forcing on snow and ice modelling.

5 Results

5.1 Surface temperature and energy budget

For the SL modelling experiments, the HIGHTSI simulated surface temperatures were compared with MODIS LIST observations over Lake Orajärvi (Fig. A.5 and A.6, and Table A.4). The coverage of MODIS observations was relatively good in time, with the exception of a few longer cloudy periods.

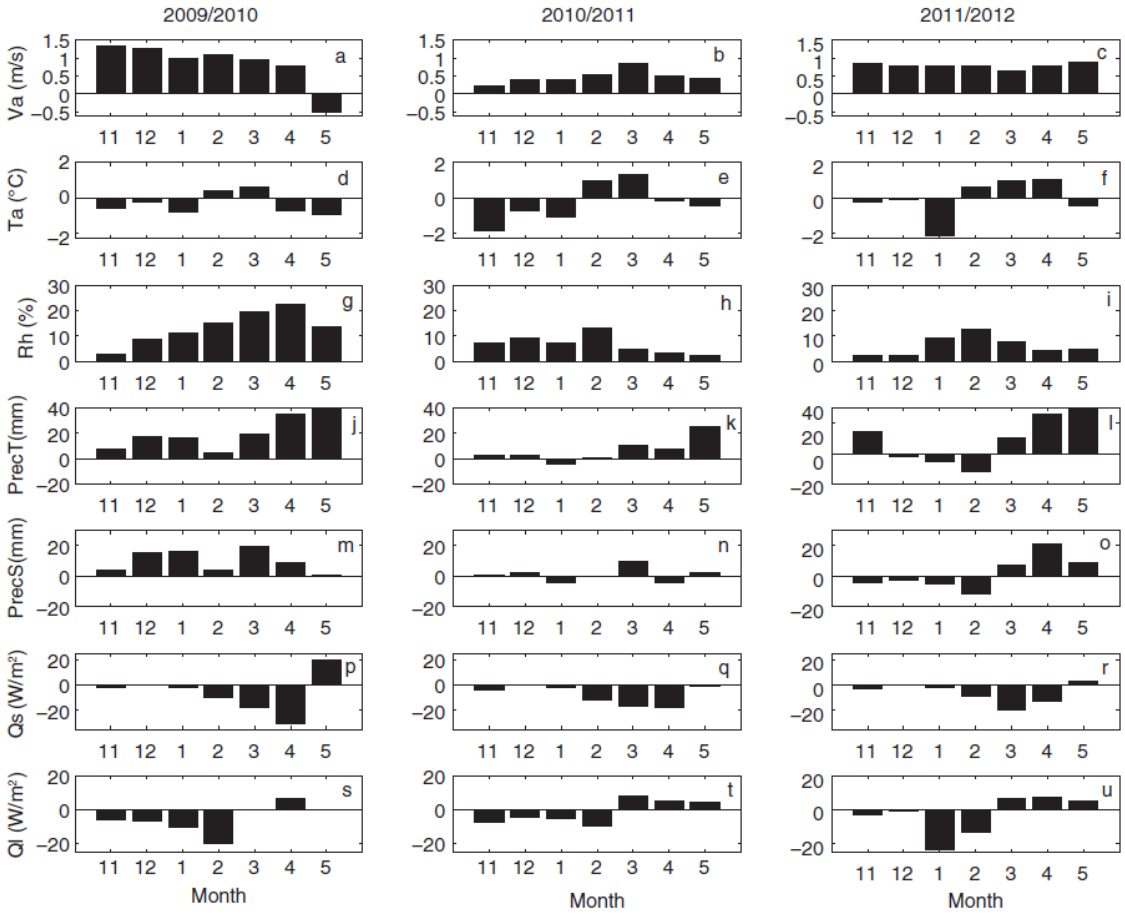

Figure A.4 The monthly mean differences between HIRLAM forecasts and weather station observations for wind speed (V_a), air temperature (T_a), relative humidity (Rh), total precipitation ($PrecT$), snow precipitation ($PrecS$), as well as shortwave (Q_s) and longwave (Q_l) radative fluxes for winters 2009/2010, 2010/2011 and 2011/2012. Note the *PrecT* has the same y-axis [-20 40], but for May of 2009/2010, the difference was 127 mm.

The comparison indicates that under cold conditions, MODIS and HIGHTSI temperatures are of the same order of magnitude. The satellite observations tend to show lower surface temperature during cold dark nights (-2.8 °C ≤ Mean Bias Error (MBE) ≤ -3.9 °C). Differences of the same magnitude have been reported by Kheyrollah Pour et al. (2012) in a comparison between MODIS and FLake modelled surface temperatures over several ice seasons (2002-2010) on Great Bear Lake and Great Slave Lake, Northwest Territories, Canada. Under melting conditions in spring, the MODIS surface

temperatures are higher than those estimated by HIGHTSI. However, MODIS and HIGHTSI surface temperatures agree better in terms of temporal variation. A summary of the statistical indices is presented in Table A.4. In Figure A.5c, SIMB data are also compared with HIGHTSI and MODIS during winter 2011/2012. The cross-comparison is shown in scatterplots in Figure A.6.

Table A.3 The names of HIGHTSI modelling experiments.

Forcing	2009/2010	2010/2011	2011/2012
with snow			
local in-situ observation	0910SL	1011SL	1112SL
HIRLAM forecasts	0910SH	1011SH	1112SH
no snow			
local in-situ observation	0910L	1011L	1112L
HIRLAM forecasts	0910H	1011H	1112H

SL: snow considered with local weather forcing; SH: snow considered with HIRLAM forecasts forcing; L: no snow with local weather forcing; H: no snow with HIRLAM forecasts forcing. The numbers (0910, 1011 and 1112) in front character represent the annual winter seasons.

In most cases, the MODIS surface temperatures were lower than the SIMB measurements and HIGTSI results during winter 2011/2012 (Figure A.5a, b; Table A.4). The agreement between HIGHTSI and SIMB surface temperature is better, particularly during warm conditions (temperature > -10 °C). For temperatures lower than -10 °C, the HIGHTSI surface temperature was usually higher than SIMB values.

To better understand the inter-annual evolution of snow and ice in Lake Orajärvi, the monthly means for various surface heat fluxes are calculated from 0910SL, 1011SL and 1112SL experiments (Table A.5). For a seasonal cycle, the net solar radiation (Q_{snet}) remains small before daytime melting season starts in April. The net longwave (Q_{lnet}) cooling dominates during the winter season. In early winter the turbulent heat fluxes were small, but when spring came the sensible heat flux increased because of positive air temperatures exceeding the lake surface temperature, which remained at or below 0 °C until the ice break-up (the air temperatures were observed over land, but we assume that they well represent conditions over the small lake). The upward conductive heat flux (F_c) represents the near surface snow/ice temperature gradient. When ice was thin, the larger F_c indicates more heat

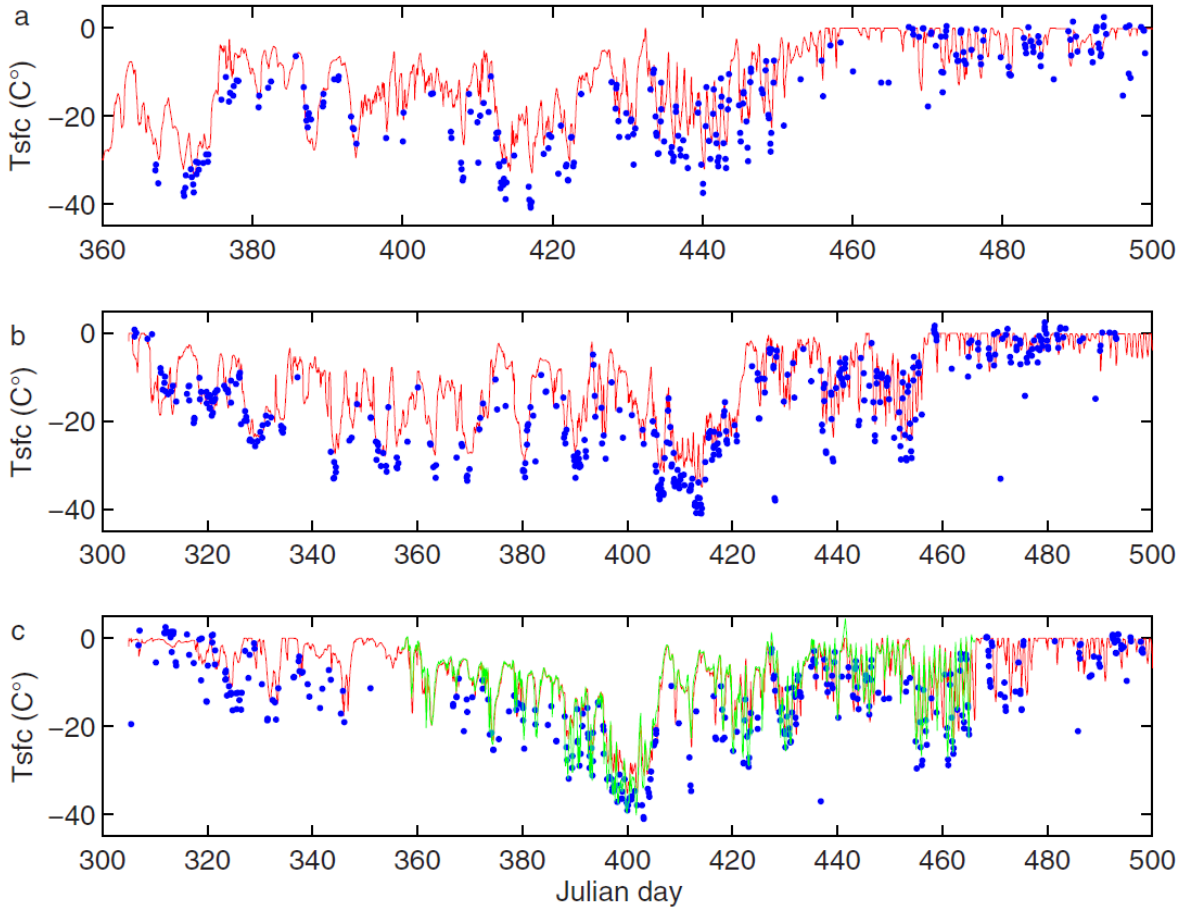

Figure A.5 The HIGHTSI (experiments SL, c.f. Table A.4) modelled (red line) and MODIS observed LIST (blue dots) for winter (a) 2009/2010; (b) 2010/2011 and (c) 2011/2012. The SIMB measured surface temperature is given as the green line in (c).

lost from the ice bottom to the snow surface and, as a results, greater ice growth. The net surface heat flux (F_{net}) indicates the overall heat gain and loss of the surface layer. In early winter, the heat gain of the surface layer results from rapid ice growth at ice bottom. In late spring, the heat gain of the surface layer results from strong solar heating (i.e. surface melting starts).

The surface energy balance in early winter 2010/2011 differed from the other seasons. The strong longwave cooling (Table A.4), associated with large F_c created rapid ice growth in early winter (note that the F_{net} in Nov. - Dec. was almost 2-3 times larger than other seasons). The modelled ice thickness (c.f. Fig. A.7), described in the next section, indeed shows thicker ice in mid-December

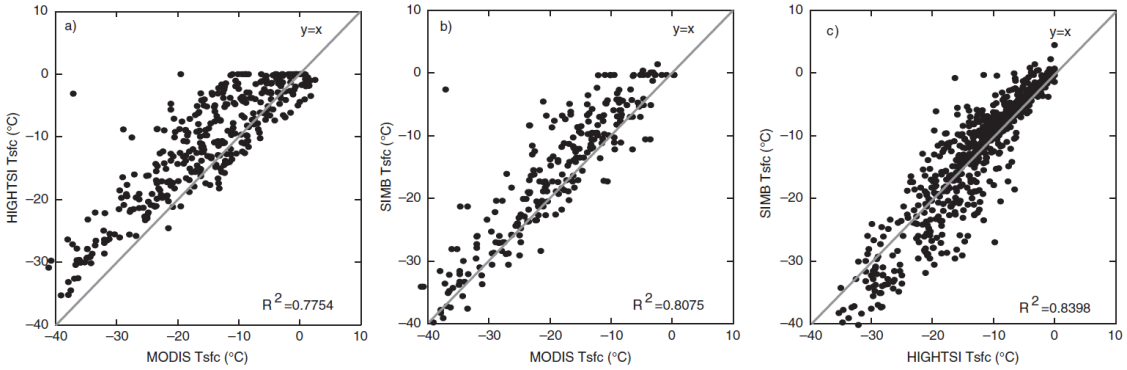

Figure A.6 The comparison of surface temperature: (a) MODIS versus HIGHTSI (SL experiments, c.f. Table A.4); (b) MODIS versus SIMB, and (c) HIGHTSI versus SIMB for winter 2011/2012.

(JD350) of 2010/2011 season compared with other seasons. Comparing the surface energy budget of 2009/2010 against 2011/2012, we see that in 2011/2012 the net surface heat flux F_{net} was smaller than in 2009/2010, which may be partly explained by slightly thinner ice in winter 2011/2012. In May, the smaller heat gain by the surface layer may have resulted in slower surface melting and consequently delayed break-up for winter 2011/2012.

Table A.4 Mean Bias Error (MBE), standard deviation (std), Root Mean Square Error (RMSE) and correlation coefficient (R) of HIGHTSI (experiments SL, c.f. Table A.4) modelled surface temperature, as well as SIMB and MODIS observations.

Winter	Results compared	MBE	std	RMSE	R	n
2009/2010	HIGHTSI – MODIS	2.9	4.5	5.4	0.93	277
2010/2011	HIGHTSI – MODIS	2.8	5.1	5.8	0.89	416
2011/2012	HIGHTSI – MODIS	3.9	4.9	6.5	0.88	375
	MODIS – SIMB	-3.1	4.6	5.5	0.9	253
	HIGHTSI – SIMB	0.03	2.8	3.8	0.91	757

5.2 Snow and ice evolution

The time series of modelled snow and ice thickness as well as freeboard are presented in Figure A.7. For winter 2009/2010, snow was modelled well until JD400 (4 Feb) for experiments 0910SL and

0910SH. The large variations in snow depth between days JD400 (4 Feb) and JD450 (26 Mar) were not well captured by the model owing to the failure to capture the large snowfall between JD418 (22 Feb) and JD427 (3 Mar). The modelled timing of snowmelt onset agreed well with observations but the melting rates were slower than observed. The differences between modelled snow thickness in 0910SL and 0910SH were large in December and March. Although, the HIRLAM total accumulated snow precipitation has a 67 mm positive bias during the season (Fig. A.4m), a cold HIRLAM T_a bias and smaller Q_l made 0910SH produce thicker ice.

For winter 2010/2011, the bias of HIRLAM seasonal accumulated snow precipitation was only 4.8 mm; therefore the 1011SL and 1011SH modelled snow thicknesses were close to each other. Again, the large errors of modelled snow thickness occurred during rapid snowfall period from JD329 (25 Nov) – JD 343(9 Dec). The 1011SH produced more ice than 1011SL towards the end of the March (JD450); the difference between modelled ice thicknesses actually started already in the early season (November) due to too small Q_l and a large cold bias in HIRLAM.

For winter 2011/2012, the modelled snow accumulations in SL and SH experiments were improved compared with results of previous winter seasons. The maximum observed snow thickness was often underestimated. The observed snow precipitation was larger than HIRLAM forecasts before March (c.f. Fig. A.4o) making the snow pack thicker in 1112SL than 1112SH (although the bias of HIRLAM seasonal accumulated snow precipitation was 5.7 mm due to the compensation effect). In this winter, the first snow-day on land was late, i.e. 17 November versus 7 and 24 October for the two other winters. However, the SL and SH gave quite similar ice growth in early November because of no snow on ice. The difference of SL and SH modelled ice thickness in the rest of the season was due to the appearance of snow in SL and SH experiments and differences in other weather forcing variables.

For each spring, the snowmelt onset dates calculated by SL and SH experiments were close to each other. Compared to the observed snowmelt onset on land, the agreements were very good, i.e. 30 March (observed) versus 1 April (calculated) for 2009/2010, 2 April (both observed and calculated) for 2010/2011, and 23 April (both observed and calculated) for 2011/2012. The earlier onset of modelled snow melt was consistent with the earlier modelled breakup date.

Table A.5 HIGHTSI (experiments SL, c.f. Table A.3) modelled monthly mean surface heat fluxes for 3 winter seasons. Q_{snet}: net shortwave radiative flux at surface; Q_{lnet}: net longwave radiative flux; Q_h: sensible heat flux; Q_{le}: latent heat flux; F_c: surface conductive heat flux; F_{net}: net surface heat flux, i.e. the sum of Q_{snet}, Q_{lnet}, Q_h, Q_{le} and F_c. All fluxes are positive toward surface (heat gain).

Year	Month	Q_{snet}	Q_{lnet}	Q_h	Q_{le}	F_c	F_{net}
		W/m^2					
09/10	11	0.1	-5.7	1.1	-0.6	6.9	2.0
	12	0.01	-19.4	2.2	-0.01	21.4	4.2
	01	0.12	-17.9	1.9	-0.9	19.5	2.8
	02	2.2	-17.9	-4.2	-1.7	16.8	-4.8
	03	9.0	-35.0	5.6	-1.8	13.9	-8.3
	04	11.4	-29.6	10.4	-3.2	13.3	2.2
	05	23.9	-7.3	12.4	4.4	9.9	43.3
10/11	11	0.2	-29.2	0.1	-0.6	40.2	11.0
	12	0.01	-23.8	-1.6	-1.0	34.3	8.0
	01	0.16	-19.1	1.8	-0.02	21.1	4.0
	02	2.3	-22.8	-1.6	-0.9	18.1	-5.1
	03	9.3	-43.7	14.7	-1.7	13.4	-8.0
	04	13.5	-31.2	12.7	-1.8	12.4	5.7
	05	26.9	-17.4	18.2	3.9	7.8	30.9
11/12	11	0.4	-15.9	3.9	2.2	9.1	-0.3
	12	0.01	-11.9	5.2	1.1	8.8	3.3
	01	0.26	-10.6	-1.1	-1.6	10.4	-2.5
	02	2.5	-15.9	-1.0	-1.3	10.6	-5.0
	03	11.2	-34.6	9.3	0.8	8.6	-6.3
	04	20.9	-30.6	5.9	-2.4	7.1	0.9
	05	25.9	-27.3	24.7	-0.1	7.3	30.5

The validation of freeboard modelling is a challenge. In this study, the rapid change of freeboard was often underestimated. In HIGHTSI, the freeboard is calculated according to Table A.1. In reality when snow is flooded, the lake water maybe merged upward due to the capillarity suction effect. We were not able to consider this micro scale process in HIGHTSI. On the other hand, HIGHTSI reproduced reasonably well the transformation of snow to ice; the model experiments revealed that the total ice formation would be largely underestimated if freezing is allowed only at the ice bottom (c.f. Table A.6)

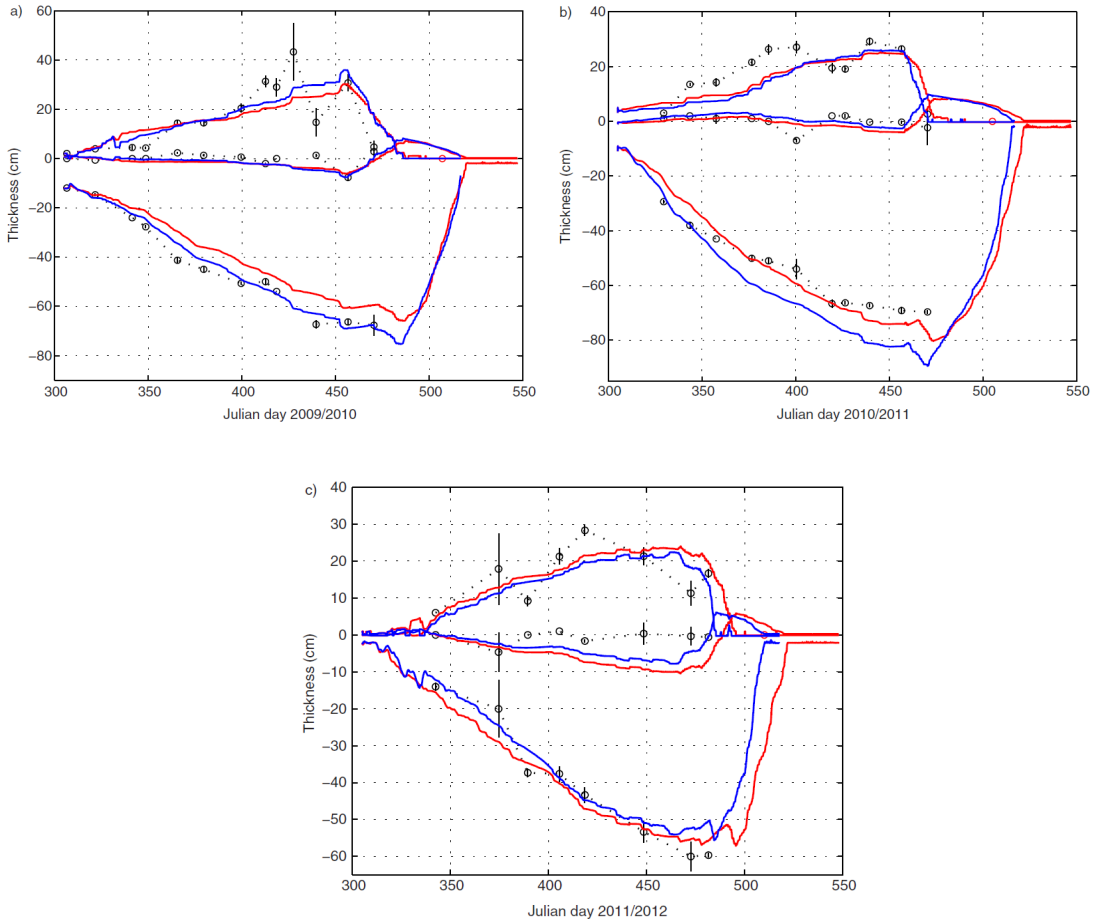

Figure A.7 HIGHTSI modelled snow thickness (upper lines), ice thicknesses (lower lines) and freeboard (middle lines) compared to in-situ observations for 2009/10 (a), 2010/11 (b) and 2011/12(c). The zero reference level is the snow-ice interface. The model runs were based on atmospheric forcing from weather station data (red lines) and HIRLAM forecasts (blue lines). The observations are given as black circles and their standard deviations are marked as vertical bars. The observed ice break-up dates of Lake Unari are indicated by red circles.

The modelled maximum ice thicknesses as well as accumulated ice bottom growth (columnar ice) and percentage of snow to ice transformation (granular ice) for the three winters are given in Table A.6 for the SL and SH experiments. For SL experiments, the bottom growth (Fig. A.8) lasted until 26 March in winter 2009/2010, but the ice thickness increased mainly during early winter (December - January). For winter 2010/2011, the pronounced bottom growth occurred until 1 March followed by a slight thickness increase until 26 March, but most of the growth occurred between November and early January. For winter 2011/2012, the bottom growth was more significant in November and early

December. Afterwards, it slowed down until 14 February and continued with a very small increase until 6 March, which was in good agreement with the SIMB measurements (Fig. A.3). The bottom ice growth for the SH experiments showed similar variation compared to SL experiments for winters 2009/2010 and 2010/2011. For winter 2011/2012, the SH run produced more bottom growth than the SL run. During the cold winter 2010/2011, snow precipitation was small and ice growth mainly took place at the ice bottom, whereas for the mild winter 2011/2012, the majority of ice growth was due to snow-ice and superimposed ice formation.

An ice core sample collected on 12 April 2012 (Fig. A.9) indicated the total ice thickness was about 57 cm, of which 24 cm (42%) was columnar ice and 33 cm (58%) was granular ice (snow-ice and superimposed ice). Compared to the initial deployment of the SIMB on 19 December 2011, when the ice thickness was 14 cm, the ice bottom growth until 12 April 2012 was 10 cm, which is in line with the SIMB detection (see section 2.3, Fig. A.3a). The 1112SL experiment yielded total ice thicknesses in good agreement with the observations during the growth season, and the observed and modelled maxima occurred within 5 days of each other.

Table A.6 The seasonal maximum ice thickness (H_{imax}), ice bottom growth and percentage of snow to ice transformation for SL and SH experiments and H_{imax} for L and H experiments for three ice seasons.

		2009/2010	2010/2011	2011/2012
SL	H_{imax}	66	81	57
SH	(cm)	75	89	55
SL	Columnar ice	36	56	27
SH	(cm)	39	67	31
SL	Granular ice	46%	30%	53%
SH	(%)	48%	24%	44%
L	H_{imax}	120	132	96
H	(cm)	123	135	99

The modelled snow and ice temperature fields for SL experiments (Fig. A.10) revealed that the snow-ice interface remained cold during the winter season, which ensured freezing of slush to form

snow-ice. After the snowmelt onset, the ice surface temperature was also low, leading to re-freezing of surface snowmelt to form superimposed ice.

The modelled and observed vertical snow and ice temperature profiles at selected time steps are shown in Figure A.11. Considering the surface temperature, the large discrepancy between observations and model results on 23 January (Fig. A.11b) was associated with inaccuracy of the SIMB snow thickness (Fig. A.3b). Under cold conditions, the snow and ice temperatures were modelled quite well. With warm conditions, the modelled and observed temperature differences in snow and ice were larger. This could be due to the error of modelled snow thickness as well as the unknown effect of solar transmission into snow and ice. The agreement between modelled and observed temperature was better in ice than in snow. On 8 April, sub-surface melting was captured by the model run (Fig. A.11g). The SIMB observations did not detect this phenomenon, but showed temperatures increasing towards the surface, with erroneous positive values due to solar heating of the sensors.

5.3. Lake ice simulations using different precipitation scenarios

Precipitation introduces a large uncertainty on snow and ice evolution in a lake. The uncertainty originates not only from the strong snow insulation effect, but also from the intensity and timing of snowfall associated with the synoptic-scale patterns and hydrostatic imbalance between snow cover and underlying ice floe. To demonstrate the uncertainty related to precipitation forcing, we carried out a few model experiments without snow. We used the same initial ice thickness (0.01 m) for each L and H experiments, which all covered the period from the beginning of November to the end of May. For each winter season, L and H modelled ice thickness (Fig. A.12) yielded a fairly similar ice evolution. For each season, the modeled maximum ice thicknesses in L and H experiments were close to each other (Table A.6), whereas for SL and SH experiments the seasonal maximum ice thicknesses differed from each other. The differences of modelled ice thickness between SL and SH and L and H experiments are shown in Figure A.13. The differences between modelled ice thickness using in-situ and HIRLAM forcing without snow are much smaller than the corresponding differences between model experiments with snow taken into account, particularly in early winter season (Nov. – Dec.).

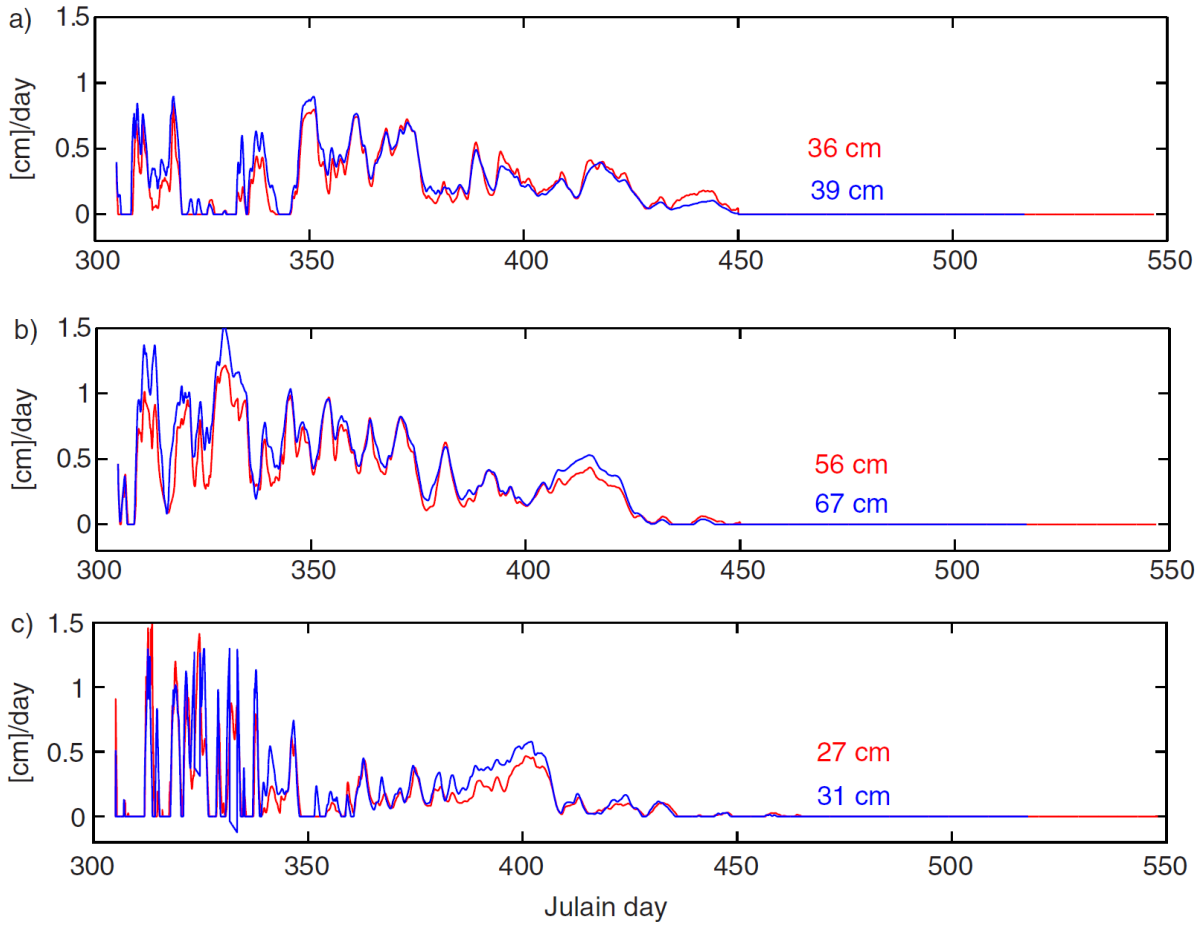

Figure A.8 The HIGHTSI modelled ice bottom growth for (a) 0910SL (red) and 0910SH (blue); (b) 1011SL (red) and 1011SH (blue), and (c) 1112SL (red) and 1112SH (blue).

This demonstrates the central role of the uncertainty in precipitation forcing. During the melt season, the differences of modeled ice thickness between SL and SH and L and H are getting large. These differences are partly due to differences in radiative forcing. Compared to in-situ observations, the monthly mean HIRLAM longwave radiative fluxes were 7 to 10 W/m^2 smaller during the winter months (November – February) and 3 to 5 W/m^2 larger in spring (March – May). The HIRLAM shortwave radiative fluxes were 4 to 7 W/m^2 larger in spring (March – May).

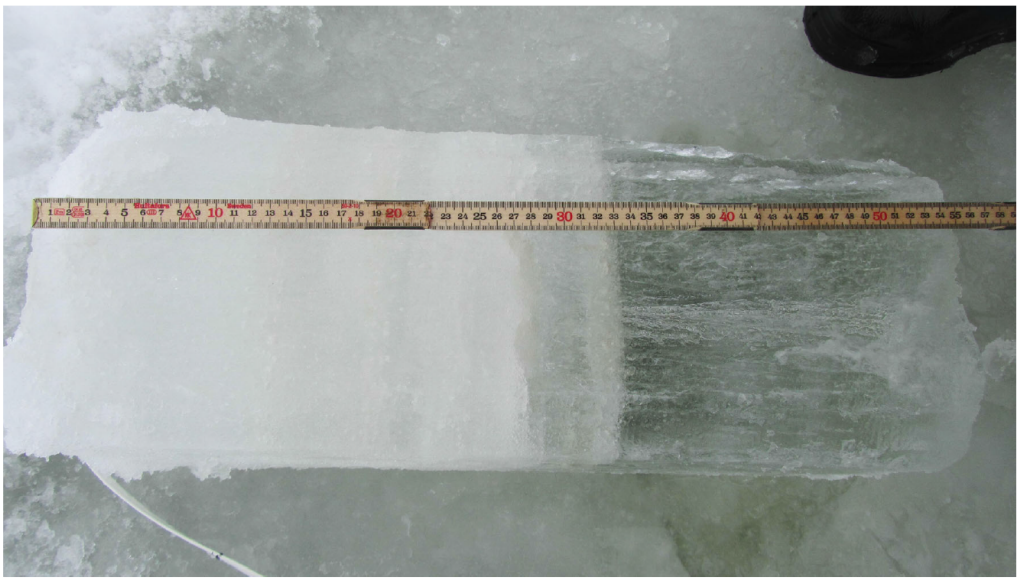

Figure A.9 Ice core sample collected on 12 April 2012 when the SIMB was recovered.

The impact of precipitation is closely linked to formation of snow-ice and superimposed ice (Table A.1). The increase of snowfall makes the snow-load heavier, promoting negative ice freeboard, which is the basis for snow-ice formation. Rain and sleet falling on snow favour snow-slush for superimposed ice formation. In winter 2011/2012, for example, a number of model sensitivity experiments indicated that when the snow precipitation was 50% of the original observed value, the maximum ice thickness only increased from 57 cm to 58 cm, but the proportions of granular and columnar ice changed a lot: from 53 to 20% for granular ice and from 47 to 80% for columnar ice. If the snow precipitation increased to 1.5 times of its original value, while keeping all other forcing factors equal, the model run ends up with 66 cm maximum ice thickness and the proportions of granular and columnar ice were 71% and 29%, respectively. We emphasize that these proportions are strongly associated with precipitation patterns as well as variations in air temperature during the winter season. The sensitivity tests merely demonstrated the impact of snow precipitation on granular and columnar ice formation. A more in-depth investigation would have required a large number of model runs taking into account different combinations of external forcings. This is a topic that we plan to pursue in a follow-up study.

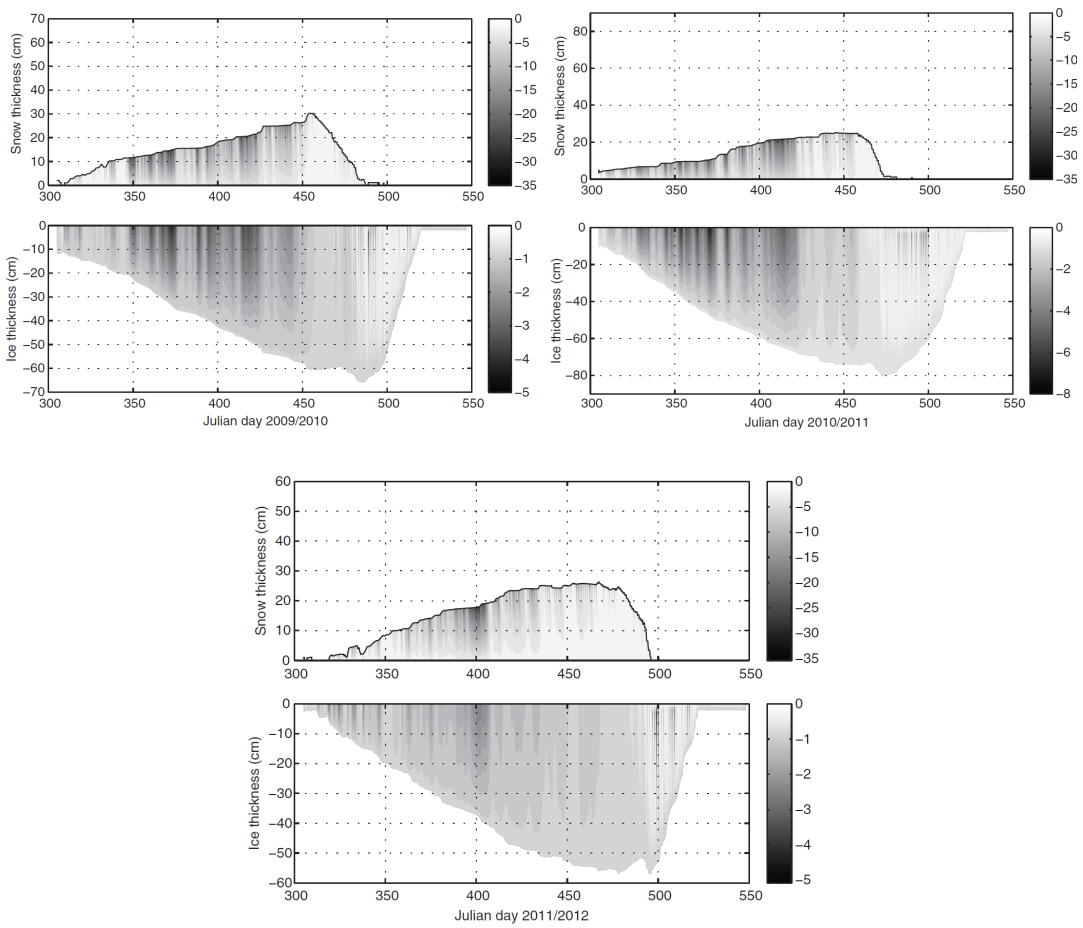

Figure A.10 HIGHTSI (SL experiments, c.f. Table A.3) modelled snow and ice temperatures for winter seasons 2009/2010, 2010/2011, and 2011/2012. For sake of clarity, snow and ice temperatures have the same vertical scales but different temperature grey scales.

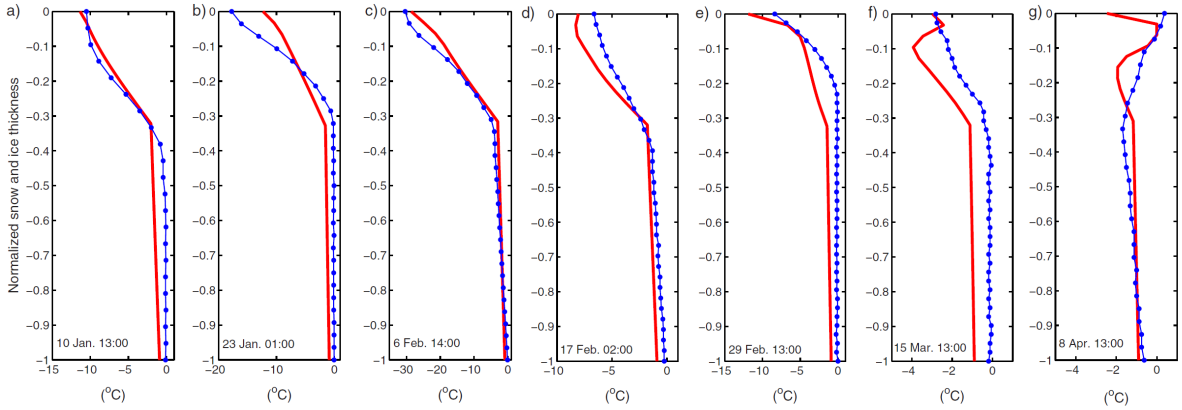

Figure A.11 The comparison of 1112SL modelled (red line) and SIMB observed (dot-blue line) vertical temperature profiles within snow and ice at selected UTC time steps. A normalized coordinate, i.e. height/(h_s+H_i) is used in the y axis (0 is surface and 1 is ice bottom).

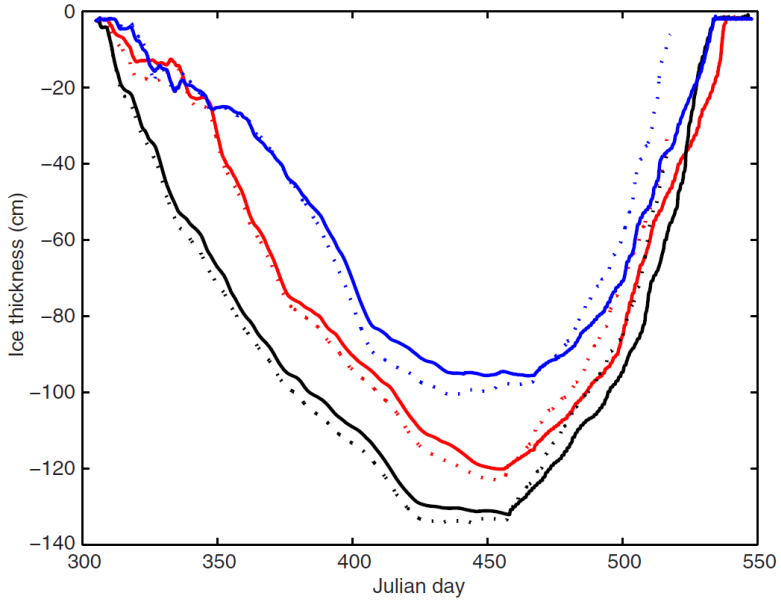

Figure A.12 HIGHTSI modelled ice evolution without taking snow into account, using in-situ weather station data (solid line) and HIRLAM forecasts (dotted line) as external forcing. The winter seasons are 2009/2010 (red), 2010/2011 (black), and 2011/2012 (blue).

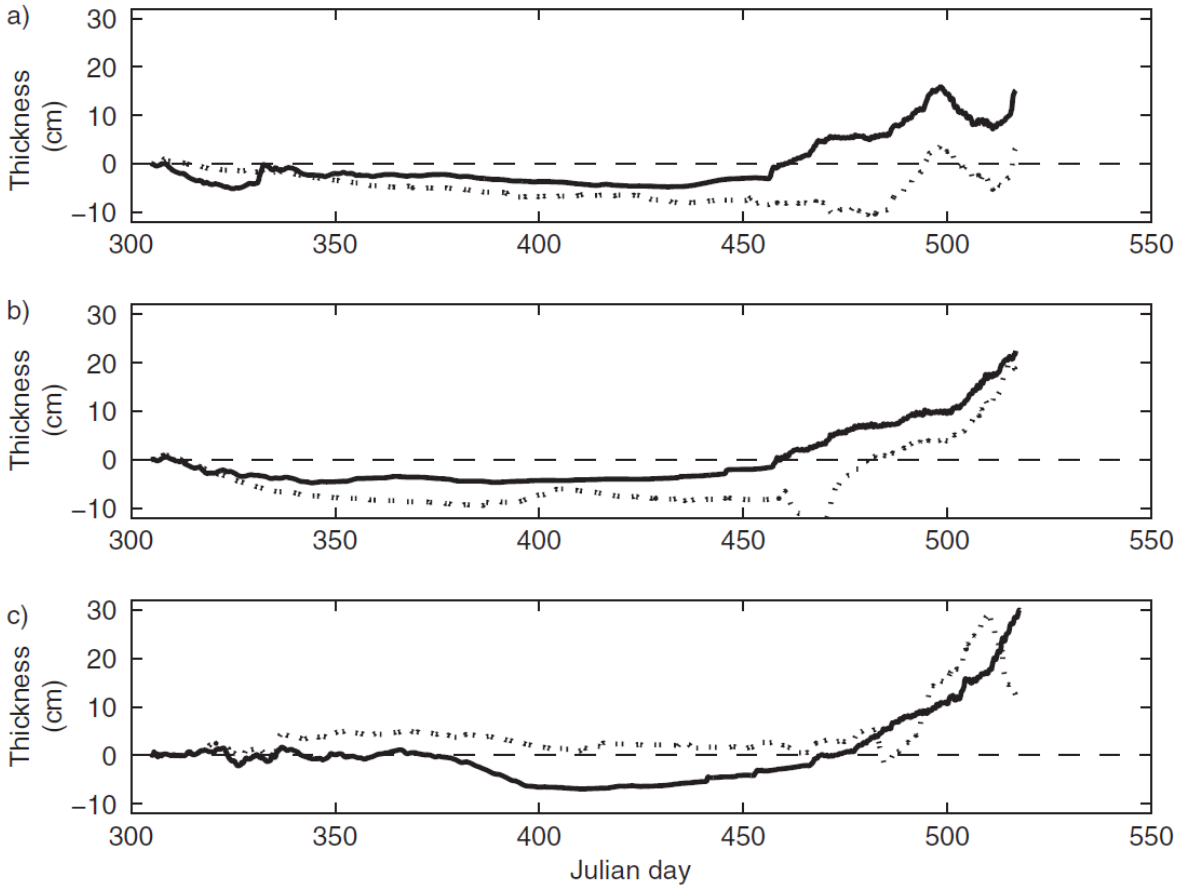

Figure A.13 The differences of modeled ice between model runs (without snow: solid lines; with snow: dotted line) using in-situ weather station data and HIRLAM forecasts as external forcing. a) 2009/2010; b) 2010/2011 and c) 2011/2012.

6 Conclusions

The evolution of snow and ice temperature, thickness and energy balance in Lake Orajärvi was investigated during three successive winter seasons (2009 – 2012). A prototype ice mass balance buoy (SIMB) was deployed to monitor snow and ice temperature profiles and thicknesses. The evolution of snow and ice in Lake Orajärvi was simulated by HIGHTSI model with external forcing data from in-situ weather station observations and HIRLAM NWP model forecasts. The performance of HIRLAM forecasts was assessed against weather station observations. The HIGHTSI results were validated using lake snow and ice measurements.

Our successful deployment of the SIMB buoy and data analyses suggest that this system is a reliable instrument set-up for monitoring snow and ice temperatures and thicknesses in an Arctic lake. The SIMB-based snow and ice thicknesses were in a reasonably good agreement with manual borehole measurements in cold conditions. The SIMB measurements clearly indicated that snow to ice transformation took place at the snow/ice interface. Challenges remain for warm conditions, in particular when the snow and ice are close to isothermal. In such situations, the detection of snow and ice thickness based on the temperature profile is likely to be uncertain. Additionally, the solar heating may cause errors in the readings of the uppermost temperature sensors during the melting season. Although the SIMB is still largely a prototype system for snow and ice monitoring (Jackson, et al, 2013), its relatively low cost and compact design make this device competitive. We have also successfully deployed SIMB buoys for snow and ice monitoring also on sea ice in the Arctic, Antarctic, and the Baltic Sea.

MODIS surface temperature observations are a promising data source for optimal interpolation surface analyses in operational NWP (Kalle Eerola, personal communication, 2014). Under clear-sky conditions, space-borne thermal remote sensing data can also be used to retrieve large-scale ice thickness during the growth season (Yu and Rothrock, 1996, Mäkynen, et al., 2013). The MODIS snow/ice (skin) surface temperatures were compared to those modelled with HIGHTSI and measured with the SIMB. Compared to simulated and in-situ LIST data, MODIS showed 2.8-3.9°C lower temperatures, with the largest differences during cold dark nights. These results are in line with those previously reported by Kheyrollah Pour et al. (2012).

The weather conditions in early winter are critical in determining the seasonal evolution of the thickness of lake ice and snow. During the freezing season, the most important forcing factors that lead to inter-annual variations in lake ice conditions are air temperature, precipitation and net longwave radiative flux. These are the essential external forcing factors for ice growth. A first-order estimate for the effect of air temperature on ice thickness can be obtained from an analytical solution for ice growth (Leppäranta, 1993). Such an estimate, however, does not take in to account the effects of precipitation and the individual terms of the surface energy balance to the snow and ice thickness, which were addressed in this study. Our results for the rate of bottom growth in early winter were comparable to previous studies (Launiainen and Cheng, 1998), being of the order of 1 to 2 cm day^{-1}. Before ice melt onset, the growth rate of superimposed ice was, however, of the same order of

magnitude as the bottom growth in the early winter. The timing of superimposed ice formation agreed reasonable well with in-situ observations carried out in a similar snow and ice environment on land-fast ice in the Baltic Sea (Granskog et al., 2006) and in an Arctic fjord (Nicolaus et al., 2003).

The largest external uncertainty originated from precipitation. This was revealed by HIGHTSI experiments in which snow on ice was not taken into account. Without precipitation, the model experiment forced by HIRLAM forecasts and in-situ observation yielded very similar seasonal ice evolution in terms of the early season ice growth and the maximum ice thickness. With external forcing including precipitation, the simulated ice thickness differed a lot between the experiments forced by HIRLAM and in-situ observations.

Improvements to the HIRLAM NWP model were made by increasing the horizontal and vertical resolution and including the FLake parameterization. The forcing fields in 2010/2011 and 2011/2012, based on the improved HIRLAM, were indeed better for the relative humidity and solar radiation compared with those in 2009/2010. The HIRLAM weather forcing time series correlated reasonable well with in-situ observations of wind speed, air temperature, shortwave and longwave radiative fluxes and daily accumulated total and snow precipitations. The increase of snow depth over lake ice is not easy to model well. Large errors originate from the uncertainty of the external forcing related to the wind impact to the in-situ precipitation observations and inaccurate NWP precipitation forecasts. The accuracy of HIRLAM total precipitation, its division between rain and snowfall, as well as prediction of individual precipitation events requires further improvements. Further efforts are also needed to implement in models the recent advances in physics of snow and ice albedo and related feedbacks, effects of aerosol deposition on snow and ice, and transmittance of snow and ice (Vihma et al., 2013).

It is vitally important to include calculation of snow to ice transformation in the lake ice modelling. Ice growth from the bottom accounted only for a portion of the total ice thickness of the lake examined in this study. At the seasonal time scale, bottom growth constituted about 50 – 70 % of the total ice growth; the percentage strongly depends on the amount of total snow precipitation as well as the air temperature regimes.

During the melting season, HIGHTSI modelled ice thickness driven by HIRLAM and by in-situ observations tend to differ from each other. The downward shortwave radiative flux and surface albedo play important roles on surface melting. Due to safety regulations, we do not have sufficient

in-situ observations on lake ice for investigation of the lake ice melting process. Although HIGHTSI reproduced well the observed timing of snow melt onset, the redistribution of melting water runoff rather than to re-freezing remains unknown and needs to be investigated in the future. We also expect further development of SIMB to improve the accuracy and reliability of the observations during melting seasons.

Appendix B

Impact of partly ice-free Lake Ladoga on temperature and cloudiness in an anticyclonic winter situation - a case study using a limited area model

Kalle Eerola[1], Laura Rontu[1], Ekaterina Kourzeneva[1], Homa Kheyrollah pour[2], and Claude Duguay[2]

[1]Finnish Meteorological Institute, Helsinki, Finland;
[2]University of Waterloo, Waterloo, Ontario, Canada,

Abstract

At the end of January 2012, a low-level cloud from partly ice-free Lake Ladoga caused very variable 2-metre temperatures in Eastern Finland. The sensitivity of the High Resolution Limited Area Model (HIRLAM) to the lake surface conditions was tested in this winter anticyclonic situation.The lake appeared to be (incorrectly) totally covered by ice when the lake surface was described with its climatology. Both parametrisation of the lake surface state by using a lake model integrated to the NWP system, and objective analysis based on satellite observations, independently resulted in a correct description of the partly ice-free Lake Ladoga. In these cases, HIRLAM model forecasts were able to predict cloud formation and its movement as well as 2-metre temperature variations in a realistic way. Three main conclusions were drawn. First, HIRLAM could predict the effect of Lake Ladoga on local weather, when the lake surface state was known. Second, the current parametrisation methods of air-surface interactions led to a reliable result in conditions where the different physical processes (local surface processes, radiation and turbulence) were not strong, but their combined effect was important. Third, these results encourage work for a better description of the lake surface state in NWP models by fully utilising satellite observations, combined with advanced lake parametrisation and data assimilation methods.

1 Introduction

At the end of January 2012, a local newspaper 'Etelä-Saimaa', published in Southeastern Finland (in Finnish), reported on an outstanding weather phenomenon. During a couple of days, the air temperature had been varying by as much as 17°C within a small area. For instance, in Imatra a temperature of -11°C was observed, while in Parikkala (60 km northeast of Imatra), the temperature at the same time was -28°C. According to the duty meteorologist of the Finnish Meteorological Institute interviewed by the newspaper, the large variability was due to a low cloud, which originated from partly ice-free Lake Ladoga. It was predicted that this situation would not last very long, because Lake Ladoga was about to freeze. The newspaper noted that Lake Ladoga, which is the largest lake in Europe (17 700 km^2, located in Russia between 30°E-35°E and 60°N-62°N) influences the weather of Eastern Finland because it is large and so close. What made the phenomenon interesting was that the low-level cloud, spread by the wind, only covered a small area at a given time. This created the large and at that time unpredicted variability in the observed temperature both in space and time.

We used this winter case to study the sensitivity of a Numerical Weather Prediction (NWP) model to the description of the lake surface state. The purpose of this work was to study the impact of partly ice-free Lake Ladoga on cloudiness and temperature in a winter anticyclonic situation and to answer the question: can a NWP model predict correctly the evolution of clouds and the consequent large 2-metre temperature variability, if it is provided with a correct description of the lake surface state? As the NWP model, we used the High Resolution Limited Area Model (HIRLAM, Undén et al., 2002, Eerola et al., 2013), where different possibilities to handle the air-lake interactions were available. In this kind of situation the balance between different surface-related processes is subtle. Thus this case provided a good test-bench for the model.

At the northern and middle latitudes, lakes regularly freeze during the winter. However, due to their large heat capacity they often stay ice-free late in the autumn and early winter. Their influence on local weather depends on the synoptic situation and on the lake surface conditions (open water, partly or totally ice-covered). Heavy snowstorms caused by the ice-free lakes are well documented, especially for the North American Great Lakes area (e.g. Niziol et al., 1995; Vavrus et al., 2013; Wright et al., 2013). Cordeira and Laird (2008) even documented two cases, where snowstorms developed over a lake mostly covered by ice. The authors stated that despite of the decreased

turbulent fluxes from the surface, a variety of ice-cover conditions and meso- and synoptic-scale factors supported the development of snowstorms. Based on earlier studies, Niziol et al. (1995) listed several factors, which have been noticed to be important in the evolution of lake-induced snowfall in this area, the most important being the air-lake temperature difference. Other influencing factors included the cloud-top inversion height and strength, the differences in temperature and surface roughness between the lake and surrounding land surfaces, as well as the orographic lift downwind of the lake. In Scandinavia, Andersson and Gustafsson (1990), Andersson and Gustafsson (1994), and Gustafsson et al., (1998) discussed the influence of the Baltic Sea, whose size is comparable to that of the Great Lakes, on convective snowfall over the ice-free water surface. According to these authors, favourable factors for the development of precipitating convective cloud bands are the ice-free conditions, suitable topography on the upwind and downwind coasts, a large temperature difference between water and air, and an optimal wind direction which allows for the longest fetch.

Skillful forecasters in Finland know by experience that Lake Ladoga or even smaller lakes may enhance snowfall in autumn or early winter. However, to the authors' knowledge, there are no documented cases where lakes would have caused heavy snowstorms at the Scandinavian high latitudes. One possible explanation is the small probability for the outbreaks of very cold air during autumn, when large lakes are still warm enough. Lakes in the Scandinavian-Karelian region are numerous but small and often shallow, with rather flat topography around them. Later in winter most of them freeze quickly due to their small size and shallowness. Because of this, the air-lake temperature differences remain moderate.

Meteorologically the case described in the newspaper differed from the severe snowstorm cases. This was a stable anticyclonic situation, with high surface pressure, cold clear-sky winter weather, weak winds, and a sharp surface-based temperature inversion. Only light snowfall was detected. However, over ice-free water a large temperature difference between the air and lake prevailed. In a cold winter-time anticyclonic situation, the near-surface air temperature is largely controlled by the cloud cover. In this case, the partly ice-free Lake Ladoga generated a low-level cloud, which spread far into Eastern Finland. Locally, under the cloud cover, temperature rose but under the clear sky it remained low. Such synoptic cases have not been popular in the scientific literature. As a synthesis, based on existing lake-effect literature, Laird et al. (2003) showed a general picture of favourable situations for different lake-effect phenomena as a function of wind speed and air-water temperature

difference. Widespread cloud coverage requires strong surface wind and a large enough air-water temperature difference. In weak-wind situations, like this case, shoreline cloud bands can occur. In cases where the air-water temperature difference exceeds 10°C in weak-wind situations, even mesoscale vortex events have been observed.

HIRLAM (Undén et al., 2002, Eerola et al., 2013) has recently been used in several studies with the aim of improving the treatment of lakes and their influence on local weather. The Freshwater Lake model FLake (Mironov, 2008, Mironov et al., 2012) was implemented into HIRLAM by Kourzeneva et al. (2008) in order to predict lake temperature as well as the evolution of lake ice and its snow cover. From the analysis side, interpolation of in-situ and remote sensing observations of Lake Surface Water Temperature (LSWT) into HIRLAM has been applied by Eerola et al. (2010), Rontu et al. (2012), and Kheyrollah Pour et al. (2014b). In this study, we present and discuss results from three HIRLAM experiments where the state of lakes was described in different ways. The first experiment relied on climatological lake surface conditions according to a method still applied in many large-scale operational NWP systems. In the second experiment, the prognostic lake parametrisation by FLake was used to predict the evolving state of the lake during the atmospheric forecast. In the third experiment, satellite observations were used for the analysis of LSWT and the diagnosis of lake ice concentration (LIC). During the forecast they were kept unchanged.

A standard verification of the NWP results against regular weather observations is sometimes insufficient to show the benefits of model improvements. This is because such a validation collects statistics from a large variety of situations so that the different effects become hidden behind the averages. A careful analysis of well-chosen cases can provide more information about the physical processes and their interactions. Here we report a case study in a situation where the extreme cloud and temperature variations lasted only a couple of days and the influence of Lake Ladoga extended only to Eastern Finland. We focus on the most striking 24-hour period, when a low-level cloud moved across the domain. Because the influence of lakes (even large lakes) on weather and climate is local, depending on local conditions and the weather parameter in question, we restrict ourselves to the closest observations around Lake Ladoga. In addition, we present results of statistical validation against observations during two weeks of the prevailing anticyclonic weather in January--February 2012.

This paper is structured as follows: After this introduction, the weather situation is described in Section 2. Special attention is paid to the cloud and temperature variability. Section 3 describes the HIRLAM NWP system, focusing on the surface-related parametrisations and surface data analysis. Also the setup of the three different experiments is described. The results are presented and discussed in Section 4. The movement of the lake-originated cloud and its influence on temperature is described. The surface energy balance is analysed over open water and snow-covered land. In addition, statistical verification results in the vicinity of the lake are shown and discussed. Finally, the results are summarised in Section 5.

2 Weather situation

During the last week of January and first week of February 2012, a strong anticyclone extended from Russia to Finland. Figure B.1 shows the weather situation in Europe on 28 January. In Eastern Finland, the highest measured mean sea level pressure in 40 years, 1063 hPa, was recorded during this period. A cold continental winter-time air mass prevailed, with 850 hPa level temperatures between -10 and -15°C in the last week of January and decreasing below -20°C during the first week of February. Typically, this kind of anticyclonic situation is characterised by clear-sky conditions, weak wind, strong and sharp surface-based inversion in temperature, and low 2-metre temperatures. Especially in Eastern Finland, very cold temperatures were recorded, with a minimum of -37.5°C at Konnunsuo (WMO station number 02733) on 5 February.

In this case, temperature and cloudiness in Eastern Finland were very variable both in time and space, illustrated by the example in Figure B.2, which shows 2-metre temperatures at the Konnunsuo (02733) and Tohmajärvi (02832) stations for the period from 24 January to 5 February. Their locations are marked in Figure B.3 with red and blue dots, respectively. Tohmajärvi is situated about 150 km northeast of Konnunsuo. On top of the diurnal cycle, with an amplitude of approximately 10°C, caused by solar radiation, there were remarkable irregularities. At the more northern station Tohmajärvi, the regular diurnal cycle was disturbed during the night of 28 January, having very small night-time cooling. In the evening on 28 January and the following night the temperature dropped by about 16°C and remained low until the end of the period. At the more southern station Konnunsuo a rapid warming of 15°C took place in the daytime on 29 January. Here the warmer period lasted several days, except for the night of 29 January, before the temperature dropped again on 1 February.

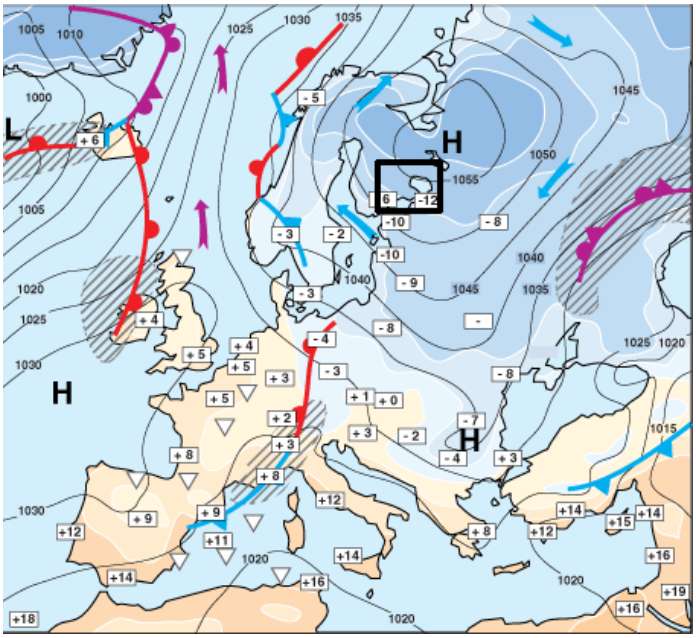

Figure B.1 General weather situation in Europe on 28 January 2012 12 UTC. Mean sea level pressure (contours) and 2-m temperature (shaded) are based on ECMWF analysis. The boxes show selected observed temperatures. The black rectangle box shows the area of interest of this study. (Source: Finnish Meteorological Institute)

The temperature drop between 31 January and 1 February was 21°C, from -11°C to -32°C. The reason for the irregular temperature variations was the changing cloudiness. During 28-29 January, the low-level cloud deck of a length of ca. 200 km and a width of 50-100 km, originating from the ice-free northern part of Lake Ladoga, moved from north to south over Southeastern Finland, as shown in Figure B.3. The clouds caused a rise of temperature first in the north (e.g. at the station Tohmajärvi), while by morning of 29 January the cloud had moved southwards, affecting the temperature there (e.g. at Konnunsuo). Based on observations and a series of satellite images acquired between 29 and 31 January (not shown), the cloud moved so that it affected the temperature only at Konnunsuo, while at Tohmajärvi the temperature kept the regular diurnal cycle with an amplitude of about 10°C. On the first days of February, the cloud occasionally affected the temperature at Konnunsuo. For instance, on 3 February the warm night temperature followed by quick cooling in the afternoon can be explained by changes in the cloud cover.

The cloud developed over Lake Ladoga because the lake was still partly ice-free. Compared to the nearby lakes, Lake Ladoga is very large and deep, with maximum and mean depths of 222 m and

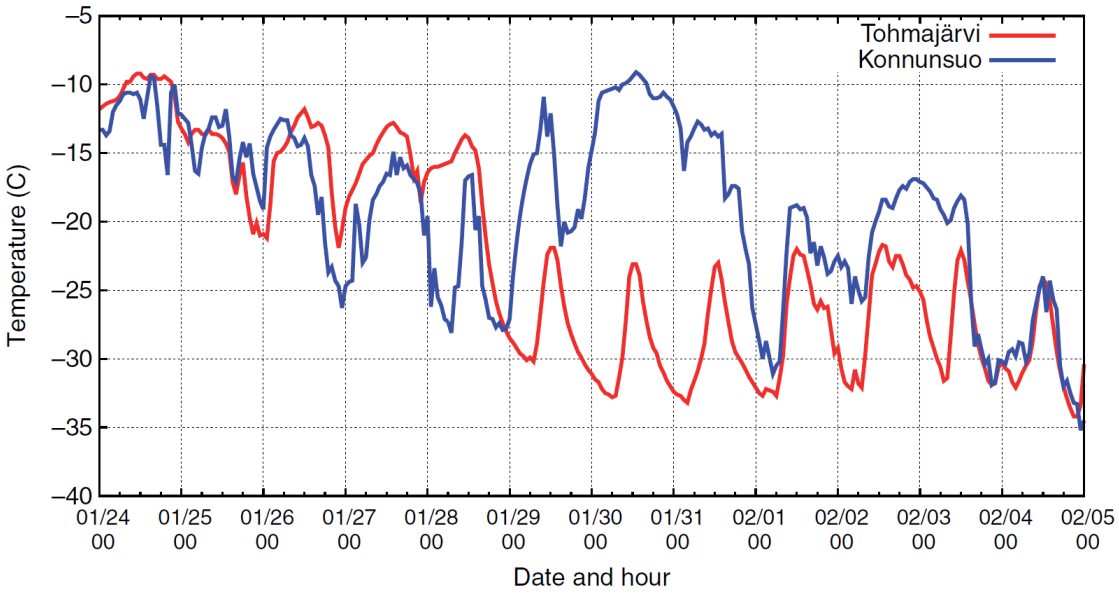

Figure B.2 Observed 2-m temperature at two stations, Konnunsuo (02733) and Tohmaja¨ rvi (02832) in Eastern Finland from 24 January to 5 February 2012. The distance between stations is about 150 km.

52 m, respectively. The northern parts are the deepest while the southern parts are relatively shallow. Lake Ladoga remains free of ice until early winter, when all other nearby lakes are already frozen. This was the case also at the end of January 2012. The northern parts of the lake were open but the shallow southern parts were covered by fractional ice, as seen in the MODIS/Terra satellite image (Figure B.4) on 28 January. A sequence of satellite images reveals that freezing advanced gradually in the cold air-mass until the whole lake was completely frozen around 5 February (not shown). This was later than on average in some years the freezing of Lake Ladoga already begins during the second half of December.

3 The model and methodology

The HIRLAM NWP system used in this study comprises an upper air and surface data assimilation system, a forecast model with a comprehensive set of physical parametrisations, and methods for pre- and post-processing observations and forecasts Undén et al., 2002, Eerola et al., 2013). This study was based on the latest reference HIRLAM (version 7.4, released in March 2012). In that version the

freshwater lake parametrisation based on FLake (Mironov, 2008, Mironov et al., 2012) may be applied for prediction of lake variables. For the atmospheric data assimilation, we used for simplicity the three-dimensional variational method (3DVAR) instead of the default four-dimensional variational analysis (4DVAR). We describe here briefly surface data assimilation and the parametrisation of atmospheric and surface processes relevant to this study.

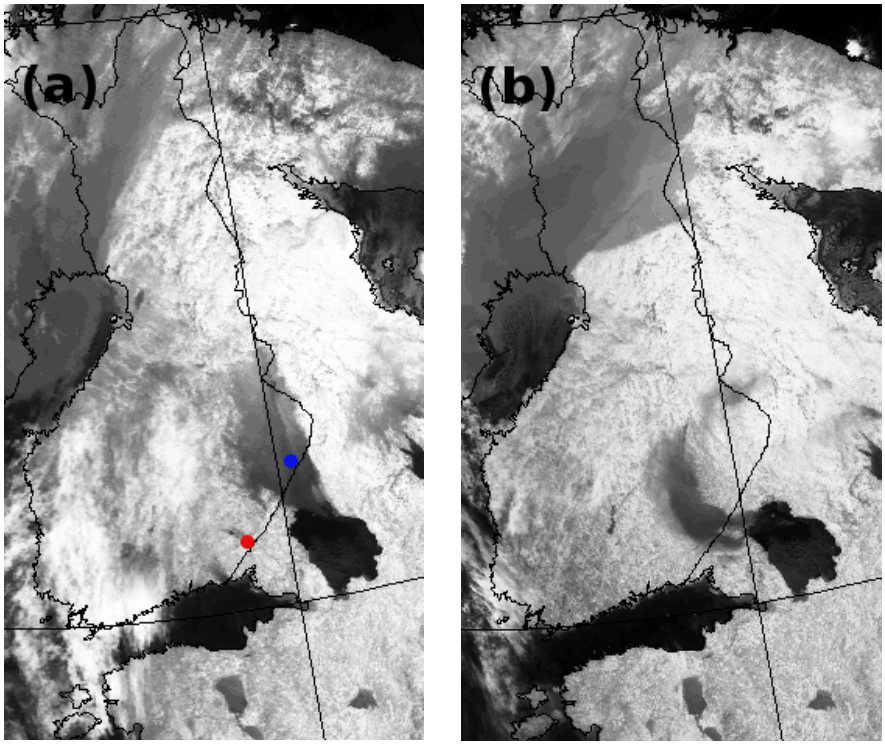

Figure B.3 NOAA AVHRR thermal IR images over Finland and Karelia on 28 January 06 UTC (a) and on 29 January 00 UTC (b) 2012. The low-level cloud cover, shown with dark-grey shades, spreads first northward (a) and later westward (b) from Lake Ladoga. In the single-channel images, the cloud over Lake Ladoga cannot be distinguished from the dark water surfaces. The stations Konnunsuo and Tohmajärvi, referred to in Fig. B.2, are marked with red and blue dots, respectively.

The method of optimal interpolation [(OI, e.g. Daley (1991)] is used for the analysis of LSWT and sea surface temperature (SST) at initial time of each forecast. LIC and sea ice concentration (SIC) are traditionally treated together with LSWT and SST using simple relations to convert from one to another (Rontu et al., 2012; Kheyrollah Pour et al., 2014b). For the current study, LSWT and LIC are

Figure B.4 MODIS-Terra colour composite image over Lake Ladoga on 28 January 2012 9:20 UTC. The dark colour in the norther part of the lake shows the ice-free part. South of it, an area of fractional ice can be seen. The white plume of the low-level cloud cover on the northeastern part of the lake is spreading northward.

of special interest. Only few conventional observations of LSWT are available regularly, so climatological information on LSWT/LIC is traditionally used in NWP models. Early versions of HIRLAM used this climatological information in the form of 'pseudo observations' (Rontu et al., 2012). Technically, the possibility of using satellite or any other extra observations of LSWT/LIC is available for numerical experiments. In the case when FLake is not applied, the background for the LSWT analysis is provided by the previous analysis, relaxed to climatology. If FLake is applied, LSWT from its short forecast is used as the background. However, the analysed LSWT does not directly influence the next forecast of the lake variables by FLake as this would require development and application of more advanced data assimilation methods (Rontu et al., 2012; Kheyrollah Pour et al., 2014b).

The HIRLAM surface scheme is based on the method of mosaic tiles (Avissar and Pielke, 1989). Each surface type is handled independently and the tiles affect each other only through the atmosphere. The total vertical turbulent and radiative fluxes in a grid square are obtained as weighted averages of fluxes over different surface types. Five surface types are defined: water, ice, bare land, forest, and agricultural terrain/low vegetation. The water and ice tiles may consist of sea or lake. For the three land surface types and sea ice, prognostic parametrisation is based on a two-layer ISBA

scheme (Interactions between Surface-Biosphere-Atmosphere) (Noilhan and Planton, 1989; Noilhan anf Mahfouf, 1996), modified according to Golvik and Samuelsson (2010) to improve interactions related to forest, snow, and ice.

Over land and ice the surface temperature is determined by the surface energy balance consisting of net radiation fluxes, heat flux from the underlying surface, and turbulent fluxes at the surface. Over sea, SST and ice cover given by the surface analysis are kept constant during the forecast and the ice surface temperature is predicted using a simple thermodynamic parametrisation based on Golvik and Samuelsson (2010). Over lakes, LSWT and LIC are treated in a similar way if the FLake parametrisation is not applied (experiments OLD and NHA described below). If FLake is used (experiment TRU), the mean lake water, ice, and snow temperatures as well as the lake ice depth are prognostic variables. At every time step, the lake surface temperature, which interacts with the atmosphere, is diagnosed from the uppermost predicted temperature (snow, ice or water).

The turbulent heat and momentum fluxes are treated separately in the surface layer (the lowest model layer) and above it. In the surface layer, stability functions by Louis (1979) and predefined roughness values are applied for calculation of the fluxes over each surface type, with own prognostic surface temperature and moisture. Above the surface layer, a scheme based on turbulent kinetic energy approach (Cuxart et al., 2000) is applied, using the grid-averaged surface fluxes as the lower boundary condition.

The weather parameters discussed in this study are the screen-level (or 2-metre) air temperature and the fractional low-level cloud cover. In HIRLAM, the screen-level temperature is estimated from the predicted temperature on the lowest model level (about 12 m above the surface) and the surface temperature, taking into account the surface layer stability. It is calculated separately for each surface type in a grid-box and the grid-scale value is obtained as an area-weighted average. The surface temperatures in the tiles are very sensitive to the radiative and heat transfer properties of the surface, which may be completely different for land, water, ice, and snow. In the current meteorological situation, the long-wave radiation was crucial for the evolution of the screen-level temperature. The net long-wave radiation flux at the surface depends on the surface temperature and on the long-wave radiation emitted by the (moist) air and clouds towards the surface. The basic prognostic variables, affecting the cloud-radiation interactions in HIRLAM, are the in-cloud specific liquid water and ice content as well as the air temperature and humidity at the level of clouds. The three-dimensional

diagnostic cloud fraction is derived from the relative humidity (Sundqvist et al., 1993; Sundqvist, 1989). The amount of low clouds is defined by taking the maximum total cloud cover from all levels from the surface to the level of about 750 hPa or about 2500 m. Details of the radiation, cloud and turbulence parametrisations applied in HIRLAM can be found in Undén et al., (2002).

For this study we defined three HIRLAM experiments: OLD, TRU, and NHA, which differed from each other only in the way how lake surface state was described. The first experiment OLD represented a traditional large-scale NWP system, where LSWT and LIC were determined by their climatological values. This was achieved by picking up LSWT values from the ECMWF analyses to be used as observations in the surface analysis (Eerola et al., 2010). Over selected large lakes, including Lake Ladoga, these analyses contained LSWT estimated from time-lagged simulated screen-level temperatures (G-P. Balsamo, personal communication). LIC was derived diagnostically from LSWT, as discussed earlier. LSWT and LIC were kept unchanged during the forecasts.

The second experiment TRU used the prognostic lake parametrisation by FLake. No observations on or close to Lake Ladoga were introduced into the LSWT analysis. Thus the lake surface state was totally determined by FLake. This experiment was similar to TRULAK in Kheyrollah Pour et al., (2014b). In the third experiment NHA, satellite data from the Moderate Resolution Imaging Spectrometer (MODIS), operating on NASA's Terra and Aqua satellites were used (Kheyrollah Pour et al., 2014a, b). MODIS observations were introduced at 15 pre-selected locations over Lake Ladoga as in the experiment NHALAK in (Kheyrollah Pour et al., 2014b).

The experiments were run independently of each other. Experiment TRU was run through the whole winter 2011-2012 and experiment NHA from the beginning of January 2012 to the end of May 2012. Experiment OLD was run for a shorter period containing the second half of January 2012. Four data assimilation-forecast cycles per day were initiated at 00, 06, 12 and, 18 UTC, but longer forecasts of 27 hours lead time started only from analyses at 00 and 12 UTC. The experiments were run over a Nordic domain shown on the upper right corner of Figure B.5a, using a horizontal resolution of ca. 7.5 km and 65 levels in vertical. The density of levels was highest in the boundary layer: 20 levels were used within the lowest one kilometre. Lateral boundary conditions of the atmospheric variables were provided by the ECMWF analyses.

4 Results and discussion

We analysed, evaluated and validated results of the three HIRLAM experiments between 25 January and 5 February, discussing in detail the results for one 27-hour forecast starting from the analysis at 28 January 00 UTC. This short (one day) period was challenging to the HIRLAM model, and would be as difficult to any other NWP-model, because of the quick changes in local cloud cover and 2-metre temperature. The predicted synoptic-scale features, such as location and strength of the anticyclone, were similar in all experiments. Therefore, the contrasting weather forecasts for Eastern Finland by the experiments were due to the differently simulated description of the state of Lake Ladoga.

4.1 Simulated ice concentration on Lake Ladoga

Figure B.5 shows LSWT and LIC according to the three experiments at 00 UTC on 28 January, i.e. at the initial (analysis) time of the forecasts in question. In OLD, Lake Ladoga was completely frozen, according to the climatology. In TRU and NHA, the northern part of the lake was ice-free as in reality (Figure B.4). In TRU, the lake model FLake predicted the northern parts of Lake Ladoga as ice-free. In NHA, the satellite observations used in the analysis allowed to describe most of the lake as ice-free. None of the experiments could describe well the area of fractional ice seen in Figure B.4 over the southern part of Lake Ladoga. In NHA, the simple relations for the diagnosis of ice fraction based on analysed LSWT and the usage of only 15 satellite pixels in the analysis were insufficient to resolve the fractional ice zone. FLake does not predict ice concentration, so in TRU, LIC was diagnosed to be 0 or 1 at every grid-point based on predicted ice thickness.

In TRU, the frozen area over Lake Ladoga increased slightly during the forecast, but even at the end of the forecast at 29 January 03 UTC most of the northern part of Lake Ladoga was still ice-free (not shown). In NHA, Lake Ladoga became totally ice-covered on 30 January and in TRU one day later. In reality, the ice concentration increased gradually from south to north during the last weeks of January and first week of February, and, according to the satellite images, the whole lake, except narrow leads, could be considered frozen by 6 February (not shown). It is worth noting that FLake, running without any support from observations but online-coupled to the weather forecast by HIRLAM, was able to predict the state of Lake Ladoga quite accurately.

4.2 Predicted cloud cover and temperature in Eastern Finland

Figure B.6 shows the 6-hour forecasts of low-level cloud cover and screen-level temperature by the three experiments. In OLD, there was only very little low-level cloudiness close to Lake Ladoga. In TRU and NHA, clouds were forecast over the northern part of the lake, in NHA also further to the south, due to the larger ice-free part of Lake Ladoga compared to TRU (Figure B.5). The cloud spread towards northwest with the prevailing weak southeastern wind. Compared to the satellite image (Figure B.3a), the cloud was located almost correctly in both experiments (TRU and NHA), only slightly shifted towards west. The corresponding charts for 24-hour forecasts are shown in Figure B.7.

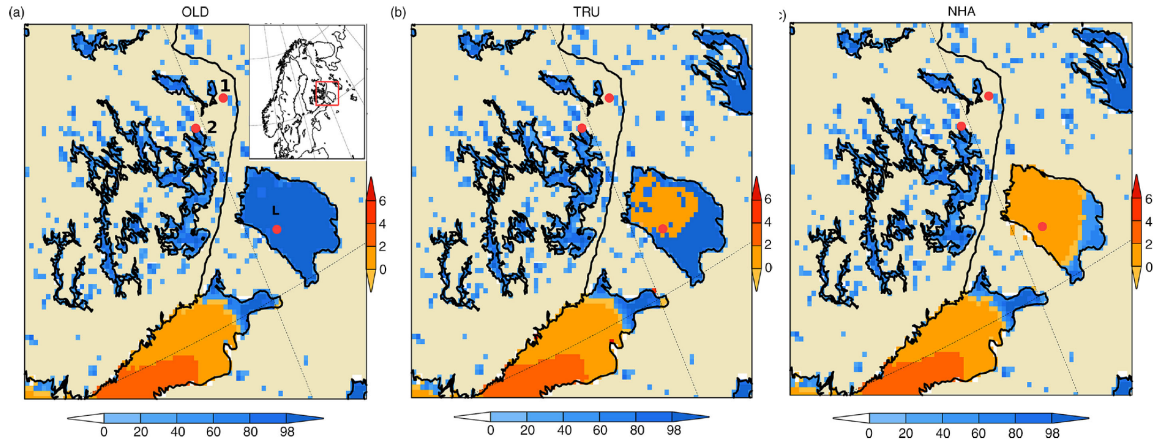

Figure B.5 Simulated ice concentration (%, scale at bottom) and surface water temperature (8C, scale on the right) on 28 January 00 UTC from the three experiments: OLD (a), TRU (b), and NHA (c). The red dots marked with 1 and 2 in (a) show the two observation stations: 1=Ilomantsi, 2=Joensuu (discussed in Sections 4.2 and 4.3). Point L over Lake Ladoga shows the grid-point discussed in Section 4.3. The embedded small map in (a) shows the whole integration area of the experiments and the red rectangle box the area of interest of this study.

According to the satellite images, the cloud moved first towards northwest, then towards west where the plume was narrower than earlier (Figure B.3b). This was well reproduced by TRU and NHA, while OLD had no sign of these clouds (Figure B.7, upper panels). Even the shape and direction of movement of the cloud cover were well predicted by TRU and NHA. It is important to note that the clouds do not necessarily appear immediately at the spot of maximum evaporation over the lake. The evolution and balance of the large-scale dynamical processes and local forcing influence

the fetch over water, modify evaporation and mixing, advect the moisture, and create conditions for cloud microphysical processes. The task of a NWP model is to simulate all these processes.

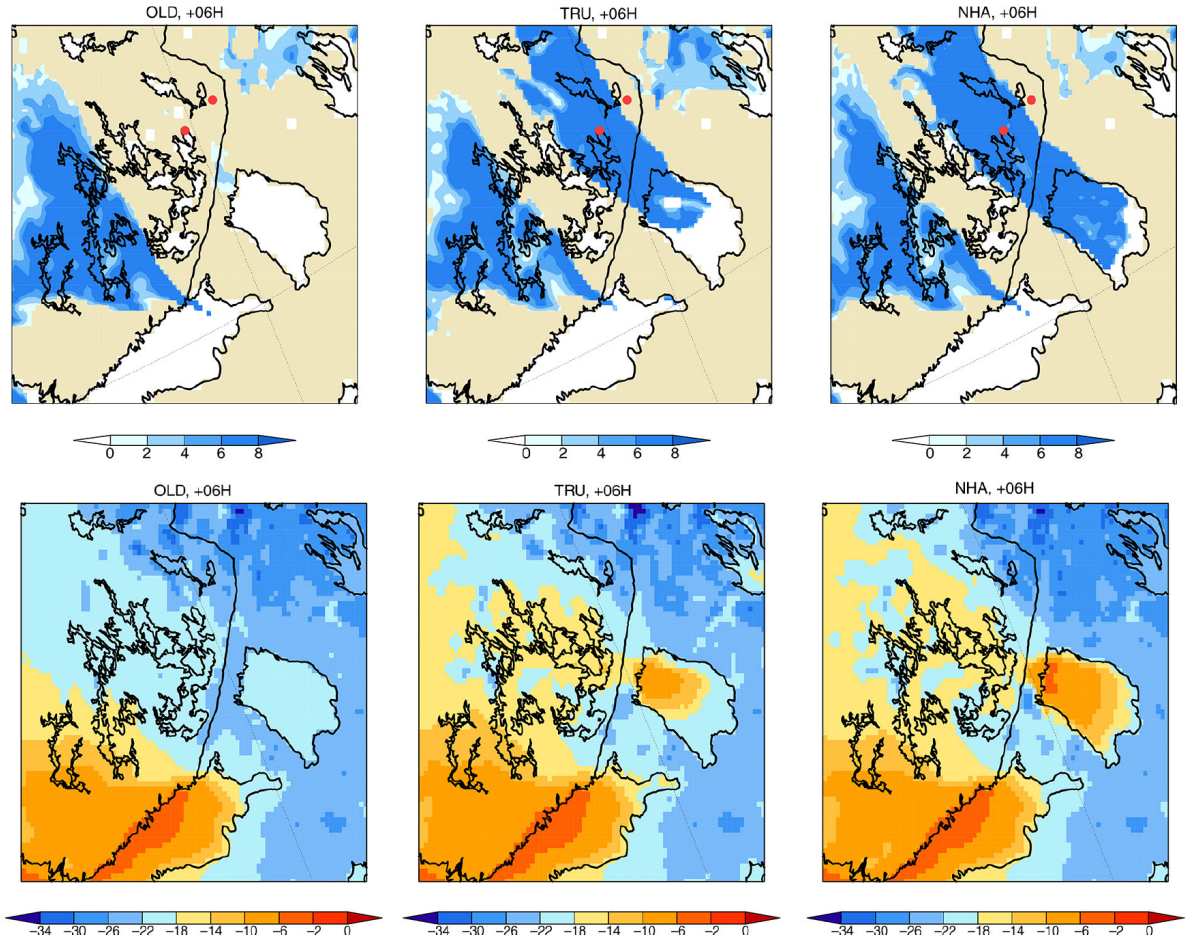

Figure B.6 Six-hour forecasts of instantaneous low-level cloud cover (octas, upper panels) and screen-level temperature (8C, lower panels) from the three experiments OLD (left), TRU (middle), and NHA (right). The analysis time (starting time of the forecasts) is 28 January 00 UTC. The red dots denote the two observation stations, Ilomantsi and Joensuu (see Fig. B.5).

The low-level cloudiness affected the predicted screen-level temperature (Figures B.6 and B.7, lower panels). OLD predicted uniformly cold temperatures, as could be expected in such meteorological situation under clear sky and over snow- or ice-covered surface. In TRU and NHA, the air temperature was higher both over Lake Ladoga and over the cloudy land areas northwest of the lake. Over the lake, the temperature followed the ice distribution, as could be expected.

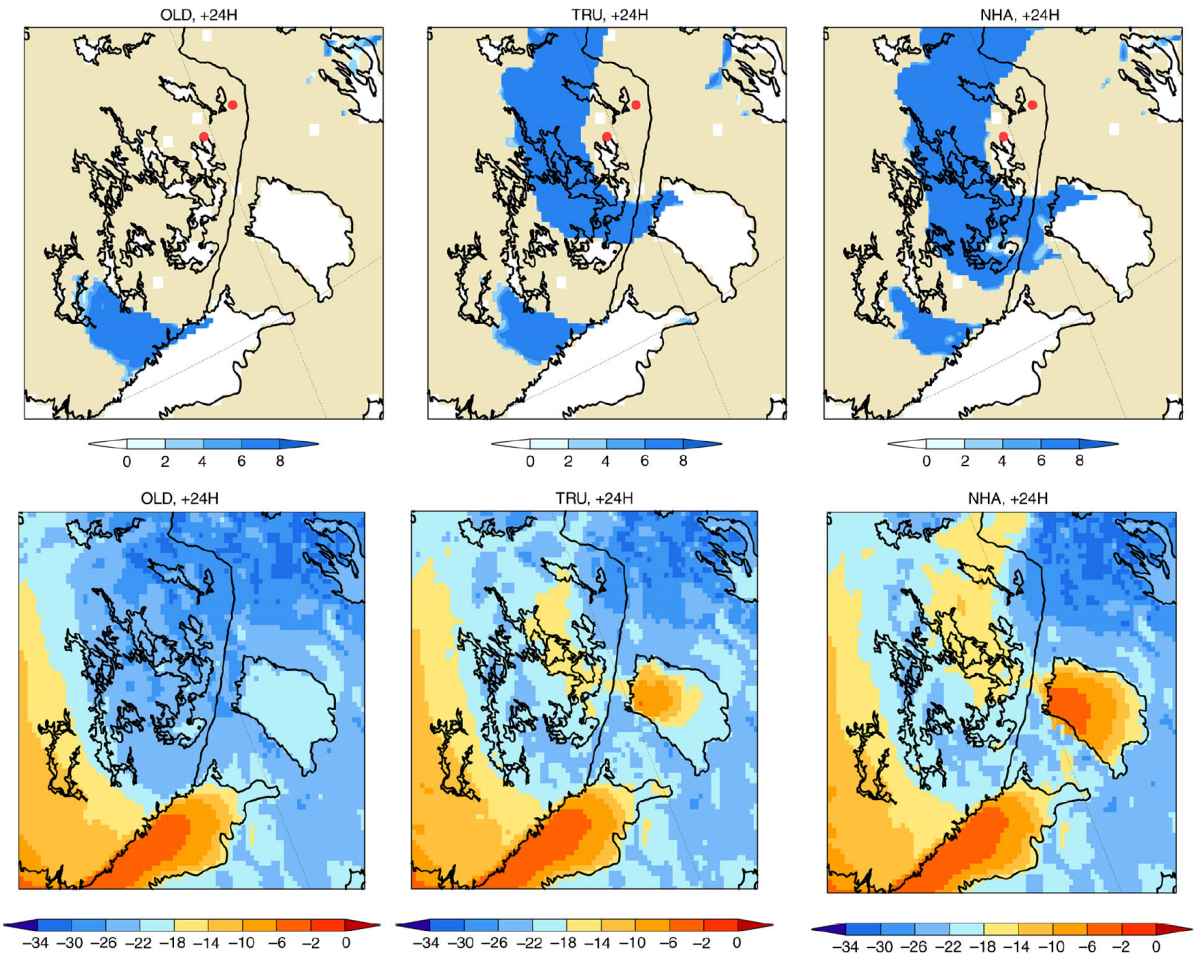

Figure B.7 Same as Fig. B.6 but for 24-hour forecasts.

Relations between the predicted and observed temperature and low-level cloudiness were studied in detail by comparing the observations and forecasts at two weather stations, Ilomantsi Mekrijärvi (02939, marked as 1 in Figure B.5a, hereafter Ilomantsi) and Joensuu Linnunlahti (02928, marked as 2, hereafter Joensuu). The distance between the stations is only about 60~km. Note that these stations are different than those chosen for illustration of the temperature fluctuations during the whole anticyclonic period in Figure B.2. The cloud passed the weather stations at slightly different times, thus motivating us to compare this timing in different experiments. The closest predicted grid-point values from the three forecasts were chosen for comparison.

The observed low-level cloud cover and temperature at Ilomantsi and Joensuu are shown in Figures B.8a and B.9a as a function of time, respectively. As observed at Ilomantsi, the sky was covered by low clouds from 06 UTC to 15 UTC, while at Joensuu the sky was cloudy from 03 UTC up till 18 UTC. As a consequence, at Ilomantsi the temperature rose from -28°C to -18°C in 12 hours when the sky became cloud-covered. Because of the clouds, the temperature change was not, at least entirely, due to the normal daily cycle driven by the solar radiation. When the cloud disappeared after 15 UTC, the temperature dropped from -18°C below -30°C. At Joensuu, the temperature was around -15°C all day due to the cloudiness, i.e. in the early morning hours it was 15°C warmer than at the nearby Ilomantsi. During the cloudy phase, the cloud base height varied at Ilomantsi from 30 m to 120 m and at Joensuu from 70 m to 180 m. At Joensuu also fog was reported. Both stations reported light snowfall, but the amount was too small to be detected in the precipitation measurements.

The corresponding forecasts (Figures B.8b-d) and 9b-d) reveal the striking differences between the experiments: there was no low-level cloud in OLD, neither at Joensuu nor at Ilomantsi. Much more realistic cloud cover was predicted by both TRU and NHA. Looking more closely at the forecasts at Ilomantsi (Figure B.8), the duration of the cloudy period was underestimated by these experiments. When there were clouds, the cloud base heights (diagnosed from the existence of liquid or ice water within the model's vertical resolution) were predicted well by both TRU and NHA: while the observed values at 09, 12, and 15 UTC were 60, 90, and 120 m, the predicted values were 66, 66 m, and no cloud in TRU, and 66, 66, and 105 m in NHA. The heights of cloud tops varied between 240 and 290 m in TRU and between 270 and 360~m in NHA. To summarise, NHA predicted more clouds than TRU and they were thicker. This difference was also seen in the values of vertically integrated cloud condensate. This is the sum of specific liquid and ice content, in this case consisting mostly of liquid. In TRU the values varied between 9-13 gm^{-2} and in NHA between 11-22 gm^{-2} when the cloud was present. The vertical distribution of cloud condensate revealed that it was in both experiments concentrated in the lower atmosphere, indicating that only low-level clouds were predicted. For the cloud condensate and the height of low cloud tops we had no observations for verification.

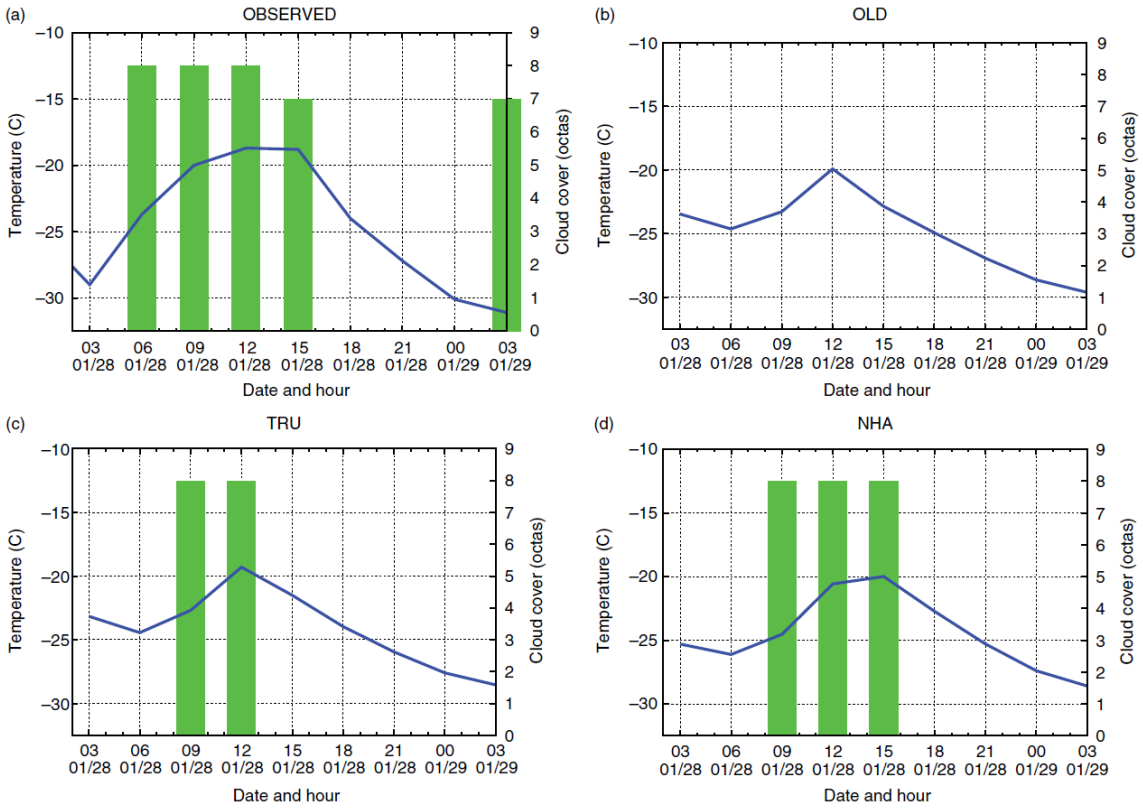

Figure B.8 Observed and predicted 2-m air temperature (8C, blue line, left y-axis) and instantaneous low-level cloud cover (octas, green bar, right y-axis) at Ilomantsi (WMO station number 02939): Observed (a), predicted by OLD (b), predicted by TRU (c), and predicted by NHA (d).

At Joensuu (Figure B.9), the low-level cloud cover and the sky clearing were forecast correctly by TRU and NHA. However, both experiments predicted similarly the cloud base heights somewhat too low, giving values between 60 and 100 m, while observations indicated values between 70 and 180 m. The cloud tops were higher in NHA, between 270 and 360 m, than those in TRU, which predicted values between 200 and 290 m. Thus the clouds were thicker in NHA than in TRU, as was the case at Ilomantsi. The vertically integrated cloud condensate varied in TRU between 8-24^{-2} and in NHA between 12-37 gm^{-2}, which are all realistic values for shallow boundary layer clouds. As at Ilomantsi, the TRU and NHA cloud condensate was concentrated in the lower atmosphere indicating that only low-level clouds were predicted.

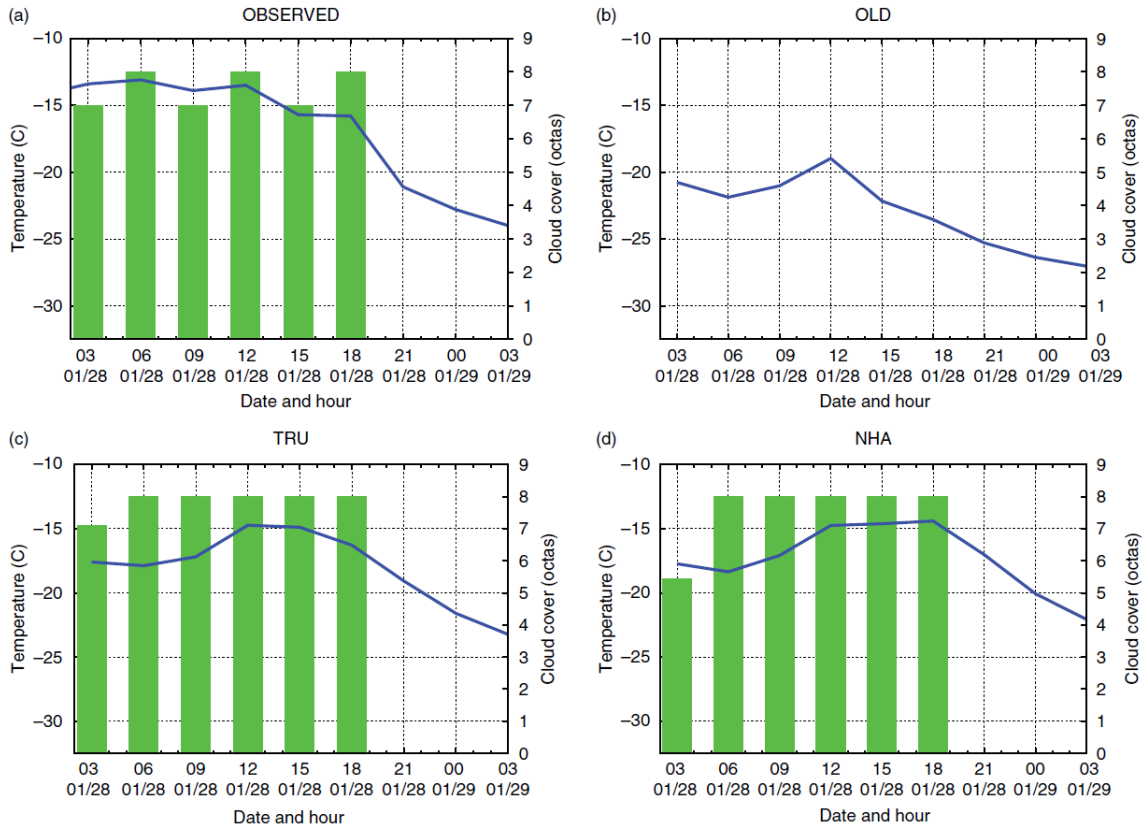

Figure B.9 As Fig. B.8 but at Joensuu (WMO station number 02928).

The thicker cloud in NHA compared to TRU both at Ilomantsi and Joensuu was indicated also by the downward long-wave radiation (LWD). LWD values were constantly around 165 Wm^{-2} in the clear-sky experiment OLD while the maximum values by TRU and NHA at Ilomantsi were in the afternoon 207 Wm^{-2} and 222 Wm^{-2}, respectively. The corresponding values for Joensuu were 231 Wm^{-2} and 263 Wm^{-2}.

The amplitude of screen-level temperature at Ilomantsi was forecast rather similarly too small by all experiments (Figure B.8). The maximum daytime temperatures were reasonable and the cooling in the evening was predicted correctly, although the night minimum temperature remained several degrees too high. At Joensuu, the temperature in OLD was too low by 5-10°C during the whole forecast due to the unpredicted clouds (Figure B.9). In TRU and NHA, the temperatures were quite well predicted, especially at noon and in the afternoon, thanks to the good low-level cloud forecast.

However, in the morning of 28 January both experiments predicted too cold temperatures by 5°C, presumably due to inaccurate prediction of the cloud evolution during the first hours of the simulations. The cooling in the evening and at night in TRU and NHA was well predicted, although the observed minimum temperatures were again not reached.

The cold morning temperature on 29 January at Ilomantsi (Figure B.8) remained unpredicted, although no experiment showed clouds. Atlaskin and Vihma (2012) reported that all NWP models have problems in predicting cold enough temperatures in the stable boundary layer situations, where they show increasing bias with decreasing temperature and strengthening temperature inversion. In a review of the results from the Global Energy and Water Exchange (GEWEX) Atmospheric Boundary Layer Studies (GABLS), Holtslag et al., 2013 reported an obvious result from their studies that operational models typically have too much mixing in stable conditions, which strongly impacts diurnal cycle of temperature and other near-surface variables. They also stated that coupling between the atmosphere and the land surface is the key for a good representation of the diurnal cycle of the boundary layer variables. Next, in Section 4.3, we analyse in detail the surface energy balance and cloudiness in order to understand the differences between experiments.

In summary, our experiments showed that a precise forecast of the cloud cover was crucial to improve the temperature forecast. Only those experiments, which relied on realistic ice conditions over Lake Ladoga, were able to predict the clouds and their movement. This in turn improved the temperature forecasts. Provided with these forecast maps by HIRLAM, a forecaster would predict the variations of temperature in Eastern Finland.

4.3 Boundary layer and conditions over land and lake

So far we have discussed the influence of frozen or unfrozen Lake Ladoga on the near-surface temperature and cloudiness in Eastern Finland. In this section, we illustrate the simulated boundary layer structure and surface energy balance with examples at two locations: one at a point over the central part of Lake Ladoga and one over land at Ilomantsi. The 24-hour predicted temperature and dew-point (Figure B.10a) and wind speed (Figure B.10b) profiles are shown for point L over Ladoga (see the map in Figure B.5) in the lowest 2 km layer. Above the atmospheric boundary layer, the results of three experiments - OLD over ice, NHA over open water and TRU over a freezing surface - were in agreement with each other. Above the inversion, the atmosphere was very dry, as characterised by the large dew point deficit $\Delta = T - T_d \approx 20$°C. The maximum wind speed was

reached at the top of the inversion layer. However, inside the boundary layer, the experiments showed remarkable differences in the profiles.

In experiment OLD (ice-covered lake surface), the surface-based temperature inversion was strong, about 15°C between the surface and the ca. 300-metre level. The wind was very weak close to the surface, where the smallest $\Delta \approx 2.5$°C was suggested by the model. These profiles over ice resemble those of the snow-covered land surface (not shown). This experiment assumed frozen Lake Ladoga, which excluded the source of moisture, available for the experiments TRU and NHA. We can assume that there was not enough humidity for formation of clouds in the shallow stable boundary layer of OLD, where mixing was also reduced. There may have been a small probability of local ice fog formation just above the ice.

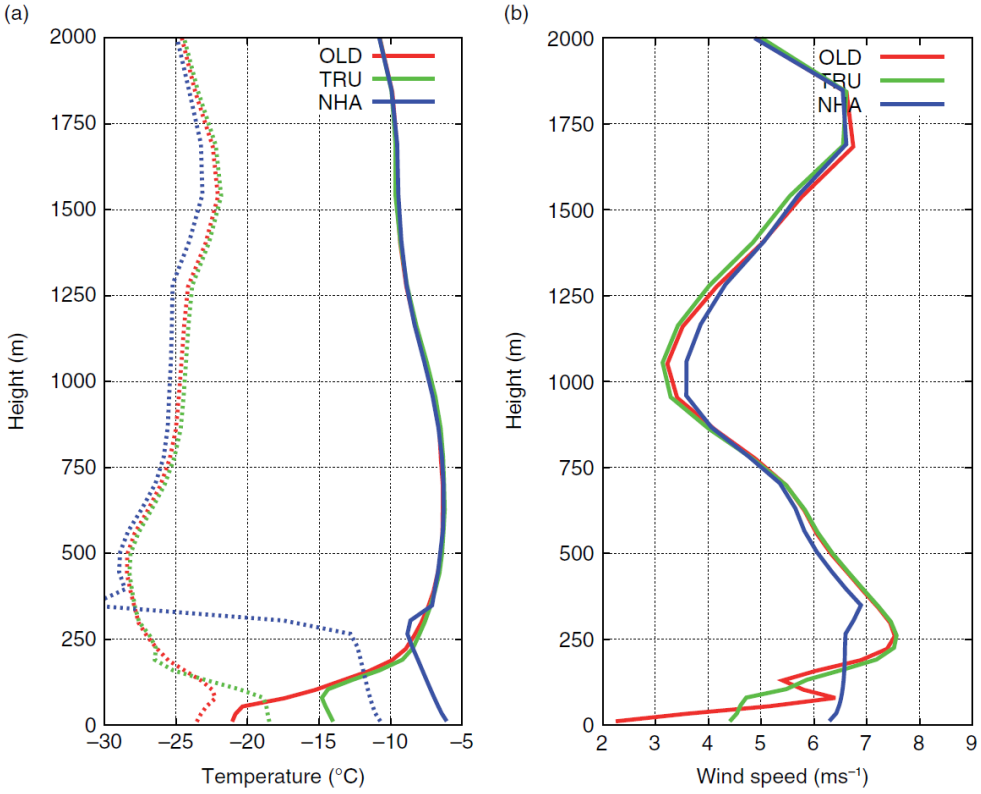

Figure B.10 Twenty-four-hour predicted temperature (solid line) and dew point (dotted line) (a) and wind speed (b) profiles at the grid-point over Lake Ladoga marked with L in Fig. B.5 from three experiments: OLD (red), TRU (green) and NHA (blue). The valid time of the profiles is 29 January 00 UTC.

NHA (open water) profiles represent conditions over an ice-free lake surface. Due to the large temperature difference between water and air, the turbulent fluxes were strong, causing strong mixing in the planetary boundary layer. The mixed layer was the thickest and warmest among the three experiments but still reached only the height of ca. 300 m, where it was capped by an elevated inversion. The near-surface turbulence lifted the inversion from surface to the top of the relatively shallow boundary layer. This is typical for anticyclonic conditions, where a large-scale descending motion is prevailing. The wind maximum at the top of the capping inversion showed only a minor difference from the mean wind speed in the boundary layer. The boundary layer temperature profile indicated neutral or slightly unstable conditions. Moisture evaporated from the lake was mixed to the whole boundary layer. However, the relatively weak wind shear reduced the simulated mixing somewhat. All this favoured cloud formation but not sufficiently to trigger deep convection and snowfall.

In experiment TRU, lake properties were handled by the prognostic parametrisation by FLake, which was coupled to the atmospheric model at every time step. Therefore, in any grid-box containing a fraction of lake, water temperature or ice depth evolved during the forecast. At the grid-point L, Lake Ladoga became frozen during this forecast about 12 hours before the time of the predicted wind, temperature and humidity profiles shown in Figure B.10. As seen in Figure B.11, the surface (now ice) temperature started to decrease after freezing at noon, but there was not enough time for the surface-based temperature inversion to build to the strength shown by OLD. Hence, the profiles were between those predicted by NHA and OLD. However, evaporation from the lake and mixing started to decrease immediately after the freezing (Figure B.11). Some of the neighbouring grid-boxes still remained ice-free, therefore influencing the profiles in L. No cloud was predicted by TRU in this grid-box.

Figure B.11 shows the evolution of the latent and sensible heat, net short-wave and long-wave radiation fluxes together with the predicted lake temperatures at the grid-point L. The figure is based on one forecast from experiment TRU, initiated from 28 January 00 UTC analysis. Note that in HIRLAM convention all fluxes are denoted positive towards the surface, both from above and below. At the beginning of the forecast the lake was ice-free. LSWT by FLake was close to zero, indicating that water was close to freezing. Due to the cold air mass above, the latent and sensible heat fluxes were quite large and negative, -70 Wm^{-2} and -150 Wm^{-2}, respectively, thus directed from the lake to

the atmosphere. Turbulent mixing in the boundary layer was reduced by the prevailing stable conditions and moderate wind shear. However, the moisture flux was sufficient for the formation of the low cloud over Lake Ladoga. This cloud then propagated downstream and dramatically affected the screen level temperatures far from the lake.

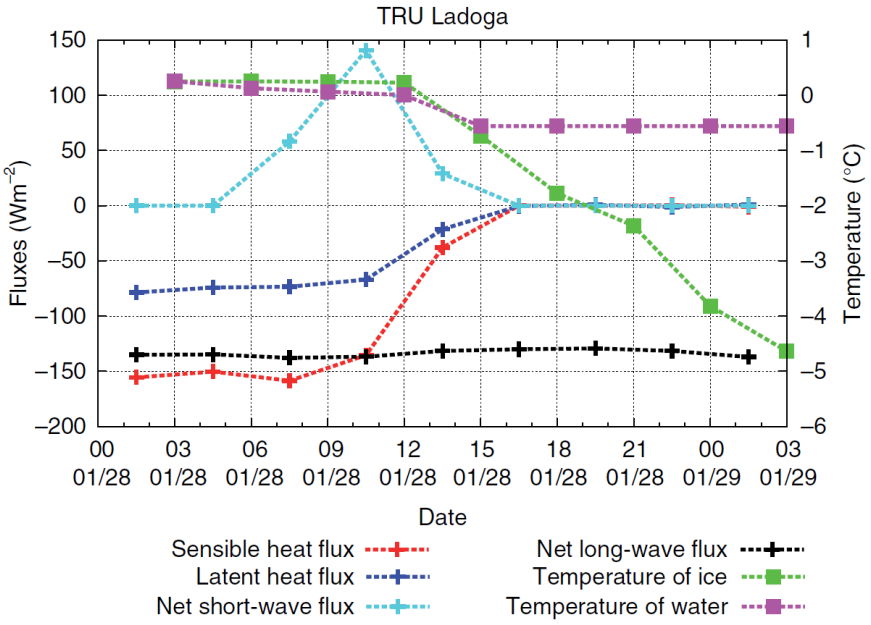

Figure B.11 Predicted surface fluxes (unit Wm^{-2}, left y-axis), averaged over 3 hours, and temperatures of ice and water (unit °C, right y-axis) during 28 January 2012 at the grid-point over Lake Ladoga marked with L in Fig. B.5 as given by the experiment TRU. No clouds were predicted by TRU at this location. All fluxes are denoted positive towards the surface, both from above and below.

Energy balance over the water or ice surface is the sum of the turbulent heat fluxes, the net long-wave and short-wave radiation fluxes and the heat transfer from below. The transfer from below, estimated by FLake in the experiment TRU, was very small before and after freezing. During the day, when there was still no ice, the water surface heat balance was negative (fluxes directed from the lake to the atmosphere). This resulted in ice formation. When ice appeared, its surface heat balance was still negative, and the ice surface temperature started to drop very fast. Hence, the turbulent heat fluxes decreased and approached zero in the stable surface layer. During the night, the surface lost heat only due to the net long-wave radiation. The ice depth continued to increase, and the ice temperature continued to drop. At the end of the forecast, the ice temperature had decreased almost to

-5°C. During the next day, the increased albedo of the now ice-covered lake surface would lead to less absorption of the solar radiation and further cooling of the surface.

At a point over land, the surface energy balance evolved differently under the clear sky and low clouds. The fluxes and surface temperatures at Ilomantsi from TRU (Figure B.12) are shown for the same period as the temperature and cloud cover in Figure B.8c. Of the Ilomantsi grid square, 41 % was covered by frozen (small) lakes, while the rest was mainly snow-covered forest. On midday 28 January, the low clouds were forecast by HIRLAM. At that time the net short-wave flux towards the surface was only one third (ca. 50 Wm^{-2}) of that at the clear-sky grid-point over Lake Ladoga (Figure B.11). The net long-wave radiative flux was small and negative, ca. -20 Wm^{-2} and thus directed from the surface to air. In this situation, the long-wave cooling was prevented by the low-level cloud cover. A small sensible heat flux (ca. -15 Wm^{-2}) was negative and thus directed from the surface to air.

The surface temperature in the snow-covered forest reached a maximum value of ca.-22°C in the afternoon (Figure B.12). The ice surface temperature, predicted by FLake for the lake part of the grid-box, was much higher during the whole period, with a maximum value of ca. -13°C. In the evening, when the cloud disappeared, the net long-wave cooling increased and approached value of -60 Wm^{-2}. This was less than half of the corresponding value at the grid-point over Lake Ladoga (Figure B.11). However, it was sufficient to cause a decrease of the forest snow and lake ice surface temperatures, since the long-wave flux was only compensated by the smaller heat flux from the snow-covered soil or lake ice. It is known that both in the model and in the nature, even a rather thin layer of snow is sufficient to insulate the relatively warm soil (or thin lake ice) from the air. As seen in Figure B.8a, cooling of the surface led to cooling of the near-surface air, which continued the whole night, as correctly suggested by experiment TRU.

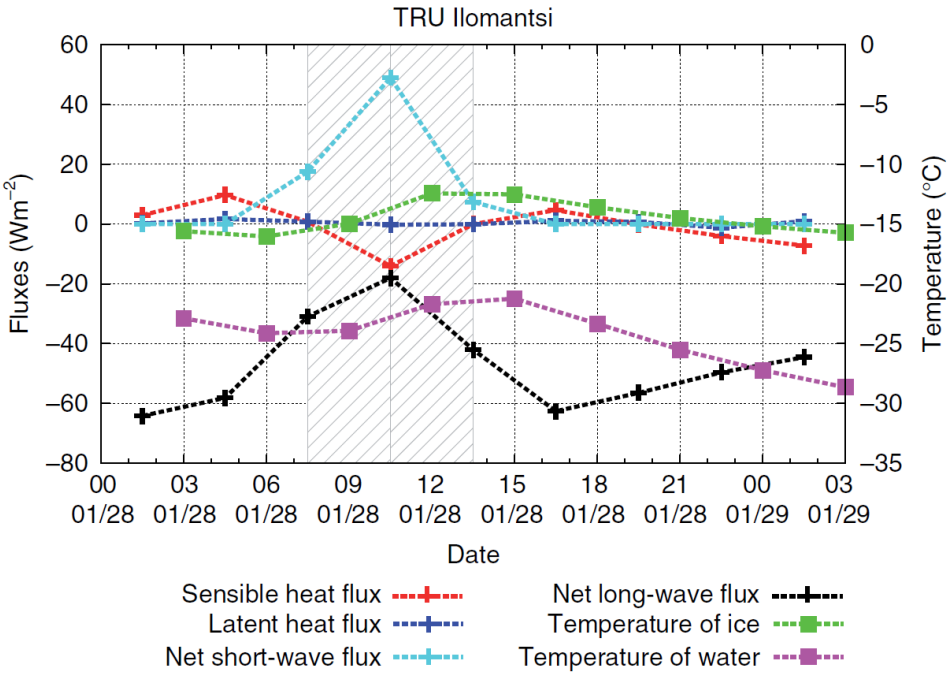

Figure B.12 As in Fig. B.11 but for Ilomantsi and temperature of forest surface instead of LSWT. Cloudy time period is shown with shading. Ice temperature represents the local small lakes in the Ilomantsi grid-box. Note that the scale in the y-axis is different to Fig. B.11.

In this section we diagnosed the boundary layer and surface conditions of the HIRLAM forecasts. There were no flux observations for the validation of the simulated surface energy balance. However, according to the resulting temperature and cloud forecasts, the winter-time boundary layer over water and snow was described well by HIRLAM.

4.4 Objective verification

Strictly speaking, the influence of lakes on weather and climate is not local but is spread to the surroundings of the lake. Scott and Huff (1996) reviewed several earlier studies and concluded that the influence of the Great Lakes extends over a distance from 10 km to more than 100 km, depending on the weather parameter and also on the lake in question. The influence can be different on different sides of the lake. These authors used a 80 km wide zone when estimating the size of climatological lake-effect of several weather parameters.

In the current case, the maximum influence of Lake Ladoga can be estimated to extend as far as the lake-originated cloud was spread by the wind. In the upwind direction the influence extent would be small. Based on Figure B.3, the cloud was detected at least 250 km to the west and northwest of the lake. The predicted wind direction over Lake Ladoga at the height of the low clouds in all experiments was from southeast, turning later more towards east and a low-level jet was predicted at the height of 250-300 m (not shown). Hence, the observing stations on the western side of Lake Ladoga up to 250 km were selected, ten stations in total, for the objective verification. Exactly the same observations were included in the verification of different experiments. The validation time period was from 25 January to 5 February.

The bias and rms-error of 2-metre temperature forecasts as a function of forecast length are shown in Figure B.13. The values at the initial time are analysis errors and are therefore not comparable to the forecast errors. Typically to the short-range 2-metre temperature forecasts, there was no large growth in the bias or rms-error with the forecast length. The differences between experiments were large, but similar at all forecast lengths. Concerning the bias, OLD had the largest negative error, of the order -2°C or more. In NHA the bias was of the order -0.5°C and in TRU even less. Because the only difference between experiments was the state of Lake Ladoga, it is evident that the correct ice conditions of Lake Ladoga improved the temperature forecasts also when measured with objective scores and averaged over a longer time period.

The large negative bias of OLD may look surprising, because normally in cold situations NWP models typically have difficulties to predict cold enough temperatures (Atlaskin and Vihma, 2012). The explanation is seen in Figure B.14, which shows the scatterplot of observed vs. predicted temperatures in different experiments. In all experiments, the extremely cold temperatures below -30°C were predicted too warm, as expected. The large negative bias in OLD was seen mainly in the observed temperature range -12°C to -18°C, which was typical for the cloudy conditions. In the observed cloudy conditions, OLD predicted too little cloud and hence too cold screen-level temperatures in this temperature range. Within the temperature range -20°C to -30°C (presumably clear-sky cases) the results were rather similar in all experiments. Far from Lake Ladoga the differences in verification scores of all parameters between experiments were very small (not shown).

The time-series of observations and forecasts indicated that largest differences between forecasts took place during the last week of January, i.e. time when the ice conditions of Lake Ladoga were

different in different experiments (not shown). The coldest period in Eastern Finland was observed during the first week of February. Lake Ladoga was then almost frozen in reality and completely frozen in all experiments. During this period, the temperature forecasts by different experiments were close to each other (not shown).

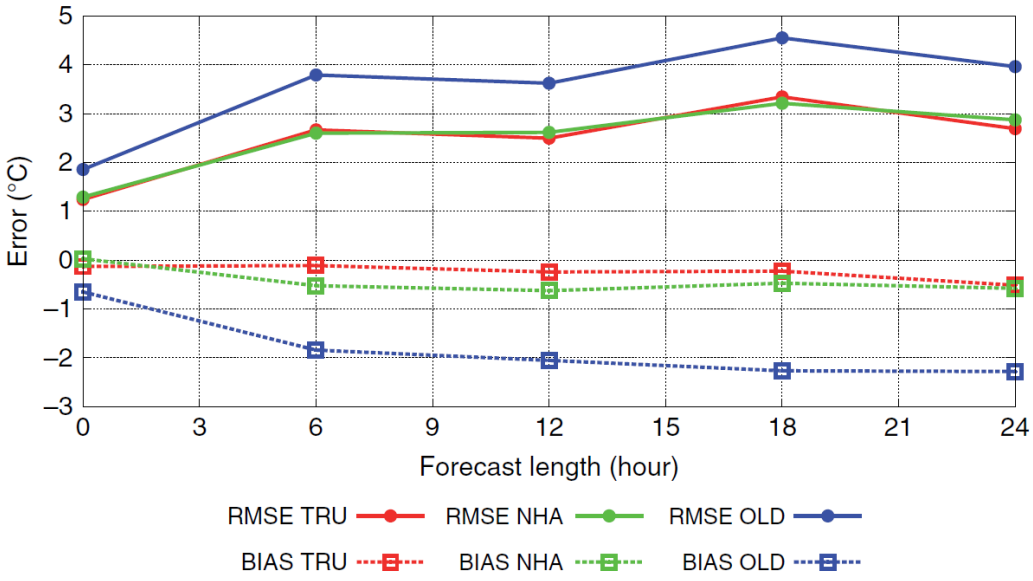

Figure B.13 Bias and rms-error of 2-m temperature as a function of forecast length for the period from 25 January to 5 February and averaged over 10 observing stations westwards and closer than 250 km from Lake Ladoga. Forecasts from 00 UTC and 12 UTC analysis are included in the statistics.

Summarising the results of objective verification, we conclude, that the correct description of the ice conditions over Lake Ladoga improved the temperature verification scores against measured temperatures in the vicinity of Lake Ladoga during the anticyclone period in January - February 2012. The verification also showed that the known inability of HIRLAM (and presumably also other NWP models) to predict very cold near-surface temperatures in the stable clear-sky cases still remains, independently of the surface description.

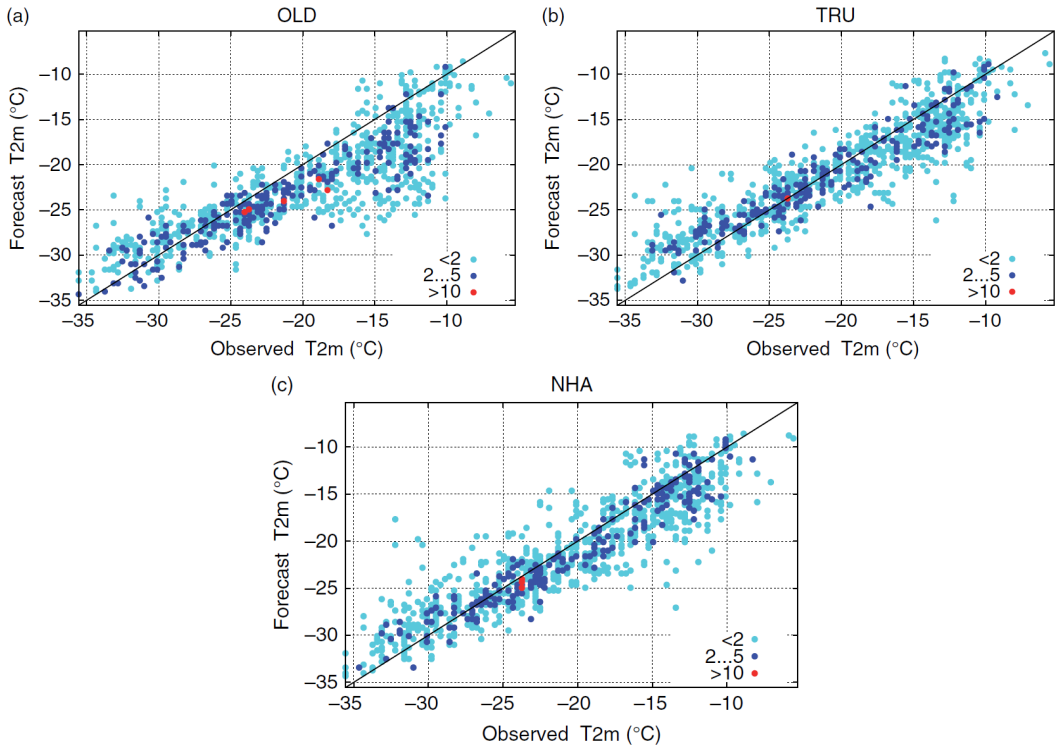

Figure B.14 Scatterplot of observed temperature vs. predicted temperature for the same 10 stations as in Fig. B.13 for OLD (a), TRU (b) and NHA (c). The time period is from 25 January to 5 February and +06-, +12-, +18- and +24-hour forecasts are included. Colours show the number of cases at each point as shown in the legend.

5 Summary

This study was inspired by a note in a local newspaper on 31 January 2012 about exceptional temperature fluctuations in the Southeastern Finland. According to the note, the reason of the observed temperature fluctuations was a cloud spread from Lake Ladoga. For the duty forecaster this situation was challenging, because a correct forecast of formation and movement of the cloud was necessary in order to predict the local temperatures. This case was also related to a series of studies, aimed at improving the treatment of lake effects in the HIRLAM NWP system.

Earlier, most of the studies on the effect of lakes on local weather have focused on severe convective snowfall cases. This case represents anticyclonic winter conditions, which typically means clear sky, stable stratification and cold near-surface temperatures. In such conditions the individual processes may not be strong, but their subtle balance and interactions determine the weather, in this

case the temperature variability. Thus, this case was a good test-bench for the physical parametrisations of HIRLAM, in particular for testing the sensitivity of the model to the description of the changing lake surface state.

We ran three experiments, which differed from each other only in the way the state of Lake Ladoga was described: based on climatology (experiment OLD), on a lake model (TRU) or on the analysis of satellite observations (NHA). Experiments based either on the assimilated satellite observations or on the prognostic lake parametrisation alone, indicated freezing of Lake Ladoga in the last days of January, which was in accordance with the observations.

When given the correct Lake Ladoga surface conditions, in one way or another (experiments TRU and NHA), the forecast model was able to predict the cloud formation and movement in a realistic way. Physically reasonable surface energy balance, predicted under clear and cloudy conditions, ensured a realistic prediction of the near-surface weather conditions. This made it possible for HIRLAM to forecast correctly also the 2-metre temperature variations, which was confirmed by comparison with the observations. However, even small errors in timing of the cloud movement were found to make the temperature forecasts less accurate.

The period with strongly varying temperatures, due to the distribution of clouds, lasted only a few days. Objective verification scores were computed using the observations within a distance of about 250~km downstream (westwards) of Lake Ladoga over the whole anticyclonic period (two weeks). They revealed a clear improvement of the 2-metre temperatures, predicted by the experiments with a correct state of Lake Ladoga, as compared to the climatology-based experiment. The influence of Lake Ladoga was visible neither in the scores of the other surface-related parameters nor in the temperatures over a large area or over a long validation period.

In this study, we arrived at three main conclusions. First, the encouraging message was that HIRLAM could predict the effect of Lake Ladoga on local weather in this meteorological case, if the lake surface state was known. Second, the current parametrisation methods of atmospheric processes and air-surface interactions may lead to realistic description of the evolving anticyclonic boundary layer conditions, with the subtle balance between processes due to the large scale atmospheric motion, local surface properties, radiation and turbulence. Third, these results encourage work towards a better description of the lake surface state in NWP models by fully utilizing satellite observations, combined with advanced lake parametrization and data assimilation methods.

Bibliography

Amlien J. and Solberg, R. 2003. A comparison of temperature retrieval algorithms for snow covered surfaces. *Proceedings of the International Geoscience and Remote Sensing Symposium*, Toulouse, France, 21-25 July 2003.

Anderson, E. 1976. A point energy and mass balance model for a snow cover. *NOAA Technical Report*, NWS 19, 150 pp.

Andersson, T. and Gustafsson, N. 1994. Coast of departure and coast of arrival: two important concepts for the formation and structure of convective snow bands overseas and lakes. *Mon. Wea. Rev.* 122, 1036-1049.

Andersson, T. and Nilsson, S. 1990. Topographically induced convective snowbands over the Baltic Sea and their precipitation distribution. *Wea. Forecast*. 5, 299-312.

Arp, C.D., Jones, B.M., Whitman, M., Larsen, A., and Urban, F.E. 2010. Lake temperature and ice cover regimes in the Alaskan subarctic and arctic; integrated monitoring, remote sensing, and modeling. *Journal of the American water resources association*, 46 (4), 777-791.

Atlaskin E. and Vihma, T. 2012. Evaluation of NWP results for wintertime nocturnal boundary-layer temperatures over Europe and Finland. *Q. J. R. Meteorol. Soc.* DOI:10.1002/qj.1885.

Avissar, R. and Pielke, R. A. 1989. A parameterization of heterogeneous land surfaces for atmospheric numerical models and its impact on regional meteorology. *Mon.Wea. Rev.* 117, 2113-2136.

Bates, G. T., Giorgi, F., and Hostetler, S. W. 1993. Toward the simulation of the effects of the Great Lakes on climate. *Monthly Weather Review,* 121**,** 1373-1387.

Bergthorsson P. and Döös, B.R. 1955. Numerical weather map analysis. *Tellus*. 7: 329-340.

Bonan, G. B. 1995. Sensitivity of a GCM simulation to inclusion of inland water surfaces. *Journal of Climate*, 8, 2691-2704.

Brown L.C. and Duguay C.R. 2010. The response and role of ice cover in lake-climate interactions. *Prog. Phys. Geogr*. 34(5): 671-704.

Blanken, P. 2003. Enhancement of Evaporation from a Large Northern Lake by the Entrainment of Warm, Dry Air. *J. Hydrometeor*, 4, 680- 693.

Blanken, P.D., Rouse, W.R., Culf, A.D., Spence, C., Boudreau, L.D., Jasper, J.N., Kochtubajda, B., Schertzer, W.M., Marsh, P., and Verseghy, D. 2000. Eddy covariance measurements of evaporation from Great Slave Lake, Northwest Territories, Canada. *Water Resources Research* 36, 1069-1077.

Bosilovich, M. G., Chen, J. Robertson, F. R. and Adler, R. F. 2008. Evaluation of Global Precipitation in Reanalyses. *J. Appl. Meteor. Climatol.,* 47, 227-2299. DOI: http://dx.doi.org/10.1175/2008JAMC1921.1

Brown, L. C. and Duguay, C. R. 2010. The response and role of ice cover in lake-climate interactions. *Prog. Phys. Geogr.* 34(5), 671-704. DOI: 10.1177/0309133310375653.

Brown, L. C. and Duguay, C. R. 2011. The fate of lake ice in the North American Arctic. *The Cryosphere,* 5, 869-892, DOI:10.5194/tc-5-869-2011.

Brown, L. C. and Duguay, C. R. 2012. Modelling lake ice phenology with an examination of satellite-detected subgrid cell variability. *Adv. Meteorol*. 19, 529064. DOI: 10.1155/2012/529064.

Brown, L. C., Howell, S. E. L., Morth, J. and Derksen, C. 2014. Evaluation of the Interactive Multisensor Snow and Ice Mapping System (IMS) for monitoring sea ice phenology. *Rem. Sens. Environ*. 147, 65-78.

Bussières, N., Verseghy, D., and MacPherson, J. I. 2002. The evolution of AVHRR-derived water temperatures over boreal lakes. *Remote Sensing of Environment*, 80, 373-384.

Bussières, N, Schertzer W. M. 2005. The Evolution of AVHRR-Derived Water Temperatures over Lakes in the Mackenzie Basin and Hydrometeorological Applications. *Journal of Hydrometeorology,* 4, 660-672.

Charney, J., Fjortoft, R. and vonNeumann, J. 1950. Numerical integration of the barotropic vorticity equation, *Tellus* 2, 237-257.

Cheng, B., Vihma, T. and Launiainen, J. 2003. Modelling of the superimposed ice formation and sub-surface melting in the Baltic Sea. *Geophysica* 39, 31-50.

Cheng, B., Vihma, T., Pirazzini. R. and Granskog, M. 2006. Modelling of superimposed ice formation during spring snowmelt period in the Baltic Sea. *Ann. Glaciol.,* 44, 139-146.

Cheng, B., Zhang, Z., Vihma, T., Johansson, M., Bian, L., Li, Z., and Wu, H. 2008. Model experiments on snow and ice thermodynamics in the Arctic Ocean with CHINAREN 2003 data. *J. Geophys. Res.* 113, C09020.

Cheng, B., Vima, T., Rontu, L., Kontu, A., Kheyrollah Pour, H., Duguay, C. R. 2014. Evolution of snow and ice temperature, thickness and energy balance in Lake Orajärvi, northern Finland. *Tellus A: Dynamic Meteorology and Oceanography*. 66, 21564.

Cole, J.J., Caraco, N.F., Kling, G.W. and Kratz, T.K. 1994. Carbon dioxide supersaturation in the surface water of lakes. *Science*, 265, 1568-1570.

Coll, C., Hook S. J. and Galve J. M. 2009. Land surface temperature from the Advanced Along-Track Scanning Radiometer: Validation over inland waters and vegetated surfaces. *IEEE Transactions on Geoscience and Remote Sensing,* 47, 350-360.

Collins, M., K. AchutaRao, K. Ashok, S. Bhandari, A. K. Mitra, S. Prakash, R. Srivastava, and A. Turner. 2013. Observational challenges in evaluating climate models, *Nat. Clim. Change*, 3, 940-941.

Cordeira, J. M. and Laird, N. F. 2008. The influence of ice cover on two lake-effect snow events over lake Erie. *Mon. Wea. Rev.* 136, 2747-2763. DOI: 10.1175/2007MWR2310.1.

Cressman, G.P.1959. An operational objective analysis system. *Mont. Wea. Rev*. 87: 367-374.

Crosman E.T. & Horel J.D. 2009: MODIS-derived surface temperature of the Great Salt Lake. *Rem. Sens. of Env*. 113: 73-81.

Cuxart, J., Bougeault, P. and Redelsberger, J.-L. 2000. A turbulence scheme allowing for mesoscale and large-eddy simulations. *Quart. J. Roy. Meteor. Soc*. 126, 1-30.

Crosman, E. T. and Horel J. D. 2009. MODIS-derived surface temperature of the Great Salt Lake. *Remote Sensing of Environment,* 113*,* 73-81.

Daley, R. 1991. Atmospheric Data Analysis. Cambridge University Press, New York, NY, USA, 457 pp.

Donlon, C. J., Martin, M., Stark, J., Robert-Jones, J., Fiedler, E. and Wimmer, W. 2012. The operational sea surface temperature and sea ice analysis (OSTIA) system. *Rem. Sens. Environ*. 116, 140-158.

Drusch, M., Vasilievic, D. and Viterbo, P. 2004. ECMWF's global snow analysis: assessment and revision based on satellite observation. *J. Appl. Meterol*. 43, 1282-1294.

Duguay, C. R., Flato, G. M., Jeffries, M. O., Ménard, P., Morris, K. and Rouse, R. 2003. Ice-cover variability on shallow lakes at high latitudes: model simulations and observations. *Hydrol. Proces.* 17, 3464-3483.

Duguay, C., Green, J. Derksen, C., English, M., Rees, A., Sturm, M., and Walker, A. 2005. preliminary assessment of the impact of lakes on passive microwave snow retrieval algorithms in the Arctic. *62nd Eastern Snow Conference Proceedings,* Waterloo Ontario Canada.

Duguay, C. R., Prowse, T. D., Bonsal, B. R., Brown, R. D., Lacroix, M. P. and M´enard, P. 2006. Recent trends in Canadian lake ice cover. *Hydrol. Proc*. 20, 781-801.

Duguay, C. R., Brown, L. C., Kang, K.-K. and Kheyrollah Pour, H. 2011. Lake ice. *Arctic report card 2011*. http://www.arctic.noaa.gov/report11/lake ice.

Duguay, C. R., Brown, L. C., Kang, K.-K. and Kheyrollah Pour, H. 2012a. [Arctic]. Lake ice. [In State of the Climate in 2011]. *Bulletin of the American Meteorological Society*. 93(7), 152-154.

Duguay, C. R., Soliman, A., Hachem, S. and Saunders, W. 2012b. Circumpolar and regional Land Surface Temperature (LST) with links to geotiff images and netCDF files. *University of Waterloo, Canada*, DOI:10.1594/PANGAEA.775962. PANGAEA: Data Publisher for Earth & Environmental Science.

Duguay, C. R., Brown, L. C., Kang, K.-K. and Kheyrollah Pour, H. 2013. [Arctic]. Lake ice. [In State of the Climate in 2012]. *Bulletin of the American Meteorological Society*. 94(7), 156-158.

Duguay, C.R., Bernier, M., Gauthier, Y., and Kouraev, A. 2015. Remote sensing of lake and river ice. *Remote Sensing of the Cryosphere*, Edited by M. Tedesco. Wiley-Blackwell (Oxford, UK), pp. 273-306.

Dupont, F., Chittibabu, P., Huang, A., Yerubandi, R.R., Fortin, V., Lu, Y. 2011. A NEMO-based modelling system for the Great Lakes. *15th Workshop on Physical Processes in Natural Waters*, Burlington, Canada.

Eerola, K. 1996. Experiences with the analysis of sea surface temperature, ice coverage and snow depth. HIRLAM 3 Workshop on Soil Processes and Soil/Surface Data Assimilation. Spanish Meteorological Institute, 27-29 November 1995, 33-37.

Eerola, K., Rontu, L., Kourzeneva, E. and Shcherbak, E. 2010. A study on effects of lake temperature and ice cover in HIRLAM. *Boreal Environ. Res*. 15, 130-142.

Eerola, K. 2013. Twenty-one years of verification from the HIRLAM NWP system. *Weather Forecasting*, 28, 270-285. DOI: http: 426 //dx.doi.org/10.1175/WAF-D-12-00068.1.

Eerola, K., Rontu, L., Kourzeneva, E., Kheyrollah Pour, H., and Duguay, C.R. 2014. Impact of partly ice-free Lake Ladoga on temperature and cloudiness in an anticyclonic witer situation- a case study using HIRLAM model. *Tellus Series A: Dynamic Meteorology and Oceanography*. 66, 23929.

Eliassen A. 1954: *Provisional report on calculation of spatial covariance and autocorrelation of the pressure field*. Inst. Weather and Climate res., Acad. Sci. Oslo, Rept. No. 5.

Fiedler, E., Martin, M. and Roberts-Jones, J. 2014. An operational analysis of lake surface water temperature. *Tellus A*. 66, 21247. DOI: 10.3402/tellusa.v66.21247.

Foster, J. L., Hall, D. K., Kelly, R. E. J., and Chiu, L. 2009. Seasonal Snow Extent and Snow Mass in South America Using SMMR and SSM/I Passive Microwave Data (1979-2003), *Remote Sensing of Environment*, 113, 291-305.

Foster, J.L., Hall, D.K., Eylander, J.B., Riggs, G.A., Ngheim, S.V., Tedesco, M., Kim, E., Montesano, P., Kelly, R.E.J., Casey, K., and Choudhury, B. 2011. A blended global snow product using visible, passive microwave and scatterometer satellite data, submitted to International Journal of Remote Sensing. *International Journal of Remote Sensing*, 32 (5), 1371-1395.

Gandin, L. 1965. Objective Analysis of Meteorological Fields. Gidrometizdat, Leningrad. Translated from Russian, Jerusalem, *Israel Program for Scientific Translations*, 242 pp.

Gilchrist B. and Cressman, G.B.1954: An experiment in objective analysis. *Tellus*, 6: 97-101.

Gollvik, S. and Samuelsson, P. 2010. A tiled land-surface scheme for 945 HIRLAM. Unpublished manuscript. Online at: http://hirlam.org.

Gustafsson, N., Nyberg, L. and Omstedt, A. 1998. Coupling of a high-resolution atmospheric model and an ocean model for the Baltic Sea. *Mon. Wea. Rev*. 126, 2822-2846.

Granskog, M., Vihma, T., Pirazzini, R. and Cheng, B. 2006. Superimposed ice formation and surface fluxes on sea ice during the spring melt-freeze period in the Baltic Sea. *J. Glaciol.* 52(176), 119-127.

Grönvall, H. and Seinä, A. 2002. Satellite data use in Finnish winter navigation. In: Operational Oceanography: Implementation at the European and Regional Scales Proceedings of the Second International Conference on EuroGOOS, 11-13 March 1999, Rome, Italy, (eds. N. C. Flemming et al.), Elsevier, pp. 429-436.

Hakala, A. 2004. Meromixis as a part of lake evolution - observations and a revised classification of true meromictic lakes in Finland. *Boreal Environment Research*, 9, 37-53.

Hall, D.K., Foster, J. L., Chang, A.T.C., and Rango, A. 1981. Freshwater ice thickness observations using passive microwave sensors. *IEEE Geoscience and Remote Sensing Letters*, 19 (4), 189-193.

Hall, D.K., Riggs, G.A., Salomonson, V.V., DiGiromamo, N., and Bayr, K.J. 2002. MODIS Snow-Cover Products, *Remote Sensing of Environment*, 83, 181-194.

Hauser, P., R., Shuttelworth, W. J., Gupta, H.V., Famiglietti, J.S., Syed, K.H., and Goodrich, D.C. 1998. Integration of soil moisture remote sensing and hydrologic modeling using data assimilation. *Water Resource Research,* 34(12), 3405-3420.

Heim, B., Overduin, P., Schirrmeister, L., and Doerffer, R. 2008. OCOC-from ocean colour to organic carbon. the '2nd MERIS / (A)ATSR User Workshop', Frascati, Italy 22–26 September 2008 (ESA SP-666, November 2008).

Helfrich, S. R., McNamara, D., Ramsay, B. H., Baldwin, T. and Kasheta, T. 2007. Enhancements to, and forthcoming developments in the Interactive Multisensor Snow and Ice Mapping System (IMS). *Hydrol. Process*. 21, 1576-1586.

Henderson-Sellers, A., and Pitman, A. J. 1992. Land-surface schemes for future climate models: Specification, aggregation, and heterogeneity. *Journal of Geophysical Research,* 97(D), 2687–2696.

Hollingsworth A. and Lönnberg R. 1986a: The statistical structure of short-range forecast errors as determined from radiosonde data. Part I: The wind field. *Tellus A*, 28: 111-136.

Hollingsworth A. and Lönnberg R. 1986b: The statistical structure of short-range forecast errors as determined from radiosonde data. Part II: The covariance of height and wind errors. *Tellus A*, 28: 137-161.

Holtslag, A. A. M., Svensson, G., Baas, P., Basu, S., Beare, B., Beljaars, A. C. M. , Bosveld, F. C., Cuxart, J., Lindvall, J., Steeneveld, G. J., Tjernström, M. and Van De Wiel, B. J. H. 2013. Stable atmospheric boundary layers and diurnal cycles: challenges for weather and climate models. *Bull. Amer. Meteor. Soc*. 94, 1691-1706. DOI: 10.1175/BAMS-D-11-00187.1.

Hook, S. J., Vaughan, R. G., Tonooka, H. and Schladow, S. G. 2007. Absolute radiometric inflight validation of mid infrared and thermal infrared data from ASTER and MODIS on the Terra Spacecraft using the Lake Tahoe, CA/NV, USA, automated validation site. *IEEE Transactions on Geoscience and Remote Sensing*, 45(6), 1798-1807.

Hook, S., Wilson, R. C., MacCallum, S. and Merchant, C. J. 2012. Lake surface temperature. *Bull. Am. Meteorol. Soc*. 93, 18-19.

Hostetler, S. W., and Giorgi, F. 1992. Use of a regional atmospheric model to simulate lake–atmosphere feedbacks associated with Pleistocene lakes Lahontan and Bonneville. *Climate Dynamics,* 7, 39-44.

Howell, S.E.L., Brown, L.C., Kang, K.K., and Duguay, C.R. 2009. Variability in Ice Phenology on Great Bear Lake and Great Slave Lake, Northwest Territories, from SeaWinds/QuikSCAT: 2000-2006. *Remote Sensing of Environment*, 113, 816-834.

Julian P.R, & Thiebaux H.J. 1975. On some properties of correlation function used in optimum interpolation scheme. *Mon. Wea. Rev*. 103: 605-616.

Huang, A., Rao, Y. R., and Lu, Y. 2010. Evaluation of a 3-D hydrodynamic model and atmospheric forecast forcing using observations in Lake Ontario, *Journal of Geophysical Research*, 115, C02004, DOI: 10. 1029/2009JC005601.

Hulley, G. C., Hook, S. and Schneider, P. 2011. Optimized split-window coefficients for deriving surface temperatures from inland water bodies. *Remotes Sensing of Environment*, 115, 3758-3769. DOI:10.1016/j.rse.2011.09.014.

Imboden, D. M. and Wüest A. 1995. Mixing mechanisms in lakes. *Physics and Chemistry of lakes,* (ed. Lerman, A., Imboden D.M., Gat J.R.), Chap. 4, Springer-Verlag, Berlin Heidelberg, New York, 83-138.

Jackson, K., Wilkinson, J., Maksym, T., Meldrum. D., Beckers, J. Haas, C. and MacKenzie, D. 2013. A Novel and Low Cost Sea Ice Mass Balance Buoy. *J. Atmos.Oceanic Technol.* 30, 2676-2688.

Jakobson, E. and Vihma, T. 2010. Atmospheric moisture budget over the Arctic on the basis of the ERA-40 reanalysis. *Int. J. Climatol.,* 30: 2175-2194, DOI: 10.1002/joc.2039.

Jeffries, M.O., Morris, K., and Duguay, C.R. 2005. Lake ice growth and decay in central Alaska, USA: observations and computer simulations compared. *Annals of Glaciology*, 40, 195-199.

Kang, K.-K., Duguay, C. R., Howell, S. E. Derksen, C. P. and Kelly, R.E.J. 2010. Sensitivity of AMSR-E brightness temperatures to the seasonal evolution of lake ice thickness. *IEEE Geoscience and Remote Sensing Letters*, 7(4), 751-755, DOI: 10.1109/LGRS.2010.2044742.

Kang, K.-K., Duguay, C. R. and Howell, S. E. L. 2012. Estimating ice phenology on large northern lakes from AMSR-E: algorithm development and application to Great Bear Lake and Great Slave Lake, Canada. *Cryosphere.* 6(2), 235-254.

Kelly, R.E.J. 2009. The AMSR-E Snow Depth Algorithm: Description and Initial Results. *Journal of the Remote Sensing Society of Japan*. 29(1): 307-317. (GLI/AMSR Special Issue).

Key, J. R., Collins, J. B., Fowler C. and Stone, R. S. 1997. High-latitude surface temperature estimates from thermal satellite data. *Remote Sensing of Environment*, 61(2), 302-309.

Kheyrollah Pour, H., Duguay, C. R., Martynov, A. and Brown, L. C. 2012. Simulation of surface temperature and ice cover of large northern lakes with 1-D models: A comparison with MODIS

satellite data and in-situ measurements. *Tellus A*: Dynamic Meteorology and Oceanography, 64, 17614, DOI: 10.3402/tellusa.v64i0.17614.

Kheyrollah Pour, H., Duguay, C. R., Solberg, R. and Rudjord, Ø. 2014a. Impact of satellite-based lake surface observations on the initial state of HIRLAM-Part I: evaluation of MODIS/AATSR lake surface water temperature observations. *Tellus A*. 66, 21534, DOI: 10.3402/tellusa.v66.21534.

Kheyrollah Pour, H., Rontu, L., Duguay, C. R., Eerola, K. and Kourzeneva, E. 2014b. Impact of satellite-based lake surface observations on the initial state of HIRLAM. Part II: analysis of lake surface temperature and ice cover. *Tellus A*. 66, 21395, DOI: 10.3402/tellusa.v66.21395.

Kourzeneva, E., Samuelsson, P., Ganbat, G. and Mironov, D. 2008. Implementation of lake model Flake into HIRLAM. HIRLAM Newsletter, no. 54, pp. 54-64. Online at: http:// hirlam.org/

Kourzeneva, E., Asensio, H., Martin, E. and Faroux, S. 2012a. Global gridded dataset of lake coverage and lake depth for use in numerical weather prediction and climate modelling. *Tellus A*. 64, 15640. DOI: 10.3402/tellusa.v64i0.15640.

Kourzeneva, E., Martin, E., Batrak, Y. and Le Moigne, P. 2012b. Climate data for parameterization of lakes in NWP models. Tellus A. 64, 17226. DOI: 10.3402/tellusa.v64i0.17226.

Kourzeneva, E. 2014: Assimilation of lake water surface temperature observations using an extended Kalman filter, *Tellus A*. 66: 21510.

Krinner, G. and Boike, J. 2010. A study of the large-scale climatic effects of a possible disappearance of high-latitude inland water surfaces during the 21st century. *Boreal Environ. Res.* 15, 203-217.

Laird, N. F., Kristovich, D. A. R. and Walsh, J. E. 2003. Idealized 970 model simulations examining the mesoscale structure of winter lake-effect circulations. *Mon. Wea. Rev*. 131, 206-221.

Latifovic, R., and Pouliot, D. 2007. Analysis of climate change impacts on lake ice phenology in Canada using the historical satellite data record. *Remote Sensing of Environment*, 106, 492-508.

Launiainen, J. 1995. Derivation of the relationship between the Obukhov stability parameter and the bulk Richardson number for the flux-profile studies. *Boundary Layer Meteorol.* 76, 165-179.

Launiainen, J. and Cheng, B. 1998. Modelling of ice thermodynamics in natural water bodies. *Cold Reg. Sci. Technol.,* 27(3), 153-178.

Lenaerts, J. T. M., and vanden Broeke, M. R. 2012. Modelling drifting snow in Antarctica with a

regional climate model: 2. Results, *J. Geophys. Res.,* 117, D05109, DOI:10.1029/2010JD015419.

Leonard, K. and Maksym, T. 2011. The importance of wind-blown snow redistribution to accumulation on and mass balance of Bellingshausen Sea ice. *Ann. Glaciol*., 52(57 Pt 2), 271-278. DOI:10.3189/172756411795931651.

Leppäranta, M. 1993. A review of analytical sea ice growth models. *Atmosphere- Ocean,* 31(1), 123 - 138.

Lehner, B. and Doell, P. 2004. Development and validation of a global database of lakes, reservoirs and wetlands. *Journal of Hydrology,* 296, 1-22.

Lindsay, R. and Zhang, J. 2006: Assimilation of ice concentration in an ice-ocean model. *J. Atmos. and Oceanic Technol.*, 23, 742-749.

Lisaeter, K. A., Rosanova, J. and Evensen, G. 2003. Assimilation of ice concentration in a coupled ice-ocean model, using the Ensemble Kalman Filter. Ocean Dynam. 53, 358-388. DOI: 10.1007/s10236-003-0049-4.

Liu, G., Ou, W., Zhang, Y., Wu, T., Zhu, G., Shi, K. and Qin, B. 2014. Validating and Mapping Surface Water Temperatures in Lake Taihu: Results From MODIS Land Surface Temperature Products, *IEEE Journal of Selected Topics in Applied Earth Observations and remote sensing*. 10, 1939-1404.

Ljungemyr, P., Gustafsson, N., and Omstedt, A. 1996. Parameterization of lake thermodymanics in a high-resolution weather forcasting model. *Tellus*, 48A, 608-621.

Lofgren, B.M. 1997. Simulated effects of idealized laurentian Great Lakes on regional and large-scale climate. *Journal of Climate,* 10, 2847-2858.

Lofgren, B. M., and Zhu, Y. 2000. Surface energy fluxes on the Great Lakes based on satellite observed surface temperatures 1992 to 1995. *Journal of Great Lakes Research,* 26, 305-314.

Long, Z., Perrie, W. Gyakum, J., Caya, D. and Laprise, R. 2007. Northern Lake impacts on local seasonal Climate. *J. Hydrometeor*, 8, 881- 896.

Lorence, A.C. 1981. A global three-dimensional multivariate statistical interpolation scheme. *Mon. Wea. Rev*. 109: 701-721.

Louis, J. F. 1979. A parametric model of vertical eddy fluxes in the atmosphere. *Bound. Lay. Met.* 17, 187-202.

Loveland, T. R., Reed, B. C., Brown, J. F., Ohlen, D. O., Zhu, J., Yang, L., and Merchant, J. W. 2000. Development of a global land cover characteristics database and IGBP DISCover from 1-km AVHRR data. *Int. J. Remote Sens*. 21, 1303-1330.

Lynch, P. 2006. *The Emergence of Numerical Weather Prediction: Richardson's Dream*. Cambridge: Cambridge University Press

MacCallum, S. N. and Merchant, C. J. 2012. Surface water temperature observations of large lakes by optimal estimation. *Can. J. Remote Sens*. 38(1), 25-45. DOI: 10.5589/m12-010.

Mahfouf, J.F. 1991. Analysis of soil moisture from near-surface parameters: a feasibility study. *Journal of Applied Meteorology*, 30, 1534-1547.

Mäkynen, M., Cheng, B. and Similä, M. 2013. On the accuracy of the thin ice thickness retrieval using MODIS thermal imagery over the Arctic first year ice, *Ann. Glaciol.,* 54(62), 87-96.

Manrique-Suñén, A., Nordbo, A., Balsamo, G., Beljaars, A. and Mammarella, I. 2013. Representing land surface heterogeneity: offline analysis of the tiling method. J. *Hydrometeor*. 14, 850-867. DOI: 10.1175/JHM-D-12-0108.1.

Mironov, D. 2008. Parameterization of 658 lakes in numerical weather prediction. Description of a lake model. *COSMO Technical Report*, No. 11, Deutscher Wetterdienst, Offenbach am Main, Germany, 41pp.

Mironov, D., Heise, E., Kourzeneva, E., Ritter, B. Schneider, N. and Terzhevik, A. 2010. Implementation of the lake parametrisation scheme FLake into the numerical weather prediction model COSMO. *Bor. Env. Res*. 15, 218-230.

Mironov, D., Ritter, B., Schulz, J.-P., Buchhold, M., Lange, M. and Machulskaya, E. 2012. Parameterisation of sea and lake ice in numerical weather prediction models of the German Weather Service. *Tellus A*. 64, 17330, DOI: 10.3402/tellusa.v64i0.17330.

Morris, K., Jeffries, M. and Duguay. C. R. 2005. Model simulation of the effects of climate variability and change on lake ice in central Alaska, USA. *Ann. Glaciol.,* 40, 113-118.

Ngai, K. L. C., Shuter, B. J., Jackson, D. A. and Chandra, S. 2013. Projecting impacts of climate change on surface water temperatures of a large subalpine lake: Lake Tahoe, USA. *Clim. Change*. 118, 841-855.

Nicolaus, M., Haas, C. and Bareiss, J. 2003. Observations of superimposed ice formation at melt-onset on fast ice on Kongsfjorden, Svalbard. *Physics and Chemistry of the Earth* 28, 1241-1248.

Niziol, T. A. 1987. Operational forecasting of lake effect snowfall in Western and Central New York. Weather Forecast. 2, 310-321.

Niziol, T. A., Snyder, W. R. and Waldstreicher, J. S. 1995. Winter weather forecasting throughout the Eastern United States. Part IV: Lake effect snow. *Weather Forecast*. 10, 61-77.

Noilhan, J. and Mahfouf, J.-F. 1996. The ISBA land surface parameterisation scheme. Global Planet. Change. 13, 145-159.

Noilhan, J. and Planton, S. 1989. A simple parameterization of land surface processes for meteorological models. *Mon. Wea. Rev*. 117, 536-549.

Noyes, E., Corlett, G., Remedios, J., Kong, X. and Llewellyn-Jones, D. 2007. An accuracy assessment of AATSR LST data using empirical and theoretical methods. In *Proceedings of the ENVISAT Symposium 2007*, Montreux, Switzerland, 23-27 April 2007; ESA SP-636.

Noyes, E., Good, S., Corlet, G., Kong, X., Remedios, J. and Llewellyn-Jones, D. 2006. AATSR LST Product Validation. In *Proceedings of the Second Working Meeting on MERIS and AATSR Calibration and Geophysical Validation (MAVT-2006),* Frascati, Italy Switzerland, 20–24 March 2006; ESA SP-615.

Oesch D. C., Jaquet J.-M. Hauser A., and Wunderle, S. 2005. Lake surface water temperature retrieval using advanced very high resolution radiometer and Moderate Resolution Imaging Spectroradiometer data: Validation and feasibility study, *J. of Geophy. Res*., 110: C12014.

Oke, T. R. 1978. *Boundary Layer Climates.* John Wiley and Sons, New York.

Panofsky, H.A.1949: Objective weather map analysis. *J.Met*. 6(6): 386-392.

Pirazzini, R. 2009. Challenges in Snow and Ice Albedo Parameterizations. *Geophysica,* 45(1-2), 41-62.

Pitman, A. J. 1991. A simple parameterization of sub-grid scale open water for climate models. *Climate Dynamics,* 6, 99-112.

Prata, F. 2002. Land Surface Temperature Measurement from Space: AATSR Algorithm Theoretical Basis Document. *CSIRO Atmospheric Research, Aspendale*, Australia, 34pp.

Prowse, T.D. and Brown, K. 2010. Hydro-ecological effects of changing Arctic river and lake ice covers: a review. *Hydrology Research,* 41:454-461.

Prowse, T., Alfredsen, K., Beltaos, S., Bonsal, B., Duguay, C. R., Korhola, A., McNamara, J., Vincent, W. F., Vuglinsky, V. and Weyhenmeyer, G. 2011. Changing Lake and River Ice Regimes: Trends, Effects and Implications. In: AMAP (2011). Snow, Water, Ice, and Permafrost in the Arctic (SWIPA): Climate Change and the Cryosphere. Arctic Monitoring and Assessment Program (AMAP). Oslo, Norway, xii + 538 pp.

Qin, J., Liang, S., Yang, K., Kaihotsu, I., Liu, R. and Koike, T. 2009. Simultaneous estimation of both soil moisture and model parameters using particle filtering method through the assimilation of microwave signal. *J. Geophys. Res*. 114, 15103. DOI: 10.1029/2008JD011358.

Ramsay, B. H. 1998. The interactive multisensor snow and ice mapping system. *Hydrol. Process*. 12, 1537-1546.

Reichle, R. H, McLaughlin, D. B., and Entekhabi, D. 2002a. Hydrologic data assimilation with the ensemble Kalman filter. *Monthly Weather Review*, 130, 103-114.

Reichle, R. H, Walker, J. P., Koster, R. D., and Houser, P. R. 2002b. Extended versus ensemble Kalman filtering for land data assimilation. *Journal of Hydrometeorology*, 3, 728-740.

Reinart, A. and Reinhold M. 2008: Mapping surface temperature in large lakes with MODIS data. *Rem. Sens. Environ*, 12 (2): 603-611.

Rodriguez, E., Navascues, B., and Ayuso, J.J. 2002. *The tiling surface scheme for HIRLAM5: feature and latest results. Proceedings of the SRNWP/HIRLAM Workshop on Surface Processes*, Turbulence and Mountain Effects, INM, Madrid 22-24 October 2001, 55-63.

Rontu, L., Eerola, K., Kourzeneva, E. and Vehviläinen, B. 2012. Data assimilation and parametrisation of lakes in HIRLAM. *Tellus A*, 64, 17611, DOI: 10.3402/tellusa.v64i0.17611.

Rouse, W. R., Oswald, C. M., Binyamin, J., Blanken, P. D., Schertzer, W. M., and Spence, C. 2003. Interannual and seasonal variability of the surface energy balance and temperature of Central Great Slave Lake. *Journal of Hydrometeorology,* 4**,** 720-730.

Rouse, W. R., Blanken, P. D., Duguay, C. R., Oswald, C. J. and Schertzer, W. M. 2008. Climate lake interactions. In: Cold Region Atmospheric and Hydrologic Studies: The Mackenzie GEWEX Experience, (ed. MK. Woo). Vol. 2, Springer, Berlin, pp. 139-160.

Saloranta, T. 2000. Modelling the evolution of snow, snow ice and ice in the Baltic Sea. *Tellus*, 52A, 93-108.

Samuelsson, P., Kourzeneva, E. and Mironov, D. 2010. The impact of lakes on the European climate as simulated by a regional climate model. Boreal Environ. Res. 15, 113-129.

Sattler K. and Huang X-Yu. 2002. Structure function characteristics for 2 meter temperature and relative humidity in different horizontal resolutions. *Tellus A*. 54A: 14-33.

Schertzer, W. M. 1997. *Freshwater Lakes*. Chapter 6 in the Surface Climates of Canada. McGill Queen's University Press, 124-148.

Schertzer, W. M., Rouse, W. R., Walker, A. E., Bussie`res, N., Leighton, H. G., and Blanken, P. D. 2002. *Heat exchange, evaporation and thermal responses of high latitude lakes*. Proceeding of the Second MAGS-GAME International Workshop, Sapporo, Japan, Institute for Low Temperature Science, University of Hokkaido, 43-51.

Svacina, N.A., Duguay, C.R. and Brown, L.C. 2014a. Modelled and satellite-derived surface albedo of lake ice - Part I: Evaluation of the albedo parameterization scheme of the Canadian Lake Ice Model. *Hydrological Processes*. 28(16), 4550-4561.

Svacina, N.A., Duguay, C.R. and King, J. 2014b. Modelled and satellite-derived surface albedo of lake ice - Part II: Evaluation of MODIS albedo products. *Hydrological Processes*. 28(16), 4562-4572.

Schneider, P., Hook, S. J., Radocinski, R. G., Corlett, G. K., Hulley, G. C., Schladow, S. G. and Steissberg, T.E. 2009. Satellite observations indicate rapid warming trend for lakes in California and Nevada. *Geophysical Research Letters*, 36, L22402.

Scott, R. W. and Huff, F. A. 1996. Impacts of the Great Lakes on regional climate conditions. *J. Great Lake. Res.* 22(4), 845-863. DOI: 10.1016/S0380-1330(96)71006-7.

Scott**,** K.A., Buehner, M.**,** Caya, A., and Carrieres, T. 2012. Direct Assimilation of AMSR-E Brightness Temperatures for Estimating Sea Ice Concentration. *Monthly Weather review*, 140, 997–1013.

Semmler, T., Cheng, B., Yang, Y. and Rontu, L. 2012. Snow and ice on Bear Lake (Alaska)-sensitivity experiments with two lake ice models. *Tellus A*. 64, 17339. DOI: 10.3402/tellusa.v64i0. 17339.

Simon, E. and Bertino, L. 2009. Application of the Gaussian anamorphosis to assimilation in a 3-D coupled physicalecosystem model of the North Atlantic with the EnEKF: a twin experiment. *Ocean Sci*. 5, 495-510.

Slater, A., Clark, M, 2005. Snow Data Assimilation via an Ensemble Kalman Filter. *Journal of Hydrometeorology,* **7**,478-493.

Solberg, R., Wangensteen, B., Rudjord, Ø., Metsämäki, S., Nagler, T., and coauthors. 2011. GlobSnow Snow Extent Product Guide - Product Version 1.2, URL: http://www.globsnow.info/se/GlobSnow_SE_product_readme_v1.2.pdf

Soliman, A., Duguay, C. R., Saunders, W. and Hachem, S. 2012. Pan-Arctic land surface temperature from MODIS and AATSR: Product development and intercomparison. *Remote Sensing,* 4, 3833-3856, DOI:10.3390/rs4123833.

Song, Y., Semazzi, F. H. M., Xie, L., and Ogallo, L. J. 2004. A coupled regional climate model for the Lake Victoria Basin of East Africa. *International Journal of Climatology,* 24, 57-75.

Stark, J., Ridley, J., Martin, M. and Hines, A. 2008. Sea ice concentration and motion assimilation in a sea ice-ocean model. *J. Geophys. Res.,* 113, C05S91.

Sundqvist, H. 1993. Inclusion of ice phase of hydro meteors in cloud parametrization for meso-scale and large scale models. *Beitr. Phys. Atmosph.* 66, 137-147.

Sundqvist, H., Berge, E. and Kristjansson, J. 1989. Condensation and cloud parametrization studies with a mesoscale numerical weather prediction model. *Mon. Wea. Rev*. 117, 1641-1657.

Surdu, C. M., Duguay, C.R., Brown, L.C., and Fernández Prieto, D. 2014. Response of ice cover on shallow lakes of the North Slope of Alaska to contemporary climate conditions (1950-2011): radar remote-sensing and numerical modelling data analysis. *The Cryosphere,* 8, 167-180, DOI:10.5194/tc-8-167-2014.

Sydor, M. 2006. Use of Hyperspectral Remote Sensing Reflectance in Extracting the Spectral Volume Absorption Coefficient for Phytoplankton in Coastal Water: Remote Sensing Relationships for the Inherent Optical Properties of Coastal Water. *Journal of Coastal Research,* 22(3), 587-594.

Thiebaux, H.J. 1975. Experiments with correlation representation for objective analysis: *Mon. Wea. Rev*. 103: 617-627.

Tikkanen, M. 2002. Long-term changes in lake and river systems in Finland. *Fennia,* 180 (1-2), 31-42. Helsinki. ISSN 0015-0010.

Tjernström, M., Sedlar, J. and Shupe, M. D. 2008. How well do regional climate models reproduce radiation and clouds in the Arctic? An Evaluation of ARCMIP Simulations. *J. Appl. Meteorol. Climatol.,* 47, 2405-2422.

Tsuang, B.-J., Tu, C.-Y., and Arpe, K. 2001. *Lake Parameterization for Climate Models*. Report No. 316, Max Planck Institute for Meteorology, Hamburg, March 2001, 72 p.

Undén, P., Rontu L., Järvinen H., Lynch P., Calvo J., Cats G., Cuxart J., Eerola K., Fortelius K., Garcia-Moya J. A., Jones C., Lenderink G., McDonald A., McGrath R., Navascues B., Nielsen N. W., Ødegaard V., Rodrigues E., Rummukainen M., Rõõm R., Sattler K., Sass B. H., Savijärvi H., Schreuer B. W., Sigg R., The H., Tijm S. 2002. HIRLAM-5 Scientific Documentation. Hirlam, scientific report.

Vavrus, S., Notaro, M. and Zarrin, A. 2013. The role of ice cover in heavy lake-effect snowstorms over the Great Lakes Basin as simulated by RegCM4. *Mon. Wea. Rev*. 141, 148-165. DOI: 10.1175/MWR-D-12-00107.1.

Vihma, T., Uotila, J., Cheng, B., and Launiainen, J. 2002. Surface heat budget over the Weddell Sea: buoy results and comparisons with large-scale models, *J. Geophys. Res.,* 107, C2, DOI:10.1029/2000JC000372.

Vihma, T., Pirazzini, R., Renfrew, I. A., Sedlar, J., Tjernström, M., Nygård, T., Fer, I., Lüpkes, C., Notz, D., Weiss, J., Marsan, D., Cheng, B., Birnbaum, G., Gerland, S., Chechin, D. and Gascard, J. C. 2014. Advances in understanding and parameterization of small-scale physical processes in the marine Arctic climate system: a review. *Atmos. Chem. Phys. Discuss*., 13, 32703-32816, DOI:10.5194/acpd-13-32703-2013.

Walsh, J.E., Anisimov, O., Hagen, J.O.M., Jakobsson, T. , Oerlemans, J., Prowse, T.D., Romanovsky, V., Savelieva, N., Serreze, M., Shiklomanov, A., Shiklomanov, I. and Solomon, S. 2005. Cryosphere and hydrology. In: Arctic Climate Impact Assessment, pp. 183-242, Cambridge University Press.

Wan, Z. and Dozier, J. 1996. A generalized split-window algorithm for retrieving land surface temperature from space. *IEEE Transactions on Geoscience and Remote Sensing*, 34(4), 892-905.

Wan, Z., Zhang, Y., Li, Z.L., Wang, R., Salomonson, V.V., Yves, A., Bosseno, R. and Hanocq, J.F. 2002: Preliminary estimate of calibration of the moderate resolution imaging spectroradiometer thermal infrared data using Lake Titicaca. *Rem. Sens. of Env*. 80: 497-515.

Wan, Z. 2005. *Refinements of the MODIS Land-Surface Temperature Products*. Technical Progress Report Submitted to the National Aeronautics and Space Administration.

Wan, Z. 2008. New refinements and validation of the MODIS land-surface temperature/emissivity products, *Rem. Sens. of Env.*, 112: 59-74.

Warner, T.T. 2011. *Numerical weather and climate prediction*. United Kingdom at University Press, Cambridge.

Wright, D. M., Posselt, D. J., Steiner, A. L. 2013. Sensitivity of Lake-Effect Snowfall to Lake Ice Cover and Temperature in the Great Lakes Region. *Mon. Wea. Rev.,* 141, 670-689. DOI: http://dx.doi.org/10.1175/MWR-D-12-00038.1

Yang, Y., Leppäranta, M., Cheng, B. and Li. Z. 2012. Numerical modelling of snow and ice thickness in Lake Vanajavesi, Finland. *Tellus A* 64, 17202, DOI: 10.3402/tellusa.v64i0.17202.

Yang Y., Cheng, B., Kourzeneva, E., Semmler, T., Rontu, R., Leppäranta, M. Shirasawa, K., and Li, Z. 2013. Modelling experiments on air-snow-ice interactions over a high Arctic lake *Boreal Env. Res.* 18: 341-358.

Yu, Y. and Rothrock, D. A. 1996. Thin ice thickness from satellite thermal imagery. *J. Geophys. Res.,*557 101(C10), 25753-25766.

Zhao, L., Jin, J., Wang, S.-Y. and Ek, M. B. 2012. Integration of remote-sensing data with WRF to improve lake-effect precipitation simulations over the Great Lakes region. *J. Geophys. Res*. 117, D09102.